Carbonyl compounds and their OH reactivities in outdoor and indoor environments

Dissertation

zur Erlangung des Grades

"Doktor der Naturwissenschaften"

im Promotionsfach Chemie

am Fachbereich Chemie, Pharmazie und Geowissenschaften

der Johannes Gutenberg-Universität Mainz

Nijing Wang

geb. in Zhejiang, China

Mainz, 2020

I hereby declare that I wrote the dissertation submitted without any unauthorized external assistance and used only sources acknowledged in the work. All textual passages that are appropriated verbatim or paraphrased from published and unpublished texts as well as all information obtained from oral sources are duly indicated and listed in accordance with bibliographical rules. In carrying out this research, I complied with the rules of standard scientific practice as formulated in the statutes of Johannes-Gutenberg-Universität Mainz to ensure standard scientific practice.

Mainz, 12.11.2020, Nijing Wang

Summary

Carbonyl compounds including aldehydes and ketones are a major chemical category of oxygenated volatile organic compounds (VOCs) in the atmosphere, which play an important role in atmospheric chemistry. They can be directly released from biogenic and anthropogenic emissions and also be produced via secondary photochemical oxidation. The formation and loss processes of carbonyls are related to tropospheric ozone formation and can influence the formation of secondary organic aerosols. Due to the various lifetimes of carbonyls, they can affect the outside air quality locally, regionally and globally. Moreover, carbonyls can be also present in indoor air. As people spend most of their time indoors and exposure to some carbonyls can cause adverse health effects, it is important to characterize indoor sources of these compounds. Indoor carbonyls can be emitted from furnishings/materials but also from humans themselves with the latter source gaining more and more prominence only in the recent decade. With the presence of indoor oxidants transported from outside or generated indoors, carbonyls can be also be generated as secondary products via oxidation. They can contribute significantly to the total loss of OH radicals, which can be used to reveal the total airborne load of reactive gases.

To better understand the role of carbonyls in air chemistry outdoors and indoors, this doctoral project conducted VOC and total OH reactivity measurements in the marine atmosphere over the Arabian Peninsula (outdoor scenario) and in a controlled human occupied climate chamber (indoor scenario). Proton-transfer-reaction mass spectrometry (PTR-MS), a soft chemical ionization technique, was the major tools used throughout the project.

For the measurements performed over the Arabian Peninsula, abundant carbonyls observed over the polluted regions were found to be related to strong photochemical oxidation, biomass burning events, and as direct emissions from oil/gas industries and marine transportation. Model-measurement comparisons indicated important missing sources of acetaldehyde in the current model. By including an oceanic source, the model simulation improved significantly for most of the areas, especially for remote areas. The total OH reactivity measured over the polluted regions was comparable to urban areas with severe air pollution. Oxygenated VOCs (mostly carbonyls) accounted for the largest fraction of the total reactivity over the region where strong photochemistry occurred. The OH reactivity can be fully attributed to measured trace gases in half of the areas including the most polluted regions. It can also help to identify different chemical regimes regarding regional ozone formation and loss.

Concerning the indoor human emissions characterization, a study was conducted in a climate chamber under controlled conditions. VOCs and total OH reactivity were measured for whole-body, breath and dermal emissions with the effect of ozone. Acetone was found to be the most emitted carbonyl compound as well as VOC for breath-only and whole-body emissions. In the

presence of ozone, the total emission rate (amount per person) of dermal emissions increased dramatically with the increase largely contributed by oxygenated VOCs, mainly carbonyls that were skin ozonolysis products. Similar species distribution was observed for whole-body emissions under ozone-free and ozone-present conditions. Emission rates obtained from the VOC measurements can be used in future indoor air models to better simulate the air chemistry of occupied environments. The total OH reactivity was applied for the first time indoors. The measured OH reactivity of four people in the ventilated chamber was comparable to the reactivity measured in cities. It agreed well with the calculated reactivity obtained from measured individual species, indicating major reactive compounds released by humans were well characterized. Ozone induced skin lipid chemistry increased the reactivity of human emissions substantially with the elevation caused mostly by carbonyl compounds.

Zusammenfassung

Carbonylverbindungen einschließlich Aldehyde und Ketone sind eine bedeutende chemische Gruppe der oxidierten, flüchtigen, organischen Verbindungen (VOC) in der Atmosphäre. Sie spielen eine wichtige Rolle in der Atmosphärenchemieund können sowohl direkt aus biogenen und anthropogenen Quellen freigesetzt werden als auch durch sekundäre photochemische Oxidation entstehen. Bildungs- und Verlustprozesse von Carbonylen hängen mit der troposphärischen Ozonbildung zusammen und können die Bildung von sekundären organischen Aerosolen beeinflussen. Aufgrund der unterschiedlichen Lebensdauer der Carbonyle können sie die Luftqualität sowohl regional als auch global beeinflussen. Außerdem können Carbonyle in Innenraumluft vorhanden sein, wo sich Menschen die meiste Zeit aufhalten. Die Exposition gegenüber einigen Carbonylen kann gesundheitsschädliche Auswirkungen haben. Carbonyle in Innenräumen können von Einrichtungsgegenständen/Materialien, aber auch vom Menschen emittiert werden, wobei letztere Quelle erst im letzten Jahrzehnt immer mehr Aufmerksamkeit gewann. Bei Vorhandensein von Oxidantien, die aus der Außenluft stammen oder innen erzeugt werden, können Carbonyle sekundär durch Oxidation gebildet werden. Sie tragen zum Gesamtverlust an OH-Radikalen bei, welcher wiederum dazu verwendet werden kann, die Gesamtheit reaktiver Spurengase in der Luft zu erklären. Um die Rolle der Carbonyle in der Luftchemie sowohl im Inneren, als auch im Freien besser zu verstehen, wurden in diesem Promotionsprojekt VOC- und OH-Gesamtreaktivitätsmessungen in der marinen Atmosphäre um die Arabische Halbinsel (Outdoor-Szenario) und in einer kontrollierten, mit Menschen besetzten Klimakammer (Indoor-Szenario) durchgeführt. Dabei wurde hauptsächlich die Protonentransfer-Reaktions-Massenspektrometrie (PTR-MS), eine weiche, chemische Ionisationstechnik, eingesetzt.

Bei den Messungen um die Arabische Halbinsel wurde festgestellt, dass die Carbonylverbindungen, die über den verschmutzten Regionen beobachtet wurden, mit starker photochemischer Oxidation, Biomasseverbrennungsereignissen sowie direkten Emissionen aus der Öl-/Gasindustrie und dem Seetransport zusammenhängen. Ein Vergleich von Modell und Messungen zeigte fehlende Acetaldehydquellen. Durch die Einbeziehung einer ozeanischen Quelle verbesserte sich die Modellsimulation für die meisten Gebiete erheblich, insbesondere für abgelegene Gebiete. Die über den verschmutzten Regionen gemessene OH-Gesamtreaktivität war vergleichbar mit städtischen Gebieten mit schwerer Luftverschmutzung. Sauerstoffhaltige VOCs (meist Carbonyle) machten den größten Anteil der Gesamtreaktivität in der Region aus, in der starke Photochemie auftrat. Die OH-Reaktivität kann durch gemessene Spurengase in der Hälfte der Gebiete, einschließlich der am stärksten verschmutzten Regionen, vollständig erklärt werden. Sie kann außerde, dazu beitragen, unterschiedliche chemische Systeme bezüglich regionaler Ozonbildung und -verluste zu identifizieren.

Was die Charakterisierung der menschlichen Emissionen in Innenräumen betrifft, so wurde die Studie in einer Klimakammer unter kontrollierten Bedingungen durchgeführt. VOCs und die OH-Gesamtreaktivität wurden für Ganzkörper-, Atem- und dermale Emissionen unter Ozoneinwirkung gemessen. Für reine Atem- und für Ganzkörperemissionen war Aceton die am stärksten emittierte Carbonylverbindung. Mit dem Vorhandensein von Ozon stieg die Gesamtemissionsrate (Menge pro Person) der dermalen Emissionen drastisch an, wobei der Anstieg hauptsächlich durch sauerstoffhaltige VOCs, größtenteils Carbonyle, verursacht wurde. Eine ähnliche Verteilung der Spezies wurde für Ganzkörperemissionen unter ozonfreien Bedingungen und solchen mit Ozon beobachtet. Die aus den VOC-Messungen gewonnenen Emissionsraten können in künftigen Modellen für Innenraumluft verwendet werden um die Luftchemie von bewohnten Umgebungen besser zu simulieren. Die Messung der OH-Gesamtreaktivität wurde zum ersten Mal in Innenräumen angewandt. Es stellte sich heraus, dass die OH-Reaktivität von vier Personen in der Kammer vergleichbar mit der in Städten gemessenen ist. Sie stimmte gut mit der berechneten Reaktivität überein, welche aus den gemessenen einzelnen Spezies erhalten wurde. Dies deutet darauf hin, dass die wichtigsten, vom Menschen freigesetzten, reaktiven Verbindungen gut charakterisiert waren. Die ozoninduzierte Chemie von Hautfetten erhöhte die Reaktivität der menschlichen Emissionen erheblich, wobei diese Erhöhung hauptsächlich durch Carbonylverbindungen verursacht wurde.

Contents

Chapter 1. Introduction

The role of carbonyl compounds in outdoor and indoor air chemistry

1.1 The role of carbonyl compounds in atmospheric chemistry

Carbonyl compounds including aldehydes (RCHO) and ketones (RC(O)R), are important species in global atmospheric chemistry. With primary sources and secondary formation pathways as well as simultaneous photochemical removal, carbonyl compounds are involved in various complex reaction pathways, some of which are related to air pollution (Carlier et al., 1986). Carbonyls can also influence atmospheric aerosol through uptake and release from particle surfaces (Kroll et al., 2005; Lary and Shallcross, 2000). Carbonyl compounds with lower molecular weight (C_1-C_3) are the most abundant carbonyls in the atmosphere (Lary and Shallcross, 2000). Therefore, formaldehyde (HCHO), acetaldehyde (CH3CHO) and acetone (CH3C(O)CH3) are the carbonyls that have been most often reported and discussed in the scientific literature.

1.1.1 Major sources

Atmospheric carbonyls have multiple primary sources that can be biogenic or anthropogenic in nature. They can be released from plants (especially those carbonyls with low molecular weight) and emission rates can vary profoundly with stress (Bourtsoukidis et al., 2014; Fall, 2003; Seco et al., 2007). Sea water is also known to be a natural source of carbonyls (Beale et al., 2013; Mopper and Stahovec, 1986; Sinha et al., 2007; Williams et al., 2004; Zhou and Mopper, 1997). Carbonyls have been also identified in biomass burning emissions (Holzinger et al., 1999; Koss et al., 2018). The anthropogenic emissions of carbonyls include industrial emissions (Kim et al., 2008; Pal et al., 2008; Vaught, 1991), vehicle exhausts (Dong et al., 2014; Erickson et al., 2014; Kean et al., 2001) and solvent use (Yuan et al., 2010).

Besides the primary emission sources, secondary photochemical oxidation of hydrocarbons is considered to be a substantial source for atmospheric carbonyls (Fortems-Cheiney et al., 2012; Jacob et al., 2002; Millet et al., 2010). In the atmosphere, the major oxidants are hydroxyl radicals (OH), ozone (O_3) and NO_3. Among the oxidants, OH is the dominant oxidant during the daytime and mostly responsible for the atmospheric oxidation capacity (Lelieveld et al., 2016). The major primary formation pathway for OH is through O_3 photolysis, that generates electronically excited oxygen atom ($O(^1D)$) that can react with water vapor (R1.1 and R1.2).

$$O_3 \xrightarrow{h\nu} O(^1D) + O_2 \quad \text{(R1.1)}$$

$$O(^1D) + H_2O \rightarrow 2OH \quad \text{(R1.2)}$$

Hydrocarbons in the atmosphere can react with OH and produce free radicals which undergo a sequence of further reactions involving nitric oxide (NO) and hydroperoxyl radcals (HO_2) to produce carbonyls. Reactions 1.3 – 1.7 demonstrate the reaction mechanism of carbonyls produced from alkane (RH) oxidation (Finlayson-Pitts and Pitts Jr, 1999).

$$RH + OH \rightarrow R\cdot + H_2O \quad \text{(R1.3)}$$

$$R\cdot + O_2 \xrightarrow{M} RO_2\cdot \quad \text{(R1.4)}$$

$$RO_2\cdot + NO \rightarrow RO\cdot + NO_2 \quad \text{(R1.5)}$$

$$RO_2\cdot + HO_2 \rightarrow \text{carbonyls} + H_2O + O_2 \quad \text{(R1.6)}$$

$$RO\cdot + O_2 \rightarrow \text{carbonyls} + HO_2 \quad \text{(R1.7)}$$

For alkenes, instead of the hydrogen abstraction observed for alkanes, OH addition to the double bond forming an adduct is more common, although the same carbonyl producing reactions follow (R1.4 – R1.7). The RO radicals formed (hydroxyalkoxy radicals for alkenes OH adduction cases) can produce carbonyls via decomposition (smaller alkenes) and isomerization (larger alkenes) (Finlayson-Pitts and Pitts Jr, 1999). During the hydrocarbon oxidation process, with sufficient NO present, HO_2 can convert NO to NO_2 (R1.8). NO_2 accumulated from R1.5 and R1.8 can produce an oxygen atom ($O(^3P)$) through photolysis, leading to ozone formation (R1.9 and R1.10). Alkenes can also react with O_3 to form carbonyl compounds via the ozonolysis reaction mechanism (detailed description in section 1.2.3). However, as the rate constants of ozone reacting with alkenes are several orders of magnitudes smaller than those of OH, the carbonyl formation contribution from O_3 oxidation is usually only important during the night or early morning (Altshuller, 1993).

$$HO_2 + NO \xrightarrow{h\nu} OH + NO_2 \quad \text{(R1.8)}$$

$$NO_2 \xrightarrow{h\nu} O(^3P) + NO \quad \text{(R1.9)}$$

$$O(^3P) + O_2 \rightarrow O_3 \quad \text{(R1.10)}$$

1.1.2 Major sinks

OH oxidation, photolysis and deposition are the major sinks for carbonyl compounds (Fortems-Cheiney et al., 2012; Jacob et al., 2002; Millet et al., 2010). Through OH oxidation and photolysis, free radicals are formed that can undergo similar reactions as for alkane OH oxidation (R1.4 – R1.7). These lead to formation of hydrogen oxide radicals (OH and HO_2) (Colomb et al., 2006) as well as peroxycaboxylic nitric anhydrides (e.g. peroxyacetayl nitrate (PAN)), an important tropospheric reservoir for NO_x (NO and NO_2) (Fischer et al., 2014; Singh and Hanst, 1981; Williams et al., 2000). The atmospheric lifetime of carbonyl compounds varies significantly. In the lower troposphere, as the OH oxidation is the major removal pathway, it is the OH rate constants with carbonyls that determine the lifetime. For carbonyls with the same carbon number, aldehydes tend to react faster with OH compared to ketones (Atkinson and Arey, 2003). By assuming the atmospheric OH concentration of 1×10^6 molecules cm^{-3}, the lifetime for acetaldehyde and acetone would be 18.5 h and 64 days, respectively according to their OH rate constants (acetaldehyde: k_{OH}=1.5×10^{-11} cm^{-3} $molecule^{-1}$ s^{-1}; acetone: k_{OH}=1.8×10^{-13} cm^{-3} $molecule^{-1}$ s^{-1}) (IUPAC, 2019). For the upper troposphere, removal via photolysis for some carbonyls becomes more important (Singh et al., 1995). Global models that consider all major sinks and transport estimated the global mean lifetime of acetaldehyde to be within one day (Millet et al., 2010) and of acetone to be around 11 days (Wang et al., 2020). Such a wide range of atmospheric lifetime allows carbonyls to be involved in local air chemistry but also in regional and even hemispheric air chemistry via air mass transportation.

Ambient measurements of carbonyl compounds have been performed worldwide in various different ecosystems (marine, forests, rural/suburban region and urban area, Table 1.1) with mixing ratios ranging from several tens of ppt to several ppb. Formaldehyde, acetaldehyde and acetone are usually the most abundant carbonyls observed. Figure 1.1 shows the acetaldehyde and acetone mixing ratios measured in various ambient air environments selected from Table 1.1. In general, acetone always had higher mixing ratios than acetaldehyde, which is consistent with acetone having a longer atmospheric lifetime than acetaldehyde. Remote marine atmosphere had much lower (but still detectable) levels of carbonyls compared to the levels observed in other environments. This is mainly due to the absence of strong direct emission sources and precursor species. However, although the observation levels were relatively low, model predictions still have a large bias compared to measured carbonyl values, indicating missing formation or uptake mechanism (Read

et al., 2012; Wang et al., 2020; Wang et al., 2019). For large forest ecosystems, although somewhat distant from anthropogenic emissions, the carbonyls mixing ratios were comparable to the mixing ratios measured in rural/suburban areas. It is mainly due to direct carbonyl emissions from the plants as mentioned in section 1.1.1 but also mainly because of abundant emissions of biogenic VOCs (e.g. isoprene and terpenes) which are precursors for carbonyl compounds (Müller et al., 2006; Yáñez-Serrano et al., 2015). Rural and suburban areas generally have lower mixing ratios of carbonyls in comparison to those in urban area (see Table 1.1). However, levels remain highly dependent on the influence from particular nearby sources (vegetation and anthropogenic emissions) and the transport pathways of the air mass arriving at the measuring point (Derstroff et al., 2017; Jordan et al., 2009b; Yang et al., 2017a; Yang et al., 2019). In densely populated urban areas, the level of carbonyls can vary greatly from place to place and from season to season. The major contribution to carbonyl formation was local primary sources (e.g. vehicular emissions), regional or long-distance transportation and secondary photochemical production which generally had larger contribution during summer time because of stronger solar radiation (Guo et al., 2013; Legreid et al., 2007; Sahu and Saxena, 2015; Sheng et al., 2018).

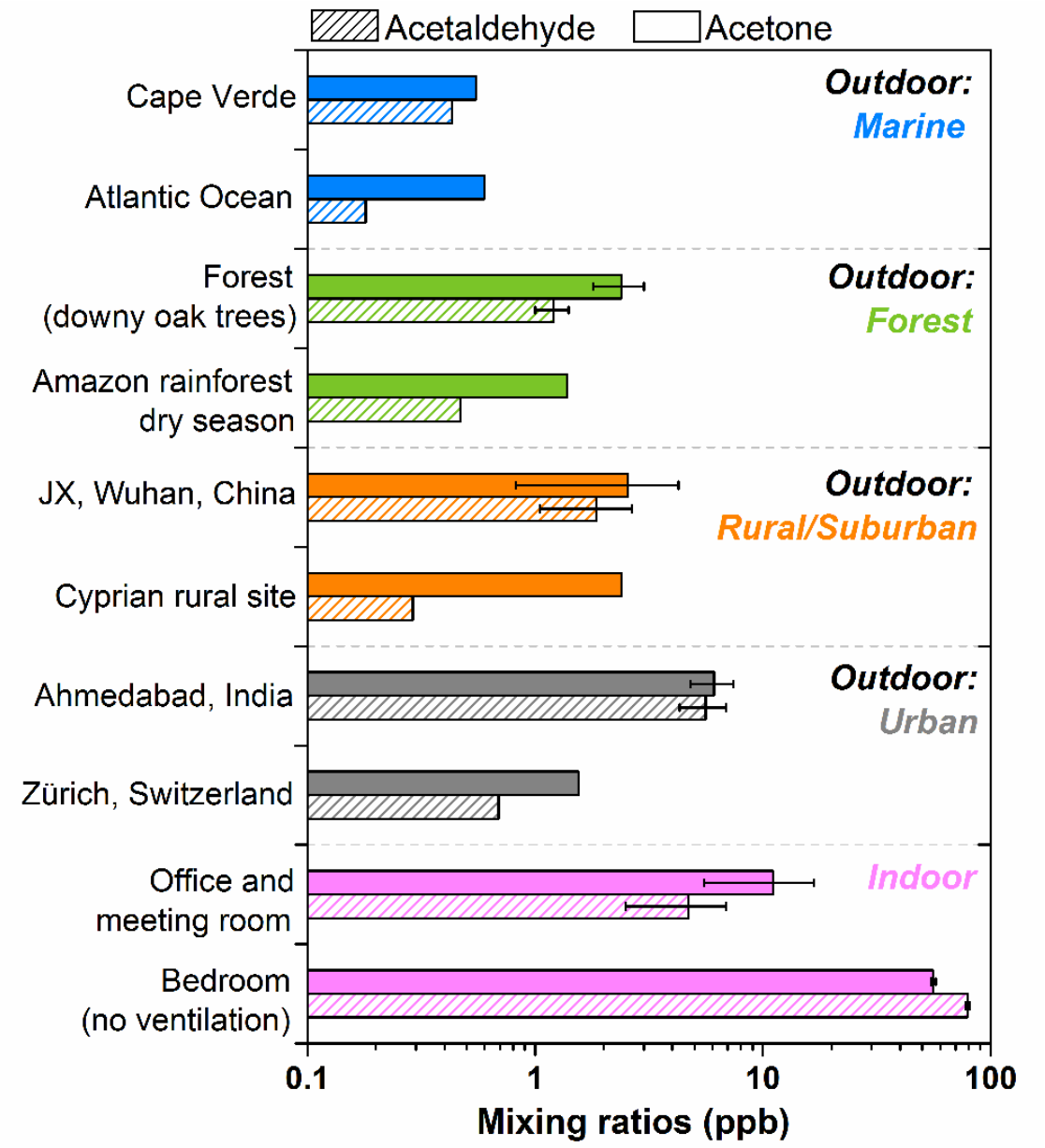

Figure 1.1 Mixing ratios of acetaldehyde and acetone in different outdoor and indoor environments (data were chosen from Table 1.1 and Table 1.2).

Table 1.1 Carbonyls measured in outdoor environments from literatures

Location	Time	Technique	Carbonyl species (ppb) (range)			Reference
			Acetaldehyde	Acetone	Other carbonyls	
Remote: marine*						
Cape Verde Atmospheric Observatory (site)	2006-2011	GC-FID	0.43 (0.19 - 0.67)	0.55 (0.23 - 0.91)	n.r	Read et al. (2012)
Appledore Island, USA (site)	Jul.-Aug. 2004	PTR-MS	0.4 ± 0.2	1.5 ± 0.7	MEK: 0.2 ± 0.2 MVK/MACR: 0.2 ± 0.3	White et al. (2008)
Atlantic Ocean (ship) (Northern Hemisphere)	Oct.-Nov.2012	PTR-MS	0.18	0.6	n.r	Yang et al. (2014)
Atlantic Ocean (ship) (Southern Hemisphere)	Oct.-Nov.2012	PTR-MS	0.08	0.2	n.r	
Remote: forest**						
Forest of downy oak trees (2 m height, inside the canopy), France	May-Jun. 2014	PTR-MS	1.2 ± 0.2	2.4 ± 0.6	MVK/MACR: 0.4 ± 0.1	Zannoni et al. (2016)
Amazon rainforest (4 m height, inside the canopy)	Sep. 2013 dry season	PTR-MS	0.47	1.38	MEK: 0.22	Yáñez-Serrano et al. (2015)
Amazon rainforest (4 m height, inside the canopy)	Feb.-Mar. 2013 wet season	PTR-MS	< 0.28	0.23	MEK: < 0.09	
Coniferous forest (12 m, in the tree top), Germany	Summer 2001 and 2002	PTR-MS HPLC	1.0	3.0	Formaldehyde: 1.6 MEK: 0.4	Müller et al. (2006)
Rural/Suburban						
Mount Tai, China	Nov.-Dec.2017	HPLC	1.27 ± 0.78	3.57 ± 0.55	Formaldehyde: 3.48 ± 0.98 MEK: 0.12 ± 0.08 Benzaldehyde: 0.16 ± 0.08	Yang et al. (2017a)
JX, Wuhan, China	2017	HPLC	1.85 ± 0.80	2.54 ± 1.72	Formaldehyde: 3.37 ± 1.99 Propanal: 0.63 ± 0.97 Benzaldehyde: 0.06 ± 0.03 Hexanal: 0.07 ± 0.03	Yang et al. (2019)
Cyprian rural site, Cyprus+	Jul.-Aug.	PTR-MS	0.29	2.4	MEK: 0.1	Derstroff et al. (2017)
Thompson Farm, USA	2004-2007	PTR-MS	0.37 (0.16-0.96)	1.02 (0.42-2.87)	MEK: 0.13 (0.05-0.37) MVK/MACR: 0.07 (0.03-0.78)	Jordan et al. (2009b)

Urban						
Central Paris, France	Winter 2010	PTR-MS GC-FID	1.87 (0.92-4.49)	1.05 (0.58-2.97)	MEK: 0.29 (0.06-0.94) MVK: 0.09 (0.02-0.44) Hexanal: 0.09 Benzaldehyde: 0.07	Dolgorouky et al. (2012)
Zürich, Switzerland	2005-2006	GC-MS	0.69 (0.23-1.21)	1.55 (0.6-2.55)	Formaldehyde: 2.09 Propanal: 0.12 MEK: 0.21 MVK: 0.04 MACR: 0.02 Benzaldehdye: 0.01 Hexanal: 0.04	Legreid et al. (2007)
Beirut, Lebanon	Aug.-Sep. 2004	HPLC	2.1 ± 1.0	5.0 ± 3.0	Formaldehyde: 4.6 ± 1.4 Propanal: 1.5 ± 1.5	Moussa et al. (2006)
Beijing, China§	Dec. 2016 (Clear day)	PTR-MS	4.37 ± 3.39	2.22 ± 1.56	Formaldehyde: 18.32 ± 7.16 MEK: 0.49 ± 0.51 Benzaldehyde: 0.25 ± 0.25	Sheng et al. (2018)
ZY, Wuhan, China	2017	HPLC	2.35 ± 0.94	2.88 ± 1.66	Formaldehyde: 4.90 ± 2.36 Propanal: 0.66 ± 0.79 Benzaldehyde: 0.08 ± 0.04 Hexanal: 0.08 ± 0.02	Yang et al. (2019)
Ahmedabad, India	Winter 2013	PTR-MS	5.6 ± 1.3	6.1 ± 1.3	n.r	Sahu and Saxena (2015)
Tsuen Wan, Hong Kong	Sep.-Nov.2010	HPLC	2.16	4.17	Formaldehyde: 2.93	Guo et al. (2013)

* More literatures reported carbonyl levels under marine-influenced atmosphere are listed in Table 2.2 in Chapter 2.

** Mixing ratios for carbonyl compounds represent daytime average values.

+ Mixing ratios are averaged from the reported values in the literature.

§ Mixing ratios are converted from concentrations in the unit of μg m^{-3}.

n.r: not reported in the literature.

1.2 The role of carbonyl compounds in indoor air chemistry

1.2.1 Indoor air vs. outdoor air

People spend most of their time indoors (80% - 90% on average), meaning indoor air quality can affect human health via long-term exposure. Outdoor air pollution was initially thought as the major driver of indoor air quality through ventilation, penetration and air exchange systems (Weschler, 2009). However later, as the buildings becoming tighter and less ventilated to save energy and expanded use of newly developed building materials and household products began, researchers identified that some volatile organic compounds were more abundant indoors. Moreover, some species were found to link with human health (Salthammer et al., 2018; Sundell, 2017; Wolkoff and Nielsen, 2001). In the past 50 years, indoor air has obtained more and more attention, which can be ascertained from indoor air regulations and guidelines that are becoming progressively stricter.

Among the indoor volatile organic compounds, carbonyls have been measured in various indoor environments (Table 1.2) due to their abundance and potential adverse health effects (formaldehyde in particular) (USEPA; Weng et al., 2009; Zhang et al., 1994). The indoor levels of carbonyls were usually found to be much higher than the outdoor levels, with the indoor to outdoor ratios up to 100 (Table 1.2). As shown in Figure 1.1, the mixing ratios of carbonyls (acetaldehyde and acetone) in a bedroom in a house located in central Washington State were over 10 times higher than the mixing ratios measured in outdoor polluted urban area in India. In those studies, besides the contribution from outdoor air, emission from building materials, furniture and indoor facilities were usually identified as the sources for carbonyls. The contribution from occupants (humans) and especially the secondary formation of those carbonyls was rarely discussed in those studies. It is true that this may not be important in less occupied environments with other significant emission sources. However, as building materials and furniture become more environmental friendly (less emissions), emissions and chemistry involving people would be of greater importance, especially for those environments with high occupancy (cinemas, theatres, restaurants, clubs etc.).

The indoor air quality not only depends on the emissions from sources but also involves multiphase chemistry as well as physical removal such as ventilation or filtration (Weschler, 2009). Therefore, in last two decades, more and more atmospheric scientists have focused their research on indoor air chemistry. Even though the same chemical reaction mechanisms for outdoor atmospheric

chemistry can also happen indoors, the indoor air chemistry differs a lot from that outdoors due to less sunlight, much more stable meteorological conditions (no rain, less fluctuation of temperature, wind and relative humidity), much less dilution, much larger surface-to-volume ratios, different driving sources for the chemicals etc. (Abbatt and Wang, 2020; Gligorovski and Weschler, 2013; Wells et al., 2017; Weschler and Carslaw, 2018; Young et al., 2019). Major aspects of indoor air carbonyl formation and removal that differ from outdoor air chemistry are listed as follows:

- **Primary emission sources:**

  For indoor environments, carbonyls can be released from building materials, decorations (e.g. carpets), furniture and consumer products (Afshari, 2003; Cheng et al., 2015; Hodgson et al., 2002; Hodgson et al., 1993; Nazaroff and Weschler, 2004; Simon et al., 2020). Human behaviors such as cooking, cleaning and incense burning are sources of carbonyls as well (Farmer et al., 2019; Lee and Wang, 2004; Zhang et al., 1994). Humans also release carbonyls via breath and skin, a source contributing to indoor carbonyls that is typically underestimated and will be discussed in detail in the section 1.2.2.

- **Major oxidants:**

  Unlike outdoor environments, solar radiation is much weaker indoors. Therefore the major OH formation pathway (R1.1 and R1.2) through ozone photolysis as well as production through other precursor photolysis (e.g. formaldehyde and nitrous acid) are limited. Photolysis can still occur due to open or closed windows and indoor artificial lighting but the reaction rate is generally much slower compared to outdoor environments and it highly depends on locations, human activities and wavelength spectra of the lighting sources (Abbatt and Wang, 2020; Weschler and Carslaw, 2018; Young et al., 2019). Indoor OH concentrations have been measured and modelled in several studies and were found to be generally on the order of 10^5 molecules cm^{-3} (Carslaw, 2007; Carslaw et al., 2017; Waring and Wells, 2015; Weschler and Shields, 1996; White et al., 2010). High levels of OH radicals (on the order of $10^6 – 10^8$ molecules cm^{-3}) were observed under special scenarios where abundant nitrous acid were measured (Gómez Alvarez et al., 2013) or intensive cleaning activities were performed (Carslaw et al., 2017). Besides, above mentioned OH sources, ozonolysis reaction between ozone and unsaturated compounds is considered an important source (Carslaw et al., 2017; Sarwar et al., 2002; Weschler and Shields, 1996). Once OH radicals are formed, they can quickly react with VOCs indoors and yield

carbonyls as products similar to outdoor atmospheric chemistry (described in section 1.1.1). Here comes another important indoor oxidant– ozone. As shown in Figure 1.2, indoor ozone can be transported from outdoor air (through door and window frames even when closed) but it also can be produced from printers and air purifiers (Britigan et al., 2006; Tuomi et al., 2000). Ozone can not only initiate ozonolysis in gas phase but it also can react with various indoor surfaces and produce OVOCs, especially carbonyls (Coleman et al., 2008; Morrison and Nazaroff, 2000; Pandrangi and Morrison, 2008; Weschler, 2000; Weschler, 2006; Zhou et al., 2016b). In addition, secondary organic aerosol (SOA) can be formed (Abbatt and Wang, 2020; Weschler and Carslaw, 2018). Ozone can also react with NO_x (NO and NO_2), producing another indoor oxidant, the nitrate radial (NO_3), an important oxidant outdoor during the nighttime. However, NO_3 radicals may be only an important oxidant under high ozone and low NO indoor conditions as high NO would titrate O_3, which prevents formation of NO_3 radicals (Young et al., 2019).

- **Air exchange:**

  The air exchange between indoor and outdoor mainly includes opening windows/doors for ventilation, air-conditioning systems and building leakage, which makes it possible for outdoor carbonyl compounds to enter inside (Figure 1.2). The production and removal of carbonyls by indoor oxidants is therefore only important if the reaction time is much faster or competitive to the air exchange rate (changes h^{-1}) (Weschler and Carslaw, 2018). It was observed by Weschler and Shields (2000) that the concentrations of compounds released from indoor pollution oxidation increased as the air exchange rate decreased. Indeed, as buildings have become more energy-efficient, the air exchange rate tends to be reduced, weakening the removal of indoor carbonyls through air exchange.

Table 1.2 Carbonyls measured in indoor environments from literatures

Location	Technique	Carbonyl species (ppb)				Indoor/Outdoor ratios	Reference
		Formaldehyde	Acetaldehyde	Acetone	Other carbonyls		
Office at research center, Mexico*	HPLC	21.2 ± 3.7	10.6 ± 3.9	37.5 ± 32.0	Propanal: 1.7 ± 1.8	1.0 – 9.6	(Báez et al., 2003)
Indoor residential, USA	HPLC	33.3 ± 17.9	10.1 ± 5.4	31.4 ± 70	Propanal: 0.91 ± 0.39 MEK: 0.71 Benzaldehyde: 0.65 ± 0.42 Hexanal: 4.0 ± 2.4	2.4-144.8	(Jurvelin et al., 2003)
Indoor residential, USA*	HPLC	16.4	10.3	3.4	Propanal: 0.7 Benzaldehyde: 0.7 Hexanal: 0.9	1.3 – 3.0	(Liu et al., 2006)
Shopping centers, China*	HPLC	49.7	4.7	13.7	Propanal: 1.0	1.5 – 3.3	(Weng et al., 2009)
School library, Japan	HPLC	45.5	12.0	n.r.	Propanal: 1.6 Benzaldehyde: 1.8 Hexanal: 0.36	5.2 – 17.3	(Yamashita et al., 2011)
Office and meeting rooms, China*	HPLC	18.4 ± 9.0	4.7 ± 2.2	11.1 ± 5.6	Propanal: 0.6 ± 0.3 C4 carbonyls: 1.1 ± 0.6 Benzaldehyde: 0.2 ± 0.1 Hexanal: 0.9	1.4 – 3.6	(Jiang and Zhang, 2012)
Bedroom in a house (ventilation off), USA*	PTR-MS	45.9 ± 0.2	79.4 ± 1.7	56.0 ± 1.3	MEK: 3.9 ± 0.2	14.6 – 27.2	(Huangfu et al., 2020)
Bedroom in a house (ventilation on), USA*	PTR-MS	30.2 ± 0.2	36.5 ± 0.2	15.5 ± 0.2	MEK: 1.1 ± 0.02	3.6 – 13.3	

* Mixing ratios are converted from concentrations in the unit of μg m^{-3}

n.r: not reported in the literature.

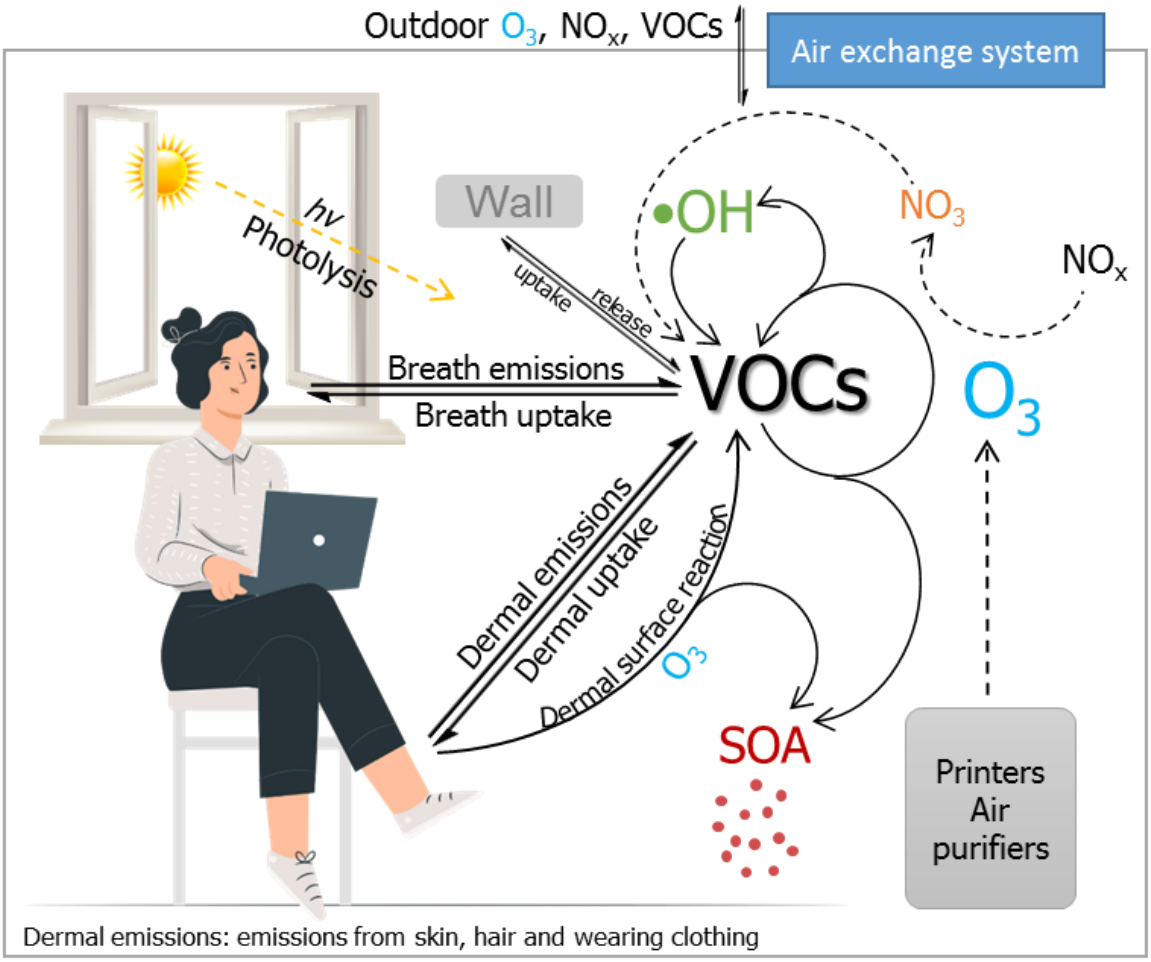

Figure 1.2 Humans as the major indoor VOCs sources and their interactions with major indoor oxidants.

1.2.2 Humans as a major source of indoor carbonyls

Humans continuously emit thousands of volatile compounds from their bodies (e.g. via breath and skin). 12 compounds are ubiquitously present in different human bioeffluents and 7 of these are carbonyls: acetaldehyde, acetone, benzaldehyde, 2-butanone (MEK), hexanal, heptanal and octanal (de Lacy Costello et al., 2014). Acetone is known to be one of the most abundant VOCs in exhalation ranging from 100 – 2000 ppb. It is an endogenous compound produced from acetoacetate decarboxylation and iso-propanol dehydrogenation in the human body (Turner et al., 2006). Other carbonyls are also present at much lower concentrations in the breath and they are mostly exogenous compounds that can vary enormously due to diet (food intake), smoking and previous exposure to compounds or pollutants under other environments (Bigazzi et al., 2016; de Lacy Costello et al., 2014; Filipiak et al., 2012). Besides acetone, isoprene is another major endogenous compound found in breath in the range of few ppb to several hundred ppb (Turner et al., 2005). Due to its two double bonds, isoprene can be quickly oxidized and can produce carbonyls indoors (e.g. methyl vinyl ketone and mathacrolein) (Tan et al., 2020).

Compared to breath, the compounds emitted from human skin are more diverse and complex. These vary from different body parts but also from person to person (de Lacy Costello et al., 2014). Mochalski et al. (2014) identified more than sixty VOCs with carbon number four to ten emitted from human skin (arm and hand), where carbonyls (mostly aldehydes) and hydrocarbons dominated the composition and acetone, 6-methyl-5-hepten-2-one (6MHO) as well as acetaldehyde had the highest emissions. Carbonyls emitted by skin can be products not only of internal metabolic processes but also from oxidative degradation of skin (Mochalski et al., 2014). People continuously produce skin oil and skin flakes which contain abundant unsaturated compounds that can react rapidly with oxidants (e.g. ozone), and can be transferred to any other surface with human contact (Weschler, 2016; Weschler and Carslaw, 2018). Several studies have shown that the ozone uptake along with formation of carbonyls due to human occupancy are significant, including soiled clothing experiments (Arata et al., 2019; Coleman et al., 2008; Rai et al., 2014; Salvador et al., 2019; Tamas et al., 2006; Wisthaler et al., 2005) and human subject experiments (Fischer et al., 2013; Tamas et al., 2006; Weschler et al., 2007; Wisthaler and Weschler, 2010). In particular, the ozone removal due to occupants in a classroom was found to be 2.6 times larger than the amount removed by the unoccupied classroom, indicating from the enormous importance of high occupancy can have on indoor air chemistry (Fischer et al., 2013). The detailed ozone-initiated

reaction mechanism as well as carbonyl formation due to human occupancy will be examined in section 1.2.3.

Several studies have reported the emission rates of carbonyls ($\mu g\ h^{-1}\ p^{-1}$) under several indoor environments (see Table 1.3). Although the emission rates for the same compound varied from place to place, acetone usually had the highest emission rates among carbonyls. It's worth noting that the amount of carbonyls (acetone and acetaldehyde) emitted per person per hour are generally much higher than the amount emitted per square meter per hour from unoccupied environments, as shown in Table 1.3. Therefore, for certain carbonyl compounds, the dominant contributor would be human emissions, especially if the indoor environment is small and fully occupied.

Overall, as illustrated in Figure 1.2, through human body emissions, VOCs can be directly released in indoor air and can also be produced via surface reactions on human skin, hair, clothing etc. Those VOCs can undergo further reactions with indoor oxidants (ozone, OH and NO_3 radicals) resulting in secondary production of VOCs (mostly oxygenated VOCs), and OH radicals can be reformed in the same reactions. Meanwhile, humans can also act as a sink of VOCs through breath and dermal uptake (He et al., 2019; Weschler and Nazaroff, 2014). In addition, human behaviors (e.g. using personal care products, eating, doing sports, cooking cleaning etc.) could make the emissions much more profound, affecting the indoor chemistry, and consequently influencing the indoor air quality as well as the exposure levels (Weschler, 2016).

Table 1.3 Indoor emission rates of carbonyls from literatures

Location	Technique	Carbonyl species			Reference
		Formaldehyde	Acetaldehyde	Acetone	
Human emission rate ($\mu g\ h^{-1} p^{-1}$)					
Lecture room, China*	HPLC	No emission	14	244	(Jiang and Zhang, 2012)
Classroom, USA	PTR-MS	n.r.	114	1060	(Tang et al., 2016)
Cinema, Germany	PTR-MS	207	221	419	(Stonner et al., 2017)
Museum gallery, USA	PTR-MS	n.r.	354	873	(Pagonis et al., 2019)
Unoccupied room emission rate ($\mu g\ h^{-1} m^{-2}$)					
Lecture room, China	HPLC	111	37	97	(Jiang and Zhang, 2012)
Bedroom in a house USA	PTR-MS	81	26	31	(Huangfu et al., 2020)

*Samples were collected after the lecture not during the lecture.
n.r.: nor reported in the literature.

1.2.3 Skin lipid ozonolysis as a carbonyl formation pathway

As mentioned in the previous section, ozone plays a critical role as an oxidant in indoor air chemistry. Figure 1.3 shows the main reaction mechanism of ozone reacting with hydrocarbons containing a double bond (alkene ozonolysis). These reactions can also be an important formation pathway for outdoor carbonyls during the night when ozone and unsaturated compounds are abundant (Altshuller, 1993). As shown in Figure 1.3, with ozone addiction to the double bond, the primary ozonide (POZ) is formed. Due to the inherent instability of the POZ, it quickly decomposes (via pathway a and b) to a carbonyl and a Criegee bioradical intermediate (Criegee, 1975). The Criegee intermediates can recombine with a carbonyl to form a larger secondary ozonide (not shown in the figure) or they can react with water to form hydroxyhydroperoxides which then decompose to carbonyls and hydrogen peroxide (Finlayson-Pitts and Pitts Jr, 1999). Criegee intermediates can also undergo isomerization, dissociation and rearrangement to form carbonyls, organic acids, esters and OH radicals. (Finlayson-Pitts and Pitts Jr, 1999). It was also found that Criegee intermediates can react with carboxylic acids to form hydroperoxide esters (Zhou et al., 2019). Recent studies have observed that environments with higher relative humidity drive the reactions more towards forming carbonyl products even though the rate of ozone loss reacting with unsaturated compounds had no apparent humidity dependence (Arata et al., 2019; Heine et al., 2017; Thornberry and Abbatt, 2004; Zhou et al., 2016a).

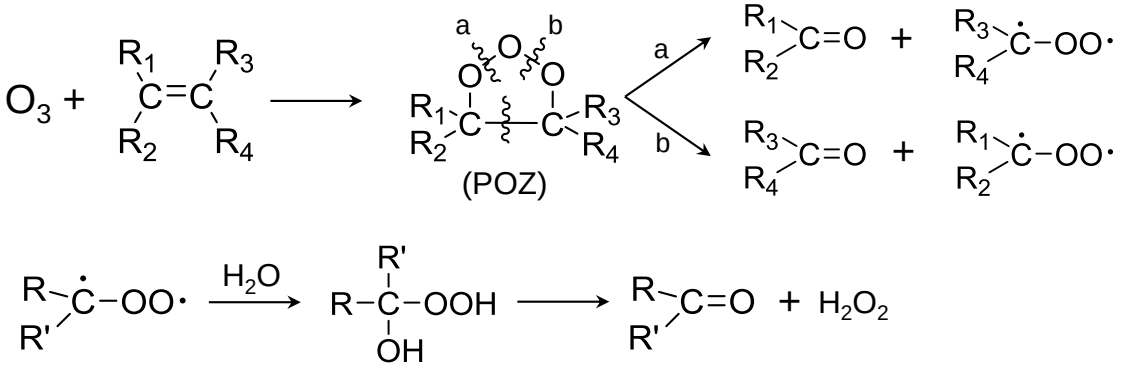

Figure 1.3 Simplified and generalized reaction mechanism of alkene ozonolysis.

Skin lipids consist of multiple chemical compounds, among which squalene, a C30 compound containing six carbon-carbon double bonds, accounts for ~ 50% of the unsaturated carbon bonds on a molar basis, followed by unsaturated fatty acids (e.g. cis-hexadec-5-enoic acid and cis-octadec-8-enoic acid) (Nicolaides, 1974; Pandrangi and Morrison, 2008). Therefore, with human

presence in any indoor environment with ozone, ozonolysis can immediately occur and generate various other compounds following the reaction mechanism mentioned above. Various laboratory experiments have been done to identify the oxidation products of ozone reacting with squalene and some unsaturated fatty acids (Fruekilde et al., 1998; Petrick and Dubowski, 2009; Thornberry and Abbatt, 2004; Wisthaler and Weschler, 2010; Zhou et al., 2016a; Zhou et al., 2014). Table 1.4 lists major gas-phase oxidation products of squalene ozonolysis. Acetone, geranyl acetone, 6-methyl-5-hepten-2-one (6MHO), hydroxyacetone and 1-hydroxy-6-methyl-5-hepten-2-one (OH-6MHO) are primary oxidation products from squalene ozonolysis but also secondary oxidation products from other precursors (larger primary oxidation products). Recently, results from a computational fluid dynamics (CFD) model have indicated that primary products showed higher mixing ratios (1.6-2 times) in the breathing zone than in the bulk room air (Lakey et al., 2019), which may increase the exposure to those carbonyls (e.g. 4OPA can cause irritancy and allergic responses) (Anderson et al., 2012). Besides the surface reactions, those produced gas-phase unsaturated carbonyls can undergo further ozone oxidation: 1) 6MHO can be formed from geranyl acetone ozonolysis; 2) 4OPA can be formed from geranyl acetone and 6MHO ozonolysis; 3) acetone and hydroxylacetone can be formed from nearly all of those unsaturated carbonyl ozonolysis reactions. In terms of ozone oxidation of unsaturated fatty acids, linear aldehydes are the dominant compounds formed (e.g. decanal, nonanal and hexanal).

Under real indoor conditions with human subjects or with skin oil soiled clothing measurements, along with the ozone drop, those aforementioned oxidation products show a substantial increase. A series of studies performed in a simulated aircraft cabin indicated that without ozone present, by simply putting worn T-shirts into the cabin, the total VOC mixing ratio was comparable to that of the empty cabin. However, with ozone present the mixing ratio doubled for the empty cabin and tripled for the cabin with T-shirts (Wisthaler et al., 2005). In addition, with ozone present, human occupancy significantly elevated the squalene oxidation products with the acetone increase even comparable to the breath acetone emissions (Weschler et al., 2007). Later on, Wisthaler and Weschler (2010) performed experiments in a simulated office and found that 6MHO was slightly elevated (0.2 ppb) when people entered the office where no ozone was present but was dramatically elevated to 1.8 ppb after ozone was injected. After people left the office, 6MHO decreased immediately while 4OPA still increased for a while, indicating it is a secondary product of squalene

oxidation. In a fully occupied classroom, both 6MHO and 4OPA were measured in the air and had higher concentrations than the levels measured after students left (Fischer et al., 2013).

Overall, ozone-initiated skin oil oxidation diversifies the indoor carbonyl species and can elevate the carbonyl concentrations. It is an essential formation pathway of unsaturated carbonyls but also a sink for those compounds. Interestingly, the same reactions also occur under ambient outdoor environments. Acetone, 6MHO and 4OPA were formed from ozone oxidation on the surface of plant leaves containing epicuticular wax (Fruekilde et al., 1998); Hexanal and other carbonyls were identified from ozone reacting with the sea surface microlayer containing unsaturated fatty acids (Zhou et al., 2014).

Table 1.4 Major gas-phase products of squalene ozonolysis (the table is modified from Table 1 in Wisthaler and Weschler (2010) and Table 1 in Lakey et al. (2017))

Squalene $C_{30}H_{50}$		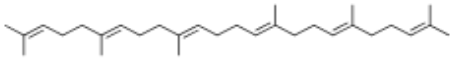			
Name	Formula	Structure	Primary /secondary	Vapor pressure at 298K (Pa)	Further ozonolysis
Acetone	C_3H_6O		P and S	3.09×10^4	×
Geranyl acetone	$C_{13}H_{22}O$	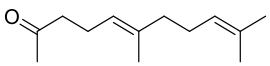	P and S	3.35	✓
6-methyl-5-hepten-2-one (6MHO)	$C_8H_{14}O$	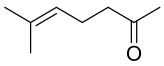	P and S	238	✓
Hydroxyacetone	$C_3H_6O_2$	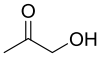	P and S	555*	×
1-Hydroxy-6-methyl-5-hepten-2-one (OH-6MHO)	$C_8H_{14}O_2$	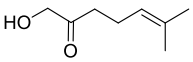	P and S	n.a.	✓
4-methyl-8-oxo-4-nonenal (4MON)	$C_{10}H_{16}O_2$	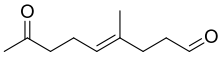	S	3.19	✓
4-methyl-4-octene-1,8-dial (4MOD)	$C_9H_{14}O_2$	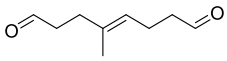	S	4.72	✓
1,4-butanedial	$C_4H_6O_2$	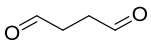	S	697	×
4-oxopentanal (4OPA)	$C_5H_8O_2$	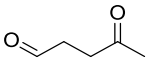	S	454	×
5-hydroxy-4-oxopentanal	$C_5H_8O_3$	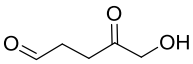	S	n.a	×
4-oxopentanoic acid	$C_5H_8O_3$	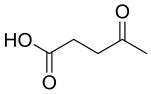	S	n.a	×
4-oxobutanoic acid	$C_4H_6O_3$	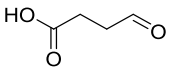	S	n.a	×

*vapor pressure is derived from Petitjean et al. (2010).

1.3 OH reactivity

As mentioned in section 1.1, OH radicals serve as an atmospheric cleaning agent or "detergent", which can react with nearly all VOCs in the air. The OH reactivity refers to the loss frequency of OH radicals, given in the unit of s^{-1}. Thus, the total OH reactivity refers to the summed reaction frequency of all components that can react with OH radicals in the air, which is the inverse of the OH lifetime (τ_{OH}):

$$R_{total} = \frac{1}{\tau_{OH}} = \sum k_{X_i+OH}[X_i] \quad \text{(Eq. 1.1)}$$

where $[X_i]$ refers to the concentration of VOC species i and k_{X_i+OH} is the rate constant (cm^3 $molecule^{-1}$ s^{-1}) of species i reacting with OH radicals.

The OH reactivity depends on the VOCs present in the measured air rather than the oxidant (OH radicals). From Eq. 1.1, the OH reactivity from certain species can be calculated if their concentrations and the OH rate constants are known. By summing up the calculated OH reactivity from measured individual species, the total OH reactivity (R_{total}) can be calculated. However, as there are thousands of VOCs present in the air, it is impossible to achieve complete characterization of VOCs. Therefore, direct measurement of the total OH reactivity is a measure that accounts for the whole reaction potential of OH radicals reacting with VOCs and any other inorganic species such as NO and NO_2. By comparing the measured OH reactivity and the estimated OH reactivity (calculated using Eq. 1.1), the completeness of VOCs measurements can be assessed. If the estimated reactivity is significantly lower than the measured reactivity, it indicates that there are important unmeasured VOC species present, resulting in the missing or unattributed OH reactivity. If the measured and estimated reactivity are comparable (no missing reactivity), a budget analysis of the fractional contribution of each VOC to OH reactivity can help to understand the major sinks of OH radicals in the atmosphere. In addition, the OH reactivity measurement gives a new perspective to determine the ozone production sensitivity using the OH reactivity of NO_x and VOCs (Kirchner et al., 2001) compared to the traditional O_3 sensitivity driven by VOCs/NO_x ratios (Seinfeld and Pandis, 2016) in which comprehensive VOC measurements are usually difficult to achieve.

The OH reactivity measurements and their comparison to the calculated OH reactivity have been performed under various atmospheric environments globally. High loadings of OH reactivity (10

to >100 s^{-1}) are usually observed in densely populated urban areas where the air pollution (including NOx) is relatively severe and in forest areas where the emissions of reactive biogenic VOCs are strong. The OH reactivity in suburban areas is highly dependent on the air mass origin (Yang et al., 2016). In contrast, the OH reactivity in the marine boundary layer has been measured at a much lower level, less than 2 s^{-1} (Thames et al., 2020). The VOC fractions contributing to the reactivity also vary from place to place. In urban areas where anthropogenic emissions drive air pollution, NO_x, CO and anthropogenic hydrocarbons usually contribute the most to the total reactivity (Kim et al., 2016; Praplan et al., 2017; Yang et al., 2017b; Yang et al., 2016). In forests, the major OH reactivity contribution is from biogenic hydrocarbons (isoprene and terpenes) (Nölscher et al., 2016; Praplan et al., 2019; Zannoni et al., 2016). For suburban areas, besides the aforementioned species, the reactivity fractions from carbonyls increase, comparable to NO_x and CO (Yang et al., 2016). Besides the limited local VOCs emission sources, the air masses reaching suburban areas are usually influenced by anthropogenic and/or biogenic emissions containing abundant hydrocarbons that are precursors of carbonyls. Therefore, more chemically aged air containing the relatively long-lived oxygenated VOCs is expected in suburban regions.

For the previously mentioned studies, where OH reactivity has been measured, missing OH reactivity was commonly identified with generally more significant missing fractions found in forests, indicating the existence of unmeasured reactive species. In recent years, due to the availability of high-resolution mass spectrometers (e.g. proton transfer reaction mass spectrometer equipped with time-of-flight as the mass analyzer, PTR-ToF-MS, details of the technique is given in section 1.4), many more VOC species (especially OVOCs) can be measured. OVOCs were hypothesized to be partially responsible for the missing reactivity in several studies in which including additional modelled OVOCs lowered the unattributed reactivity (Lou et al., 2010; Whalley et al., 2016). A recent study done by Millet et al. (2018) confirmed that by including more ions measured by PTR-ToF-MS (over 100), the measured reactivity flux in the forest (Michigan, USA) can be mostly attributed by the calculated reactivity flux (> 99%). While at the same site Di Carlo et al. (2004) reported significant missing reactivity (30%) many years ago in which only 8 OVOCs were measured.

As the OH radicals are of great importance in tropospheric chemistry, the OH reactivity has been often studied in outdoor air. Only in recent years, researchers have started to realize that the indoor OH radicals can also be a meaningful oxidant, impacting the indoor chemistry as introduced in

section 1.2.1. Thus, it is also important to characterize the overall loss rate of indoor OH radicals (total OH reactivity). However, up to now, studies focusing on this topic are limited. Price et al. (2019) estimated the total OH reactivity of a museum gallery room based on VOCs measured by high-resolution mass spectrometers and compared the level with the calculated total OH reactivity of other indoor (classroom and residence) and outdoor (megacity, urban, rural and remote areas) environments. The indoor total OH reactivity (10 - 50 s^{-1}) are generally comparable to polluted urban areas and are higher than those rural and remote areas. The average OH reactivity in the gallery room was 19 s^{-1} with low occupancy and it increased by 73% with high occupancy during an opening event, which indicates the great impact brought about by humans to the indoor OH loss frequency. However, prior to the work contained in this thesis the direct measurement of indoor OH reactivity was still lacking let alone indoor environments dominated by human emissions. Furthermore, the question of whether there is missing reactivity in indoor environments remained unknown.

1.4 Proton transfer reaction mass spectrometer (PTR-MS)

Proton-transfer-reaction mass spectrometry (PTR-MS) is a chemical ionization technique, which was developed in late 20th century by Lindinger and co-workers in Austria (Lindinger et al., 1998). Due to its fast response time, high sensitivity and no need for pre-concentration, PTR-MS has been widely applied in various research areas for real-time VOC measurements in last two decades (Ellis and Mayhew, 2013; Yuan et al., 2017), such as environmental science (outdoor and indoor), food science, medical science and homeland security. As PTR-MS is the key monitoring technique used among the work presented in the thesis, detailed working principles, instrument set-up as well as its implementation in the total OH reactivity measurement method are described in this section.

1.4.1 PTR-QMS and PTR-ToF-MS

The key working principle of PTR-MS is that a trace gas (R) that has proton affinity (PA) higher than water (691 kJ mol^{-1} (NIST, 2018)) can be protonated via proton transfer reaction with hydronium ions (H_3O^+); and the product ions (RH^+) are then measured by mass spectrometers. The major atmosphere components (N_2, O_2, Ar and CO_2) have lower PAs than water, while trace-level VOCs especially oxygenated VOCs usually have higher PAs than water (NIST, 2018), which makes PTR-MS an ideal technique for ambient measurements.

As shown in Figure 1.4, by introducing water vapor into the ion source, the primary ions (H_3O^+) are generated by a hollow cathode discharge in the ion source (not shown in the figure). The primary ions are then transported to the drift tube where the proton transfer reactions of trace gases occur. Inside the drift tube, a homogeneous electric field is established, which limits the cluster-ion formation and helps the ion transport over the drift tube (de Gouw and Warneke, 2007). The ions are then measured by mass spectrometers.

The quadrupole mass spectrometer (QMS) was originally utilized as the detector for PTR-MS. As shown in the left diagram of Figure 1.4, ions are extracted from the drift tube through a nose cone to the QMS which consists of a mass filter and an electron multiplier (de Gouw and Warneke, 2007). The selected-ion mode is usually used to monitor masses of interest instead of scan mode due to the limited time resolution. As PTR-QMS can only measure nominal masses, it is not able to identify isobaric compounds. Therefore, PTR-QMS is suitable for measurements where the compounds of interest are known and have no interference from isobaric compounds. Later, PTR-MS using a time-of-flight mass spectrometer (PTR-ToF-MS) was developed with high sensitivity and mass resolution (Graus et al., 2010; Jordan et al., 2009a). As shown in Figure 1.4 (right), ions from the drift tube are transferred to the detector lens system. Before being extracted to the reflectron time-of-flight area, ions are accelerated along the direction perpendicular to the continuous ion beams (so-called orthogonal acceleration). As there is no electrical field within the flight region, the velocity remained constant for ions entering the time-of-flight region. Since the kinetic energy of ions after acceleration is the same, the time for ions to reach the detector depends on the mass-to-charge ratio (m/z). Therefore, heavier ions need longer time to reach the detector than those lighter ions. Compared to PTR-QMS, PTR-ToF-MS significantly improved the time resolution (down to 10 Hz) and the mass identification range by giving a whole spectrum (m/z up to 500). In addition, due to much higher mass resolution ($m/\Delta m$ in the range of 4000-5000), PTR-ToF-MS is able to separate some nominally isobaric compounds, which allows assignment of chemical formulas to the measured exact masses. This significantly enlarges the number of compounds that can be quantified and reduces the interference issues existing for the PTR-QMS.

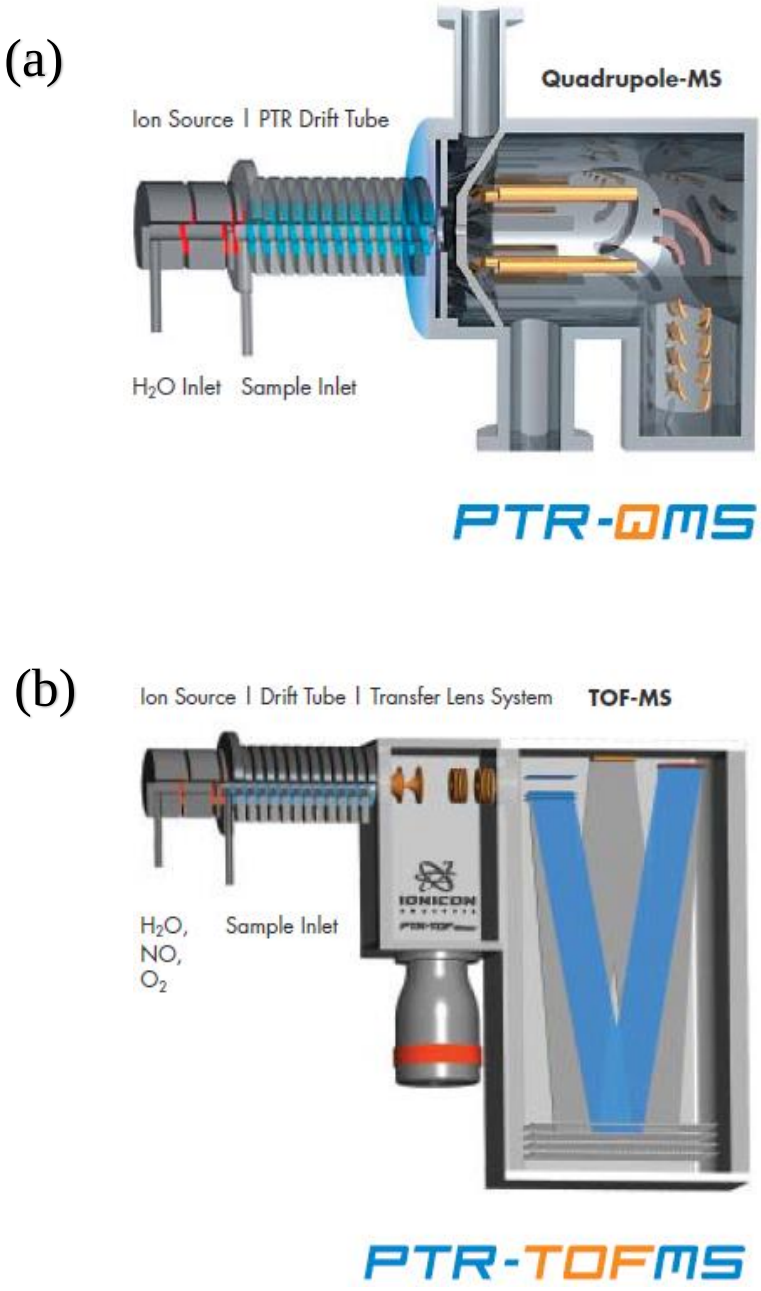

Figure 1.4 Diagram of working process for PTR-QMS (a) and PTR-ToF-MS (b). Picture source: https://www.ionicon.com

In theory, no standard calibrations are needed for compound quantification by using PTR-MS. Based on the proton transfer reactions, the concentration of protonated trace gas (RH^+) is linear to the concentration of the trace gas (R) as shown by following equation:

$$[RH^+] = [H_3O^+]k[R]\Delta t \quad \text{(Eq.1.2)}$$

In the equation, $[H_3O^+]$ is the concentration of hydronium ions. k is the proton-transfer reaction rate constant of trace gas R, *and* Δt is the reaction time in the drift region. What is eventually detected by the detector is the signal intensity I (count rate), which is proportional to the compound concentration in the drift tube and related to its transmission efficiency T. The transmission efficiency varies with *m/z* and a relative transmission curve (T_{RH^+}/T_{H3O^+} vs. m/z) can be derived for each instrument by measuring the gained signal of RH^+ and lost signal of H_3O^+ with varying trace gases which should have negligible fragments in PTR. Therefore, for compounds known to have no fragmentation, the mixing ratio of that trace gas can be determined by knowing the relative transmission ratio, the rate constant and the reaction time. However, fragmentations do occur for some compounds especially for those with large molecular weight, for example, dehydration of alcohols, aldehydes and carboxylic acids, loss of alkyl group for hydrocarbons and so on (Yuan et al., 2017). Large uncertainty will occur if above mentioned calculation method is used for those compounds. In addition, the uncertainty from the rate constant determination (both theoretic calculation and experimental values) remains relatively large, which is around 25% and can be as large as 50% (Ellis and Mayhew, 2013). Therefore, if one needs to accurately quantify the concentrations, calibrations with standard gases are necessary. Moreover, measuring the air sample with changing humidity would impact the sensitivity of some compounds, which complicates the ion chemistry in the drift tube (Warneke et al., 2001). Calibrations under varying humidity should also be performed for more accurate quantitative analysis.

PTR-MS has been widely used in various outdoor environments to monitor the VOCs (especially OVOCs) compared to indoor environments (Farmer, 2019). Selected studies characterized outdoor and indoor carbonyl compounds using PTR-MS can be found in Table 1.1, Table 1.2 and Table 1.3.

1.4.2 Total OH reactivity measurement: comparative reactivity method (CRM)

The direct measurement of total OH reactivity started around 2000, and was based on laser induced fluorescence (LIF) detection of OH decay (Calpini et al., 1999; Kovacs and Brune, 2001). Later on in 2008, a new method termed comparative reactivity method (CRM) was developed, based on comparing the OH reactivity of a known reference reagent (a VOC) with the OH reactivity of ambient air (Sinha et al., 2008). Instead of directly measuring the OH, as for the LIF method, CRM tracks the variation of the reference species where PTR-QMS is used as the detector. Compared to LIF instruments, the CRM set-up is more affordable, transportable and does not require a large inlet flow. Since the CRM was developed, it has been improved and applied in various ambient measurements (Hansen et al., 2015; Kim et al., 2016; Michoud et al., 2015; Nölscher et al., 2016; Praplan et al., 2019; Williams et al., 2016; Zannoni et al., 2017). A recent inter-comparison study between LIF instruments and CRM setups done by Fuchs et al. (2017) showed that although the CRM has higher detection limit compared to LIF, the two setups have a generally good agreement with each other.

The major components of the CRM are a glass reactor and the detector (PTR-QMS) as shown in Figure 1.5. A gas chromatograph coupled with a photo ionization detector (GC-PID) can be used as the detector as well (Nölscher et al., 2012; Praplan et al., 2019). Pyrrole (C_4H_5N) is the most widely used reference reagent for the CRM as it is rarely present in the ambient air; it has a known relatively fast rate constant reacting with OH ($k_{Pyrrol+OH} = 1.26 \times 10^{-10}$ cm^3 molecule^{-1} s^{-1}, (Dillon et al., 2012)) and it can be measured by the detector with good sensitivity (Sinha et al., 2008). The OH radicals are generated inside the reactor via water photolysis using a pen-ray mercury UV lamp (λ=185 nm, located inside the arm where humidified pure nitrogen is introduced, see Figure 1.5). There are three running modes (C1, C2 and C3) implemented to determine the total OH reactivity in which pyrrole are measured by PTR-QMS at m/z 68 ($C_4H_5NH^+$).

The pyrrole level under C1 mode represents the total amount of the reference reagent that is introduced in the system without any reaction with OH radicals. It was originally achieved by introducing dry pure nitrogen through the arm where the UV lamp is located (switched on) together with pyrrole and zero air introduced from the other arm (Sinha et al., 2008). However, it is difficult and usually takes long time to reach pure dry condition inside the reactor. Therefore, the scavenger

method was developed by introducing a high concentration of a specific VOC (e.g. propane) mixed with zero air through the sample air arm shown in Figure 1.5. In this way, there is no need to achieve dry conditions in the reactor. Instead, the humidified nitrogen airflow can be kept the same as it is needed for C2 and C3 modes because the OH radicals produced are fully consumed by the scavenger (Zannoni et al., 2015). The UV lamp needs to be switched on in C1 mode so that the loss of pyrrole due to photolysis (up to 15%) is taken into account. In C2 mode, the flow setup is the same as C1 except for the scavenger in which only zero air is introduced. Due to reaction with OH radicals, the measured pyrrole level drops under the C2 mode of operation. The difference between C1 and C2 mode corresponds to the amount of OH radicals generated inside the reactor. In C3 mode, the zero air is replaced by the sampling air which causes pyrrole level elevation as VOCs in the sample air compete with pyrrole to react with OH radicals. By switching between C2 mode and C3 modes, the real-time total OH reactivity can be calculated using following equation:

$$R = \frac{[C3-C2]}{[C1-C3)]} \cdot C1 \cdot k_{Pyrrol+OH} \qquad \text{(Eq. 1.3)}$$

where C1, C2 and C3 refer to pyrrole concentrations (molecules cm^{-3}) measured in the corresponding mode, and $k_{pyrrol+OH}$ refers to the rate constant of pyrrole reacting with OH radical (Dillon et al., 2012). As the pyrrole level under C1 mode tends to be stable if the introduced pyrrole concentration is fixed throughout the measurements, the C1 determination mode can be performed before and after the measurement depending on the real measurement time schedule.

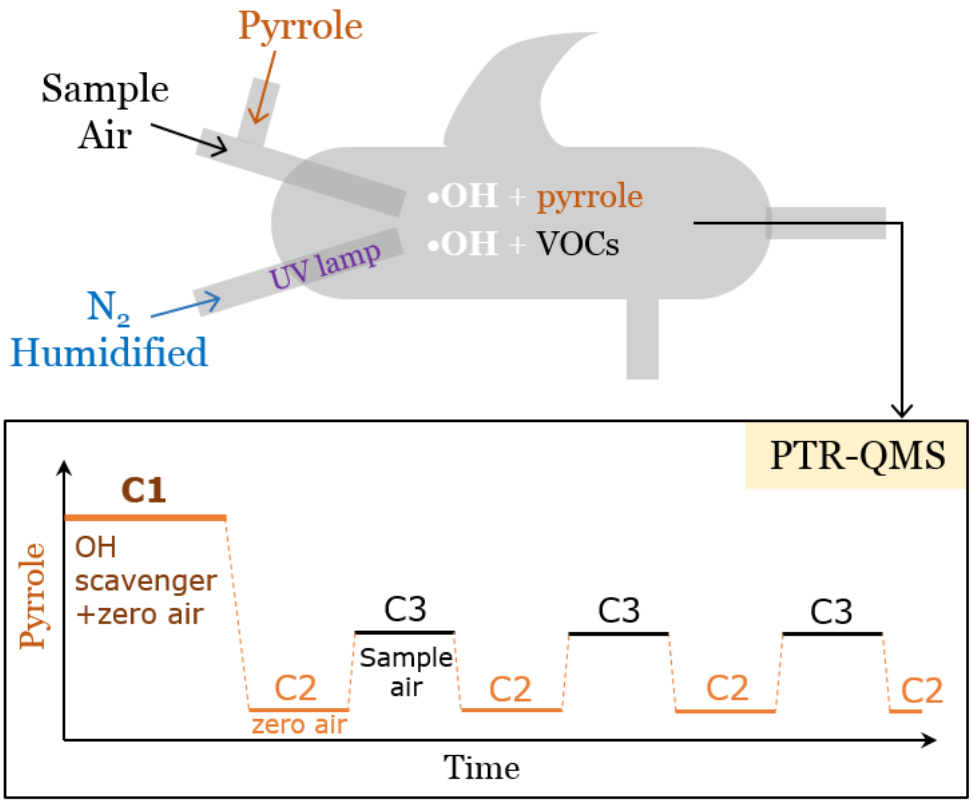

Figure 1.5 Key working principle of the comparative reactivity method (CRM)

Several interferences do exist for the CRM system and corrections need to be applied depending on the measured environments (Fuchs et al., 2017; Michoud et al., 2015; Sinha et al., 2008). In general, following corrections need to be considered:

- **PTR-MS humidity dependence of pyrrole:**
  As mentioned in 1.4.1, for some compounds the sensitivity is dependent on the relative humidity of sample air. Pyrrole is found to have such an effect (Sinha et al., 2009), thus calibrations under different humidities are needed to correct this effect.
- **Humidity difference between C2 mode and C3 mode:**
  The zero air running for C2 mode is usually generated by introducing the sample air into a catalytic converter so that the relative humidity can be kept comparable with the sampled air under C3 mode. However, the difference still exists (usually C3 mode has slightly higher humidity than C2 mode) and this leads to extra production of OH radicals inside the reactor. Therefore, tests involving introducing zero air with different humidities need to be done to correct the pyrrole level in C2 mode (Michoud et al., 2015).

- **Extra OH radicals produced under high NO_x and ozone environments:**
  As OH radicals are produced via water photolysis, hydrogen radicals are formed as well, and these further react with oxygen producing hydroperoxyl radicals (HO_2). NO and ozone can rapidly react with HO_2 radicals to generate extra OH radicals inside the reactor. Although NO_2 would not directly react with HO_2 radicals, it can be photolyzed to NO due to the UV lamp. Therefore, extra tests of adding NO_x and ozone at different levels into the reactor are needed to obtain the correction factor (Fuchs et al., 2017).
- **Correction for not being at pseudo-first-order conditions:**
  Eq. 1.3 is based on the assumption of pseudo-first-order conditions where [pyrrole] >> [OH]. However, it is difficult to fully achieve this condition together with a reasonable sensitivity (pyrrole level difference between C3 mode and C2 mode) (Sinha et al., 2008). A relationship between [pyrrole] to [OH] ratio obtained as C1/(C1-C2) and the deviation of different VOC species from pseudo-first-order condition (true reactivity as expected) can help to correct the interference (Michoud et al., 2015). The deviation can be obtained by introducing varying known amount of VOC species in to the reactor and compare the measured reactivity to the expected reactivity.

As the CRM setup condition can vary over time (aging of the reactor as well as the UV lamp, PTR-MS sensitivity etc.) and the measuring conditions are different, ideally, characterization of the aforementioned interferences should be performed onsite and justified according to the measuring conditions (relative humidity range, temperature, expected dominant reactive species etc.). The corrections applied under specific measurements are described in greater details in Chapter 3 and 5.

1.5 Open research questions and thesis outline

For both outdoor and indoor air, carbonyl compounds can be generated from primary and secondary sources and they can play important roles in air chemistry. Exposure to high levels of carbonyls (aldehydes in particular) can cause adverse health effects (USEPA). These compounds are especially important for indoor air environments as people usually spend much more time indoors than outside. Meanwhile, due to the various chemical reactions that carbonyls can be involved in, they can impact ozone formation (outdoor), free radical budget (outdoor and indoor), secondary organic particle formation (indoor and outdoor) as well as producing other organic

compounds having higher toxicity (indoor and outdoor). Therefore, real-time measurement of carbonyl compounds as well as other VOCs can help to document their variations so that we can better understand the air chemistry involving carbonyls. In addition, through the comparison between direct measurement of the total OH reactivity and the estimated OH reactivity, we can determine the existence of important reactive species in the air that are not captured by current measurement techniques and see how important the carbonyl contribution to the total OH reactivity is in air.

PTR-MS is a soft ionization technique that has been widely applied in various research fields to monitor VOCs due to its rapid response and high sensitivity (Ellis and Mayhew, 2013; Yuan et al., 2017). It is the main technique applied in this doctoral project to characterize VOCs and measure the total OH reactivity outdoor (Chapter 2 and 3) and indoor (Chapter 4 and 5).

Chapter 2 and 3 focus on the outdoor carbonyl characterization and the total OH reactivity around the Arabian Peninsula. Due to strong solar radiation, high temperature and hotspots of anthropogenic emissions (petroleum industries), the regional ozone air pollution is predicted to be severe (Lelieveld et al., 2009). However, ambient measurement data over the region is scarce. Therefore, on-line VOCs and total OH reactivity measurements were implemented on a research vessel that travelled around the Arabian Peninsula. **Chapter 2** presents the regional concentration distributions and budget assessment of carbonyls measured by PTR-ToF-MS. In addition, comparisons between the measurement results and model estimations were performed for major carbonyls (acetaldehyde, acetone and methyl ethyl ketone) to further identify their sources and formation pathways. In **Chapter 3**, the measured total OH reactivity was compared to the calculated OH reactivity by considering more than 120 species measured by PTR-ToF-MS and other instruments. Budget analysis indicates that OVOCs (mostly carbonyls) dominated the fractional contribution to the total OH reactivity. The measured OH reactivity was also utilized to identify the favorable conditions for ozone formation over the region.

Chapters 4 and 5 focus on the characterization of carbonyls as well as the total OH reactivity under a well-controlled indoor environment dominated by human emissions. Humans are a potent source of thousands of VOCs (de Lacy Costello et al., 2014). With the development of technology as well as the stringent rules and regulations, the emissions from building materials, decorations and furniture are expected to decrease in the future, which makes the role of human emissions more

and more important in indoor environments. Several studies have reported human VOC emissions in real life indoor environments (Liu et al., 2016; Pagonis et al., 2019; Stonner et al., 2017; Tang et al., 2016), which were usually characterized together with other variables such as use of personal care products and fragrance, indoor furnishings and furniture. Detailed characterization of indoor human whole-body emissions, separate breath and skin emissions under controlled conditions (temperature, relative humidity and ozone) are lacking. **Chapter 4** describes the emission rates of VOCs from the human whole body, breath and skin under ozone-free and ozone-present conditions, which were also compared with the emission rates reported by other studies. The emission rates of carbonyl compounds increased sharply when people were exposed to high levels of ozone. A first indoor OH reactivity measurement is presented in **Chapter 5**, which aims to determine whether the indoor human emissions are completely characterized by the current trace gas measurements, and to know to what extent ozone can influence the OH reactivity and the contribution from carbonyl compounds to the total OH reactivity.

In **Chapter 6**, major observations and findings for the doctoral project are summarized with further discussion of the links between outdoor and indoor air chemistry related to carbonyl compounds. Implications and future outlooks are discussed as well in this chapter.

References

Abbatt, J. P. D. and Wang, C.: The atmospheric chemistry of indoor environments, Environ Sci Process Impacts, 22, 25-48, 2020.

Afshari, A., Lundgren, B. and Ekberg, L.E.: Comparison of three small chamber test methods for the measurement of VOC emission rates from paint, Indoor Air, 13, 156-165, 2003.

Altshuller, A. P.: Production of aldehydes as primary emissions and from secondary atmospheric reactions of alkenes and alkanes during the night and early morning hours, Atmospheric Environment. Part A. General Topics, 27, 21-32, 1993.

Anderson, S. E., Franko, J., Jackson, L. G., Wells, J. R., Ham, J. E., and Meade, B. J.: Irritancy and allergic responses induced by exposure to the indoor air chemical 4-oxopentanal, Toxicol Sci, 127, 371-381, 2012.

Arata, C., Heine, N., Wang, N., Misztal, P. K., Wargocki, P., Beko, G., Williams, J., Nazaroff, W. W., Wilson, K. R., and Goldstein, A. H.: Heterogeneous Ozonolysis of Squalene: Gas-Phase Products Depend on Water Vapor Concentration, Environ Sci Technol, 53, 14441-14448, 2019.

Atkinson, R. and Arey, J.: Atmospheric Degradation of Volatile Organic Compounds, Chemical Reviews, 103, 4605-4638, 2003.

Báez, A., Padilla, H., García, R. o., Torres, M. d. C., Rosas, I., and Belmont, R.: Carbonyl levels in indoor and outdoor air in Mexico City and Xalapa, Mexico, Science of The Total Environment, 302, 211-226, 2003.

Beale, R., Dixon, J. L., Arnold, S. R., Liss, P. S., and Nightingale, P. D.: Methanol, acetaldehyde, and acetone in the surface waters of the Atlantic Ocean, Journal of Geophysical Research: Oceans, 118, 5412-5425, 2013.

Bigazzi, A. Y., Figliozzi, M. A., Luo, W., and Pankow, J. F.: Breath Biomarkers to Measure Uptake of Volatile Organic Compounds by Bicyclists, Environmental Science & Technology, 50, 5357-5363, 2016.

Bourtsoukidis, E., Williams, J., Kesselmeier, J., Jacobi, S., and Bonn, B.: From emissions to ambient mixing ratios: online seasonal field measurements of volatile organic compounds over a Norway spruce-dominated forest in central Germany, Atmos. Chem. Phys., 14, 6495-6510, 2014.

Britigan, N., Alshawa, A., and Nizkorodov, S. A.: Quantification of ozone levels in indoor environments generated by ionization and ozonolysis air purifiers, J Air Waste Manag Assoc, 56, 601-610, 2006.

Calpini, B., Jeanneret, F., Bourqui, M., Clappier, A., Vajtai, R., and van den Bergh, H.: Direct measurement of the total reaction rate of OH in the atmosphere, Analusis, 27, 328-336, 1999.

Carlier, P., Hannachi, H., and Mouvier, G.: The chemistry of carbonyl compounds in the atmosphere—A review, Atmospheric Environment (1967), 20, 2079-2099, 1986.

Carslaw, N.: A new detailed chemical model for indoor air pollution, Atmospheric Environment, 41, 1164-1179, 2007.

Carslaw, N., Fletcher, L., Heard, D., Ingham, T., and Walker, H.: Significant OH production under surface cleaning and air cleaning conditions: Impact on indoor air quality, Indoor Air, 27, 1091-1100, 2017.

Cheng, Y.-H., Lin, C.-C., and Hsu, S.-C.: Comparison of conventional and green building materials in respect of VOC emissions and ozone impact on secondary carbonyl emissions, Building and Environment, 87, 274-282, 2015.

Coleman, B. K., Destaillats, H., Hodgson, A. T., and Nazaroff, W. W.: Ozone consumption and volatile byproduct formation from surface reactions with aircraft cabin materials and clothing fabrics, Atmospheric Environment, 42, 642-654, 2008.

Colomb, A., Williams, J., Crowley, J., Gros, V., Hofmann, R., Salisbury, G., Klüpfel, T., Kormann, R., Stickler, A., Forster, C., and Lelieveld, J.: Airborne Measurements of Trace Organic Species in the Upper Troposphere Over Europe: the Impact of Deep Convection, Environmental Chemistry, 3, 244, 2006.

Criegee, R.: Mechanism of Ozonolysis, Angewandte Chemie International Edition in English, 14, 745-752, 1975.

de Gouw, J. and Warneke, C.: Measurements of volatile organic compounds in the earth's atmosphere using proton-transfer-reaction mass spectrometry, Mass Spectrometry Reviews, 26, 223-257, 2007.

de Lacy Costello, B., Amann, A., Al-Kateb, H., Flynn, C., Filipiak, W., Khalid, T., Osborne, D., and Ratcliffe, N. M.: A review of the volatiles from the healthy human body, J Breath Res, 8, 014001, 2014.

Derstroff, B., Hüser, I., Bourtsoukidis, E., Crowley, J. N., Fischer, H., Gromov, S., Harder, H., Janssen, R. H. H., Kesselmeier, J., Lelieveld, J., Mallik, C., Martinez, M., Novelli, A., Parchatka, U., Phillips, G. J., Sander, R., Sauvage, C., Schuladen, J., Stönner, C., Tomsche, L., and Williams, J.: Volatile organic compounds (VOCs) in photochemically aged air from the eastern and western Mediterranean, Atmospheric Chemistry and Physics, 17, 9547-9566, 2017.

Di Carlo, P., Brune, W. H., Martinez, M., Harder, H., Lesher, R., Ren, X., Thornberry, T., Carroll, M. A., Young, V., and Shepson, P. B.: Missing OH reactivity in a forest: Evidence for unknown reactive biogenic VOCs, Science, 304, 722-725, 2004.

Dillon, T. J., Tucceri, M. E., Dulitz, K., Horowitz, A., Vereecken, L., and Crowley, J. N.: Reaction of Hydroxyl Radicals with C4H5N (Pyrrole): Temperature and Pressure Dependent Rate Coefficients, The Journal of Physical Chemistry A, 116, 6051-6058, 2012.

Dolgorouky, C., Gros, V., Sarda-Esteve, R., Sinha, V., Williams, J., Marchand, N., Sauvage, S., Poulain, L., Sciare, J., and Bonsang, B.: Total OH reactivity measurements in Paris during the 2010 MEGAPOLI winter campaign, Atmospheric Chemistry and Physics, 12, 9593-9612, 2012.

Dong, D., Shao, M., Li, Y., Lu, S., Wang, Y., Ji, Z., and Tang, D.: Carbonyl emissions from heavy-duty diesel vehicle exhaust in China and the contribution to ozone formation potential, Journal of Environmental Sciences, 26, 122-128, 2014.

Ellis, A. M. and Mayhew, C. A.: Proton transfer reaction mass spectrometry: principles and applications, John Wiley & Sons, 2013.

Erickson, M. H., Gueneron, M., and Jobson, B. T.: Measuring long chain alkanes in diesel engine exhaust by thermal desorption PTR-MS, Atmospheric Measurement Techniques, 7, 225-239, 2014.

Fall, R.: Abundant Oxygenates in the Atmosphere: A Biochemical Perspective, Chemical Reviews, 103, 4941-4952, 2003.

Farmer, D. K.: Analytical Challenges and Opportunities For Indoor Air Chemistry Field Studies, Anal Chem, 91, 3761-3767, 2019.

Farmer, D. K., Vance, M. E., Abbatt, J. P. D., Abeleira, A., Alves, M. R., Arata, C., Boedicker, E., Bourne, S., Cardoso-Saldana, F., Corsi, R., DeCarlo, P. F., Goldstein, A. H., Grassian, V. H., Hildebrandt Ruiz, L., Jimenez, J. L., Kahan, T. F., Katz, E. F., Mattila, J. M., Nazaroff, W. W., Novoselac, A., O'Brien, R. E., Or, V. W., Patel, S., Sankhyan, S., Stevens, P. S., Tian, Y., Wade, M., Wang, C., Zhou, S., and Zhou, Y.: Overview of HOMEChem: House Observations of Microbial and Environmental Chemistry, Environ Sci Process Impacts, 21, 1280-1300, 2019.

Filipiak, W., Ruzsanyi, V., Mochalski, P., Filipiak, A., Bajtarevic, A., Ager, C., Denz, H., Hilbe, W., Jamnig, H., Hackl, M., Dzien, A., and Amann, A.: Dependence of exhaled breath composition on exogenous factors, smoking habits and exposure to air pollutants, J Breath Res, 6, 036008, 2012.

Finlayson-Pitts, B. J. and Pitts Jr, J. N.: Chemistry of the upper and lower atmosphere: theory, experiments, and applications, Elsevier, 1999.

Fischer, A., Ljungström, E., and Langer, S.: Ozone removal by occupants in a classroom, Atmospheric Environment, 81, 11-17, 2013.

Fischer, E. V., Jacob, D. J., Yantosca, R. M., Sulprizio, M. P., Millet, D. B., Mao, J., Paulot, F., Singh, H. B., Roiger, A., Ries, L., Talbot, R. W., Dzepina, K., and Pandey Deolal, S.: Atmospheric peroxyacetyl nitrate (PAN): a global budget and source attribution, Atmospheric Chemistry and Physics, 14, 2679-2698, 2014.

Fortems-Cheiney, A., Chevallier, F., Pison, I., Bousquet, P., Saunois, M., Szopa, S., Cressot, C., Kurosu, T. P., Chance, K., and Fried, A.: The formaldehyde budget as seen by a global-scale multi-constraint and multi-species inversion system, Atmospheric Chemistry and Physics, 12, 6699-6721, 2012.

Fruekilde, P., Hjorth, J., Jensen, N. R., Kotzias, D., and Larsen, B.: Ozonolysis at vegetation surfaces: a source of acetone, 4-oxopentanal, 6-methyl-5-hepten-2-one, and geranyl acetone in the troposphere, Atmospheric Environment, 32, 1893-1902, 1998.

Fuchs, H., Novelli, A., Rolletter, M., Hofzumahaus, A., Pfannerstill, E. Y., Kessel, S., Edtbauer, A., Williams, J., Michoud, V., Dusanter, S., Locoge, N., Zannoni, N., Gros, V., Truong, F., Sarda-Esteve, R., Cryer, D. R., Brumby, C. A., Whalley, L. K., Stone, D., Seakins, P. W., Heard, D. E., Schoemaecker, C., Blocquet, M., Coudert, S., Batut, S., Fittschen, C., Thames, A. B., Brune, W. H., Ernest, C., Harder, H., Muller, J. B. A., Elste, T., Kubistin, D., Andres, S., Bohn, B., Hohaus, T., Holland, F., Li, X., Rohrer, F., Kiendler-Scharr, A., Tillmann, R., Wegener, R., Yu, Z., Zou, Q., and Wahner, A.: Comparison of OH reactivity measurements in the atmospheric simulation chamber SAPHIR, Atmospheric Measurement Techniques, 10, 4023-4053, 2017.

Gligorovski, S. and Weschler, C. J.: The oxidative capacity of indoor atmospheres, Environ Sci Technol, 47, 13905-13906, 2013.

Gómez Alvarez, E., Amedro, D., Afif, C., Gligorovski, S., Schoemaecker, C., Fittschen, C., Doussin, J.-F., and Wortham, H.: Unexpectedly high indoor hydroxyl radical concentrations associated with nitrous acid, Proceedings of the National Academy of Sciences, 110, 13294, 2013.

Graus, M., Müller, M., and Hansel, A.: High Resolution PTR-TOF: Quantification and Formula Confirmation of VOC in Real Time, Journal of the American Society for Mass Spectrometry, 21, 1037-1044, 2010.

Guo, H., Ling, Z. H., Cheung, K., Wang, D. W., Simpson, I. J., and Blake, D. R.: Acetone in the atmosphere of Hong Kong: Abundance, sources and photochemical precursors, Atmospheric Environment, 65, 80-88, 2013.

Hansen, R. F., Blocquet, M., Schoemaecker, C., Léonardis, T., Locoge, N., Fittschen, C., Hanoune, B., Stevens, P. S., Sinha, V., and Dusanter, S.: Intercomparison of the comparative reactivity method (CRM) and pump–probe technique for measuring total OH reactivity in an urban environment, Atmospheric Measurement Techniques, 8, 4243-4264, 2015.

He, J., Sun, X., and Yang, X.: Human respiratory system as sink for volatile organic compounds: Evidence from field measurements, Indoor Air, 29, 968-978, 2019.

Heine, N., Houle, F. A., and Wilson, K. R.: Connecting the Elementary Reaction Pathways of Criegee Intermediates to the Chemical Erosion of Squalene Interfaces during Ozonolysis, Environ Sci Technol, 51, 13740-13748, 2017.

Hodgson, A. T., Beal, D., and McIlvaine, J. E. R.: Sources of formaldehyde, other aldehydes and terpenes in a new manufactured house, Indoor Air, 12, 235-242, 2002.

Hodgson, A. T., Wooley, J. D., and Daisey, J. M.: Emissions of volatile organic compounds from new carpets measured in a large-scale environmental chamber, Air & Waste, 43, 316-324, 1993.

Holzinger, R., Warneke, C., Hansel, A., Jordan, A., Lindinger, W., Scharffe, D. H., Schade, G., and Crutzen, P. J.: Biomass burning as a source of formaldehyde, acetaldehyde, methanol, acetone, acetonitrile, and hydrogen cyanide, Geophysical Research Letters, 26, 1161-1164, 1999.

Huangfu, Y., Lima, N. M., O'Keeffe, P. T., Kirk, W. M., Lamb, B. K., Walden, V. P., and Jobson, B. T.: Whole-House Emission Rates and Loss Coefficients of Formaldehyde and Other Volatile Organic Compounds as a Function of the Air Change Rate, Environ Sci Technol, 54, 2143-2151, 2020.

IUPAC: http://iupac.pole-ether.fr, 2019.

Jacob, D. J., Field, B. D., Jin, E. M., Bey, I., Li, Q., Logan, J. A., Yantosca, R. M., and Singh, H. B.: Atmospheric budget of acetone, Journal of Geophysical Research: Atmospheres, 107, ACH 5-1-ACH 5-17, 2002.

Jiang, C. and Zhang, P.: Indoor carbonyl compounds in an academic building in Beijing, China: concentrations and influencing factors, Frontiers of Environmental Science & Engineering, 6, 184-194, 2012.

Jordan, A., Haidacher, S., Hanel, G., Hartungen, E., Märk, L., Seehauser, H., Schottkowsky, R., Sulzer, P., and Märk, T. D.: A high resolution and high sensitivity proton-transfer-reaction time-of-flight mass spectrometer (PTR-TOF-MS), International Journal of Mass Spectrometry, 286, 122-128, 2009a.

Jordan, C., Fitz, E., Hagan, T., Sive, B., Frinak, E., Haase, K., Cottrell, L., Buckley, S., and Talbot, R.: Long-term study of VOCs measured with PTR-MS at a rural site in New Hampshire with urban influences, Atmospheric Chemistry and Physics, 9, 4677-4697, 2009b.

Jurvelin, J. A., Edwards, R. D., Vartiainen, M., Pasanen, P., and Jantunen, M. J.: Residential indoor, outdoor, and workplace concentrations of carbonyl compounds: relationships with personal exposure concentrations and correlation with sources, J Air Waste Manag Assoc, 53, 560-573, 2003.

Kean, A. J., Grosjean, E., Grosjean, D., and Harley, R. A.: On-Road Measurement of Carbonyls in California Light-Duty Vehicle Emissions, Environmental Science & Technology, 35, 4198-4204, 2001.

Kim, K.-H., Hong, Y.-J., Pal, R., Jeon, E.-C., Koo, Y.-S., and Sunwoo, Y.: Investigation of carbonyl compounds in air from various industrial emission sources, Chemosphere, 70, 807-820, 2008.

Kim, S., Sanchez, D., Wang, M., Seco, R., Jeong, D., Hughes, S., Barletta, B., Blake, D. R., Jung, J., Kim, D., Lee, G., Lee, M., Ahn, J., Lee, S. D., Cho, G., Sung, M. Y., Lee, Y. H., Kim, D. B., Kim, Y., Woo, J. H., Jo, D., Park, R., Park, J. H., Hong, Y. D., and Hong, J. H.: OH reactivity in urban and suburban regions in Seoul, South Korea - an East Asian megacity in a rapid transition, Faraday Discuss, 189, 231-251, 2016.

Kirchner, F., Jeanneret, F., Clappier, A., Krüger, B., van den Bergh, H., and Calpini, B.: Total VOC reactivity in the planetary boundary layer: 2. A new indicator for determining the sensitivity of the ozone production to VOC and NOx, Journal of Geophysical Research: Atmospheres, 106, 3095-3110, 2001.

Koss, A. R., Sekimoto, K., Gilman, J. B., Selimovic, V., Coggon, M. M., Zarzana, K. J., Yuan, B., Lerner, B. M., Brown, S. S., Jimenez, J. L., Krechmer, J., Roberts, J. M., Warneke, C., Yokelson, R. J., and de Gouw, J.: Non-methane organic gas emissions from biomass burning: identification, quantification, and emission factors from PTR-ToF during the FIREX 2016 laboratory experiment, Atmospheric Chemistry and Physics, 18, 3299-3319, 2018.

Kovacs, T. A. and Brune, W. H.: Total OH Loss Rate Measurement, Journal of Atmospheric Chemistry, 39, 105-122, 2001.

Kroll, J. H., Ng, N. L., Murphy, S. M., Varutbangkul, V., Flagan, R. C., and Seinfeld, J. H.: Chamber studies of secondary organic aerosol growth by reactive uptake of simple carbonyl compounds, Journal of Geophysical Research, 110, 2005.

Lakey, P. S. J., Morrison, G. C., Won, Y., Parry, K. M., von Domaros, M., Tobias, D. J., Rim, D., and Shiraiwa, M.: The impact of clothing on ozone and squalene ozonolysis products in indoor environments, Communications Chemistry, 2, 2019.

Lakey, P. S. J., Wisthaler, A., Berkemeier, T., Mikoviny, T., Poschl, U., and Shiraiwa, M.: Chemical kinetics of multiphase reactions between ozone and human skin lipids: Implications for indoor air quality and health effects, Indoor Air, 27, 816-828, 2017.

Lary, D. J. and Shallcross, D. E.: Central role of carbonyl compounds in atmospheric chemistry, Journal of Geophysical Research: Atmospheres, 105, 19771-19778, 2000.

Lee, S.-C. and Wang, B.: Characteristics of emissions of air pollutants from burning of incense in a large environmental chamber, Atmospheric Environment, 38, 941-951, 2004.

Legreid, G., Lööv, J. B., Staehelin, J., Hueglin, C., Hill, M., Buchmann, B., Prevot, A. S. H., and Reimann, S.: Oxygenated volatile organic compounds (OVOCs) at an urban background site in Zürich (Europe): Seasonal variation and source allocation, Atmospheric Environment, 41, 8409-8423, 2007.

Lelieveld, J., Gromov, S., Pozzer, A., and Taraborrelli, D.: Global tropospheric hydroxyl distribution, budget and reactivity, Atmospheric Chemistry and Physics, 16, 12477-12493, 2016.

Lelieveld, J., Hoor, P., Jöckel, P., Pozzer, A., Hadjinicolaou, P., Cammas, J. P., and Beirle, S.: Severe ozone air pollution in the Persian Gulf region, Atmos. Chem. Phys., 9, 1393-1406, 2009.

Lindinger, W., Hansel, A., and Jordan, A.: On-line monitoring of volatile organic compounds at pptv levels by means of proton-transfer-reaction mass spectrometry (PTR-MS) medical applications, food control and environmental research, International Journal of Mass Spectrometry and Ion Processes, 173, 191-241, 1998.

Liu, S., Li, R., Wild, R. J., Warneke, C., de Gouw, J. A., Brown, S. S., Miller, S. L., Luongo, J. C., Jimenez, J. L., and Ziemann, P. J.: Contribution of human-related sources to indoor volatile organic compounds in a university classroom, Indoor Air, 26, 925-938, 2016.

Liu, W., Zhang, J., Zhang, L., Turpin, B. J., Weisel, C. P., Morandi, M. T., Stock, T. H., Colome, S., and Korn, L. R.: Estimating contributions of indoor and outdoor sources to indoor carbonyl concentrations in three urban areas of the United States, Atmospheric Environment, 40, 2202-2214, 2006.

Lou, S., Holland, F., Rohrer, F., Lu, K., Bohn, B., Brauers, T., Chang, C. C., Fuchs, H., Häseler, R., Kita, K., Kondo, Y., Li, X., Shao, M., Zeng, L., Wahner, A., Zhang, Y., Wang, W., and Hofzumahaus, A.: Atmospheric OH reactivities in the Pearl River Delta – China in summer 2006: measurement and model results, Atmos. Chem. Phys., 10, 11243-11260, 2010.

Michoud, V., Hansen, R. F., Locoge, N., Stevens, P. S., and Dusanter, S.: Detailed characterizations of the new Mines Douai comparative reactivity method instrument via laboratory experiments and modeling, Atmospheric Measurement Techniques, 8, 3537-3553, 2015.

Millet, D. B., Alwe, H. D., Chen, X., Deventer, M. J., Griffis, T. J., Holzinger, R., Bertman, S. B., Rickly, P. S., Stevens, P. S., Léonardis, T., Locoge, N., Dusanter, S., Tyndall, G. S., Alvarez, S. L., Erickson, M. H., and Flynn, J. H.: Bidirectional Ecosystem–Atmosphere Fluxes of Volatile Organic Compounds Across the Mass Spectrum: How Many Matter?, ACS Earth and Space Chemistry, 2, 764-777, 2018.

Millet, D. B., Guenther, A., Siegel, D. A., Nelson, N. B., Singh, H. B., de Gouw, J. A., Warneke, C., Williams, J., Eerdekens, G., and Sinha, V.: Global atmospheric budget of acetaldehyde: 3-D model analysis and constraints from in-situ and satellite observations, Atmospheric Chemistry and Physics, 10, 3405-3425, 2010.

Mochalski, P., King, J., Unterkofler, K., Hinterhuber, H., and Amann, A.: Emission rates of selected volatile organic compounds from skin of healthy volunteers, J Chromatogr B Analyt Technol Biomed Life Sci, 959, 62-70, 2014.

Mopper, K. and Stahovec, W. L.: Sources and sinks of low molecular weight organic carbonyl compounds in seawater, Marine Chemistry, 19, 305-321, 1986.

Morrison, G. C. and Nazaroff, W. W.: The Rate of Ozone Uptake on Carpets: Experimental Studies, Environmental Science & Technology, 34, 4963-4968, 2000.

Moussa, S. G., El-Fadel, M., and Saliba, N. A.: Seasonal, diurnal and nocturnal behaviors of lower carbonyl compounds in the urban environment of Beirut, Lebanon, Atmospheric Environment, 40, 2459-2468, 2006.

Müller, K., Haferkorn, S., Grabmer, W., Wisthaler, A., Hansel, A., Kreuzwieser, J., Cojocariu, C., Rennenberg, H., and Herrmann, H.: Biogenic carbonyl compounds within and above a coniferous forest in Germany, Atmospheric Environment, 40, 81-91, 2006.

Nazaroff, W. W. and Weschler, C. J.: Cleaning products and air fresheners: exposure to primary and secondary air pollutants, Atmospheric Environment, 38, 2841-2865, 2004.

Nicolaides, N.: Skin Lipids: Their Biochemical Uniqueness, Science, 186, 19, 1974.

NIST: https://webbook.nist.gov/chemistry/2020.

Nölscher, A. C., Sinha, V., Bockisch, S., Klüpfel, T., and Williams, J.: Total OH reactivity measurements using a new fast Gas Chromatographic Photo-Ionization Detector (GC-PID), Atmospheric Measurement Techniques, 5, 2981-2992, 2012.

Nölscher, A. C., Yanez-Serrano, A. M., Wolff, S., de Araujo, A. C., Lavric, J. V., Kesselmeier, J., and Williams, J.: Unexpected seasonality in quantity and composition of Amazon rainforest air reactivity, Nat Commun, 7, 10383, 2016.

Pagonis, D., Price, D. J., Algrim, L. B., Day, D. A., Handschy, A. V., Stark, H., Miller, S. L., de Gouw, J., Jimenez, J. L., and Ziemann, P. J.: Time-Resolved Measurements of Indoor Chemical Emissions, Deposition, and Reactions in a University Art Museum, Environ Sci Technol, 53, 4794-4802, 2019.

Pal, R., Kim, K.-H., Hong, Y.-J., and Jeon, E.-C.: The pollution status of atmospheric carbonyls in a highly industrialized area, Journal of Hazardous Materials, 153, 1122-1135, 2008.

Pandrangi, L. S. and Morrison, G. C.: Ozone interactions with human hair: Ozone uptake rates and product formation, Atmospheric Environment, 42, 5079-5089, 2008.

Petitjean, M., Reyès-Pérez, E., Pérez, D., Mirabel, P., and Le Calvé, S.: Vapor Pressure Measurements of Hydroxyacetaldehyde and Hydroxyacetone in the Temperature Range (273 to 356) K, Journal of Chemical & Engineering Data, 55, 852-855, 2010.

Petrick, L. and Dubowski, Y.: Heterogeneous oxidation of squalene film by ozone under various indoor conditions, Indoor Air, 19, 381-391, 2009.

Praplan, A. P., Pfannerstill, E. Y., Williams, J., and Hellén, H.: OH reactivity of the urban air in Helsinki, Finland, during winter, Atmospheric Environment, 169, 150-161, 2017.

Praplan, A. P., Tykkä, T., Chen, D., Boy, M., Taipale, D., Vakkari, V., Zhou, P., Petäjä, T., and Hellén, H.: Long-term total OH reactivity measurements in a boreal forest, Atmos. Chem. Phys., 19, 14431-14453, 2019.

Price, D. J., Day, D. A., Pagonis, D., Stark, H., Algrim, L. B., Handschy, A. V., Liu, S., Krechmer, J. E., Miller, S. L., Hunter, J. F., de Gouw, J. A., Ziemann, P. J., and Jimenez, J. L.: Budgets of Organic Carbon Composition and Oxidation in Indoor Air, Environ Sci Technol, 53, 13053-13063, 2019.

Rai, A. C., Guo, B., Lin, C. H., Zhang, J., Pei, J., and Chen, Q.: Ozone reaction with clothing and its initiated VOC emissions in an environmental chamber, Indoor Air, 24, 49-58, 2014.

Read, K. A., Carpenter, L. J., Arnold, S. R., Beale, R., Nightingale, P. D., Hopkins, J. R., Lewis, A. C., Lee, J. D., Mendes, L., and Pickering, S. J.: Multiannual observations of acetone, methanol, and acetaldehyde in remote tropical atlantic air: implications for atmospheric OVOC budgets and oxidative capacity, Environ Sci Technol, 46, 11028-11039, 2012.

Sahu, L. K. and Saxena, P.: High time and mass resolved PTR-TOF-MS measurements of VOCs at an urban site of India during winter: Role of anthropogenic, biomass burning, biogenic and photochemical sources, Atmospheric Research, 164-165, 84-94, 2015.

Salthammer, T., Zhang, Y., Mo, J., Koch, H. M., and Weschler, C. J.: Assessing Human Exposure to Organic Pollutants in the Indoor Environment, Angew Chem Int Ed Engl, 57, 12228-12263, 2018.

Salvador, C. M., Beko, G., Weschler, C. J., Morrison, G., Le Breton, M., Hallquist, M., Ekberg, L., and Langer, S.: Indoor ozone/human chemistry and ventilation strategies, Indoor Air, 29, 913-925, 2019.

Sarwar, G., Corsi, R., Kimura, Y., Allen, D., and Weschler, C. J.: Hydroxyl radicals in indoor environments, Atmospheric Environment, 36, 3973-3988, 2002.

Seco, R., Peñuelas, J., and Filella, I.: Short-chain oxygenated VOCs: Emission and uptake by plants and atmospheric sources, sinks, and concentrations, Atmospheric Environment, 41, 2477-2499, 2007.

Seinfeld, J. H. and Pandis, S. N.: Atmospheric Chemistry and Physics: From Air Pollution to Climate Change: Chapter 6, Wiley, 2016.

Sheng, J., Zhao, D., Ding, D., Li, X., Huang, M., Gao, Y., Quan, J., and Zhang, Q.: Characterizing the level, photochemical reactivity, emission, and source contribution of the volatile organic compounds based on PTR-TOF-MS during winter haze period in Beijing, China, Atmospheric Research, 212, 54-63, 2018.

Simon, V., Uitterhaegen, E., Robillard, A., Ballas, S., Veronese, T., Vilarem, G., Merah, O., Talou, T., and Evon, P.: VOC and carbonyl compound emissions of a fiberboard resulting from a coriander biorefinery: comparison with two commercial wood-based building materials, Environ Sci Pollut Res Int, 27, 16121-16133, 2020.

Singh, H. B. and Hanst, P. L.: Peroxyacetyl nitrate (PAN) in the unpolluted atmosphere: An important reservoir for nitrogen oxides, Geophysical Research Letters, 8, 941-944, 1981.

Singh, H. B., Kanakidou, M., Crutzen, P. J., and Jacob, D. J.: High concentrations and photochemical fate of oxygenated hydrocarbons in the global troposphere, Nature, 378, 50-54, 1995.

Sinha, V., Custer, T. G., Kluepfel, T., and Williams, J.: The effect of relative humidity on the detection of pyrrole by PTR-MS for OH reactivity measurements, International Journal of Mass Spectrometry, 282, 108-111, 2009.

Sinha, V., Williams, J., Crowley, J., and Lelieveld, J.: The Comparative Reactivity Method–a new tool to measure total OH Reactivity in ambient air, Atmospheric Chemistry and Physics, 8, 2213-2227, 2008.

Sinha, V., Williams, J., Meyerhöfer, M., Riebesell, U., Paulino, A. I., and Larsen, A.: Air-sea fluxes of methanol, acetone, acetaldehyde, isoprene and DMS from a Norwegian fjord following a phytoplankton bloom in a mesocosm experiment, Atmos. Chem. Phys., 7, 739-755, 2007.

Stonner, C., Edtbauer, A., and Williams, J.: Real-world volatile organic compound emission rates from seated adults and children for use in indoor air studies, Indoor Air, 28, 164-172, 2017.

Sundell, J.: Reflections on the history of indoor air science, focusing on the last 50 years, Indoor Air, 27, 708-724, 2017.

Tamas, G., Weschler, C., Bakobiro, Z., Wyon, D., and Stromtejsen, P.: Factors affecting ozone removal rates in a simulated aircraft cabin environment, Atmospheric Environment, 40, 6122-6133, 2006.

Tan, Y., Liu, C., Ho, K., Ma, Q., and Lee, S.-C.: Characterization of an indoor environmental chamber and identification of C1–C4 OVOCs during isoprene ozonolysis, Indoor and Built Environment, 0, 1420326X20922880, 2020.

Tang, X., Misztal, P. K., Nazaroff, W. W., and Goldstein, A. H.: Volatile Organic Compound Emissions from Humans Indoors, Environ Sci Technol, 50, 12686-12694, 2016.

Thames, A. B., Brune, W. H., Miller, D. O., Allen, H. M., Apel, E. C., Blake, D. R., Bui, T. P., Commane, R., Crounse, J. D., Daube, B. C., Diskin, G. S., DiGangi, J. P., Elkins, J. W., Hall, S. R., Hanisco, T. F., Hannun, R. A., Hintsa, E., Hornbrook, R. S., Kim, M. J., McKain, K., Moore, F. L., Nicely, J. M., Peischl, J., Ryerson, T. B., St. Clair, J. M., Sweeney, C., Teng, A., Thompson, C. R., Ullmann, K., Wennberg, P. O., and Wolfe, G. M.: Missing OH reactivity in the global marine boundary layer, Atmospheric Chemistry and Physics, 20, 4013-4029, 2020.

Thornberry, T. and Abbatt, J. P. D.: Heterogeneous reaction of ozone with liquid unsaturated fatty acids: detailed kinetics and gas-phase product studies, Physical Chemistry Chemical Physics, 6, 84, 2004.

Tuomi, T., Engström, B., Niemelä, R., Svinhufvud, J., and Reijula, K.: Emission of Ozone and Organic Volatiles from a Selection of Laser Printers and Photocopiers, Applied Occupational and Environmental Hygiene, 15, 629-634, 2000.

Turner, C., Spanel, P., and Smith, D.: A longitudinal study of ammonia, acetone and propanol in the exhaled breath of 30 subjects using selected ion flow tube mass spectrometry, SIFT-MS, Physiol Meas, 27, 321-337, 2006.

Turner, C., Španěl, P., and Smith, D.: A longitudinal study of breath isoprene in healthy volunteers using selected ion flow tube mass spectrometry (SIFT-MS), Physiological Measurement, 27, 13-22, 2005.

USEPA: https://cfpub.epa.gov/ncea/iris_drafts/atoz.cfm?list_type=alpha.

Vaught, C.: Locating and estimating air emissions from sources of formaldehyde (revised), Midwest Research Inst., Cary, NC (United States), 1991.

Wang, S., Apel, E. C., Schwantes, R. H., Bates, K. H., Jacob, D. J., Fischer, E. V., Hornbrook, R. S., Hills, A. J., Emmons, L. K., Pan, L. L., Honomichl, S., Tilmes, S., Lamarque, J. F., Yang, M., Marandino, C. A., Saltzman, E. S., Bruyn, W., Kameyama, S., Tanimoto, H., Omori, Y., Hall, S. R., Ullmann, K., Ryerson, T. B., Thompson, C. R., Peischl, J., Daube, B. C., Commane, R., McKain, K., Sweeney, C., Thames, A. B., Miller, D. O., Brune, W. H., Diskin, G. S., DiGangi, J. P., and Wofsy, S. C.: Global Atmospheric Budget of Acetone: Air-Sea Exchange and the Contribution to Hydroxyl Radicals, Journal of Geophysical Research: Atmospheres, 125, 2020.

Wang, S., Hornbrook, R. S., Hills, A., Emmons, L. K., Tilmes, S., Lamarque, J. F., Jimenez, J. L., Campuzano-Jost, P., Nault, B. A., Crounse, J. D., Wennberg, P. O., Kim, M., Allen, H., Ryerson, T. B., Thompson, C. R., Peischl, J., Moore, F., Nance, D., Hall, B., Elkins, J., Tanner, D., Huey, L. G., Hall, S. R., Ullmann, K., Orlando, J. J., Tyndall, G. S., Flocke, F. M., Ray, E., Hanisco, T. F., Wolfe, G. M., St. Clair, J., Commane, R., Daube, B., Barletta, B., Blake, D. R., Weinzierl, B., Dollner, M., Conley, A., Vitt, F., Wofsy, S. C., Riemer, D. D., and Apel, E. C.: Atmospheric Acetaldehyde: Importance of Air-Sea Exchange and a Missing Source in the Remote Troposphere, Geophysical Research Letters, doi: 10.1029/2019gl082034, 2019. 2019.

Waring, M. S. and Wells, J. R.: Volatile organic compound conversion by ozone, hydroxyl radicals, and nitrate radicals in residential indoor air: Magnitudes and impacts of oxidant sources, Atmos Environ (1994), 106, 382-391, 2015.

Warneke, C., van der Veen, C., Luxembourg, S., de Gouw, J. A., and Kok, A.: Measurements of benzene and toluene in ambient air using proton-transfer-reaction mass spectrometry: calibration, humidity dependence, and field intercomparison, International Journal of Mass Spectrometry, 207, 167-182, 2001.

Wells, J. R., Schoemaecker, C., Carslaw, N., Waring, M. S., Ham, J. E., Nelissen, I., and Wolkoff, P.: Reactive indoor air chemistry and health—A workshop summary, International Journal of Hygiene and Environmental Health, 220, 1222-1229, 2017.

Weng, M., Zhu, L., Yang, K., and Chen, S.: Levels and health risks of carbonyl compounds in selected public places in Hangzhou, China, J Hazard Mater, 164, 700-706, 2009.

Weschler, C. J.: Changes in indoor pollutants since the 1950s, Atmospheric Environment, 43, 153-169, 2009.

Weschler, C. J.: Ozone in indoor environments: concentration and chemistry, Indoor air, 10, 269-288, 2000.

Weschler, C. J.: Ozone's Impact on Public Health: Contributions from Indoor Exposures to Ozone and Products of Ozone-Initiated Chemistry, Environmental Health Perspectives, 114, 1489-1496, 2006.

Weschler, C. J.: Roles of the human occupant in indoor chemistry, Indoor Air, 26, 6-24, 2016.

Weschler, C. J. and Carslaw, N.: Indoor Chemistry, Environ Sci Technol, 52, 2419-2428, 2018.

Weschler, C. J. and Nazaroff, W. W.: Dermal Uptake of Organic Vapors Commonly Found in Indoor Air, Environmental Science & Technology, 48, 1230-1237, 2014.

Weschler, C. J. and Shields, H. C.: The Influence of Ventilation on Reactions Among Indoor Pollutants: Modeling and Experimental Observations, Indoor Air, 10, 92-100, 2000.

Weschler, C. J. and Shields, H. C.: Production of the hydroxyl radical in indoor air, Environmental Science & Technology, 30, 3250-3258, 1996.

Weschler, C. J., Wisthaler, A., Cowlin, S., Tamás, G., Strøm-Tejsen, P., Hodgson, A. T., Destaillats, H., Herrington, J., Zhang, J., and Nazaroff, W. W.: Ozone-initiated chemistry in an occupied simulated aircraft cabin, Environmental Science & Technology, 41, 6177-6184, 2007.

Whalley, L. K., Stone, D., Bandy, B., Dunmore, R., Hamilton, J. F., Hopkins, J., Lee, J. D., Lewis, A. C., and Heard, D. E.: Atmospheric OH reactivity in central London: observations, model predictions and estimates of in situ ozone production, Atmos. Chem. Phys., 16, 2109-2122, 2016.

White, I. R., Martin, D., Muñoz, M. P., Petersson, F. K., Henshaw, S. J., Nickless, G., Lloyd-Jones, G. C., Clemitshaw, K. C., and Shallcross, D. E.: Use of Reactive Tracers To Determine Ambient OH Radical Concentrations: Application within the Indoor Environment, Environmental Science & Technology, 44, 6269-6274, 2010.

White, M. L., Russo, R. S., Zhou, Y., Mao, H., Varner, R. K., Ambrose, J., Veres, P., Wingenter, O. W., Haase, K., Stutz, J., Talbot, R., and Sive, B. C.: Volatile organic compounds in northern New England marine and continental environments during the ICARTT 2004 campaign, Journal of Geophysical Research, 113, 2008.

Williams, J., Holzinger, R., Gros, V., Xu, X., Atlas, E., and Wallace, D. W. R.: Measurements of organic species in air and seawater from the tropical Atlantic, Geophysical Research Letters, 31, 2004.

Williams, J., Keßel, S. U., Nölscher, A. C., Yang, Y., Lee, Y., Yáñez-Serrano, A. M., Wolff, S., Kesselmeier, J., Klüpfel, T., Lelieveld, J., and Shao, M.: Opposite OH reactivity and ozone cycles in the Amazon rainforest and megacity Beijing: Subversion of biospheric oxidant control by anthropogenic emissions, Atmospheric Environment, 125, 112-118, 2016.

Williams, J., Roberts, J. M., Bertman, S. B., Stroud, C. A., Fehsenfeld, F. C., Baumann, K., Buhr, M. P., Knapp, K., Murphy, P. C., Nowick, M., and Williams, E. J.: A method for the airborne measurement of PAN, PPN, and MPAN, Journal of Geophysical Research: Atmospheres, 105, 28943-28960, 2000.

Wisthaler, A., Tamás, G., Wyon, D. P., Strøm-Tejsen, P., Space, D., Beauchamp, J., Hansel, A., Märk, T. D., and Weschler, C. J.: Products of ozone-initiated chemistry in a simulated aircraft environment, Environmental Science & Technology, 39, 4823-4832, 2005.

Wisthaler, A. and Weschler, C. J.: Reactions of ozone with human skin lipids: sources of carbonyls, dicarbonyls, and hydroxycarbonyls in indoor air, Proceedings of the National Academy of Sciences, 107, 6568-6575, 2010.

Wolkoff, P. and Nielsen, G. D.: Organic compounds in indoor air—their relevance for perceived indoor air quality?, Atmospheric Environment, 35, 4407-4417, 2001.

Yamashita, S., Kume, K., Horiike, T., Honma, N., Masahiro, F., and Amagai, T.: Emission Sources and their Contribution to Indoor Air Pollution by Carbonyl Compounds in a School and a Residential Building in Shizuoka, Japan, Indoor and Built Environment, 21, 392-402, 2011.

Yáñez-Serrano, A. M., Nölscher, A. C., Williams, J., Wolff, S., Alves, E., Martins, G. A., Bourtsoukidis, E., Brito, J., Jardine, K., Artaxo, P., and Kesselmeier, J.: Diel and seasonal changes of biogenic volatile organic compounds within and above an Amazonian rainforest, Atmospheric Chemistry and Physics, 15, 3359-3378, 2015.

Yang, M., Beale, R., Liss, P., Johnson, M., Blomquist, B., and Nightingale, P.: Air–sea fluxes of oxygenated volatile organic compounds across the Atlantic Ocean, Atmospheric Chemistry and Physics, 14, 7499-7517, 2014.

Yang, X., Xue, L., Yao, L., Li, Q., Wen, L., Zhu, Y., Chen, T., Wang, X., Yang, L., Wang, T., Lee, S., Chen, J., and Wang, W.: Carbonyl compounds at Mount Tai in the North China Plain: Characteristics, sources, and effects on ozone formation, Atmospheric Research, 196, 53-61, 2017a.

Yang, Y., Shao, M., Keßel, S., Li, Y., Lu, K., Lu, S., Williams, J., Zhang, Y., Zeng, L., Nölscher, A. C., Wu, Y., Wang, X., and Zheng, J.: How the OH reactivity affects the ozone production efficiency: case studies in Beijing and Heshan, China, Atmos. Chem. Phys., 17, 7127-7142, 2017b.

Yang, Y., Shao, M., Wang, X., Nölscher, A. C., Kessel, S., Guenther, A., and Williams, J.: Towards a quantitative understanding of total OH reactivity: A review, Atmospheric Environment, 134, 147-161, 2016.

Yang, Z., Cheng, H. R., Wang, Z. W., Peng, J., Zhu, J. X., Lyu, X. P., and Guo, H.: Chemical characteristics of atmospheric carbonyl compounds and source identification of formaldehyde in Wuhan, Central China, Atmospheric Research, 228, 95-106, 2019.

Young, C. J., Zhou, S., Siegel, J. A., and Kahan, T. F.: Illuminating the dark side of indoor oxidants, Environ Sci Process Impacts, 21, 1229-1239, 2019.

Yuan, B., Koss, A. R., Warneke, C., Coggon, M., Sekimoto, K., and de Gouw, J. A.: Proton-Transfer-Reaction Mass Spectrometry: Applications in Atmospheric Sciences, Chem Rev, 117, 13187-13229, 2017.

Yuan, B., Shao, M., Lu, S., and Wang, B.: Source profiles of volatile organic compounds associated with solvent use in Beijing, China, Atmospheric Environment, 44, 1919-1926, 2010.

Zannoni, N., Dusanter, S., Gros, V., Sarda Esteve, R., Michoud, V., Sinha, V., Locoge, N., and Bonsang, B.: Intercomparison of two comparative reactivity method instruments inf the Mediterranean basin during summer 2013, Atmospheric Measurement Techniques, 8, 3851-3865, 2015.

Zannoni, N., Gros, V., Lanza, M., Sarda, R., Bonsang, B., Kalogridis, C., Preunkert, S., Legrand, M., Jambert, C., Boissard, C., and Lathiere, J.: OH reactivity and concentrations of biogenic volatile organic compounds in a Mediterranean forest of downy oak trees, Atmospheric Chemistry and Physics, 16, 1619-1636, 2016.

Zannoni, N., Gros, V., Sarda Esteve, R., Kalogridis, C., Michoud, V., Dusanter, S., Sauvage, S., Locoge, N., Colomb, A., and Bonsang, B.: Summertime OH reactivity from a receptor coastal site in the Mediterranean Basin, Atmos. Chem. Phys., 17, 12645-12658, 2017.

Zhang, J., Lioy, P. J., and He, Q.: Characteristics of aldehydes: concentrations, sources, and exposures for indoor and outdoor residential microenvironments, Environmental Science & Technology, 28, 146-152, 1994.

Zhou, S., Forbes, M. W., and Abbatt, J. P.: Kinetics and Products from Heterogeneous Oxidation of Squalene with Ozone, Environ Sci Technol, 50, 11688-11697, 2016a.

Zhou, S., Forbes, M. W., Katrib, Y., and Abbatt, J. P. D.: Rapid Oxidation of Skin Oil by Ozone, Environmental Science & Technology Letters, 3, 170-174, 2016b.

Zhou, S., Gonzalez, L., Leithead, A., Finewax, Z., Thalman, R., Vlasenko, A., Vagle, S., Miller, L. A., Li, S. M., Bureekul, S., Furutani, H., Uematsu, M., Volkamer, R., and Abbatt, J.: Formation of gas-phase carbonyls from heterogeneous oxidation of polyunsaturated fatty acids at the air–water interface and of the sea surface microlayer, Atmospheric Chemistry and Physics, 14, 1371-1384, 2014.

Zhou, S., Joudan, S., Forbes, M. W., Zhou, Z., and Abbatt, J. P. D.: Reaction of Condensed-Phase Criegee Intermediates with Carboxylic Acids and Perfluoroalkyl Carboxylic Acids, Environmental Science & Technology Letters, 6, 243-250, 2019.

Zhou, X. and Mopper, K.: Photochemical production of low-molecular-weight carbonyl compounds in seawater and surface microlayer and their air-sea exchange, Marine Chemistry, 56, 201-213, 1997.

Chapter 2. Measurements of carbonyl compounds around the Arabian Peninsula: overview and model comparison

The entire chapter has been published as:

Wang, N., Edtbauer, A., Stönner, C., Pozzer, A., Bourtsoukidis, E., Ernle, L., Dienhart, D., Hottmann, B., Fischer, H., Schuladen, J., Crowley, J. N., Paris, J.-D., Lelieveld, J., and Williams, J.: Measurements of carbonyl compounds around the Arabian Peninsula: overview and model comparison, Atmospheric Chemistry and Physics, 20, 10807-10829**.**

Contribution to this publication by Nijing Wang: helped with the measurements during the second leg of the campaign; conducted data analysis including results overview, case studies and model comparison; drafted the entire article and is the corresponding author of the publication.

Abstract

Volatile organic compounds (VOCs) were measured around the Arabian Peninsula using a research vessel during the AQABA campaign (Air Quality and Climate Change in the Arabian Basin) from June to August 2017. In this study we examine carbonyl compounds, measured by a proton transfer reaction mass spectrometer (PTR-ToF-MS), and present both a regional concentration distribution and a budget assessment for these key atmospheric species. Among the aliphatic carbonyls, acetone had the highest mixing ratios in most of the regions traversed, varying from 0.43 ppb over the Arabian Sea to 4.5 ppb over the Arabian Gulf, followed by formaldehyde (measured by a Hantzsch monitor, 0.82 ppb over the Arabian Sea and 3.8 ppb over the Arabian Gulf) and acetaldehyde (0.13 ppb over the Arabian Sea and 1.7 ppb over the Arabian Gulf). Unsaturated carbonyls (C_4–C_9) varied from 10 to 700 ppt during the campaign and followed similar regional mixing ratio dependence to aliphatic carbonyls, which were identified as oxidation products of cycloalkanes over polluted areas. We compared the measurements of acetaldehyde, acetone, and methyl ethyl ketone to global chemistry-transport model (ECHAM5/MESSy Atmospheric Chemistry – EMAC) results. A significant discrepancy was found for acetaldehyde, with the model underestimating the measured acetaldehyde mixing ratio by up to an order of magnitude. Implementing a photolytically driven marine source of acetaldehyde significantly improved the agreement between measurements and model, particularly over the remote regions (e.g. Arabian Sea). However, the newly introduced acetaldehyde source was still insufficient to describe the observations over the most polluted regions (Arabian Gulf and Suez), where model underestimation of primary emissions and biomass burning events are possible reasons.

2.1 Introduction

Carbonyl compounds (aldehydes and ketones) can be released into the air directly from a variety of primary biogenic and anthropogenic sources. These include biomass burning (Holzinger et al., 1999, 2005; Koss et al., 2018), fossil fuel combustion (Reda et al., 2014; Huang et al., 2018) including vehicles (Erickson et al., 2014; Dong et al., 2014), industrial solvent use (Kim et al., 2008), and natural sources including plants and plankton (Zhou and Mopper, 1997;Warneke et al., 1999; Jacob et al., 2002; Fall, 2003; Williams et al., 2004; Bourtsoukidis et al., 2014). However, secondary production via the atmospheric oxidation of hydrocarbons is considered to be more important for many carbonyl compounds including acetone and acetaldehyde (Jacob et al., 2002; Millet et al., 2010).

Carbonyls have several important roles in the atmosphere. They form as stable intermediates directly after hydrocarbon oxidation by hydroxyl radicals, O_3, or NO_3 when the peroxy radicals initially formed react with each other (permutation reactions) or with NO. Their production is linked to tropospheric ozone formation (Carlier et al., 1986), and their loss, through oxidation and photolysis, is an important source of hydroxyl and hydroperoxyl radicals (HO_x) in the dry upper troposphere (Colomb et al., 2006). Carbonyls serve as precursors of peroxyacetyl nitrates (PANs), which are important atmospheric NOx (NO and NO2/ reservoir species (Finlayson-Pitts and Pitts, 1997; Edwards et al., 2014; Williams et al., 2000). Carbonyl compounds are also important for the growth of atmospheric particles (Kroll et al., 2005), thereby indirectly impacting the Earth's radiative balance. The atmospheric lifetimes of carbonyl compounds vary considerably, from less than 1 d for acetaldehyde (Millet et al., 2010) to more than 15 d for acetone (Jacob et al., 2002; Khan et al., 2015) in terms of tropospheric mean lifetime. A multi-day lifetime means that carbonyl compounds can impact the air chemistry on local, regional, and even hemispheric scales. The numerous primary and secondary sources of carbonyl compounds as well as their multiple loss routes (photolysis, OH, NO3, and O3 oxidation) make budget assessments difficult.

The most predominant atmospheric carbonyl compounds besides formaldehyde are acetaldehyde and acetone. They have been reported to vary from tens or hundreds of ppt in remote areas (Warneke and de Gouw, 2001;Wisthaler, 2002; Lewis et al., 2005; White et al., 2008; Colomb et al., 2009; Read et al., 2012; Sjostedt et al., 2012; Tanimoto et al., 2014; Yang et al., 2014; Hornbrook et al., 2016; Wang et al., 2019) to several ppb in urban and polluted areas (Dolgorouky et al., 2012; Guo et al., 2013; Stoeckenius and McNally, 2014; Koss et al., 2015; Sahu et al., 2017; Sheng et al., 2018). Generally, secondary photochemical formation from various precursors is the main source of those carbonyl compounds. However, several recent studies have shown that acetaldehyde mixing ratios in both the remote marine boundary layer and the free troposphere could not be explained by known photochemistry as implemented in various atmospheric chemistry

models, which consistently underestimated the measurements by an order of magnitude or more (Singh et al., 2003; Read et al., 2012; Wang et al., 2019). Several potential additional acetaldehyde sources have been proposed, including new hydrocarbon oxidation mechanisms, aerosol-related sources, and oceanic sources. One possible source of acetaldehyde in the remote marine boundary layer is oceanic emission from the photodegradation of coloured dissolved organic matter (CDOM) in sea-surface water, where acetaldehyde could be produced together with other low-molecular-weight carbonyl compounds (Kieber et al., 1990; Zhou and Mopper, 1997; Sinha et al., 2007; Dixon et al., 2013). Nevertheless, due to both limited airborne and seawater measurements of acetaldehyde, the importance of oceanic emission is still under debate (Millet et al., 2010;Wang et al., 2019). In order to better understand the atmospheric budgets of acetaldehyde (and the other carbonyl compounds), it is informative to analyze a dataset of multiple carbonyl compounds in both polluted and clean environments, with influence from marine emissions, varying particulate loadings, and high rates of oxidation as shown in Figure 2.1, which demonstrates the main formation pathways of acetaldehyde during this campaign.

During the AQABA (Air Quality and Climate Change in the Arabian Basin) shipborne research campaign, carbonyl compounds were continuously measured by PTR-ToF-MS onboard a research vessel that circumnavigated the Arabian Peninsula. During the campaign, chemically distinct air masses were sampled, which had been influenced by primary emissions of hydrocarbons and inorganic pollutants (NO_x, SO_2, and CO) from petroleum industries and marine transport (Bourtsoukidis et al., 2019; Celik et al., 2019), by pollution from urban areas (Pfannerstill et al., 2019), and clean marine-influenced air (Edtbauer et al., 2020). It is a unique dataset of carbonyl compounds encompassing starkly different environmental conditions from a region with few (or no) available in situ measurements to date.

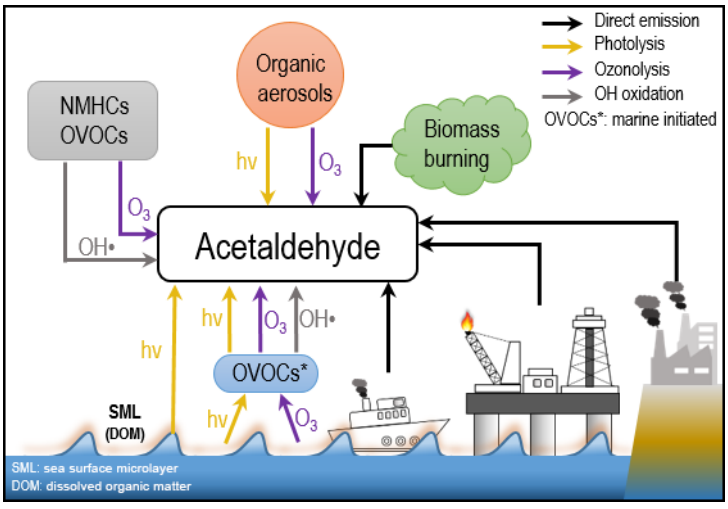

Figure 2.1. Diagram of possible sources and formation pathways of acetaldehyde during the AQABA campaign.

In this study, we provide an overview of carbonyl compound mixing ratios (aliphatic, unsaturated, and aromatic) over the Mediterranean Sea, Suez, Red Sea, Arabian Sea, and Arabian Gulf. Using an empirical method based on measured hydrocarbon precursors, we have analyzed the relative importance of the photochemical sources of the carbonyl compounds observed. The analysis is then extended to include sources and transport by using an EMAC global model (5th generation European Centre – Hamburg general model, ECHAM5, coupled to the modular earth submodel system, MESSy, applied to atmospheric chemistry). Model measurement differences are investigated in both clean and polluted regions, with particular emphasis on acetaldehyde.

2.2 Method

2.2.1 AQABA campaign

The AQABA campaign was conducted onboard R/V *Kommandor Iona* (KI) from the end of June to the end of August 2017. The ship started from southern France, proceeded across the Mediterranean, through the Suez Canal, around the Arabian Peninsula into the Arabian Gulf and on to Kuwait, thereafter returning along the same route. Five laboratory containers were loaded onto the vessel, containing multiple gas- and particle-phase measurement instruments as well as a weather station.

2.2.2 PTR-ToF-MS

2.2.2.1 Sampling and instrument set-up

A high-flow inlet (stainless steel tubing, 0.2 m diameter, 5.5 m tall and 3 m above the top of the containers and the front deck) was installed at the front of the ship where the laboratory containers were located. A high flow of air (approximately 10 $m^3 min^{-1}$) was drawn through the inlet which provided a common attachment point for sub-sampling lines for all gas-phase measurement instruments. An air flow of 5 standard L min^{-1} for the first leg and 3.5 standard L min^{-1} for the second leg was pumped into the onboard lab container through an ½" (O.D. = 1.27cm) FEP (fluorinated ethylene propylene) tubing (about 10 m long) insulated and heated to 50-60 °C. A PTFE (polytetrafluoroethylene) filter was placed at the beginning of the inlet to prevent insects, dust, and particles from entering the instruments. Every 2-5 days, the filter was replaced depending on the degree of pollution encountered. Inside the volatile organic compound (VOC) instrument container, the PTR-ToF-MS (8000, Ionicon Analytik GmbH Innsbruck, Austria) sampled a sub-flow at 80-100 sccm through 1/8" (0.3175 cm) FEP tubing (~ 10 m in length, insulated and heated to 60 °C) from the main fast air flow and then to the instrument's PEEK (polyether ether ketone) inlet which was likewise heated to 60 °C. The inlet system was shared with total OH reactivity measurement (Pfannerstill et al., 2019).

The working principle of PTR-MS has been described in detail in previous studies (Lindinger et al., 1998;Ellis and Mayhew, 2013;Yuan et al., 2017). In brief, H_3O^+ primary ions are generated in the ion source, and then drawn into the drift tube where they interact with sampled ambient air. Inside the drift tube, VOCs with a proton affinity greater than that of H_2O (691 kJ mol^{-1}) are protonated by proton transfer from H_3O^+. The resulting secondary ions are transferred to the detector, in this case a time-of-flight mass spectrometer with mass resolution around 3500 for the first leg and 4500 for the second leg at mass 96amu. An internal standard of trichlorobenzene ($C_6H_3Cl_3$) was continuously introduced into the instrument to ensure accurate mass calibration. Every minute a spectrum with mass range (m/z) 0-450 was generated. The data reported in this study are all at 1 minute resolution unless otherwise specified.

2.2.2.2 Instrument characterization

The instrument background was determined every 3h for 10 minutes with synthetic air. Four-point calibrations were performed five times during the whole campaign using a standard gas mixture (Apel-Riemer Environmental inc., Broomfield, USA) containing 14 compounds (methanol, acetonitrile, acetaldehyde, acetone, dimethyl sulfide, isoprene, methyl vinyl ketone, methacrolein, methyl ethyl ketone, benzene, toluene, xylene, 1,3,5-trimethylbenzene and α-pinene). It has been previously reported that the sensitivities of some compounds measured by PTR-MS are humidity dependent (de Gouw and Warneke, 2007). As the relative humidity (RH) was expected to be high and varying (marine boundary layer with occasional desert air influence), humidity calibration was combined with four-point calibration by humidifying the gas mixture at different levels from 0% to 100% RH.

2.2.2.3 Data analysis

The data were initially processed by the PTR Analyzer software (Müller et al., 2013) to identify and integrate the peaks. After obtaining the raw data (counts per second for each mass identified), a custom-developed python-based program was used to further process the data to final mixing ratios. For compounds present in the standard gas cylinder, interpolated sensitivities based on the five in-campaign calibrations were applied to derive the mixing ratios; while mixing ratios of the other masses were calculated by using a proton transfer reaction rate constant (k_{PTR}) of 2.0×10^{-9} cm^3 s^{-1}. The uncertainty associated with the mixing ratios of the calibrated compounds was around 6-17% (see Table S2.1). For the mixing ratios derived by assuming k_{PTR}, the accuracy was around ±50% (Zhao and Zhang, 2004). The detection limit (LOD) was calculated from the background measurement with 3 times the standard deviation (3σ), 52 ± 26 ppt for acetaldehyde, 22 ± 9 ppt for acetone and 9 ± 6 ppt for methyl ethyl ketone (MEK) (Table S2.1). Data below LOD were kept as determined for further statistical analysis (Figure 2.1 and Table 2.1).

In this study, we have interpreted ion masses with the exact masses corresponding to $C_nH_{2n}O$, $C_nH_{2n-2}O$ and $C_nH_{2n-8}O$ as aliphatic, unsaturated and aromatic carbonyls, respectively (see the exact protonated m/z in Table S2.2). Carbonyl compounds with a carbon number of three and above can be either aldehydes or ketones, which are not distinguishable with PTR-ToF-MS using H_3O^+ as the primary ion. However, laboratory experiments have shown that protonated aldehydic ions with carbon atoms more than three tend to lose a H_2O molecule and fragment to other masses (Buhr et al., 2002;Spanel et al., 2002). Moreover, although both ketones and aldehydes can be produced via atmospheric oxidation processes, ketones tend to have longer atmospheric lifetimes and higher photochemical yields than aldehydes as mentioned in the introduction. The ratio of measured propanal to acetone was 0.07 in the western Pacific coastal region (Schlundt et al., 2017), 0.06 in urban Los Angeles (Borbon et al., 2013) and 0.17 - 0.22 in oil and gas production regions (summarized by Koss et al., 2017). Therefore, signals on the exact mass of carbonyl compounds from the PTR-ToF-MS are expected to be dominated by ketones, particularly in regions remote from the sources.

2.2.3 Meteorological data and other trace gases

The meteorological data were obtained by using a commercial weather station (Sterela) which monitored wind speed, wind direction, RH, temperature, speed of the vessel, GPS, etc. The actinic flux was measured by a spectral radiometer (Metcon GmbH; Meusel et al., 2016). Non-methane hydrocarbons (NMHC) mixing ratios were measured by a gas chromatograph with a flame ionization detector (GC−FID) online with a time resolution of 50 minutes. It measured hydrocarbons (C2-C8) and aromatics (C6-C8) with an average LOD < 10 ppt for most of the compounds. For a detailed instrumental description see Bourtsoukidis et al. (2019). Formaldehyde mixing ratios were determined by a modified and optimized version of the commercially available AL4021 (Aero-Laser, Germany), which utilizes the Hantzsch technique (Stickler et al., 2006). Methane and carbon monoxide (CO) levels were monitored by a cavity ring-down spectroscopy analyzer (Picarro G2401). Ozone was measured with an absorption photometer (Model 202 Ozone Monitor, 2B Technologies, Boulder, Colorado). Due to the potential interference from sampling our own ship exhaust in which carbonyl compounds may be present (Reda et al., 2014), a filter was applied to the dataset based on the wind direction and NO_x, SO_2 and ethene levels.

2.2.4 Model simulations

The EMAC model was used to simulate atmospheric mixing ratios of several carbonyl compounds along the cruise track covered during the AQABA campaign. The EMAC model is an atmospheric chemistry-general circulation model simulating the process of tropospheric air by considering processes which could influence trace-gas mixing ratios, such as transport, chemistry, interaction with ocean/land, and dry deposition (Pozzer et al., 2007;Pozzer et al., 2012;Lelieveld et al., 2016).

The model applied in this study is a combination of the 5th generation of the European Centre Hamburg general circulation model (ECHAM5) (Roeckner et al., 2006) and the 2nd version of the Modular Earth Submodel System (MESSy2) (Jöckel et al., 2010), where a comprehensive chemistry mechanism MOM (Mainz Organic Mechanism) was deployed (Sander et al., 2019). The model considers direct emissions (such as anthropogenic, biogenic, biomass burning.), atmospheric transport and mixing, photochemical production of carbonyls (by OH, O_3 and NO_3), as well as physical and chemical removal processes. The global fire assimilation system was used for biomass burning emissions (Kaiser et.al., 2012). The exchange of organic compounds between ocean and atmosphere was considered in EMAC via the AIRSEA submodel, described in detail in Pozzer et al. (2006). The transfer velocity is calculated online and the concentration in the water is prescribed by the user. For acetone, a constant water concentration of 15 nmol/L is used, following the suggestion of Fischer et al. (2012). The model configuration in the study is the same as the model applied in Bourtsoukidis et al. (2020), where a natural non-methane hydrocarbon source (ethane and propane) was implemented. The model is at the resolution of T106L31 (i.e. ~ $1.1^o \times 1.1^o$ horizontal resolution and , 31 vertical hybrid pressure levels up to 10 hPa) and the time resolution of 10 minutes. The measurement data of PTR-ToF-MS were averaged to 10-minute resolution to match the model data resolution for further comparison.

2.3 Results and discussion

Around the Arabian Peninsula, the mixing ratios of individual carbonyl compounds varied over a wide range, from tens of ppt to ppb levels. In this study, we divided the dataset geographically into eight regions (Figure 2.2, middle graph) to classify and characterize the primary and secondary origins of carbonyl compounds. The regional delineations were: the Mediterranean Sea (MS), Suez, Red Sea North (RSN), Red Sea South (RSS), Gulf of Aden (GA), Arabian Sea (AS), Gulf of Oman (GO) and Arabian Gulf (AG), the same as those described by Bourtsoukidis et al. (2019). Figure 2.2 shows the abundance of aliphatic, aromatic and unsaturated carbonyl compounds (carbonyls) for each region. Generally, aliphatic carbonyls were present at much higher mixing ratios than aromatic and unsaturated carbonyls, with smaller carbonyl compounds (formaldehyde, acetaldehyde, C3 and C4 carbonyls) dominating the distribution. The mixing ratios of aliphatic carbonyls decreased dramatically from C5 carbonyls with increasing carbon number. The box plots (Figure 2.2) also show that carbonyl compounds were measured at higher mixing ratios and were more variable over the Suez region and the Arabian Gulf. The abundance of carbonyl compounds varied markedly from region to region, with the highest and lowest values found in the Arabian Gulf and the Arabian Sea, respectively. Table 2.1 shows the mean, standard deviation and the median values for carbonyls in each region. In the following sections, each class of carbonyl compounds is investigated in greater detail.

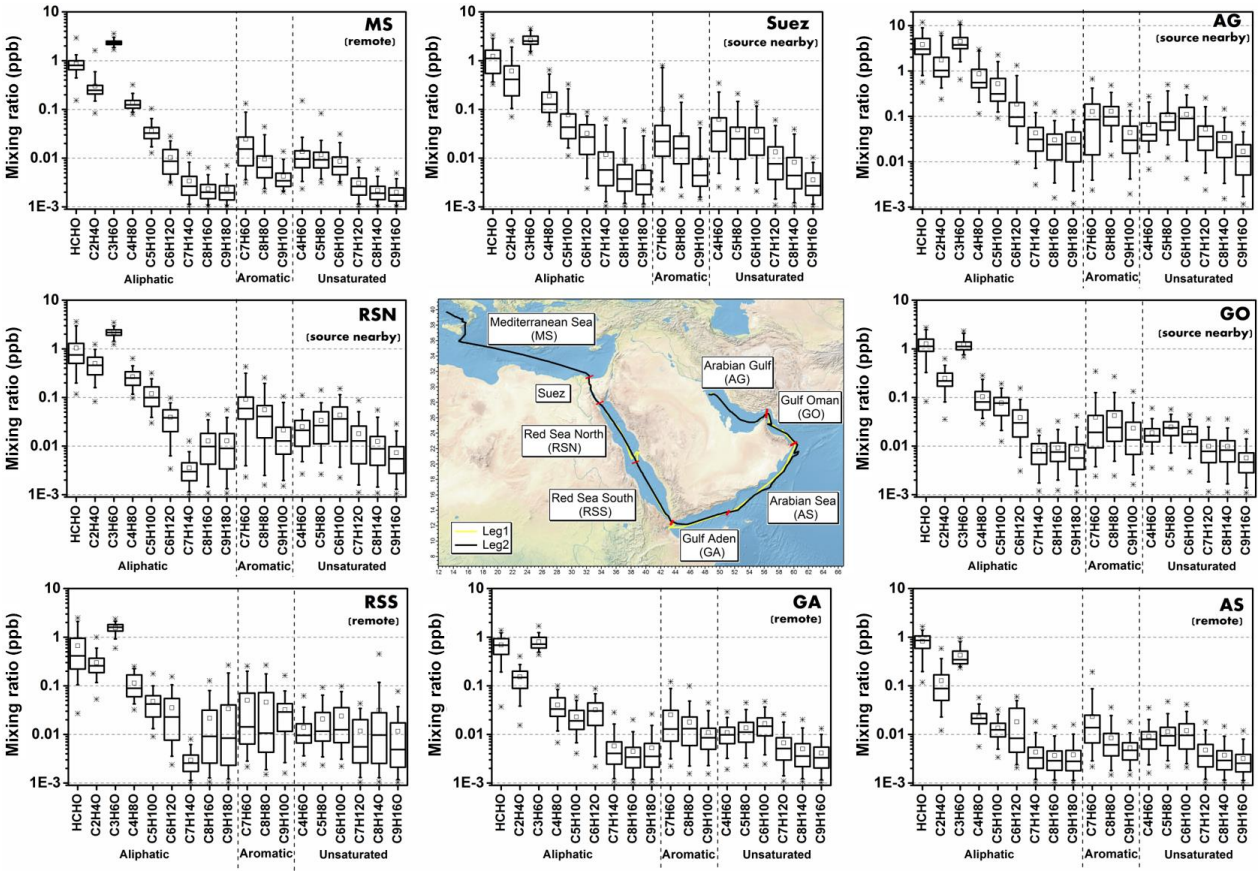

Figure 2.2. Overview of mixing ratios for aliphatic, aromatic, and unsaturated carbonyl compounds (CxHyO). The boxes represent 25% to 75% of the data, with the central line and square indicating the median and the mean values, respectively. The whiskers show data from 5% to 95%, and stars were drawn for the minimum and maximum data points within 1% to 99% of the dataset. Within brackets under the region acronyms the main characteristics of the air masses are indicated, based on non-methane hydrocarbon variability-lifetime results (b factor) from Bourtsoukidis et al. (2019). The data used for map plotting were from public domain GIS data found on the Natural Earth website (http://www.naturalearthdata.com, last access: 23 January 2019) and ere read into Igor using the IgorGIS XOP beta.

2.3.1 Aliphatic carbonyls ($C_nH_{2n}O$)

2.3.1.1 Overview

Relatively high mean mixing ratios of aliphatic carbonyls were observed over the Arabian Gulf, the highest being acetone (C3 carbonyl compound) at 4.50 ± 2.40 ppb (median: 3.77 ppb), followed by formaldehyde at 3.83 ± 2.55 ppb (median: 3.02 ppb), acetaldehyde at 1.73 ± 1.61 ppb (median: 1.02 ppb) and MEK (C4 carbonyl compound) at 0.87 ± 0.71 ppb (median: 0.56 ppb). As the Arabian Gulf is highly impacted by the oil and gas industry, we compared the measurements of the four aforementioned carbonyl compounds with those measured in the oil and gas region (Table 2.2). Except for formaldehyde, acetaldehyde, acetone and MEK were lower than the mixing ratios measured in the Uintah Basin, which was influenced by intensive oil and natural gas activities

(Koss et al., 2015). The general distribution of the aliphatic carbonyls in the Uintah Basin is similar to the Arabian Gulf, with acetone levels being approximately twice those of acetaldehyde. The carbonyl mixing ratios in the Arabian Gulf were comparable to those measured in Hickory (PA, USA) surrounded by natural gas wells (Swarthout et al., 2015). Koss et al. (2017) reported the maximum boundary layer enhancement of carbonyl compounds (C2-C7) measured during an aircraft measurement above the most productive oil field in the United States (Permian Basin). Within the boundary layer of the Permian Basin, C5-C7 aliphatic carbonyls had mixing ratios of 0.34 ppb, 0.08 ppb and 0.03 ppb, which are of the same magnitude but lower than the levels measured over the Arabian Gulf for C5 (0.52 ± 0.48 ppb), C6 (0.19 ± 0.25ppb), and C7 (0.04 ± 0.04 ppb) carbonyl compounds. The sources of the major carbonyls in the Arabian Gulf will be discussed in detail in section 3.1.2 and 3.4.3.

In contrast, aliphatic carbonyls had much lower average mixing ratios over the Arabian Sea and the Gulf of Aden especially for C7-C9 carbonyls with mean mixing ratios below the detection limit for most of the time. During the summertime AQABA campaign, the prevailing wind direction over the Arabian Sea was south-west (Figure S 2.1). Four-day back trajectories indicate the air was transported from the Arabian Sea (north-western Indian Ocean), passing the eastern Africa coast, which brought relatively clean, photochemically aged air masses (Bourtsoukidis et al., 2019). The mean level of acetone over the Arabian Sea (0.43 ± 0.18 ppb, median: 0.34 ppb) is close to the level measured in the marine boundary layer of the western Indian Ocean (0.49 ppb) (Warneke and de Gouw, 2001) and comparable to other reported values from open-sea air measurement (see Table 2.2). Acetaldehyde was measured at relatively low mixing ratios over the Arabian Sea (0.13 ± 0.12 ppb, median: 0.09 ppb), which is comparable than the levels reported by the measurements done in the Northern Hemisphere open ocean (see Table 2.2). Over the Gulf of Aden, acetaldehyde, acetone and MEK had slightly higher mixing ratios than those over the Arabian Sea.

The Mediterranean Sea had somewhat higher levels of aliphatic carbonyls than the clean regions (the Arabian Sea and the Gulf of Aden) but with acetone (above 2ppb) dominating the distribution. A much higher acetone level than the acetaldehyde level was also observed for coastal site measurements, which were impacted by continental air (White et al., 2008; Schlundt et al., 2017; see Table 2.2). Larger aliphatic carbonyls (C6-C9) were below the detection limit most of the time. The aliphatic carbonyl levels over the Gulf of Oman were higher than the clean regions, while C1-C5 carbonyls were more variable over the Gulf of Oman compared to those over the Mediterranean Sea. This is probably because the Gulf of Oman connects to the Arabian Gulf where intense oil and gas industrial activities are located. Over the Gulf of Oman, polluted air from the nearby sources of the Arabian Gulf is occasionally mixed with the clean air from the open sea (the Arabian Sea) under south-easterly wind conditions (Figure S2.1).

Another region where abundant aliphatic carbonyls were observed was the Suez region. The air in this region was mainly influenced by nearby cities and marine transportation (ship emissions within the Suez Canal) (Bourtsoukidis et al., 2019;Pfannerstill et al., 2019). Therefore abundant precursors were available in the Suez region, producing more carbonyls regionally, especially for shorter-lived compounds (formaldehyde and acetaldehyde). Besides the local-scale emissions and photochemical production contribution to the carbonyls over the Suez, the longer-lived carbonyls (e.g. acetone) could also be transported from the Mediterranean Sea (where acetone was high). Four-day back trajectories indicate the air reaching the Suez region mostly originated from the European continent, passing over the Mediterranean Sea (Bourtsoukidis et al., 2019). Meanwhile, ocean uptake of acetone from the air due to polluted continental outflow (Marandino et al., 2005) as well as dilution and mixing with free tropospheric air during transport can modulate acetone mixing ratios. Although the mean mixing ratios of aliphatic carbonyls over the Suez were much lower than those over the Arabian Gulf, the variations were still more significant than other regions (not including the Arabian Gulf; see Table 2.1).

Over the Red Sea, acetone was the most abundant aliphatic carbonyl, followed by formaldehyde and acetaldehyde. The mixing ratios of acetaldehyde and acetone over the northern part of the Red Sea were similar to those levels measured in western Pacific coastal regions (South China Sea, Table 2.2). It is worth noticing that the levels of aliphatic carbonyls in the northern part of the Red Sea were almost 2 times higher than the southern part of the Red Sea. According to the 4 d back trajectories reported by Bourtsoukidis et al. (2019), the measured air masses that travelled to the northern part were from southern Europe and north-eastern Africa, while the southern part was more influenced by air from the northern part of the Red Sea mixed with the air masses from desertic areas of central Africa. Therefore, fewer primary precursors as well as carbonyls were transported to the souhtern part of the Red Sea compared to the northern part. Moreover, the unexpected sources of hydrocarbons (ethane and propane) from northern Red Sea deep water reported by Bourtsoukidis et al. (2020) would lead to higher carbonyl levels in the northen part compared with the sourthern part due to the additional precursors in the Red Sea North. However, acetaldehyde was still found to be significantly underestimated compared to the model results, even taking the deep-water source into consideration (section 3.3). This indicates that extra sources of acetaldehyde may exist, which will be discussed in detail in section 3.4.

Table 2.1. Mean, standard deviation (SD) and median mixing ratios of aliphatic, unsaturated and aromatic carbonyls in different regions.

		Aliphatic Carbonyls								
		HCHO	CH3CHO	C3H6O	C4H8O	C5H10O	C6H12O	C7H14O	C8H16O	C9H18O
MS	mean	0.86	0.30	2.37	0.14	0.04	0.01	< LOD	< LOD	< LOD
	SD	0.41	0.25	0.37	0.05	0.02	0.01	NA	NA	NA
	median	0.80	0.25	2.32	0.12	0.03	0.01	< LOD	< LOD	< LOD
Suez	mean	1.23	0.62	2.64	0.19	0.08	0.03	0.01	0.01	0.01
	SD	0.76	0.58	0.77	0.15	0.08	0.02	0.01	0.01	0.01
	median	1.11	0.41	2.52	0.13	0.04	0.03	< LOD	< LOD	< LOD
RSN	mean	0.99	0.50	2.17	0.27	0.12	0.04	< LOD	0.01	0.01
	SD	0.78	0.26	0.45	0.11	0.07	0.02	NA	0.01	0.01
	median	0.73	0.46	2.17	0.25	0.10	0.04	< LOD	0.01	0.01
RSS	mean	0.66	0.29	1.56	0.11	0.05	0.03	< LOD	0.02	0.03
	SD	0.62	0.17	0.38	0.06	0.03	0.03	NA	0.03	0.05
	median	0.40	0.25	1.60	0.09	0.04	0.02	< LOD	< LOD	< LOD
GA	mean	0.69	0.15	0.81	0.04	0.02	0.03	0.01	< LOD	< LOD
	SD	0.33	0.09	0.27	0.02	0.01	0.02	0.01	NA	NA
	median	0.68	0.15	0.72	0.03	0.02	0.03	< LOD	< LOD	< LOD
AS	mean	0.82	0.13	0.43	0.02	0.01	0.01	< LOD	< LOD	< LOD
	SD	0.35	0.12	0.18	0.01	0.01	0.02	NA	NA	NA
	median	0.86	0.09	0.34	0.02	0.01	0.01	< LOD	< LOD	< LOD
GO	mean	1.27	0.25	1.23	0.10	0.08	0.04	0.01	0.01	0.01
	SD	0.59	0.12	0.40	0.06	0.04	0.03	0.00	0.01	0.01
	median	1.13	0.22	1.12	0.08	0.08	0.03	0.01	0.01	0.01
AG	mean	3.83	1.73	4.50	0.87	0.52	0.19	0.04	0.03	0.03
	SD	2.55	1.61	2.40	0.71	0.48	0.25	0.04	0.03	0.03
	median	3.02	1.02	3.77	0.56	0.31	0.10	0.03	0.02	0.02

Table 2.1 Continued

		Aromatic Carbonyls			Unsaturated Carbonyls					
		C7H6O	C8H8O	C9H10O	C4H6O	C5H8O	C6H10O	C7H12O	C8H14O	C9H16O
MS	mean	0.02	0.01	< LOD	0.01	0.01	0.01	< LOD	< LOD	< LOD
	SD	0.03	0.01	NA	0.02	0.01	0.01	NA	NA	NA
	median	0.02	0.01	< LOD	0.01	0.01	0.01	< LOD	< LOD	< LOD
Suez	mean	0.09	0.03	< LOD	0.06	0.04	0.03	0.01	0.01	< LOD
	SD	0.20	0.04	NA	0.08	0.04	0.03	0.01	0.01	NA
	median	0.02	0.01	< LOD	0.04	0.02	0.02	0.01	< LOD	< LOD
RSN	mean	0.09	0.05	0.02	0.03	0.03	0.04	0.02	0.01	0.01
	SD	0.10	0.06	0.02	0.02	0.03	0.04	0.02	0.01	0.01
	median	0.06	0.04	0.01	0.02	0.03	0.03	0.01	0.01	< LOD
RSS	mean	0.05	0.04	0.03	0.01	0.02	0.02	0.01	0.03	0.01
	SD	0.06	0.06	0.03	0.01	0.02	0.02	0.01	0.07	0.01
	median	0.01	0.01	0.03	0.01	0.01	0.01	< LOD	< LOD	< LOD
GA	mean	0.02	0.02	0.01	0.01	0.01	0.02	0.01	< LOD	< LOD
	SD	0.03	0.02	0.01	0.01	0.01	0.01	0.01	NA	NA
	median	0.01	0.01	0.01	0.01	0.01	0.01	< LOD	< LOD	< LOD
AS	mean	0.02	0.01	< LOD	0.01	0.01	0.01	< LOD	< LOD	< LOD
	SD	0.03	0.01	NA	0.01	0.01	0.01	NA	NA	NA
	median	0.01	0.01	< LOD	0.01	0.01	0.01	< LOD	< LOD	< LOD
GO	mean	0.04	0.04	0.02	0.02	0.02	0.02	0.01	0.01	0.01
	SD	0.06	0.05	0.03	0.01	0.01	0.01	0.01	0.01	NA
	median	0.02	0.02	0.01	0.02	0.02	0.02	0.01	0.01	< LOD
AG	mean	0.12	0.13	0.04	0.07	0.11	0.12	0.05	0.03	0.02
	SD	0.14	0.10	0.04	0.06	0.10	0.10	0.05	0.03	0.02
	median	0.08	0.10	0.03	0.04	0.07	0.09	0.04	0.03	0.01

< LOD: the mixing ratios were lower than the limit of detection. NA: not available.

Table 2.2. Mixing ratios (ppb) of OVOCs reported in previous observation in the literature

Locations	Lon./Lat.	Height	Time	Technique	Formal-dehyde	Acetal-dehyde	Acetone	MEK	Literature
Open sea		m							
Tropical Atlantic Ocean	10◦ N-0◦ N 35◦ W-5◦ E	18	Oct.-Nov.	PTR-MS	n.r.	n.r.	0.53	n.r.	(Williams et al., 2004)
Atlantic Ocean	50◦ N-50◦ S 10-60◦ W	18	Oct.-Nov.	PTR-MS	n.r.	0.18 (NorthernH) 0.08 (Southern H)	0.6 (North) 0.2 (South)	n.r.	(Yang et al., 2014)
Western North Pacific Ocean	15-20◦ N 137◦ E	6.5 - 14	May	PTR-MS	n.r.	n.r.	0.20-0.70	n.r.	(Tanimoto et al., 2014)
Western Indian Ocean	12◦ N-5◦ S 43-55◦ E	15	Feb.-Mar.	PTR-MS	n.r.	n.r.	0.49	n.r.	(Warneke and de Gouw, 2001)
Indian Ocean	19◦ N-13◦ S 67-75◦ E	10	Mar.	PTR-MS	n.r.	0.32-0.42 (continental outflow) 0.18-0.21 (equatorial marine)	1.11-2.08 (continental outflow) 0.51-0.62 (equatorial marine)	n.r.	(Wisthaler, 2002)
Southern Indian Ocean	30◦ S-49◦ S 30-100◦ E	15	Dec.	PTR-MS	n.r.	0.12-0.52	0.42-1.08	n.r.	(Colomb et al., 2009)
Costal									
Caribbean Sea	10-30◦ N 60-80◦ W	10	Oct.	HPLC	0.61	0.57	0.40	0.03	(Zhou and Mopper, 1993)
Cape Verde Atmospheric Observatory	16.86◦ N 24.87◦ W	10	2006-2011	GC-FID	n.r.	0.43 (0.19-0.67)	0.55 (0.23-0.91)	n.r	(Read et al., 2012)
Appledore Island, USA	42.97◦ N 70.62◦ W	5	Jul.-Aug.	PTR-MS	n.r.	0.40	1.5	0.20	(White et al., 2008)
Mace Head, Ireland	53.3◦ N 9.9◦ W	25	Jul.-Sep.	GC-FID	n.r.	0.44 (0.12-2.12)	0.50 (0.16-1.67)	n.r.	(Lewis et al., 2005)
Canadian Archipelago	68-75◦ N 60-100◦ W	Ship cruise	Aug.-Sep.	PTR-MS	n.r.	n.r	0.34	n.r	(Sjostedt et al., 2012)
Barrow Arctic	71.30◦ N 156.77◦ W	6	Mar.-Apr.	TOGA		0.10 ± 0.20	0.90 ± 0.30	0.19 ± 0.05	(Hornbrook et al., 2016)
South China Sea, Sulu Sea	2◦ N-15◦ N 108-124◦ E	10	Nov.	GC-MS	n.r.	0.86	2.1	0.06	(Schlundt et al., 2017)
Oil & Gas									
Horse Pool site, Uintah Basin, USA		Ground site	2012-2013	PTR-MS	3.71	4.27	7.97	2.81	(Koss et al., 2015)

Central United State	<600	Mar.-April	ToF-CIMS	1.13[a]	0.5	1.5	0.2	(Koss et al., 2017)
Eagle Mountain Lake site, Texas, USA	Ground site	June	PTR-MS	n.r.	n.r.	3.2 (1.2-6.7)	0.3 (0.09 - 0.85)	(Rutter et al., 2015)
Hickory, Pennsylvania, USA	Ground site	June	PTR-MS	n.r.	1.29 (0.28-2.03)	3.22 (1.45-4.99)	0.73 (0.4-0.97)	(Swartho ut et al., 2015)

n.r.: not reported in the literature.
a: formaldehyde was measured by laser-induced fluorescence (LIF)

2.3.1.2 Case studies of polluted regions: the Arabian Gulf and Suez

The primary emission sources in the Arabian Gulf and Suez regions are quite different. While the Arabian Gulf is dominated by oil and gas operations, the Suez is more influenced by ship emissions and urban areas (Bourtsoukidis et al., 2019). Carbonyl compounds were most abundant in these two areas. For further insight, we focused on a time series of selected trace gases and their inter-correlations to better identify the sources of the major aliphatic carbonyls. Meanwhile, we calculated the OH exposure ($[OH]\Delta t$) based on hydrocarbon ratios (Roberts et al., 1984;de Gouw et al., 2005;Yuan et al., 2012) for the polluted regions (Arabian Gulf and Suez) where primary emissions have been identified (Bourtsoukidis et al., 2019; Bourtsoukidis et al. 2020), to better understand the photochemical aging of the major carbonyls using the following equation:

$$[OH]\Delta t = \frac{1}{k_X - k_Y} \cdot \left(ln\frac{[X]}{[Y]}\Big|_{t=0} - ln\frac{[X]}{[Y]}\right), \quad \text{Eq. (2.1)}$$

where X and Y refer to two hydrocarbon compounds with different rates of reaction with the OH radical (k). For this study, we chose toluene ($k_{OH+toluene}$: 5.63×10^{-12} cm^3 $molecule^{-1}s^{-1}$) and benzene ($k_{OH+benzene}$: 1.22×10^{-12} cm^3 $molecule^{-1}s^{-1}$) (Atkinson and Arey, 2003), because both compounds were measured by PTR-ToF-MS at high frequency and these values showed a good agreement with values measured by GC-FID (Figure S2.2). The approach detailed by Yuan et al. (2012) was applied to determine the initial emission ratio $\frac{[X]}{[Y]}\Big|_{t=0}$ in those two regions by only including nighttime data of benzene and toluene. We obtained initial emission ratios (toluene-to-benzene ratios) of 1.38 for the Arabian Gulf and 2.12 for the Suez region. Koss et al. (2017) summarized the toluene-to-benzene ratios observed in various locations and showed that urban and vehicle sources tend to have higher toluene to benzene ratio (mean ~ 2.5) than the ratios of oil & gas sources (mean ~ 1.2). Therefore, the toluene to benzene ratios obtained for those two regions agreed well with other studies done with similar emission sources. The corresponding correlation plots of toluene and benzene for those two regions can be found in Figure S2.3.

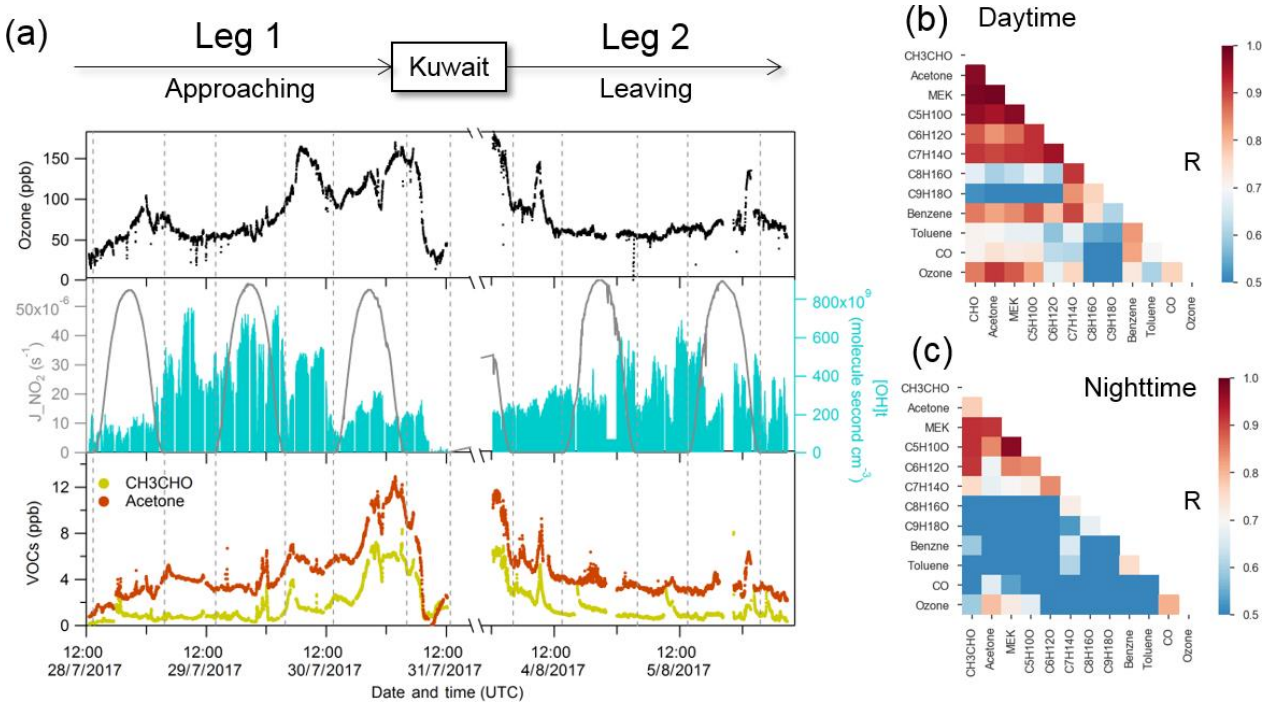

Figure 2.3. Case study of the Arabian Gulf. (a) Time series of selected species measured over the Arabian Gulf; (b) daytime correlation heat map of selected species; (c) nighttime correlation heat map of selected species.

Figure 2.3(a) shows the time series of acetaldehyde and acetone over the Arabian Gulf along with OH exposure ($[OH]t$) and ozone. We further separated the data into daytime and nighttime and calculated correlations among the carbonyls and other selected species (see Fig. 2.4b and c). Aliphatic carbonyls were well correlated with each other during the daytime and ozone had a generally good correlation with C2-C7 carbonyls (r > 0.7) during the daytime but a much lower correlation during the night, indicating ozone and carbonyls were co-produced via photochemical oxidation. Tadic et al. (2020) reported that the net ozone production rate over the Arabian Gulf (32 ppb d^{-1}) was greatest over the Arabian Peninsula. They show that strong ozone-forming photochemistry occurred in this region, which would lead to abundant secondary photochemically produced products (including carbonyls). However, it should be noted that the good correlation between ozone and carbonyls could in part be due to carbonyls co-emitted with ozone precursors (hydrocarbons) as primary emissions. In Figure 2.3 (a), the calculated OH exposure was high during the first night in leg 1, where an elevation of the acetone mixing ratio was observed while the mixing ratio of acetaldehyde remained relatively constant. With limited OH radical abundance during the nighttime, the increased OH exposure indicates that the air reaching the ship was photochemically processed (aged). Therefore, the increase in acetone was mainly from long-distance transport as acetone has a much longer atmospheric lifetime than acetaldehyde. As the

ship approached Kuwait, the calculated OH exposure was low (starting from 7/30/2017, 00:00 UTC), which is an indicator of nearby emission sources. The lifetime of the OH radical derived from the measured OH reactivity also decreased from ~ 0.1 s to ~ 0.04 s during the same period (Pfannerstill et al., 2019). Oil fields and associated refineries are densely distributed in the north-west of the Arabian Gulf region (United States Central Intelligence Agency). The air reaching the ship when mixing ratios of acetone and acetaldehyde were highest was mainly from the north-west (Iraq oil field region) according to the back trajectories (Bourtsoukidis et al., 2019). This suggests that the air masses encountered in the north-western Arabian Gulf were a combination of fresh emissions from nearby sources and photochemically processed air transported from elsewhere. During the second leg, relatively low mixing ratios were identified in the same region (north-western Arabian Gulf), which was mainly due to a greater influence of air masses originating from less populated desert regions of Northeast Iran (Bourtsoukidis et al., 2019) with much less influence from the oil field emissions, meaning fewer precursors were available for carbonyl production. Several plumes (extending over 2-3 hours) of elevated carbonyls with increased ozone were observed during the nighttime for both legs (Fig. 2.4a), indicating transport of highly polluted air.

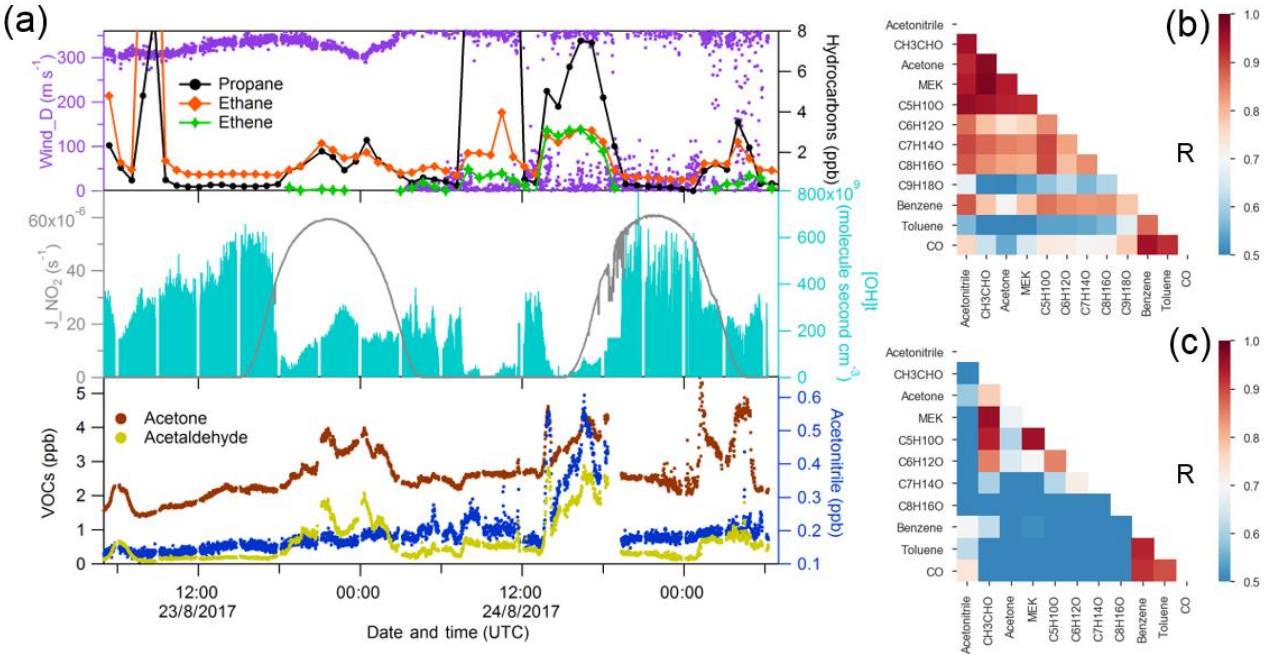

Figure 2.4. Case study of Suez. (a) Time series of selected species measured over Suez; (b) correlation heat map of selected species during biomass burning plume (UTC 01:00 -06:00 August 24th 2017); (c) correlation heat map of selected species without the period of biomass burning plume.

For the Suez region (Gulf of Suez and Suez Canal), data were only available for the second leg. A significant increase in acetonitrile (over 400 ppt) was observed just before entering the Great Bitter

Lake (see Figure 2.4a), indicating an increasing influence of biomass burning on the air composition (Lobert et al., 1990). Carbonyl compounds are important primary emissions in fresh biomass burning plumes (Holzinger et al., 1999;Schauer et al., 2001;Holzinger et al., 2001;Koss et al., 2018) as well as being formed as secondary products in more aged plumes (Holzinger et al., 2005). We further investigated the correlation coefficient among carbonyls during the biomass burning plume (Figure 2.4b) in the Suez. Carbonyls had a high correlation with acetonitrile, benzene, and themselves, particularly for smaller carbonyls (acetaldehyde, C3-C5 carbonyls). The biomass burning emissions were probably transported by the prevailing northerly wind (Figure S2.1) above north-eastern Egypt, where crop residues especially rice straw, are often directly burned in the open fields (Abdelhady et al., 2014;Said et al., 2013;Youssef et al., 2009). Besides the direct biomass burning emission, the high mixing ratios and the good correlations of carbonyls could also have resulted from other sources such as hydrocarbons (alkanes, alkenes and aromatics) which were elevated at the same time. Similar to conditions identified over the Arabian Gulf, elevated OH exposure accompanied by an increasing acetone mixing ratio was observed during the first night over the Gulf of Suez, indicating aged air-mass transportation. The OH exposure was then significantly lower during the daytime, when mixing ratios of carbonyls and alkanes increased as well. This indicates the presence of emission sources nearby. Oil refineries located on the coastal side of the Suez and oil tank terminals located in the northern part of the Gulf of Suez are likely sources.

2.3.2 Unsaturated and aromatic carbonyls ($C_nH_{2n-2}O$), ($C_nH_{2n-8}O$)

2.3.2.1 Overview

The mixing ratios of unsaturated carbonyls were generally ~ 10 ppt or lower than the LOD over the Mediterranean Sea and the clean regions (the Arabian Sea and the Gulf of Aden). The Red Sea region and the Gulf of Oman had slightly higher levels (LOD – 40 ppt). The highest values were again observed in the Arabian Gulf (20 – 110 ppt), followed by the Suez (LOD – 60 ppt). The numbers represent the range of the mean mixing ratios of unsaturated carbonyls in each region. In terms of the mixing ratio distribution (Figure 2.2), the peak value was usually observed at C5 or C6 unsaturated carbonyls over most regions except for the Suez where C4 carbonyl had the highest mixing ratio. Based on chemical formulas, unsaturated carbonyls can be either cyclic carbonyl compounds or carbonyls containing a carbon-carbon double bond. Therefore, the air chemistry could differ considerably depending on the compound assignment. A detailed analysis of the chemistry of the unsaturated carbonyls measured will be given in the following section 3.2.2.

Regional variability was also observed for aromatic carbonyls, with the highest levels observed over the Arabian Gulf and Suez and much lower mixing ratios over the Arabian Sea, Mediterranean Sea and Gulf of Aden (Table 2.1). Several studies using PTR-MS have reported values for m/z 107.049 (C7 aromatic carbonyls) attributed to benzaldehyde (Brilli et al., 2014; Koss et al., 2017;Koss et al., 2018), m/z 121.065 (C8 aromatic carbonyls) attributed to tolualdehyde (Koss et al., 2018) or acetophenone (Brilli et al., 2014), and *m/z* 135.080 (C9 aromatic carbonyls) attributed to methyl acetophenone (Koss et al., 2018) or benzyl methyl ketone (Brilli et al., 2014) or 3,5-dimethylbenzaldehyde (Müller et al., 2012). Atmospheric aromatic carbonyls are produced via photochemical oxidation of aromatic hydrocarbons (Finlayson-Pitts and Pitts Jr, 1999;Wyche et al., 2009;Müller et al., 2012), and benzaldehyde was reported as having primary sources from biomass burning and anthropogenic emissions (Cabrera-Perez et al., 2016). Around the Arabian Peninsula, the level of aromatic carbonyls declined with increasing carbon number over most of the regions except in the Red Sea South, Gulf of Oman and Arabian Gulf where C7 carbonyls were comparable to C8 carbonyls (Figure 2.2). Interestingly, only in the Suez region, were the C7 aromatic carbonyls more abundant than other aromatic carbonyls, whereby the mean value (90 ± 200 ppt) was much higher than the median value (20 ppt), indicating strong primary sources of benzaldehyde in the Suez. Otherwise, toluene was found to be more abundant over the Suez with mean mixing ratios of 271 ± 459 ppt than over other regions (the mean over the Arabian Gulf: 130 ± 160 ppt) which would also lead to higher benzaldehyde as it is one of the OH-induced oxidation products of toluene via H abstraction (Ji et al., 2017).

2.3.2.2 Potential precursors and sources of unsaturated carbonyls

Unsaturated carbonyls measured by PTR-MS have only rarely been reported in the atmosphere, with the exception of methyl vinyl ketone and methacrolein (C4 carbonyls) which are frequently reported as the oxidation products of isoprene (Williams et al., 2001; Fan and Zhang, 2004;Wennberg et al., 2018). According to the GC-FID measurement, isoprene was below the detection limit for most of the time during the AQABA cruise with the highest values observed in the Suez (10 - 350 ppt). This shows that the AQABA campaign was little influenced by either terrestrial or marine isoprene emissions. However, we observed unexpected high levels on mass 69.070, which is usually interpreted as isoprene for PTR-MS measurements. Significant enhancements were even identified while sampling our own ship exhaust (in PTR-MS but not GC-FID), suggesting the presence of an anthropogenic interference at that mass under these extremely polluted conditions. Several studies have reported possible fragmentations of cyclic alkanes giving mass (m/z) 69.070. These include: a laboratory study on gasoline hydrocarbon measurements by

PTR-MS (Gueneron et al., 2015), a GC-PTR-MS study of an oil spill site combined with analysis of crude oil samples (Yuan et al., 2014) and an inter-comparison of PTR-MS and GC in an O&G industrial site (Warneke et al., 2014). From those studies, other fragmentations from C5 to C9 cycloalkanes including m/z 43, m/z 57, m/z 83, m/z 111 and m/z 125 were identified together with m/z 69. Cyclic alkanes were directly measured in oil and gas fields (Simpson et al., 2010;Gilman et al., 2013; Li et al., 2017;Aklilu et al., 2018), and vehicle exhaust (Gentner et al., 2012;Erickson et al., 2014), vessel exhaust (Xiao et al., 2018), accounting for a non-negligible amount of the total VOC mass depending on the fuel type. Koss et al. (2017) reported enhancement of cyclic alkane fragment signals and increased levels of unsaturated carbonyls measured by PTR-ToF-MS over the O&G region in the US. The unsaturated carbonyls (C5-C9) were assigned as oxidation products of cycloalkanes. Therefore, we examined the correlations between m/z 69.070 and other cycloalkane fragments over the Arabian Gulf and Suez, where anthropogenic primary emissions were significant. As shown in Figure 2.5, m/z 83 was the most abundant fragment, and it correlated better with m/z 69 than the other two masses, strongly supporting the presence of C6 cycloalkanes (methylcyclopentane and cyclohexane). The other two masses are distributed in two or three clusters, suggesting compositions of different cycloalkanes. M/z 43 and m/z 57 (fragments of C5 cycloalkanes) had lower correlations with other fragments (not shown in the graph) as they are also fragments of other higher hydrocarbons. Thereby we could assign those unsaturated carbonyls as photochemical oxidation products (i.e. cyclic ketones or aldehydes) from their precursor cycloalkanes.

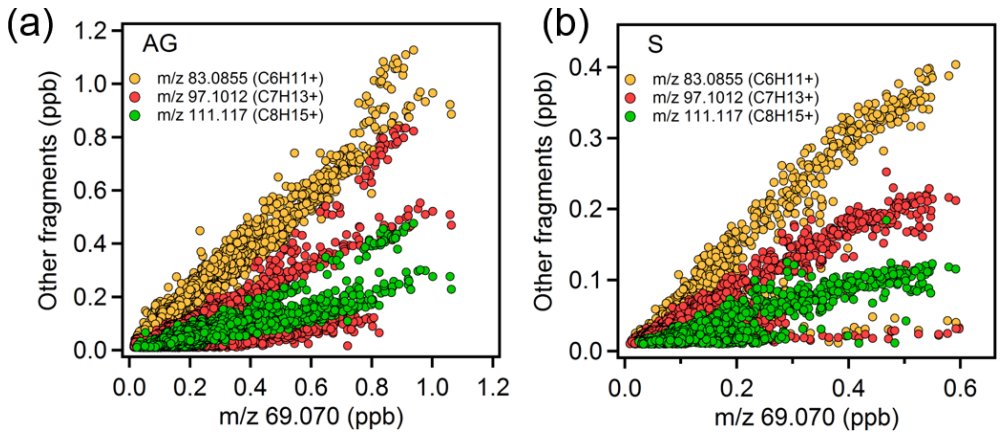

Figure 2.5. Scatter plots of m/z 69.070 and other cycloalkane fragment masses over the (a) Arabian Gulf and (b) Suez region.

As shown in Figure 2.2 and Table 2.1, C6 unsaturated carbonyls displayed higher mixing ratios than any other unsaturated carbonyls over the Arabian Gulf while C5 unsaturated carbonyl was slightly higher than C6 in the Suez. Bourtsoukidis et al. (2019) derived enhancement ratio slopes

from pentane isomers and established that the Arabian Gulf is dominated by oil and gas operations and that the Suez is more influenced by ship emissions. Therefore, as the Arabian Gulf had much more active O&G activities than the Suez, our findings agree with Koss et al. (2017) who showed that C6 unsaturated carbonyls should be more abundant than C5 carbonyls since more precursors for C6 unsaturated carbonyls are emitted from active oil fields. It is worth mentioning that in Figure 2.5 (b) one cluster at the bottom showed m/z 69.070 had no correlation with the other three masses. Those points correspond to the time when the GC measured significantly elevated isoprene while passing through the narrow Suez Canal where some vegetation (e.g. palms and some agriculture) was present close to the shore, meaning m/z 69.070 during this period was isoprene. At the same time, m/z 71.049 (C4 unsaturated carbonyl) increased from 20 ppt to 220 ppt. Isoprene oxidation products (MVK and methacrolein) were probably the major contribution to the C4 unsaturated carbonyls in this period. This also explains why C4 carbonyl dominated the distribution of unsaturated carbonyls over the Suez.

In the other regions (especially more remote areas), the cyclic alkane fragmentation masses had much lower abundance, leading to much less unsaturated carbonyls due to lack of precursors. Meanwhile, m/z 69.070 ($C_5H_8H^+$), m/z 83.086 ($C_6H_{10}H^+$) and m/z 97.101 ($C_7H_{12}H^+$) could also be fragmentations from corresponding aldehydes losing one water molecule as mentioned in section 2.3.3. Missing information of the chemical structure on unsaturated carbonyls and knowledge of their precursors preclude detailed investigation of the sources of large unsaturated carbonyls in these areas.

2.3.3 Model comparison of acetaldehyde, acetone, and MEK

We compared our measurement results of acetaldehyde, acetone and MEK to those predicted by EMAC global model (ECHAM5/MESSy2 for Atmospheric Chemistry). From the results shown in Figure 2.6, the model predicted acetone much better than acetaldehyde and MEK. In general, the model broadly captured the major features identified during the campaign, such as much higher levels of carbonyl mixing ratios over the Arabian Gulf and Suez and relatively low levels over the Arabian Sea. The mean measurement-to-model ratios indicated that acetone was overestimated by a factor within 1.5 over the Arabian Sea, Gulf of Aden, and Gulf of Oman, and underestimated by a factor within 2.5 over the other regions. In contrast, the model underestimated MEK within a factor of 4 over most of the regions except for the Gulf of Oman where MEK was overestimated (median values were taken here as the mean values substantially deviated from the medians over the Suez, Gulf of Oman and Arabian Gulf). The model underestimation was most significant for acetaldehyde, which is under predicted by a factor (median values) of more than 6 over the Red Sea North, ~ 4 over the Arabian Sea and Arabian Gulf and between 1 and 4 over other regions. A strong natural non-methane hydrocarbon source from deep water in the northern Red Sea was

implemented in the model (Bourtsoukidis et al., 2020). Although the model representation of acetaldehyde and other carbonyls was clearly improved after including the deep-water source of ethane and propane (Figure S2.4), the underestimation of acetaldehyde was still significant over the Red Sea North as shown in Figure 2.6(a), indicating further missing sources. For acetaldehyde and MEK, the discrepancy was also significant over the Arabian Sea where acetone was in contrast, overestimated. Since acetaldehyde had the biggest bias from the model prediction, we further investigate the possible missing sources of acetaldehyde.

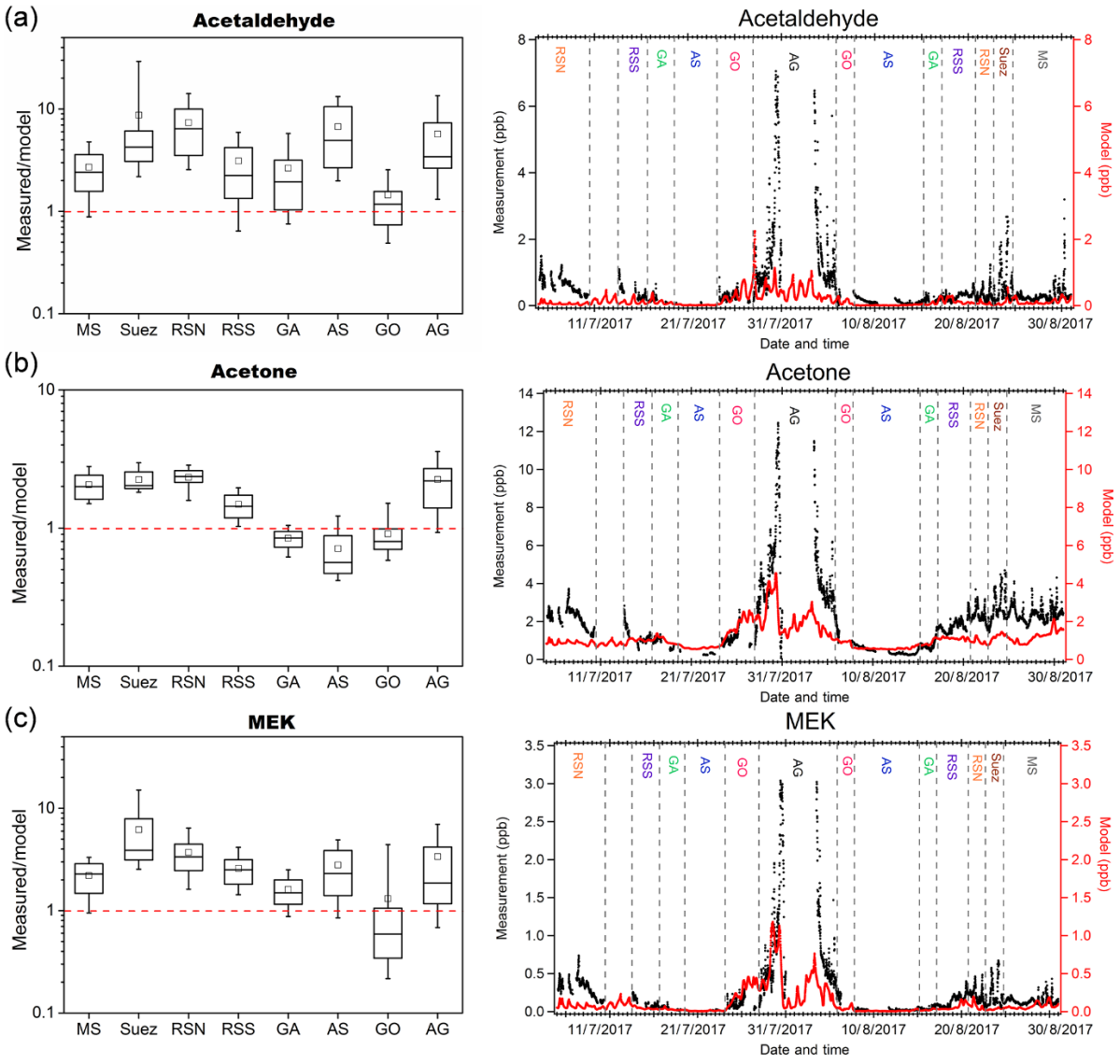

Figure 2.6. Measurement-to-model ratios (left) and time series (right) of measurements (in black) and model simulation (in red) of (a) acetaldehyde; (b) acetone; and (c) MEK in each area. In each box plot, the box represents 25% to 75% of the dataset with central line and square indicating the median value and the mean value respectively. The whiskers show data from 10% to 90%. The red dashed lines represent the 1:1 ratio.

2.3.4 Missing sources of acetaldehyde

In this section we investigate the following processes as potential sources of acetaldehyde: (1) production as an inlet artifact, (2) oceanic emission of acetaldehyde, (3) anthropogenic primary sources, (4) biomass burning sources, and (5) other possible secondary formation pathways.

2.3.4.1 Inlet artifact

Northway et al. (2004) and Apel et al. (2008) reported that heterogeneous reactions of unsaturated organic species with ozone on the wall of the Teflon inlet can cause artifact signal of acetaldehyde but not of acetone. During AQABA, the highest and most variable ozone mixing ratios were observed during the campaign over the Arabian Gulf (mean: 80 ± 34 ppb) and the Red Sea North (66 ± 12 ppb), where a modest correlation was found between acetaldehyde and ozone over the Arabian Gulf (r^2=0.54) and no significant correlation over the Red Sea North (r^2=0.40). However larger correlation coefficients were identified between ozone and other carbonyls over the Arabian Gulf (see Figure S2.5), which suggests that the correlation was due to atmospheric photochemical production rather than artifacts. Moreover, acetaldehyde was found to have a much worse correlation with ozone during the nighttime compared to the correlation during the daytime over the Arabian Gulf (Figure 2.3b and c), which also indicates that inlet generation of acetaldehyde was insignificant. Over other regions, especially the remote area (the Arabian Sea and Gulf of Aden), ozone was relatively constant and low, with poor correlation with acetaldehyde mixing ratios. Although we cannot completely exclude the possible existence of artifacts, the interference is likely to be insignificant in this dataset.

2.3.4.2 Oceanic emission

A bias between measured acetaldehyde and global model simulations has been observed in previous studies conducted in the remote troposphere (Singh et al., 2003; Singh, 2004;Wang et al., 2019) and in the marine boundary layer (Read et al., 2012). The aforementioned studies emphasized the potential importance of the seawater acting as a source of acetaldehyde emission via air-sea exchange. No significant correlation was found between acetaldehyde and dimethyl sulfide (DMS), a marker of marine biogenic emission which is produced by phytoplankton in seawater (Bates et al., 1992) (see Figure S2.6). This indicates that the direct biogenic acetaldehyde emissions from the ocean are probably insufficient to explain the measured acetaldehyde. More likely, acetaldehyde and other small carbonyl compounds can be formed in the sea especially in the surface microlayer (SML) via photodegradation of coloured dissolved organic matter (CDOM) (Kieber et al., 1990;Zhou and Mopper, 1997;Ciuraru et al., 2015). Zhou and Mopper (1997) calculated the exchange direction of small carbonyls based on measurement results and identified that the net flux of acetaldehyde was from the sea to the air, whereas formaldehyde was taken up

by the sea. Sinha et al. (2007) characterized air-sea flux of several VOCs in a mesocosm experiment and found that acetaldehyde emissions were in close correlation with light intensity (r=0.7). By using a 3-D model, Millet et al. (2010) estimated the net oceanic emission of acetaldehyde to be as high as 57 Tg a^{-1} (in a global total budget: 213 Tg a^{-1}), being the second largest global source. A similar approach was applied in a recent study done by Wang et al. (2019), reporting the upper limit of the net ocean emission of acetaldehyde to be 34 Tg a^{-1}. Yang et al. (2014) quantified the air-sea fluxes of several oxygenated VOCs (OVOCs) over the Atlantic Ocean by eddy covariance measurements, showing the ocean is a net source of acetaldehyde. Although Schlundt et al. (2017) reported uptake of acetaldehyde by the ocean from measurement-inferred fluxes in western Pacific coastal regions, to our knowledge, there is no direct experimental evidence showing the ocean to be a sink for acetaldehyde.

In order to test the importance of the oceanic emission of acetaldehyde, we implemented this source in the EMAC model. The measured seawater concentration of acetaldehyde was not available for the water area around the Arabian Peninsula. Wang et al. (2019) estimated the global average acetaldehyde surface seawater concentrations of the ocean mixed layer using a satellite-based approach similar to Millet et al. (2010), where the model estimation agreed well with limited reported measurements. From the Wang et al. (2019) results, the averaged seawater concentration of acetaldehyde around the Arabian Peninsula was generally much higher from June to August. As the photodegradation of CDOM is highly dependent on sunlight, the air-sea submodel (Pozzer et al., 2006) was augmented to include throughout the campaign a scaled acetaldehyde seawater concentration in the range of 0 ~ 50 nM according to the solar radiation (Figure S2.7). With this approach, the average of acetaldehyde seawater concentration estimated by the model is 13.4 nM, a reasonable level compared to the predicted level by Wang et al. (2019).

After adding the oceanic source of acetaldehyde, the model estimation was significantly improved (Figure 2.7). As the oceanic source in the model is scaled according to the solar radiation, the measurement-to-model ratios were more strongly reduced during the day compared to the night. With oceanic emission included, the model underestimation was less significant, within a factor of 3 during the day and 4 during the night over the Mediterranean Sea, Red Sea and Gulf of Aden. The most significant improvement was identified over the Red Sea North. As shown in Figure 2.8, the model had much better agreement with the measurement after adding the oceanic source. The scatter plots for other regions can be found in Figure S2.8. Over the Arabian Sea, the model significantly overestimated acetaldehyde mixing ratios, indicating the input seawater concentration of acetaldehyde might be too high. The SML layer starts to be effectively destroyed by the wave breaking when the wind speed exceeds 8 m s^{-1} (Gantt et al., 2011). As the average wind speed over the Arabian Sea was highest among the cruised areas (8.1 ± 2.4 m s^{-1}, Figure S2.1), less contribution

from the CDOM photodegradation to acetaldehyde in the surface seawater would be expected. For the Suez region, due to the limited model resolution (1.1° × 1.1°), little seawater was identified in the model, leading to negligible influence from the oceanic source.

Model underestimation of acetaldehyde, especially over the Suez, Red Sea, and Arabian Gulf, is also likely to be related to the coarse model resolution (~ 1.1° × 1.1°) (Fischer et al., 2015). Where model grid points contain areas of land the higher and more variable terrestrial boundary layer height impacts the model prediction, whereas the measurements may only by influenced by a shallower and more stable marine boundary layer.

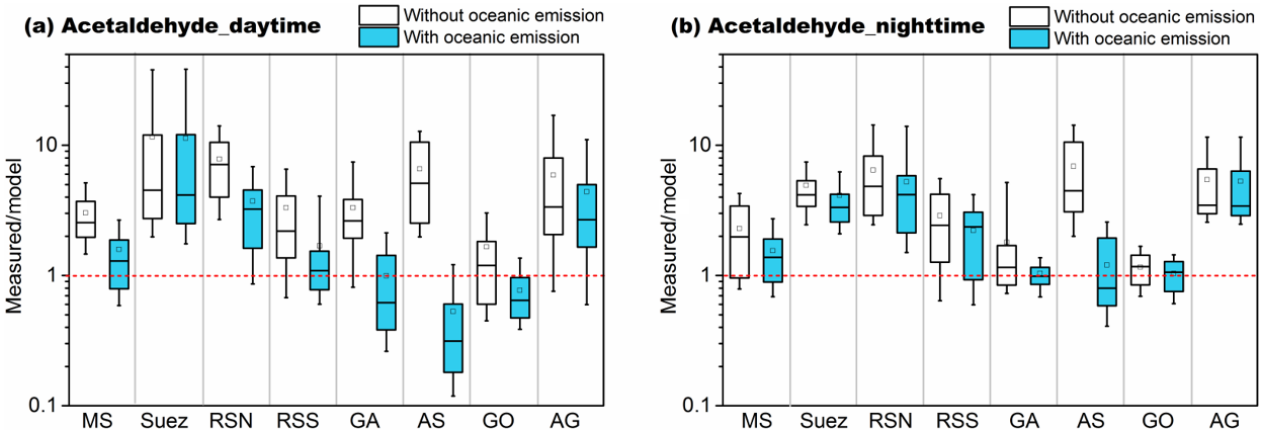

Figure 2.7. Acetaldehyde measurement-to-model ratios without the oceanic source (white boxes) and with the oceanic source (blue boxes) in the model during (a) daytime and (b) nighttime in different regions. The boxes represent 25% to 75% of the dataset with the central line and square indicating the median and mean values, respectively. The whiskers show data from 10% to 90%. The red dashed lines represent the 1:1 ratio.

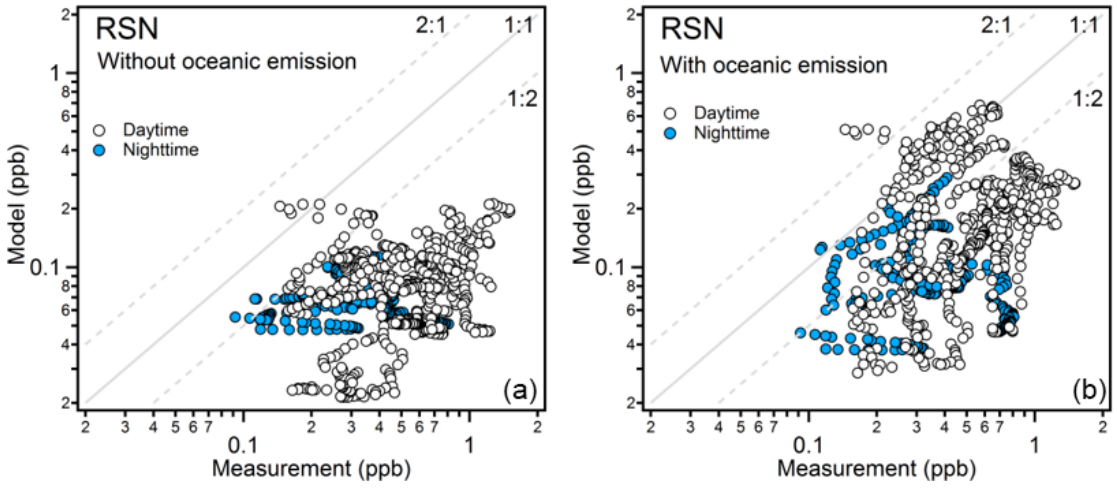

Figure 2.8. Observed and simulated mixing ratios of acetaldehyde over the Red Sea North without oceanic emission (left) and with oceanic emission (right). The data points are separated into daytime and nighttime according to solar radiation.

2.3.4.3 Anthropogenic primary sources

Over the Arabian Gulf and Suez, the intensive photochemical production of carbonyls is apparent. Bourtsoukidis et al. (2020) compared measured hydrocarbons (ethane, propane, and butane) with the results from model simulations (the same model used in this study with the newly discovered deep water source implemented). The model was able to reproduce the measurement over most regions expect for some significant model underestimations in the Suez and Arabian Gulf, in which local and small-scale emissions were difficult for the model to capture. Therefore, an underestimation of the precursor hydrocarbons, as well as those large alkanes, alkenes and cyclic hydrocarbons which were not measured (> C8) or included in the model (> C5), could be a reason for the model underestimation of acetaldehyde, especially in polluted regions. In addition, as mentioned in the previous case studies, high-ozone mixing ratios were observed over the Arabian Gulf especially during the nighttime. Ethene and propene were found to be significantly underestimated during the nighttime high-ozone period by a factor over 10 (Figure S2.9), which indicates that the nighttime ozonolysis of alkenes could be another important source of acetaldehyde, formaldehyde, and other carbonyls (Atkinson et al., 1995;Altshuller, 1993) in the Arabian Gulf.

Acetaldehyde, an oxygenated VOC, is not generally considered an important primary emission from oil and gas fields, but instead a photochemical product of hydrocarbon oxidation (Yuan et al., 2014;Koss et al., 2015;Koss et al., 2017). In contrast, primary sources of formaldehyde from oil and gas production processes including both combustion and non-combustion processes, have been ascertained (Vaught, 1991). Le Baron and Stoeckenius (2015) concluded in their report onthe Uinta Basin winter ozone study that besides formaldehyde, the other carbonyls were poorly understood in terms of their primary sources. Acetaldehyde and other carbonyls (aldehydes and ketones) have been reported as primary emissions from fossil fuel combustion, including ship emissions (Reda et al., 2014;Xiao et al., 2018;Huang et al., 2018) and vehicle emissions (Nogueira et al., 2014;Erickson et al., 2014;Dong et al., 2014). A possible explanation for the measurement-model discrepancy is that the active petroleum industry located in the Arabian Gulf and intensive marine transportation in the Suez are primary sources of acetaldehyde and other carbonyls which were not well constrained in the model. The Suez region, where the largest acetaldehyde discrepancy was identified, had a significant influence from biomass burning (see section 3.2.2). Biomass burning emissions are notoriously difficult to model as they are highly variable in both time and space. In this study, the model failed to reproduce the acetonitrile level with a range of only 40-50 ppt rather than 100-550 ppt measured over the Suez. Thus, besides the possibility of seawater emission from the Gulf of Suez and the Suez Canal, the underestimated biomass burning source in the model over the Suez, will lead to an underestimation of acetaldehyde as well as other carbonyl compounds in this region.

2.3.4.4 Other possible secondary formation pathways

Although the model estimation was generally improved with the addition of an oceanic source, the model to measured ratios still varied over a wide range. As mentioned above, photodegradation of CDOM on the surface of seawater is a known source of acetaldehyde although some studies focusing on real seawater samples did not observe clear diel cycles of seawater acetaldehyde (Beale et al., 2013;Yang et al., 2014). Fast microbial oxidation could be a reason (Dixon et al., 2013), while other non-light-driven sources of acetaldehyde could be an alternative explanation. In a recent study, Zhou et al. (2014) reported enhanced gas-phase carbonyl compounds including acetaldehyde during a laboratory experiment of ozone reacting with SML samples, indicating acetaldehyde could also be produced under non-light-driven heterogeneous oxidation. Wang et al. (2019) ventured a hypothetical source that organic aerosol can be an extra source of unattributed acetaldehyde in the free troposphere through light-driven production and ozonolysis. However, since the yield of acetaldehyde from such reactions is unknown, large uncertainties remain. Previous studies have shown that the organic matter fraction was highest in smaller sea spray aerosols and that the aerosols contain both saturated and unsaturated fatty acids originating from the seawater surface (i.e. SML) (Mochida et al., 2002;Cochran et al., 2016). Thus, for the AQABA campaign, both photodegradation and heterogeneous oxidation could occur on the surface of sea spray and pollution-associated aerosols, even over the remote open ocean therefore being an extra source of acetaldehyde and other carbonyl compounds.

Another acetaldehyde formation pathway reported is gas-phase photolysis of pyruvic acid (Eger et al., 2020;Reed Harris et al., 2016), a compound mainly of biogenic origin. Pyruvic acid has been also observed in seawater (Kieber and Mopper, 1987;Zhou and Mopper, 1997) and was found up to 50 nM in the surface water of the eastern Pacific Ocean (Steinberg and Bada, 1984), while acetaldehyde was not the major product of aqueous-phase photolysis of pyruvic acid (Griffith et al., 2013). Zhou and Mopper (1997) pointed out that the net exchange direction for pyruvic acid is expected to be from the air to the sea due to high solubility, with a Henry's law constant of 3.1×10^{3} mol m^{-3} Pa^{-1} (Sander, 2015). Moreover, partitioning to aerosols could be an important sink for pyruvic acid (Reed et al.,2014; Griffith et al., 2013) : an increasing concentration trend of pyruvic acid was observed in marine aerosols over the western North Pacific Ocean (Boreddy et al., 2017). Therefore, due to limited terrestrial biogenic sources of pyruvic acid for the AQABA campaign, the gas-phase level of pyruvic acid was expected to be low. Limited studies reported pyruvic acid level in marine the boundary layer and Baboukas et al. (2000) measured 1.1 ± 1.0 ppt of pyruvic acid above the Atlantic Ocean. Pyruvic acid was measured by Jardine et al. (2010) using a PTR-MS at m/z 89 in a forested environment. For the AQABA PTR-ToF-MS dataset, enhanced signals were observed at m/z 89.024, with a mean mixing ratio of 35-110 ppt over different regions (Table S2.4), which is much more abundant than reported pyruvic acid levels by Baboukas et al. (2000).

This might be due to the uncertainty associated with the theoretical methods of quantification used here or the presence of isomeric compounds on that mass, since pyruvic acid was not calibrated with the standard. Even if we assume the m/z 89.024 to be entirely pyruvic acid, with 60% yield of acetaldehyde via photolysis (IUPAC, 2019), it gave a maximum of 13 ppt of acetaldehyde over the Arabian Gulf and 5-9 ppt over other regions, which were only 0.8% - 6% of the mean mixing ratios (Table S2.4). Detailed information on the calculation can be found in the Supporting Information. Therefore, we conclude that the contribution from the photolysis of pyruvic acid is not an important source of the unattributed acetaldehyde during the AQABA campaign.

2.4 Summary and conclusion

Observations of carbonyl compounds around the Arabian Peninsula were investigated in terms of mixing ratio abundance over different areas. Aliphatic carbonyl compounds were generally more abundant than the unsaturated and aromatic carbonyl compounds and were dominated by low-molecular-weight compounds (carbon number less than five). Aliphatic carbonyl compounds were found at the highest mixing ratios over the Arabian Gulf followed by the Suez region, while the lowest mixing ratios were observed over the Arabian Sea and the Gulf of Aden. Over the Mediterranean Sea, aliphatic carbonyls were low except for acetone, which was much higher compared to the levels observed over clean remote areas (i.e. Arabian Sea). The atmospheric composition over the Red Sea showed obvious differences between the northern and southern parts, with higher mixing ratios in the north. Similar region-dependent distributions were observed for unsaturated and aromatic carbonyls. Generally, the mixing ratios of aromatic carbonyl compounds decreased as the carbon number increased. Particularly over the Suez region, benzaldehyde (C7 aromatic carbonyls) was much more abundant than other aromatic carbonyls, indicating direct sources as well as abundant oxidation precursors. For unsaturated carbonyl compounds, C5 and C6 carbonyl compounds dominated the mixing ratio distribution, while the air chemistry highly depends on the chemical structure assignment of those masses.

Further case studies showed that the carbonyl compounds were highly correlated with the high ozone levels during daytime over the Arabian Gulf while the air chemistry in the Suez region was strongly influenced by regional biomass burning. Due to the unexpectedly high loading of m/z 69 (usually assigned as isoprene) observed in highly polluted regions, we further identified the correlations between m/z 69 and other fragmentation masses of cycloalkanes according to previous studies conducted in oil and gas regions (Warneke et al., 2014;Yuan et al., 2014;Koss et al., 2017). The high correlations among fragments implied the existence of cycloalkanes in the polluted regions, which could be further oxidized to unsaturated carbonyl compounds (cyclic ketones or aldehydes).

As acetaldehyde was identified as having important additional sources, we further compared the measurements of major carbonyl species (acetaldehyde, acetone, and MEK) with a comprehensive global atmospheric chemistry model (EMAC). Acetaldehyde was found to have the highest discrepancy between the observations and model simulations, with the simulated values lower by up to a factor of 10. By adding an oceanic source of acetaldehyde produced via light-driven photodegradation of CDOM in the seawater, the model estimation improved significantly, especially over the Red Sea North. With the oceanic source added, modelled acetaldehyde became slightly overestimated in clean regions, suggesting that the emission rate employed represents an upper limit. The results indicate that the ocean plays an important role in the atmospheric acetaldehyde budget, under both clean and polluted conditions. The underestimated acetaldehyde in the model is significant as it will influence the atmospheric budget of e.g. PAN. As shown in Figure 2.1, multiple sources and formation pathways need to be considered to better understand the atmospheric budget of acetaldehyde. Additional laboratory experiments and field measurements are necessary in order to verify all possible atmospheric formation mechanisms and to improve model simulations.

Data availability. The data used in this study are available to all scientists agreeing to the AQABA protocol at: http://doi.org/10.5281/zenodo.3974228 (Wang et al., 2020).

Supplement. The supplement related to this article is available online at: https://doi.org/10.5194/acp-20-10807-2020-supplement.

Author contributions. AE and CS performed PTR-ToF-MS measurement and preliminary data processing. NW conducted data analysis and drafted the article. AP performed EMAC model simulation. EB and LE were responsible for NMHC measurements and data. DD, BH and HF provided formaldehyde data. Ozone and actinic flux data were contributed by JS and JNC. Methane and carbon monoxide data were provided by JP. JL designed and realized the campaign. JW supervised the study. All the authors contributed to editing the draft and approved the submitted version.

Competing interests. The authors declare that they have no conflict of interest.

Acknowledgements. We are grateful for the collaboration with the King Abdullah University of Science and Technology (KAUST), the Kuwait Institute for Scientific Research (KISR), and the Cyprus Institute (CyI) to fulfill the campaign. We would like to thank Captain Pavel Kirzner and the crew for their full support onboard the Kommandor Iona, Hays Ships Ltd. We are grateful for the support from all members involved in the AQABA campaign, especially Hartwig Harder for his general organization onboard the campaign, and Marcel Dorf, Claus Koeppel, Thomas Klüpfel, and Rolf Hofmann for logistical organization and their help with preparation and set-up. We would

like to express our gratitude to Ivan Tadic and Philipp Eger for the use of a ship exhaust contamination flag.

Financial support. The position of Nijing Wang was funded by the European Commission, H2020 Research Infrastructures (IMPACT (grant no. 674911)).

The article processing charges for this open-access publication were covered by the Max Planck Society

Review statement. This paper was edited by Robert Harley and reviewed by two anonymous referees.

References

Abdelhady, S., Borello, D., Shaban, A., and Rispoli, F.: Viability Study of Biomass Power Plant Fired with Rice Straw in Egypt, Energy Procedia, 61, 211-215, https://doi.org/10.1016/j.egypro.2014.11.1072, 2014.

Aklilu, Y.-a., Cho, S., Zhang, Q., and Taylor, E.: Source apportionment of volatile organic compounds measured near a cold heavy oil production area, Atmospheric Research, 206, 75-86, https://doi.org/10.1016/j.atmosres.2018.02.007, 2018.

Altshuller, A. P.: Production of aldehydes as primary emissions and from secondary atmospheric reactions of alkenes and alkanes during the night and early morning hours, Atmospheric Environment. Part A. General Topics, 27, 21-32, https://doi.org/10.1016/0960-1686(93)90067-9, 1993.

Apel, E. C., Brauers, T., Koppmann, R., Bandowe, B., Boßmeyer, J., Holzke, C., Tillmann, R., Wahner, A., Wegener, R., Brunner, A., Jocher, M., Ruuskanen, T., Spirig, C., Steigner, D., Steinbrecher, R., Gomez Alvarez, E., Müller, K., Burrows, J. P., Schade, G., Solomon, S. J., Ladstätter-Weißenmayer, A., Simmonds, P., Young, D., Hopkins, J. R., Lewis, A. C., Legreid, G., Reimann, S., Hansel, A., Wisthaler, A., Blake, R. S., Ellis, A. M., Monks, P. S., and Wyche, K. P.: Intercomparison of oxygenated volatile organic compound measurements at the SAPHIR atmosphere simulation chamber, Journal of Geophysical Research, 113, 10.1029/2008jd009865, 2008.

Atkinson, R., Tuazon, E. C., and Aschmann, S. M.: Products of the Gas-Phase Reactions of a Series of 1-Alkenes and 1-Methylcyclohexene with the OH Radical in the Presence of NO, Environmental Science & Technology, 29, 1674-1680, 10.1021/es00006a035, 1995.

Atkinson, R., and Arey, J.: Atmospheric Degradation of Volatile Organic Compounds, Chemical Reviews, 103, 4605-4638, 10.1021/cr0206420, 2003.

Baboukas, E. D., Kanakidou, M., and Mihalopoulos, N.: Carboxylic acids in gas and particulate phase above the Atlantic Ocean, Journal of Geophysical Research: Atmospheres, 105, 14459-14471, 10.1029/1999jd900977, 2000.

Bates, T. S., Lamb, B. K., Guenther, A., Dignon, J., and Stoiber, R. E.: Sulfur emissions to the atmosphere from natural sourees, Journal of Atmospheric Chemistry, 14, 315-337, 10.1007/bf00115242, 1992.

Beale, R., Dixon, J. L., Arnold, S. R., Liss, P. S., and Nightingale, P. D.: Methanol, acetaldehyde, and acetone in the surface waters of the Atlantic Ocean, Journal of Geophysical Research: Oceans, 118, 5412-5425, 10.1002/jgrc.20322, 2013.

Borbon, A., Gilman, J. B., Kuster, W. C., Grand, N., Chevaillier, S., Colomb, A., Dolgorouky, C., Gros, V., Lopez, M., Sarda-Esteve, R., Holloway, J., Stutz, J., Petetin, H., McKeen, S., Beekmann, M., Warneke, C., Parrish, D. D., and de Gouw, J. A.: Emission ratios of anthropogenic volatile organic compounds in northern

mid-latitude megacities: Observations versus emission inventories in Los Angeles and Paris, Journal of Geophysical Research: Atmospheres, 118, 2041-2057, 10.1002/jgrd.50059, 2013.

Bourtsoukidis, E., Williams, J., Kesselmeier, J., Jacobi, S., and Bonn, B.: From emissions to ambient mixing ratios: online seasonal field measurements of volatile organic compounds over a Norway spruce-dominated forest in central Germany, Atmos. Chem. Phys., 14, 6495–6510, https://doi.org/10.5194/acp-14-6495-2014, 2014.

Bourtsoukidis, E., Ernle, L., Crowley, J. N., Lelieveld, J., Paris, J.-D., Pozzer, A., Walter, D., and Williams, J.: Non-methane hydrocarbon (C2–C8) sources and sinks around the Arabian Peninsula, Atmospheric Chemistry and Physics, 19, 7209-7232, 10.5194/acp-19-7209-2019, 2019.

Bourtsoukidis, E., Pozzer, A., Sattler, T., Matthaios, V. N., Ernle, L., Edtbauer, A., Fischer, H., Konemann, T., Osipov, S., Paris, J. D., Pfannerstill, E. Y., Stonner, C., Tadic, I., Walter, D., Wang, N., Lelieveld, J., and Williams, J.: The Red Sea Deep Water is a potent source of atmospheric ethane and propane, Nat Commun, 11, 447, 10.1038/s41467-020-14375-0, 2020.

Boreddy, S. K. R., Kawamura, K., and Tachibana, E.: Long-term (2001–2013) observations of water-soluble dicarboxylic acids and related compounds over the western North Pacific: trends, seasonality and source apportionment, Scientific Reports, 7, 8518, 10.1038/s41598-017-08745-w, 2017.

Brilli, F., Gioli, B., Ciccioli, P., Zona, D., Loreto, F., Janssens, I. A., and Ceulemans, R.: Proton Transfer Reaction Time-of-Flight Mass Spectrometric (PTR-TOF-MS) determination of volatile organic compounds (VOCs) emitted from a biomass fire developed under stable nocturnal conditions, Atmospheric Environment, 97, 54-67, 10.1016/j.atmosenv.2014.08.007, 2014.

Buhr, K., van Ruth, S., and Delahunty, C.: Analysis of volatile flavour compounds by Proton Transfer Reaction-Mass Spectrometry: fragmentation patterns and discrimination between isobaric and isomeric compounds, International Journal of Mass Spectrometry, 221, 1-7, https://doi.org/10.1016/S1387-3806(02)00896-5, 2002.

Cabrera-Perez, D., Taraborrelli, D., Sander, R., and Pozzer, A.: Global atmospheric budget of simple monocyclic aromatic compounds, Atmospheric Chemistry and Physics, 16, 6931-6947, 10.5194/acp-16-6931-2016, 2016.

Carlier, P., Hannachi, H., and Mouvier, G.: The chemistry of carbonyl compounds in the atmosphere—A review, Atmospheric Environment (1967), 20, 2079-2099, https://doi.org/10.1016/0004-6981(86)90304-5, 1986.

Celik, S., Drewnick, F., Fachinger, F., Brooks, J., Darbyshire, E., Coe, H., Paris, J. D., Eger, P. G., Schuladen, J., Tadic, I., Friedrich, N., Dienhart, D., Hottmann, B., Fischer, H., Crowley, J. N., Harder, H., and Borrmann, S.: Influence of vessel characteristics and atmospheric processes on the gas and particle phase of ship emission plumes: In-situ measurements in the Mediterranean Sea and around the Arabian Peninsula, Atmos. Chem. Phys. Discuss., 2019, 1-36, 10.5194/acp-2019-859, 2019.

Ciuraru, R., Fine, L., van Pinxteren, M., D'Anna, B., Herrmann, H., and George, C.: Photosensitized production of functionalized and unsaturated organic compounds at the air-sea interface, Sci Rep, 5, 12741, 10.1038/srep12741, 2015.

Cochran, R. E., Laskina, O., Jayarathne, T., Laskin, A., Laskin, J., Lin, P., Sultana, C., Lee, C., Moore, K. A., Cappa, C. D., Bertram, T. H., Prather, K. A., Grassian, V. H., and Stone, E. A.: Analysis of Organic Anionic Surfactants in Fine and Coarse Fractions of Freshly Emitted Sea Spray Aerosol, Environ Sci Technol, 50, 2477-2486, 10.1021/acs.est.5b04053, 2016.

Colomb, A., Williams, J., Crowley, J., Gros, V., Hofmann, R., Salisbury, G., Klüpfel, T., Kormann, R., Stickler, A., Forster, C., and Lelieveld, J.: Airborne Measurements of Trace Organic Species in the Upper Troposphere Over Europe: the Impact of Deep Convection, Environmental Chemistry, 3, 244, 10.1071/en06020, 2006.

Colomb, A., Gros, V., Alvain, S., Sarda-Esteve, R., Bonsang, B., Moulin, C., Klüpfel, T., and Williams, J.: Variation of atmospheric volatile organic compounds over the Southern Indian Ocean (30 - 49°S), Environmental Chemistry, 6, 70, 10.1071/en08072, 2009.

de Gouw, J., and Warneke, C.: Measurements of volatile organic compounds in the earth's atmosphere using proton-transfer-reaction mass spectrometry, Mass Spectrometry Reviews, 26, 223-257, 2007.

de Gouw, J. A., Middlebrook, A. M., Warneke, C., Goldan, P. D., Kuster, W. C., Roberts, J. M., Fehsenfeld, F. C., Worsnop, D. R., Canagaratna, M. R., Pszenny, A. A. P., Keene, W. C., Marchewka, M., Bertman, S. B., and Bates, T. S.: Budget of organic carbon in a polluted atmosphere: Results from the New England Air Quality Study in 2002, Journal of Geophysical Research: Atmospheres, 110, doi:10.1029/2004JD005623, 2005.

Dixon, J. L., Beale, R., and Nightingale, P. D.: Production of methanol, acetaldehyde, and acetone in the Atlantic Ocean, Geophysical Research Letters, 40, 4700-4705, 10.1002/grl.50922, 2013.

Dolgorouky, C., Gros, V., Sarda-Esteve, R., Sinha, V., Williams, J., Marchand, N., Sauvage, S., Poulain, L., Sciare, J., and Bonsang, B.: Total OH reactivity measurements in Paris during the 2010 MEGAPOLI winter campaign, Atmospheric Chemistry and Physics, 12, 9593-9612, 10.5194/acp-12-9593-2012, 2012.

Dong, D., Shao, M., Li, Y., Lu, S., Wang, Y., Ji, Z., and Tang, D.: Carbonyl emissions from heavy-duty diesel vehicle exhaust in China and the contribution to ozone formation potential, Journal of Environmental Sciences, 26, 122-128, https://doi.org/10.1016/S1001-0742(13)60387-3, 2014.

Edtbauer, A., Stönner, C., Pfannerstill, E. Y., Berasategui, M., Walter, D., Crowley, J. N., Lelieveld, J., and Williams, J.: A new marine biogenic emission: methane sulfonamide (MSAM), dimethyl sulfide (DMS), and dimethyl sulfone ($DMSO_2$) measured in air over the Arabian Sea, Atmospheric Chemistry and Physics, 20, 6081-6094, 10.5194/acp-20-6081-2020, 2020.

Edwards, P. M., Brown, S. S., Roberts, J. M., Ahmadov, R., Banta, R. M., deGouw, J. A., Dube, W. P., Field, R. A., Flynn, J. H., Gilman, J. B., Graus, M., Helmig, D., Koss, A., Langford, A. O., Lefer, B. L., Lerner, B. M., Li, R., Li, S. M., McKeen, S. A., Murphy, S. M., Parrish, D. D., Senff, C. J., Soltis, J., Stutz, J., Sweeney, C., Thompson, C. R., Trainer, M. K., Tsai, C., Veres, P. R., Washenfelder, R. A., Warneke, C., Wild, R. J., Young, C. J., Yuan, B., and Zamora, R.: High winter ozone pollution from carbonyl photolysis in an oil and gas basin, Nature, 514, 351-354, 10.1038/nature13767, 2014.

Eger, P. G., Schuladen, J., Sobanski, N., Fischer, H., Karu, E., Williams, J., Riva, M., Zha, Q., Ehn, M., Quéléver, L. L. J., Schallhart, S., Lelieveld, J., and Crowley, J. N.: Pyruvic acid in the boreal forest: gas-phase mixing ratios and impact on radical chemistry, Atmos. Chem. Phys., 20, 3697–3711, 10.5194/acp-20-3697-2020, 2020.

Ellis, A. M., and Mayhew, C. A.: Proton transfer reaction mass spectrometry: principles and applications, John Wiley & Sons, UK, 2013.

Erickson, M. H., Gueneron, M., and Jobson, B. T.: Measuring long chain alkanes in diesel engine exhaust by thermal desorption PTR-MS, Atmospheric Measurement Techniques, 7, 225-239, 10.5194/amt-7-225-2014, 2014.

Fall, R.: Abundant Oxygenates in the Atmosphere: A Biochemical Perspective, Chemical Reviews, 103, 4941-4952, 10.1021/cr0206521, 2003.

Fan, J., and Zhang, R.: Atmospheric Oxidation Mechanism of Isoprene, Environmental Chemistry, 1, 140-149, https://doi.org/10.1071/EN04045, 2004.

Finlayson-Pitts, B. J., and Pitts, J. N.: Tropospheric Air Pollution: Ozone, Airborne Toxics, Polycyclic Aromatic Hydrocarbons, and Particles, Science, 276, 1045, 10.1126/science.276.5315.1045, 1997.

Finlayson-Pitts, B. J., and Pitts Jr, J. N.: Chemistry of the upper and lower atmosphere: theory, experiments, and applications, Elsevier, USA, 1999.

Fischer, E. V., Jacob, D. J., Millet, D. B., Yantosca, R. M., and Mao, J.: The role of the ocean in the global atmospheric budget of acetone, Geophysical Research Letters, 39, n/a-n/a, 10.1029/2011gl050086, 2012.

Fischer, H., Pozzer, A., Schmitt, T., Jöckel, P., Klippel, T., Taraborrelli, D., and Lelieveld, J.: Hydrogen peroxide in the marine boundary layer over the South Atlantic during the OOMPH cruise in March 2007, Atmospheric Chemistry and Physics, 15, 6971-6980, 10.5194/acp-15-6971-2015, 2015.

Gantt, B., Meskhidze, N., Facchini, M. C., Rinaldi, M., Ceburnis, D., amp, apos, and Dowd, C. D.: Wind speed dependent size-resolved parameterization for the organic mass fraction of sea spray aerosol, Atmospheric Chemistry and Physics, 11, 8777-8790, 10.5194/acp-11-8777-2011, 2011.

Gentner, D. R., Isaacman, G., Worton, D. R., Chan, A. W. H., Dallmann, T. R., Davis, L., Liu, S., Day, D. A., Russell, L. M., Wilson, K. R., Weber, R., Guha, A., Harley, R. A., and Goldstein, A. H.: Elucidating secondary organic aerosol from diesel and gasoline vehicles through detailed characterization of organic carbon emissions, Proceedings of the National Academy of Sciences, 109, 18318, 10.1073/pnas.1212272109, 2012.

Gilman, J. B., Lerner, B. M., Kuster, W. C., and de Gouw, J. A.: Source signature of volatile organic compounds from oil and natural gas operations in northeastern Colorado, Environ Sci Technol, 47, 1297-1305, 10.1021/es304119a, 2013.

Griffith, E. C., Carpenter, B. K., Shoemaker, R. K., and Vaida, V.: Photochemistry of aqueous pyruvic acid, Proceedings of the National Academy of Sciences, 110, 11714, 10.1073/pnas.1303206110, 2013.

Gueneron, M., Erickson, M. H., VanderSchelden, G. S., and Jobson, B. T.: PTR-MS fragmentation patterns of gasoline hydrocarbons, International Journal of Mass Spectrometry, 379, 97-109, 10.1016/j.ijms.2015.01.001, 2015.

Guo, H., Ling, Z. H., Cheung, K., Wang, D. W., Simpson, I. J., and Blake, D. R.: Acetone in the atmosphere of Hong Kong: Abundance, sources and photochemical precursors, Atmospheric Environment, 65, 80-88, 10.1016/j.atmosenv.2012.10.027, 2013.

Holzinger, R., Warneke, C., Hansel, A., Jordan, A., Lindinger, W., Scharffe, D. H., Schade, G., and Crutzen, P. J.: Biomass burning as a source of formaldehyde, acetaldehyde, methanol, acetone, acetonitrile, and hydrogen cyanide, Geophysical Research Letters, 26, 1161-1164, 10.1029/1999gl900156, 1999.

Holzinger, R., Jordan, A., Hansel, A., and Lindinger, W.: Automobile Emissions of Acetonitrile: Assessment of its Contribution to the Global Source, Journal of Atmospheric Chemistry, 38, 187-193, 10.1023/A:1006435723375, 2001.

Holzinger, R., Williams, J., Salisbury, G., Klüpfel, T., de Reus, M., Traub, M., Crutzen, P. J., and Lelieveld, J.: Oxygenated compounds in aged biomass burning plumes over the Eastern Mediterranean: evidence for strong secondary production of methanol and acetone, Atmos. Chem. Phys., 5, 39-46, 10.5194/acp-5-39-2005, 2005.

Hornbrook, R. S., Hills, A. J., Riemer, D. D., Abdelhamid, A., Flocke, F. M., Hall, S. R., Huey, L. G., Knapp, D. J., Liao, J., Mauldin III, R. L., Montzka, D. D., Orlando, J. J., Shepson, P. B., Sive, B., Staebler, R. M., Tanner, D. J., Thompson, C. R., Turnipseed, A., Ullmann, K., Weinheimer, A. J., and Apel, E. C.: Arctic springtime observations of volatile organic compounds during the OASIS-2009 campaign, Journal of Geophysical Research: Atmospheres, 121, 9789-9813, 10.1002/2015jd024360, 2016.

Huang, C., Hu, Q., Wang, H., Qiao, L., Jing, S., Wang, H., Zhou, M., Zhu, S., Ma, Y., Lou, S., Li, L., Tao, S., Li, Y., and Lou, D.: Emission factors of particulate and gaseous compounds from a large cargo vessel operated under real-world conditions, Environ Pollut, 242, 667-674, 10.1016/j.envpol.2018.07.036, 2018.

IUPAC Task Group on Atmospheric Chemical Kinetic Data Evaluation, (http://iupac.pole-ether.fr, last access:14 July 2020).

Jacob, D. J., Field, B. D., Jin, E. M., Bey, I., Li, Q., Logan, J. A., Yantosca, R. M., and Singh, H. B.: Atmospheric budget of acetone, Journal of Geophysical Research: Atmospheres, 107, ACH 5-1-ACH 5-17, 10.1029/2001jd000694, 2002.

Jardine, K. J., Sommer, E. D., Saleska, S. R., Huxman, T. E., Harley, P. C., and Abrell, L.: Gas Phase Measurements of Pyruvic Acid and Its Volatile Metabolites, Environmental Science & Technology, 44, 2454-2460, 10.1021/es903544p, 2010.

Ji, Y., Zhao, J., Terazono, H., Misawa, K., Levitt, N. P., Li, Y., Lin, Y., Peng, J., Wang, Y., Duan, L., Pan, B., Zhang, F., Feng, X., An, T., Marrero-Ortiz, W., Secrest, J., Zhang, A. L., Shibuya, K., Molina, M. J., and Zhang, R.: Reassessing the atmospheric oxidation mechanism of toluene, Proceedings of the National Academy of Sciences, 114, 8169, 10.1073/pnas.1705463114, 2017.

Jöckel, P., Kerkweg, A., Pozzer, A., Sander, R., Tost, H., Riede, H., Baumgaertner, A., Gromov, S., and Kern, B.: Development cycle 2 of the Modular Earth Submodel System (MESSy2), Geoscientific Model Development, 3, 717-752, 10.5194/gmd-3-717-2010, 2010.

Khan, M. A. H., Cooke, M. C., Utembe, S. R., Archibald, A. T., Maxwell, P., Morris, W. C., Xiao, P., Derwent, R. G., Jenkin, M. E., Percival, C. J., Walsh, R. C., Young, T. D. S., Simmonds, P. G., Nickless, G., O'Doherty, S., and Shallcross, D. E.: A study of global atmospheric budget and distribution of acetone using global atmospheric model STOCHEM-CRI, Atmospheric Environment, 112, 269-277, 10.1016/j.atmosenv.2015.04.056, 2015.

Kieber, D. J., and Mopper, K.: Photochemical formation of glyoxylic and pyruvic acids in seawater, Marine Chemistry, 21, 135-149, https://doi.org/10.1016/0304-4203(87)90034-X, 1987.

Kieber, R. J., Zhou, X., and Mopper, K.: Formation of carbonyl compounds from UV-induced photodegradation of humic substances in natural waters: Fate of riverine carbon in the sea, Limnology and Oceanography, 35, 1503-1515, 10.4319/lo.1990.35.7.1503, 1990.

Kim, K.-H., Hong, Y.-J., Pal, R., Jeon, E.-C., Koo, Y.-S., and Sunwoo, Y.: Investigation of carbonyl compounds in air from various industrial emission sources, Chemosphere, 70, 807-820, https://doi.org/10.1016/j.chemosphere.2007.07.025, 2008.

Koss, A., Yuan, B., Warneke, C., Gilman, J. B., Lerner, B. M., Veres, P. R., Peischl, J., Eilerman, S., Wild, R., Brown, S. S., Thompson, C. R., Ryerson, T., Hanisco, T., Wolfe, G. M., Clair, J. M. S., Thayer, M., Keutsch, F. N., Murphy, S., and de Gouw, J.: Observations of VOC emissions and photochemical products over US oil- and gas-producing regions using high-resolution H3O+ CIMS (PTR-ToF-MS), Atmos. Meas. Tech., 10, 2941-2968, 10.5194/amt-10-2941-2017, 2017.

Koss, A. R., de Gouw, J., Warneke, C., Gilman, J. B., Lerner, B. M., Graus, M., Yuan, B., Edwards, P., Brown, S. S., Wild, R., Roberts, J. M., Bates, T. S., and Quinn, P. K.: Photochemical aging of volatile organic compounds associated with oil and natural gas extraction in the Uintah Basin, UT, during a wintertime ozone formation event, Atmospheric Chemistry and Physics, 15, 5727-5741, 10.5194/acp-15-5727-2015, 2015.

Koss, A. R., Sekimoto, K., Gilman, J. B., Selimovic, V., Coggon, M. M., Zarzana, K. J., Yuan, B., Lerner, B. M., Brown, S. S., Jimenez, J. L., Krechmer, J., Roberts, J. M., Warneke, C., Yokelson, R. J., and de Gouw, J.: Non-methane organic gas emissions from biomass burning: identification, quantification, and emission factors from PTR-ToF during the FIREX 2016 laboratory experiment, Atmospheric Chemistry and Physics, 18, 3299-3319, 10.5194/acp-18-3299-2018, 2018.

Kroll, J. H., Ng, N. L., Murphy, S. M., Varutbangkul, V., Flagan, R. C., and Seinfeld, J. H.: Chamber studies of secondary organic aerosol growth by reactive uptake of simple carbonyl compounds, Journal of Geophysical Research, 110, 10.1029/2005jd006004, 2005.

Lelieveld, J., Gromov, S., Pozzer, A., and Taraborrelli, D.: Global tropospheric hydroxyl distribution, budget and reactivity, Atmospheric Chemistry and Physics, 16, 12477-12493, 10.5194/acp-16-12477-2016, 2016.

Lewis, A., Hopkins, J., Carpenter, L., Stanton, J., Read, K., and Pilling, M.: Sources and sinks of acetone, methanol, and acetaldehyde in North Atlantic marine air, Atmospheric Chemistry and Physics, 5, 1963-1974, 2005.

Li, S.-M., Leithead, A., Moussa, S. G., Liggio, J., Moran, M. D., Wang, D., Hayden, K., Darlington, A., Gordon, M., Staebler, R., Makar, P. A., Stroud, C. A., McLaren, R., Liu, P. S. K., O'Brien, J., Mittermeier, R. L., Zhang, J., Marson, G., Cober, S. G., Wolde, M., and Wentzell, J. J. B.: Differences between measured and reported volatile organic compound emissions from oil sands facilities in Alberta, Canada, Proceedings of the National Academy of Sciences, 114, E3756, 10.1073/pnas.1617862114, 2017.

Lindinger, W., Hansel, A., and Jordan, A.: On-line monitoring of volatile organic compounds at pptv levels by means of proton-transfer-reaction mass spectrometry (PTR-MS) medical applications, food control and environmental research, International Journal of Mass Spectrometry and Ion Processes, 173, 191-241, 1998.

Lobert, J. M., Scharffe, D. H., Hao, W. M., and Crutzen, P. J.: Importance of biomass burning in the atmospheric budgets of nitrogen-containing gases, Nature, 346, 552-554, 10.1038/346552a0, 1990.

Marandino, C. A., De Bruyn, W. J., Miller, S. D., Prather, M. J., and Saltzman, E. S.: Oceanic uptake and the global atmospheric acetone budget, Geophysical Research Letters, 32, 10.1029/2005GL023285, 2005.

Millet, D. B., Guenther, A., Siegel, D. A., Nelson, N. B., Singh, H. B., de Gouw, J. A., Warneke, C., Williams, J., Eerdekens, G., and Sinha, V.: Global atmospheric budget of acetaldehyde: 3-D model analysis and constraints from in-situ and satellite observations, Atmospheric Chemistry and Physics, 10, 3405-3425, 2010.

Mochida, M., Kitamori, Y., Kawamura, K., Nojiri, Y., and Suzuki, K.: Fatty acids in the marine atmosphere: Factors governing their concentrations and evaluation of organic films on sea-salt particles, Journal of Geophysical Research: Atmospheres, 107, AAC 1-1-AAC 1-10, 10.1029/2001jd001278, 2002.

Müller, M., Graus, M., Wisthaler, A., Hansel, A., Metzger, A., Dommen, J., and Baltensperger, U.: Analysis of high mass resolution PTR-TOF mass spectra from 1,3,5-trimethylbenzene (TMB) environmental chamber experiments, Atmospheric Chemistry and Physics, 12, 829-843, 10.5194/acp-12-829-2012, 2012.

Müller, M., Mikoviny, T., Jud, W., D'Anna, B., and Wisthaler, A.: A new software tool for the analysis of high resolution PTR-TOF mass spectra, Chemometrics and Intelligent Laboratory Systems, 127, 158-165, 10.1016/j.chemolab.2013.06.011, 2013.

Meusel, H., Kuhn, U., Reiffs, A., Mallik, C., Harder, H., Martinez, M., Schuladen, J., Bohn, B., Parchatka, U., and Crowley, J. N.: Daytime formation of nitrous acid at a coastal remote site in Cyprus indicating a common ground source of atmospheric HONO and NO, Atmospheric Chemistry and Physics, 16, 14475-14493, 2016.

Nogueira, T., Dominutti, P. A., de Carvalho, L. R. F., Fornaro, A., and Andrade, M. d. F.: Formaldehyde and acetaldehyde measurements in urban atmosphere impacted by the use of ethanol biofuel: Metropolitan Area of Sao Paulo (MASP), 2012–2013, Fuel, 134, 505-513, 10.1016/j.fuel.2014.05.091, 2014.

Northway, M. J., de Gouw, J. A., Fahey, D. W., Gao, R. S., Warneke, C., Roberts, J. M., and Flocke, F.: Evaluation of the role of heterogeneous oxidation of alkenes in the detection of atmospheric acetaldehyde, Atmospheric Environment, 38, 6017-6028, 10.1016/j.atmosenv.2004.06.039, 2004.

Pfannerstill, E. Y., Wang, N., Edtbauer, A., Bourtsoukidis, E., Crowley, J. N., Dienhart, D., Eger, P. G., Ernle, L., Fischer, H., Hottmann, B., Paris, J.-D., Stönner, C., Tadic, I., Walter, D., Lelieveld, J., and Williams, J.: Shipborne measurements of total OH reactivity around the Arabian Peninsula and its role in ozone chemistry, Atmospheric Chemistry and Physics, 19, 11501-11523, 10.5194/acp-19-11501-2019, 2019.

Pozzer, A., Jöckel, P., Sander, R., Williams, J., Ganzeveld, L., and Lelieveld, J.: Technical Note: The MESSy-submodel AIRSEA calculating the air-sea exchange of chemical species, Atmos. Chem. Phys., 6, 5435-5444, 10.5194/acp-6-5435-2006, 2006.

Pozzer, A., Jöckel, P., Tost, H., Sander, R., Ganzeveld, L., Kerkweg, A., and Lelieveld, J.: Simulating organic species with the global atmospheric chemistry general circulation model ECHAM5/MESSy1: a comparison of model results with observations, Atmos. Chem. Phys., 7, 2527-2550, 10.5194/acp-7-2527-2007, 2007.

Pozzer, A., de Meij, A., Pringle, K. J., Tost, H., Doering, U. M., van Aardenne, J., and Lelieveld, J.: Distributions and regional budgets of aerosols and their precursors simulated with the EMAC chemistry-climate model, Atmospheric Chemistry and Physics, 12, 961-987, 10.5194/acp-12-961-2012, 2012.

Read, K. A., Carpenter, L. J., Arnold, S. R., Beale, R., Nightingale, P. D., Hopkins, J. R., Lewis, A. C., Lee, J. D., Mendes, L., and Pickering, S. J.: Multiannual observations of acetone, methanol, and acetaldehyde in

remote tropical atlantic air: implications for atmospheric OVOC budgets and oxidative capacity, Environ Sci Technol, 46, 11028-11039, 10.1021/es302082p, 2012.

Reda, A. A., Schnelle-Kreis, J., Orasche, J., Abbaszade, G., Lintelmann, J., Arteaga-Salas, J. M., Stengel, B., Rabe, R., Harndorf, H., Sippula, O., Streibel, T., and Zimmermann, R.: Gas phase carbonyl compounds in ship emissions: Differences between diesel fuel and heavy fuel oil operation, Atmospheric Environment, 94, 467-478, 10.1016/j.atmosenv.2014.05.053, 2014.

Reed Harris, A. E., Ervens, B., Shoemaker, R. K., Kroll, J. A., Rapf, R. J., Griffith, E. C., Monod, A., and Vaida, V.: Photochemical kinetics of pyruvic acid in aqueous solution, J Phys Chem A, 118, 8505-8516, 10.1021/jp502186q, 2014.

Reed Harris, A. E., Doussin, J.-F., Carpenter, B. K., and Vaida, V.: Gas-Phase Photolysis of Pyruvic Acid: The Effect of Pressure on Reaction Rates and Products, The Journal of Physical Chemistry A, 120, 10123-10133, 10.1021/acs.jpca.6b09058, 2016.

Roberts, J. M., Fehsenfeld, F. C., Liu, S. C., Bollinger, M. J., Hahn, C., Albritton, D. L., and Sievers, R. E.: Measurements of aromatic hydrocarbon ratios and NOx concentrations in the rural troposphere: Observation of air mass photochemical aging and NOx removal, Atmospheric Environment (1967), 18, 2421-2432, https://doi.org/10.1016/0004-6981(84)90012-X, 1984.

Roeckner, E., Brokopf, R., Esch, M., Giorgetta, M., Hagemann, S., Kornblueh, L., Manzini, E., Schlese, U., and Schulzweida, U.: Sensitivity of Simulated Climate to Horizontal and Vertical Resolution in the ECHAM5 Atmosphere Model, Journal of Climate, 19, 3771-3791, 10.1175/JCLI3824.1, 2006.

Rutter, A. P., Griffin, R. J., Cevik, B. K., Shakya, K. M., Gong, L., Kim, S., Flynn, J. H., and Lefer, B. L.: Sources of air pollution in a region of oil and gas exploration downwind of a large city, Atmospheric Environment, 120, 89-99, 10.1016/j.atmosenv.2015.08.073, 2015.

Sahu, L. K., Tripathi, N., and Yadav, R.: Contribution of biogenic and photochemical sources to ambient VOCs during winter to summer transition at a semi-arid urban site in India, Environ Pollut, 229, 595-606, 10.1016/j.envpol.2017.06.091, 2017.

Said, N., El-Shatoury, S. A., Díaz, L. F., and Zamorano, M.: Quantitative appraisal of biomass resources and their energy potential in Egypt, Renewable and Sustainable Energy Reviews, 24, 84-91, https://doi.org/10.1016/j.rser.2013.03.014, 2013.

Sander, R.: Compilation of Henry's law constants (version 4.0) for water as solvent, Atmospheric Chemistry and Physics, 15, 4399-4981, 10.5194/acp-15-4399-2015, 2015.

Sander, R., Baumgaertner, A., Cabrera-Perez, D., Frank, F., Gromov, S., Grooß, J.-U., Harder, H., Huijnen, V., Jöckel, P., Karydis, V. A., Niemeyer, K. E., Pozzer, A., Riede, H., Schultz, M. G., Taraborrelli, D., and Tauer, S.: The community atmospheric chemistry box model CAABA/MECCA-4.0, Geoscientific Model Development, 12, 1365-1385, 10.5194/gmd-12-1365-2019, 2019.

Schauer, J. J., Kleeman, M. J., Cass, G. R., and Simoneit, B. R. T.: Measurement of Emissions from Air Pollution Sources. 3. C1−C29 Organic Compounds from Fireplace Combustion of Wood, Environmental Science & Technology, 35, 1716-1728, 10.1021/es001331e, 2001.

Schlundt, C., Tegtmeier, S., Lennartz, S. T., Bracher, A., Cheah, W., Krüger, K., Quack, B., and Marandino, C. A.: Oxygenated volatile organic carbon in the western Pacific convective center: ocean cycling, air–sea gas exchange and atmospheric transport, Atmospheric Chemistry and Physics, 17, 10837-10854, 10.5194/acp-17-10837-2017, 2017.

Sheng, J., Zhao, D., Ding, D., Li, X., Huang, M., Gao, Y., Quan, J., and Zhang, Q.: Characterizing the level, photochemical reactivity, emission, and source contribution of the volatile organic compounds based on PTR-TOF-MS during winter haze period in Beijing, China, Atmospheric Research, 212, 54-63, https://doi.org/10.1016/j.atmosres.2018.05.005, 2018.

Simpson, I. J., Blake, N. J., Barletta, B., Diskin, G. S., Fuelberg, H. E., Gorham, K., Huey, L. G., Meinardi, S., Rowland, F. S., Vay, S. A., Weinheimer, A. J., Yang, M., and Blake, D. R.: Characterization of trace gases measured over Alberta oil sands mining operations: 76 speciated C_2–C_{10} volatile organic compounds

(VOCs), CO_2, CH_4, CO, NO, NO_2, NO_y, O_3 and SO_2, Atmos. Chem. Phys., 10, 11931-11954, 10.5194/acp-10-11931-2010, 2010.

Singh, H. B., O'hara, D., Herlth, D., Sachse, W., Blake, D., Bradshaw, J., Kanakidou, M., and Crutzen, P.: Acetone in the atmosphere: Distribution, sources, and sinks, Journal of Geophysical Research: Atmospheres, 99, 1805-1819, 1994.

Singh, H. B., Tabazadeh, A., Evans, M. J., Field, B. D., Jacob, D. J., Sachse, G., Crawford, J. H., Shetter, R., and Brune, W. H.: Oxygenated volatile organic chemicals in the oceans: Inferences and implications based on atmospheric observations and air-sea exchange models, Geophysical Research Letters, 30, 10.1029/2003gl017933, 2003.

Singh, H. B.: Analysis of the atmospheric distribution, sources, and sinks of oxygenated volatile organic chemicals based on measurements over the Pacific during TRACE-P, Journal of Geophysical Research, 109, 10.1029/2003jd003883, 2004.

Sinha, V., Williams, J., Meyerhöfer, M., Riebesell, U., Paulino, A. I., and Larsen, A.: Air-sea fluxes of methanol, acetone, acetaldehyde, isoprene and DMS from a Norwegian fjord following a phytoplankton bloom in a mesocosm experiment, Atmos. Chem. Phys., 7, 739-755, 10.5194/acp-7-739-2007, 2007.

Sjostedt, S. J., Leaitch, W. R., Levasseur, M., Scarratt, M., Michaud, S., Motard-Côté, J., Burkhart, J. H., and Abbatt, J. P. D.: Evidence for the uptake of atmospheric acetone and methanol by the Arctic Ocean during late summer DMS-Emission plumes, Journal of Geophysical Research: Atmospheres, 117, n/a-n/a, 10.1029/2011jd017086, 2012.

Spanel, P., Doren, J., and Smith, D.: A selected ion flow tube study of the reactions of H3O+, NO+, and O2+ with saturated and unsaturated aldehydes and subsequent hydration of the product ions, International Journal of Mass Spectrometry, 213, 163-176, 10.1016/S1387-3806(01)00531-0, 2002.

Steinberg, S. M., and Bada, J. L.: Oxalic, glyoxalic and pyruvic acids in eastern Pacific Ocean waters, Journal of Marine Research, 42, 697-708, 10.1357/002224084788506068, 1984.

Stickler, A., Fischer, H., Williams, J., de Reus, M., Sander, R., Lawrence, M. G., Crowley, J. N., and Lelieveld, J.: Influence of summertime deep convection on formaldehyde in the middle and upper troposphere over Europe, Journal of Geophysical Research, 111, 10.1029/2005jd007001, 2006.

Swarthout, R. F., Russo, R. S., Zhou, Y., Miller, B. M., Mitchell, B., Horsman, E., Lipsky, E., McCabe, D. C., Baum, E., and Sive, B. C.: Impact of Marcellus Shale natural gas development in southwest Pennsylvania on volatile organic compound emissions and regional air quality, Environ Sci Technol, 49, 3175-3184, 10.1021/es504315f, 2015.

Tadic, I., Crowley, J. N., Dienhart, D., Eger, P., Harder, H., Hottmann, B., Martinez, M., Parchatka, U., Paris, J.-D., Pozzer, A., Rohloff, R., Schuladen, J., Shenolikar, J., Tauer, S., Lelieveld, J., and Fischer, H.: Net ozone production and its relationship to nitrogen oxides and volatile organic compounds in the marine boundary layer around the Arabian Peninsula, Atmospheric Chemistry and Physics, 20, 6769-6787, 10.5194/acp-20-6769-2020, 2020.

Tanimoto, H., Kameyama, S., Iwata, T., Inomata, S., and Omori, Y.: Measurement of air-sea exchange of dimethyl sulfide and acetone by PTR-MS coupled with gradient flux technique, Environ Sci Technol, 48, 526-533, 10.1021/es4032562, 2014.

Vaught, C.: Locating and estimating air emissions from sources of formaldehyde (revised), Midwest Research Inst., Cary, NC (United States), 1991.

United States Central Intelligence Agency: Middle East oil and gas, Washington, D.C.: Central Intelligence Agency, available at: https://www.loc.gov/item/2007631392/ (last access: 26 November 2019), 2007.

Utah Division of Air Quality: Final Report: Uinta Basin Winter Ozone Study, ENVIRON International Corporation, Novato, California 2014.

Wang, S., Hornbrook, R. S., Hills, A., Emmons, L. K., Tilmes, S., Lamarque, J. F., Jimenez, J. L., Campuzano-Jost, P., Nault, B. A., Crounse, J. D., Wennberg, P. O., Kim, M., Allen, H., Ryerson, T. B., Thompson, C. R., Peischl, J., Moore, F., Nance, D., Hall, B., Elkins, J., Tanner, D., Huey, L. G., Hall, S. R.,

Ullmann, K., Orlando, J. J., Tyndall, G. S., Flocke, F. M., Ray, E., Hanisco, T. F., Wolfe, G. M., St. Clair, J., Commane, R., Daube, B., Barletta, B., Blake, D. R., Weinzierl, B., Dollner, M., Conley, A., Vitt, F., Wofsy, S. C., Riemer, D. D., and Apel, E. C.: Atmospheric Acetaldehyde: Importance of Air-Sea Exchange and a Missing Source in the Remote Troposphere, Geophysical Research Letters, 10.1029/2019gl082034, 2019.

Warneke, C., Karl, T., Judmaier, H., Hansel, A., Jordan, A., Lindinger, W., and Crutzen, P. J.: Acetone, methanol, and other partially oxidized volatile organic emissions from dead plant matter by abiological processes: Significance for atmospheric HOx chemistry, Global Biogeochemical Cycles, 13, 9-17, 10.1029/98GB02428, 1999.

Warneke, C., and de Gouw, J. A.: Organic trace gas composition of the marine boundary layer over the northwest Indian Ocean in April 2000, Atmospheric Environment, 35, 5923-5933, https://doi.org/10.1016/S1352-2310(01)00384-3, 2001.

Warneke, C., Geiger, F., Edwards, P. M., Dube, W., Pétron, G., Kofler, J., Zahn, A., Brown, S. S., Graus, M., Gilman, J. B., Lerner, B. M., Peischl, J., Ryerson, T. B., de Gouw, J. A., and Roberts, J. M.: Volatile organic compound emissions from the oil and natural gas industry in the Uintah Basin, Utah: oil and gas well pad emissions compared to ambient air composition, Atmospheric Chemistry and Physics, 14, 10977-10988, 10.5194/acp-14-10977-2014, 2014.

Wennberg, P. O., Bates, K. H., Crounse, J. D., Dodson, L. G., McVay, R. C., Mertens, L. A., Nguyen, T. B., Praske, E., Schwantes, R. H., Smarte, M. D., St Clair, J. M., Teng, A. P., Zhang, X., and Seinfeld, J. H.: Gas-Phase Reactions of Isoprene and Its Major Oxidation Products, Chemical Reviews, 118, 3337-3390, 10.1021/acs.chemrev.7b00439, 2018.

Williams, J., Roberts, J. M., Bertman, S. B., Stroud, C. A., Fehsenfeld, F. C., Baumann, K., Buhr, M. P., Knapp, K., Murphy, P. C., Nowick, M., and Williams, E. J.: A method for the airborne measurement of PAN, PPN, and MPAN, Journal of Geophysical Research: Atmospheres, 105, 28943-28960, 10.1029/2000JD900373, 2000.

Williams, J., Pöschl, U., Crutzen, P. J., Hansel, A., Holzinger, R., Warneke, C., Lindinger, W., and Lelieveld, J.: An Atmospheric Chemistry Interpretation of Mass Scans Obtained from a Proton Transfer Mass Spectrometer Flown over the Tropical Rainforest of Surinam, Journal of Atmospheric Chemistry, 38, 133-166, 10.1023/A:1006322701523, 2001.

Williams, J., Holzinger, R., Gros, V., Xu, X., Atlas, E., and Wallace, D. W. R.: Measurements of organic species in air and seawater from the tropical Atlantic, Geophysical Research Letters, 31, 10.1029/2004gl020012, 2004.

Wisthaler, A.: Organic trace gas measurements by PTR-MS during INDOEX 1999, Journal of Geophysical Research, 107, 10.1029/2001jd000576, 2002.

White, M. L., Russo, R. S., Zhou, Y., Mao, H., Varner, R. K., Ambrose, J., Veres, P., Wingenter, O. W., Haase, K., Stutz, J., Talbot, R., and Sive, B. C.: Volatile organic compounds in northern New England marine and continental environments during the ICARTT 2004 campaign, Journal of Geophysical Research, 113, 10.1029/2007jd009161, 2008.

Wyche, K. P., Monks, P. S., Ellis, A. M., Cordell, R. L., Parker, A. E., Whyte, C., Metzger, A., Dommen, J., Duplissy, J., Prevot, A. S. H., Baltensperger, U., Rickard, A. R., and Wulfert, F.: Gas phase precursors to anthropogenic secondary organic aerosol: detailed observations of 1,3,5-trimethylbenzene photooxidation, Atmos. Chem. Phys., 9, 635-665, 10.5194/acp-9-635-2009, 2009.

Xiao, Q., Li, M., Liu, H., Fu, M., Deng, F., Lv, Z., Man, H., Jin, X., Liu, S., and He, K.: Characteristics of marine shipping emissions at berth: profiles for particulate matter and volatile organic compounds, Atmos. Chem. Phys., 18, 9527-9545, 10.5194/acp-18-9527-2018, 2018.

Yang, M., Beale, R., Liss, P., Johnson, M., Blomquist, B., and Nightingale, P.: Air–sea fluxes of oxygenated volatile organic compounds across the Atlantic Ocean, Atmospheric Chemistry and Physics, 14, 7499-7517, 10.5194/acp-14-7499-2014, 2014.

Youssef, M. A., Wahid, S. S., Mohamed, M. A., and Askalany, A. A.: Experimental study on Egyptian biomass combustion in circulating fluidized bed, Applied Energy, 86, 2644-2650, https://doi.org/10.1016/j.apenergy.2009.04.021, 2009.

Yuan, B., Shao, M., de Gouw, J., Parrish, D. D., Lu, S., Wang, M., Zeng, L., Zhang, Q., Song, Y., Zhang, J., and Hu, M.: Volatile organic compounds (VOCs) in urban air: How chemistry affects the interpretation of positive matrix factorization (PMF) analysis, Journal of Geophysical Research: Atmospheres, 117, n/a-n/a, 10.1029/2012jd018236, 2012.

Yuan, B., Warneke, C., Shao, M., and de Gouw, J. A.: Interpretation of volatile organic compound measurements by proton-transfer-reaction mass spectrometry over the deepwater horizon oil spill, International Journal of Mass Spectrometry, 358, 43-48, 10.1016/j.ijms.2013.11.006, 2014.

Yuan, B., Koss, A. R., Warneke, C., Coggon, M., Sekimoto, K., and de Gouw, J. A.: Proton-Transfer-Reaction Mass Spectrometry: Applications in Atmospheric Sciences, Chem Rev, 117, 13187-13229, 10.1021/acs.chemrev.7b00325, 2017.

Zhao, J., and Zhang, R.: Proton transfer reaction rate constants between hydronium ion (H3O+) and volatile organic compounds, Atmospheric Environment, 38, 2177-2185, 10.1016/j.atmosenv.2004.01.019, 2004.

Zhou, S., Gonzalez, L., Leithead, A., Finewax, Z., Thalman, R., Vlasenko, A., Vagle, S., Miller, L. A., Li, S. M., Bureekul, S., Furutani, H., Uematsu, M., Volkamer, R., and Abbatt, J.: Formation of gas-phase carbonyls from heterogeneous oxidation of polyunsaturated fatty acids at the air–water interface and of the sea surface microlayer, Atmospheric Chemistry and Physics, 14, 1371-1384, 10.5194/acp-14-1371-2014, 2014.

Zhou, X., and Mopper, K.: Carbonyl compounds in the lower marine troposphere over the Caribbean Sea and Bahamas, Journal of Geophysical Research: Oceans, 98, 2385-2392, 10.1029/92jc02772, 1993.

Zhou, X., and Mopper, K.: Photochemical production of low-molecular-weight carbonyl compounds in seawater and surface microlayer and their air-sea exchange, Marine Chemistry, 56, 201-213, https://doi.org/10.1016/S0304-4203(96)00076-X, 1997.

Supplementary

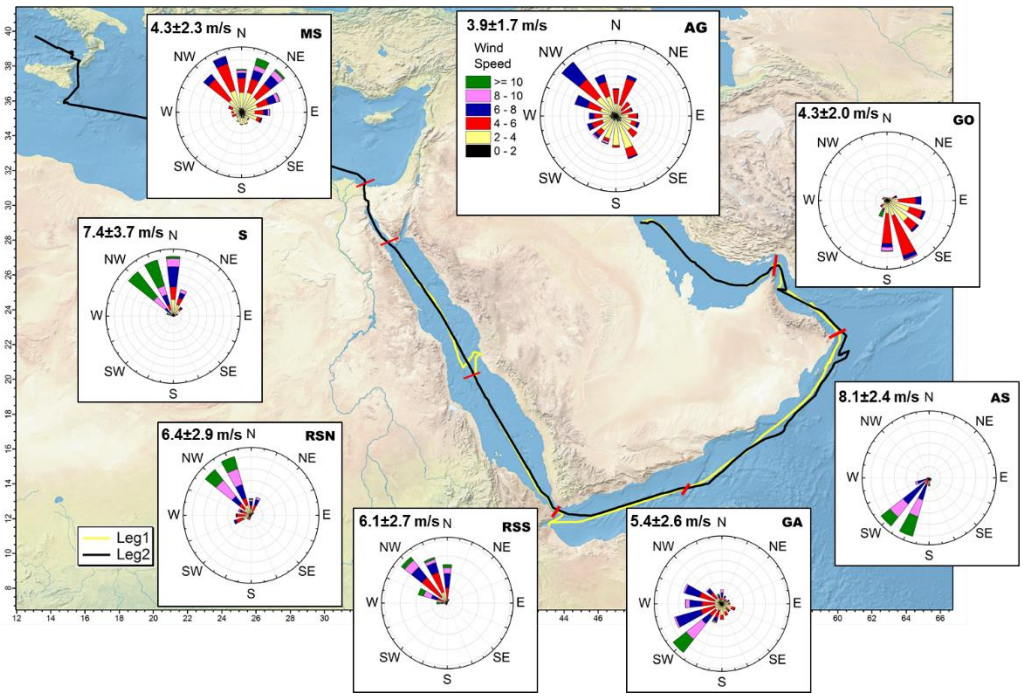

Figure S2.1. Wind map of each area and ship cruise. The number on the left top of each map represents the mean ± standard deviation of the wind speed in each area. The data used for map plotting was from public domain GIS data found on the Natural Earth web site (http://www.naturalearthdata.com) was read into Igor using the IgorGIS XOP beta.

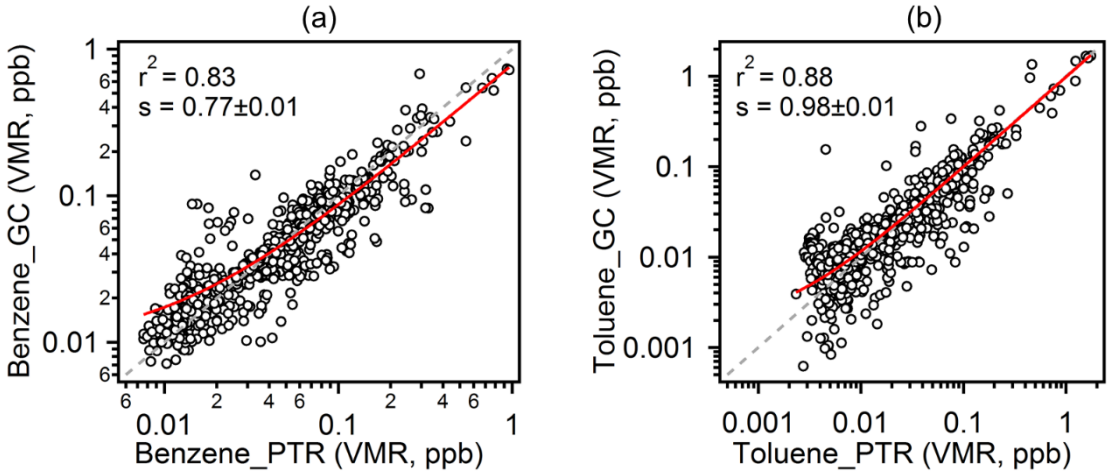

Figure S2.2. Comparison of (a) benzene and (b) toluene measured by GC-FID and PTR-ToF-MS (data from PTR-Tof-MS was averaged to GC time resolution of 50 min).

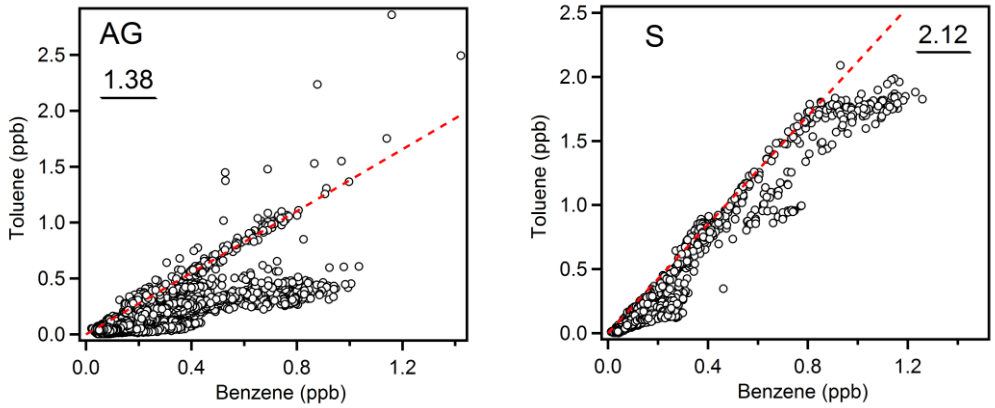

Figure S2.3. Scatter plots between benzene and toluene mixing ratios for Arabian Gulf and Suez. Red dashed line represents the initial emission ratio (values with underlined numbers on the top right of each figure) determined for further OH exposure calculation.

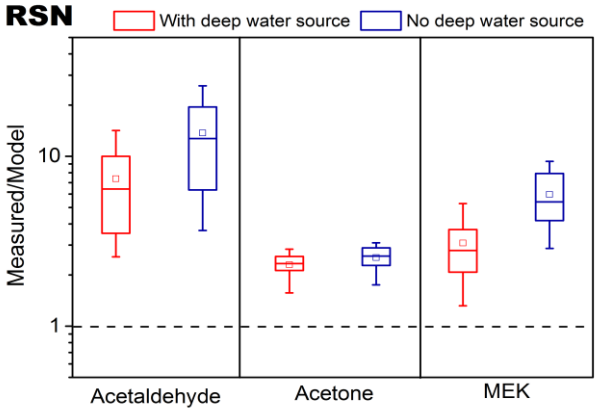

Figure S2.4. Comparison of model results for carbonyls with and without input of the ethane and propane deep water source in the North Red Sea.

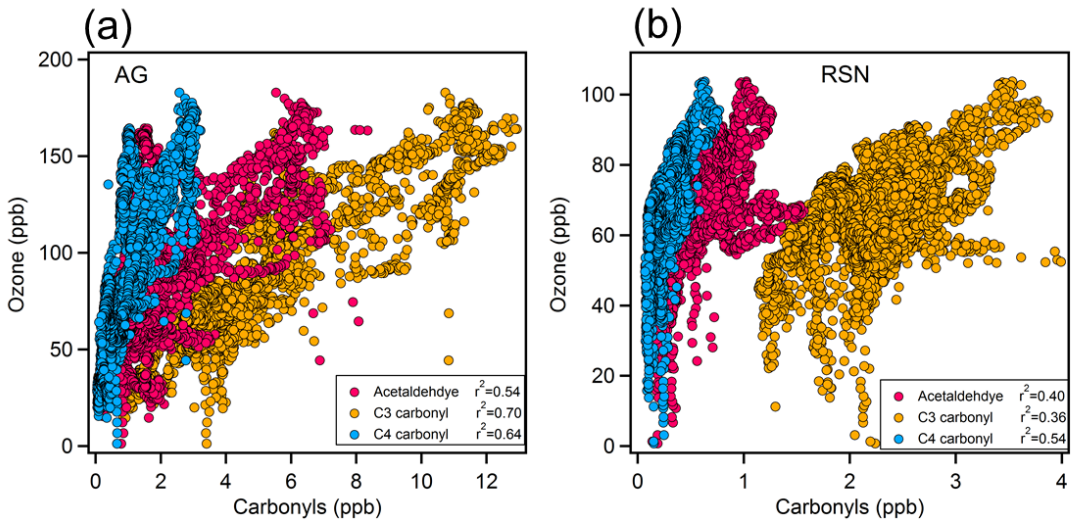

Figure S2.5. Scatter plots of carbonyls and ozone mixing ratios over the (a) Arabian Gulf (AG) and (b) Red Sea North (RSN).

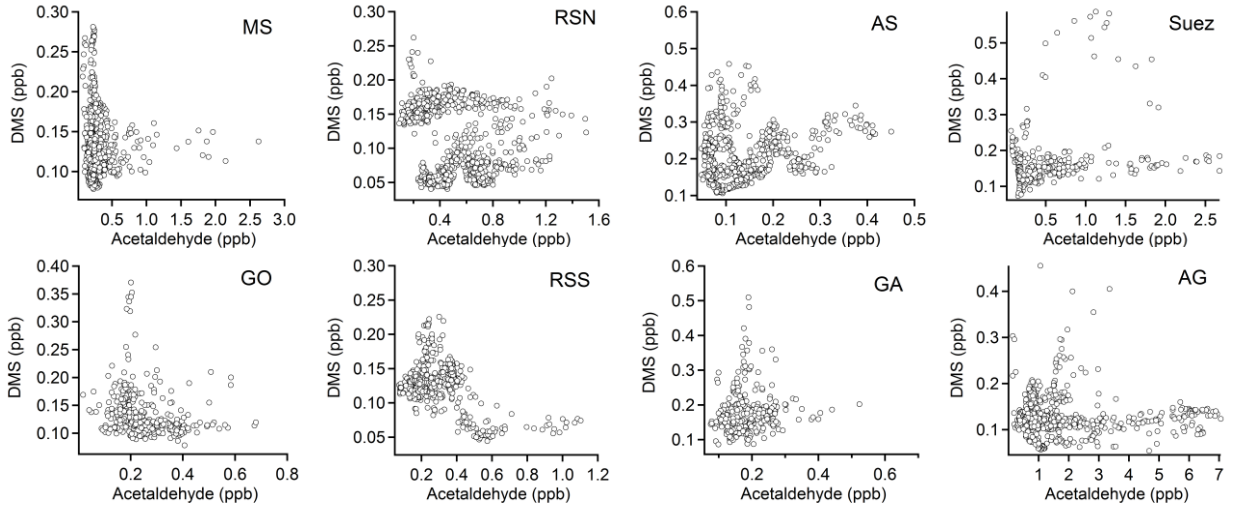

Figure S2.6. Scatter plots between dimethyl sulfide (DMS) and acetaldehyde mixing ratios over the eight regions (10 minute average).

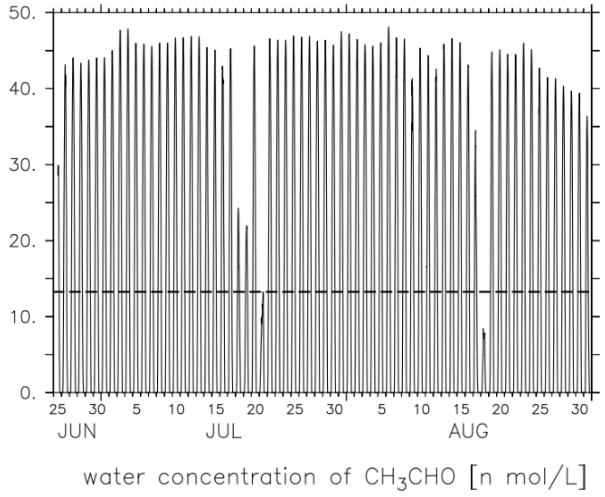

Figure S2.7. Estimated water concentration of acetaldehyde (nM) scaled according to solar radiation. The black dash line indicates the mean level 13.4 nM.

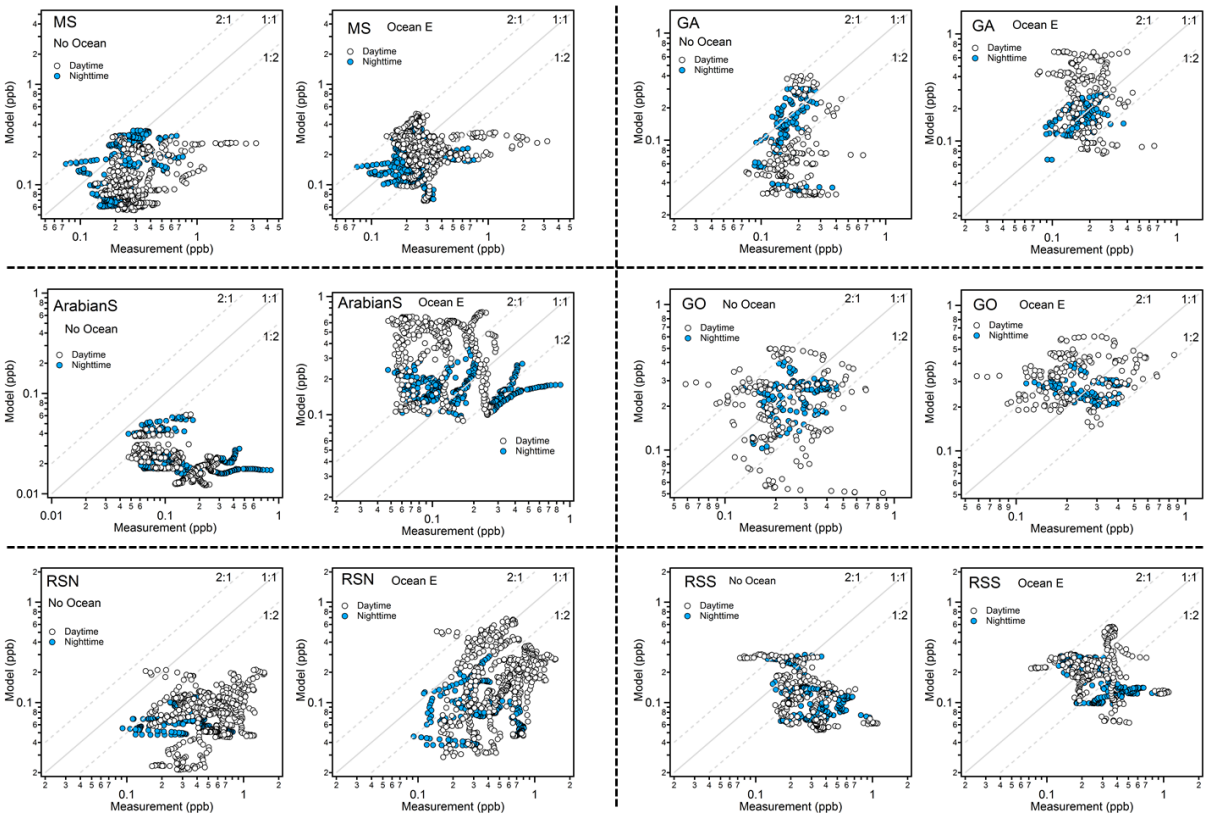

Figure S2.8. Scatter plots between measured and model simulated mixing ratios for acetaldehyde in different regions without ocean source (graph on the left side of each region labeled with No Ocean) and with ocean emission source (graph on the right side of each region labeled with Ocean E). The data points are further separated into day- and nighttime according to solar radiation.

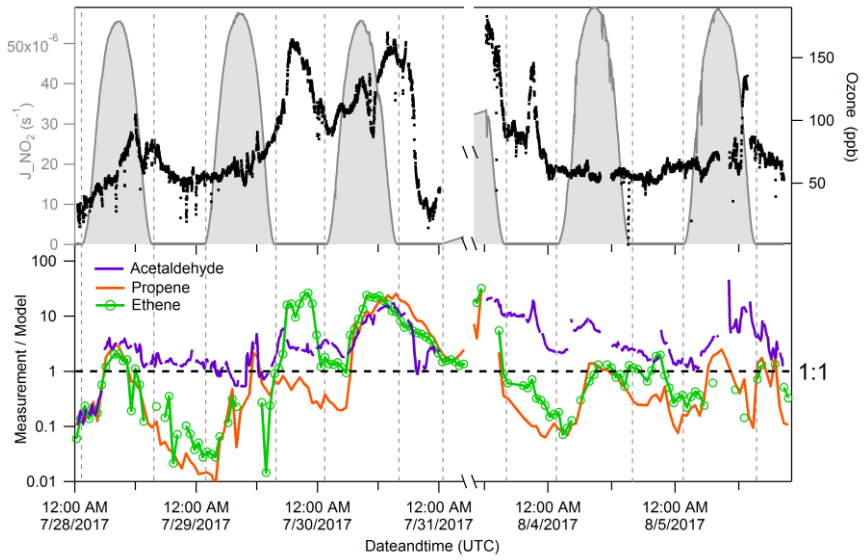

Figure S2.9. Time series of ozone mixing ratios and measurement to model ratios of acetaldehyde, propene and ethene over the Arabian Gulf (shaded area represents daytime).

Table S2.1. Detection limit (LOD) and total uncertainty of standard gas calibrated trace gases during AQABA

Compounds	Protonated Masses	LOD (mean ± 3σ) (ppt)	LOD Range (ppt)	Total Uncertainty (%)
Methanol	33.0335	105 ± 40	31-302	17
Acetonitrile	42.0339	13 ± 3	4-23	6
Acetaldehyde	45.0335	52 ± 26	10-194	8
Acetone	59.0492	22 ± 9	6-122	6
DMS	63.0263	13 ±5	2-30	12
Isoprene	69.0699	15 ± 10	2-98	6
Methacrolein/ Methyl Vinyl Ketone	71.0492	7 ± 2	2-19	6
MEK	73.0648	9 ± 6	3-80	6
Benzene	79.0543	6 ± 2	2-16	7
Toluene	93.0699	4 ± 1	1-8	8
Xylene	107.0856	4 ± 1	1-10	7
1,3,5-Trimethylbenzene	121.1012	3 ± 1	1-13	7
α-pinene	137.1325	5 ± 3	2-38	7

Table S2.2. Protonated masses, chemical formula and limit of detection of carbonyl compounds.

Protonated Masses	Chemical Formula	LOD Average (ppt)	LOD Range (ppt)
Aliphatic CCs	**$C_nH_{2n}OH^+$**		
87.0805	$C_5H_{10}OH^+$	10	4-28
101.0961	$C_6H_{12}OH^+$	11	3-34
115.1118	$C_7H_{14}OH^+$	7	1-22
129.1274	$C_8H_{16}OH^+$	6	1-24
143.1431	$C_9H_{18}OH^+$	5	1-28
Unsaturated CCs	**$C_nH_{2n-2}OH^+$**		
85.0648	$C_5H_8OH^+$	12	3-34
99.0805	$C_6H_{10}OH^+$	12	3-39
113.0961	$C_7H_{12}OH^+$	6	1-19
127.1118	$C_8H_{14}OH^+$	5	1-9
141.1274	$C_9H_{16}OH^+$	4	1-12
Aromatic CCs	**$C_nH_{2n-8}OH^+$**		
107.0492	$C_7H_6OH^+$	10	3-31
121.0648	$C_8H_8OH^+$	7	2-21
135.0805	$C_9H_{10}OH^+$	12	2-45

Table S2.3. OH rate constant of hydrocarbons and carbonyls mentioned in the study

Formula	Compound	CAS	k (OH) cm^3 $molecule^{-1}s^{-1}$ at 298K
Alkanes			
CH4	methane*	74-82-8	6.40E-15
C2H6	ethane*	74-84-0	2.40E-13
C3H8	propane*	74-98-6	1.10E-12
C4H10	i-butane	75-28-5	2.12E-12
C4H10	n-butane*	106-97-8	2.35E-12
C5H12	i-pentane	78-78-4	3.60E-12
C5H12	n-pentane	109-66-0	3.80E-12
C6H14	i-hexane	107-83-5	5.20E-12
C6H14	n-hexane	110-54-3	5.20E-12
C7H16	n-heptane	142-82-5	6.76E-12
C8H18	octane	111-65-9	8.11E-12
Alkenes			
C2H4	ethene		8.52E-12
Aliphatic Carbonyls			
CH2O	formaldehyde*	50-00-0	8.50E-12
C2H4O	acetaldehyde*	75-07-0	1.50E-11
C3H6O	acetone*	67-64-1	1.80E-13
C4H8O	methyl ethyl ketone*	78-93-3	1.10E-12
C5H10O	2-pentanone	107-87-9	4.40E-12
	3-pentanone	96-22-0	2.00E-12
	3-methyl-2-butanone	563-80-4	2.90E-12
C6H12O	3,3-dimethyl-2-butanone	75-97-8	1.20E-12
	2-hexanone	591-78-6	9.10E-12
	3-hexanone	589-38-8	6.90E-12
	4-methyl-2-pentanone	108-10-1	1.30E-11
	3-methyl-2-pentanone	565-61-7	6.90E-12
C7H14O	2,4-dimethyl-3-pentanone	565-80-0	5.00E-12
	2-heptanone	110-43-0	1.10E-11
	5-methyl-2-hexanone	110-12-3	1.00E-11
C8H16O	2-octanone	111-13-7	1.10E-11

Compounds marked with * represent k(OH) taken from Atkinson et.al. (2006). Otherwise k (OH) were taken from Atkinson and Arey (2003).

Calculation of acetaldehyde yield from pyruvic acid photolysis

In order to verify the contribution from the photolysis of pyruvic acid to acetaldehyde, we calculated the expected acetaldehyde produced through pyruvic acid photolysis over different regions assuming: (1) *m/z* 89.0234 is fully assigned to pyruvic acid; (2) the loss of pyruvic acid is only through photolysis; (3) 60% is the yield of acetaldehyde via pyruvic acid photolysis recommended by IUPAC (2019); (4) the loss of acetaldehyde is only through OH oxidation. The acetaldehyde produced via pyruvic acid photolysis can be calculated using following equation (consecutive reactions):

$$[Acetaldehyde] = [Pyruvic\ acid]\frac{J_{PA}}{k_{OH}[OH]-J_{PA}}[\exp(-J_{PA}\Delta t) - \exp(-k_{OH} \times [OH]\Delta t\ )] \quad \text{Eq. S2.1}$$

$[Pyruvic\ acid]$ is the mean of pyruvic acid mixing ratio in each region. J_{PA} represents the mean photolysis rate constant of pyruvic acid during the daytime (dawn to dusk) in each region calculated from the wavelength resolved actinic flux data using quantum yield of 0.2 as suggested by IUPAC (2019). The k_{OH} is the rate constant of acetaldehyde reacting with OH radical (1.5×10^{-11} cm^3 $molecule^{-1}s^{-1}$, Table S2.3). The $[OH]$ concentrations in each area were the mean values during the daytime obtained from the EMAC model. The maximum acetaldehyde level as well as the corresponding time (Δt) can be derived from Eq. S2.1 as Δt is the only variable. The results are shown in Table S4.

Table S2.4. Mean photolysis rate constant of pyruvic acid, OH concentrations, relative time (Δt) needed to reach the maximum acetaldehyde yield from pyruvic acid photolysis, maximum acetaldehyde and its fraction accounting the mean level over regions.

Regions	J_{PA} (s^{-1})	OH (molecules cm^{-3})	m/z 89.0234 pyruvic acid (H^+) (ppt)	Δt (h)	Acetaldehyde maximum (ppt)	Fractions (%)
MS	3.51×10^{-5}	6.52×10^{6}	39 ± 8	5.6	5.6	1.85
SC	3.44×10^{-5}	7.42×10^{6}	42 ± 9	5.2	5.3	0.85
RSN	3.52×10^{-5}	7.14×10^{6}	35 ± 14	5.2	4.7	0.92
RSS	3.00×10^{-5}	8.74×10^{6}	61 ± 15	4.9	6.2	1.98
GA	3.11×10^{-5}	7.20×10^{6}	57 ± 12	5.5	6.8	3.60
AS	2.74×10^{-5}	4.35×10^{6}	59 ± 12	7.8	9.4	5.88
GO	3.31×10^{-5}	7.89×10^{6}	65 ± 10	5.0	7.6	2.91
AG	3.29×10^{-5}	7.81×10^{6}	110 ± 53	5.1	12.9	0.75

References

Atkinson, R., and Arey, J.: Atmospheric Degradation of Volatile Organic Compounds, Chemical Reviews, 103, 4605-4638, 10.1021/cr0206420, 2003.

Atkinson, R., Baulch, D. L., Cox, R. A., Crowley, J. N., Hampson, R. F., Hynes, R. G., Jenkin, M. E., Rossi, M. J., Troe, J., and Subcommittee, I.: Evaluated kinetic and photochemical data for atmospheric chemistry: Volume II – gas phase reactions of organic species, Atmos. Chem. Phys., 6, 3625-4055, 10.5194/acp-6-3625-2006, 2006.

IUPAC Task Group on Atmospheric Chemical Kinetic Data Evaluation, (http://iupac.pole-ether.fr).

Chapter 3. Shipborne measurements of total OH reactivity around the Arabian Peninsula and its role in ozone chemistry

This chapter has been published as:

Pfannerstill, Eva Y., Nijing Wang, Achim Edtbauer, Efstratios Bourtsoukidis, John N. Crowley, Dirk Dienhart, Philipp G. Eger et al. "Shipborne measurements of total OH reactivity around the Arabian Peninsula and its role in ozone chemistry." Atmospheric Chemistry and Physics 19, no. 17 (2019): 11501-11523.

Contribution to this publication by Nijing Wang: responsible for the OH reactivity measurements during the second half of the campaign; contributed to the data analysis of the OH reactivity including raw data process, OH reactivity calculation and ozone production regime analysis; contributed to the manuscript revision.

Abstract

The Arabian Peninsula is characterized by high and increasing levels of photochemical air pollution. Strong solar irradiation, high temperatures and large anthropogenic emissions of reactive trace gases result in intense photochemical activity, especially during the summer months. However, air chemistry measurements in the region are scarce. In order to assess regional pollution sources and oxidation rates, the first ship-based direct measurements of total OH reactivity were performed in summer 2017 from a vessel travelling around the peninsula during the AQABA (Air Quality and Climate Change in the Arabian Basin) campaign. Total OH reactivity is the total loss frequency of OH radicals due to all reactive compounds present in air and defines the local lifetime of OH, the most important oxidant in the troposphere. During the AQABA campaign, the total OH reactivity ranged from below the detection limit (5.4 s^{-1}) over the north-western Indian Ocean (Arabian Sea) to a maximum of 32.8 ± 9.6 s^{-1} over the Arabian Gulf (also known as Persian Gulf) when air originated from large petroleum extraction/processing facilities in Iraq and Kuwait. In the polluted marine regions, OH reactivity was broadly comparable to highly populated urban centers in intensity and composition. The permanent influence of heavy maritime traffic over the seaways of the Red Sea, Gulf of Aden and Gulf of Oman resulted in median OH sinks of 7.9−8.5 s^{-1}. Due to the rapid oxidation of direct volatile organic compound (VOC) emissions, oxygenated volatile organic compounds (OVOCs) were observed to be the main contributor to OH reactivity around the Arabian Peninsula (9−35 % by region). Over the Arabian Gulf, alkanes and alkenes from the petroleum extraction and processing industry were an important OH sink with ~9 % of total OH reactivity each, whereas NO_x and aromatic hydrocarbons (~10 % each) played a larger role in the Suez Canal, which is influenced more by ship traffic and urban emissions. We investigated the number and identity of chemical species necessary to explain the total OH sink. Taking into account ~100 individually measured chemical species, the observed total OH reactivity can typically be accounted for within the measurement uncertainty (50 %), with 10 dominant trace gases accounting for 20−39 % of regional total OH reactivity. The chemical regimes causing the intense ozone pollution around the Arabian Peninsula were investigated using total OH reactivity measurements. Ozone vs. OH reactivity relationships were found to be a useful tool for differentiating between ozone titration in fresh emissions and photochemically aged air masses. Our results show that the ratio of NO_x- and VOC-attributed OH reactivity was favorable for ozone formation almost all around the Arabian Peninsula, which is due to NO_x and VOCs from ship exhausts and, often, oil/gas production. Therewith, total OH reactivity measurements help to elucidate the chemical processes underlying the extreme tropospheric ozone concentrations observed in summer over the Arabian Basin.

3.1 Introduction

The Arabian Peninsula is a hotspot of global change. It is already subject to extremes of heat and drought, which are predicted to intensify (Zhang et al., 2005; Wasimi, 2010; Chenoweth et al., 2011; Tanarhte et al., 2012; Lelieveld et al., 2012; Terink et al., 2013; Donat et al., 2014; Cook et al., 2016; Lelieveld et al., 2016), and to photochemical air pollution (Lelieveld et al., 2009; Smoydzin et al., 2012; Abdelkader et al., 2015; Farahat, 2016). The Middle East accommodates densely populated urban centers with a total of 350 million people, and is a hub of fossil fuel extraction and processing with more than half of the world's known oil and gas reserves (Khatib, 2014). Moreover, the waters surrounding the Arabian Peninsula are key routes of global trade and bottlenecks for marine traffic, another source of air pollution (Endresen, 2003; Eyring, 2005; Boersma et al., 2015; Mertens et al., 2018) that is expected to increase in the future (Eyring et al., 2007).

Photochemistry in the region is thought to be particularly active due to a combination of factors: large anthropogenic emissions of reactive hydrocarbons and NO_x (= NO + NO_2) from the petroleum industry, shipping and energy-intensive urban areas; with high levels of solar irradiation and hence photolysis rates; and high temperature, which disfavors NO_x reservoirs such as PAN and N_2O_5. The main regional photochemical oxidation process is initiated by ozone photolysis to $O(^1D)$, which reacts with water vapor to form hydroxyl radicals (OH). The OH radicals react with volatile organic compounds (VOCs) to yield peroxy radicals that can convert NO to NO_2, leading to ozone formation (Haagen-Smit, 1952; Sillman, 1999; Ren et al., 2013). The abundance of precursors and intense photochemistry make conditions in the Arabian Basin very favorable for photochemical ozone production, leading to extremely high ozone mixing ratios up to 200 ppb (Lelieveld et al., 2009; Smoydzin et al., 2012; Krotkov et al., 2016). Ozone formation was reported to be enhanced even 300 km downwind of a hydrocarbon processing facility at the coast of the Arabian Gulf (Moradzadeh et al., 2019). In addition, VOC oxidation by OH and ozone can generate secondary organic aerosol (Grosjean and Seinfeld, 1989; Kroll and Seinfeld, 2008) with implications for human health (Lelieveld et al., 2015) and regional radiative budgets (Ezhova et al., 2018).

Despite being an air pollution hotspot, very few observational atmospheric data exist from the Arabian Basin, and studies of VOCs in the region are scarce and mostly urban (Doskey et al., 1999; Matysik et al., 2010; Salameh et al., 2014; Simpson et al., 2014; Khalil et al., 2016; Salameh et al., 2016; Barletta et al., 2017). In order to chemically map the region, a comprehensive suite of atmospheric measurements was performed from a ship sailing around the Arabian Peninsula in summer 2017 during the AQABA (Air Quality and Climate Change in the Arabian Basin) cruise.

The number of known VOCs in air has been estimated to be between 10^4 and 10^5 species (Goldstein and Galbally, 2007), and it is assumed that many more remain unknown. Accounting for all of

these chemical compounds individually with quantitative measurements is currently unfeasible. Instead, the combined load of OH reactive species (mainly VOCs and CO) in ambient air, termed the total OH reactivity, can be measured directly. Total OH reactivity denotes the total sink, or loss frequency, of the OH radical. When compared to the OH reactivity calculated from all individually measured compounds (termed the speciated OH reactivity), total OH reactivity can be used to infer the occurrence of VOCs that were not measured (termed the unattributed or "missing" OH reactivity). Moreover, total OH reactivity is necessary for a quantitative understanding of ozone production and can help estimating its sensitivity to VOCs and NO_x (Kirchner et al., 2001; Sinha et al., 2010; Pusede et al., 2014; Yang et al., 2017). The OH sink also affects the atmospheric residence time of methane and therewith its global budget, which still poses a challenge in models (Zhao et al., 2019).

With VOC and NO_x emissions from ship exhausts (Boersma et al., 2015; Endresen, 2003; Huang et al., 2018) and VOCs from oil and gas operations (Buzcu and Fraser, 2006; Gilman et al., 2009; Gilman et al., 2013; Schade and Roest, 2016; Milazzo et al., 2017), the air around the Arabian Peninsula is expected to contain significant levels of pollution. In Saudi Arabian cities, OH reactivity has been reported to range from 14 to 42 s^{-1} (from the sum of individual measurements), dominated by alkenes (Barletta et al., 2017). Downwind of oil and gas production in Colorado, OH reactivity of VOCs was dominated by alkanes (60 %), followed by OVOCs (27 %) and alkenes (8 %; Gilman et al., 2013). The largest OH sink among the VOCs in the exhaust plume of a ship operating at full speed are alkenes (42 %), followed by aromatics (40 %), OVOCs (12 %) and alkanes (5 %; estimated using emission factors from Huang et al., 2018).

Unattributed OH reactivity in locations dominated by anthropogenic VOCs has been measured to be as low as zero in Lille, France (Hansen et al., 2015) or New York, U.S. (Ren et al., 2006), to 10−54 % in Paris, France (Dolgorouky et al., 2012) and 10−80 % in Tokyo, Japan (Yoshino et al., 2006). However, comparing unattributed OH reactivity between different studies is difficult, because it depends on the air mass and coverage of inorganic trace gases and VOCs measured in each campaign. In this work, we apply an approach that aims to use comprehensive trace gas information gathered by various instruments, even compounds with unidentified chemical structure measured by PTR−ToF−MS, for calculation of speciated OH reactivity. Therewith, we identify the trace gases representing the major OH sinks and try to obtain closure on apportioning OH reactivity.

This study provides an overview of total OH reactivity around the Arabian Peninsula and investigates its sources in the different environments along the route of the campaign. Total OH reactivity is applied for assessing the regional oxidation chemistry and the underlying reasons for the extreme ozone concentrations observed in summer over the Arabian Basin. By combining OH reactivity and ozone measurements, we aim to investigate ozone production processes and to

identify differentiated chemical regimes. We demonstrate the utility of in-situ OH reactivity measurements to characterize the role of anthropogenic emissions in modifying the chemical composition of the air.

3.2 Materials and methods

3.2.1 AQABA campaign

The Air Quality and Climate Change in the Arabian Basin (AQABA) measurements took place on-board the vessel *Kommandor Iona* from June 25 till September 3, 2017. The first leg began in La-Seyne-sur-mer (near Toulon, France), continued via the Mediterranean, the Suez Canal, the Red Sea, the Indian Ocean, the Gulf of Oman and the Arabian Gulf to Kuwait. On the second leg, the vessel returned via the same route (Fig. 3.1a/b). The ship was equipped with a weather station and four laboratory containers with instrumentation for in-situ and offline monitoring of a large suite of (trace) gases, particles and radicals.

3.2.2 Sampling

Air sampling was performed from a high-flow (10 m^3 min^{-1}) cylindrical stainless steel inlet (sampling height: 5.5 m above deck, diameter: 0.2 m), situated between the containers on the front deck of the ship. This position ensured that inlets were ahead of any contamination sources from the vessel itself when pointed into the wind. Air was drawn from the center of the high-flow inlet and sub-sampled at a rate of approximately 5 slpm (standard L min^{-1}, first leg) and 3 slpm (second leg) into an air conditioned laboratory container using a FEP (fluorinated ethylene propylene) inlet tube (1/2" = 1.27 cm o.d., length ca. 10 m), heated to 50−60 °C. A PTFE (polytetrafluoroethylene) filter, changed weekly (and additionally after intense particle contamination events such as dust storms), prevented contamination of the sub-sampling line by particles or sea spray. This inlet system was used for monitoring both VOCs and total OH reactivity simultaneously. We assume that the length of the inlet prevented some of the larger, extremely low volatile VOCs from reaching the instruments (see Sect. 3.3.3). The combined inlet residence time in FEP tubing and reactor for the OH reactivity instrument was determined as ≈ 15 s during the first leg and ≈ 25 s during the second leg by spiking with acetone.

3.3.3 OH reactivity and trace gas measurements

Total OH reactivity was measured using the Comparative Reactivity Method (CRM, Sinha et al., 2008), which proved to be robust enough to run nearly continuously for 10 weeks on a ship, often in rough conditions due to high waves. The method has been applied in many regions of the world (Yang et al., 2016) and has recently been compared to other methods (Fuchs et al., 2017). The CRM is based on a competitive reaction between reactive compounds from ambient air and a

reagent, pyrrole (Westfalen AG, Münster, Germany), inside a glass reactor. OH radicals are produced in the reactor by flushing humidified nitrogen (6.0 grade, Westfalen AG, Münster, Germany) over a Hg/Ar UV lamp (LOT Quantum Design, Darmstadt, Germany). CRM uses three different modes: C1 (pyrrole + OH scavenger + UV light, at ≈ ambient humidity), C2 (OH + pyrrole, ambient humidity), and C3 (ambient air + pyrrole + OH). For more details of the method see Sinha et al. (2008) and Michoud et al. (2015). The system was operated at a pyrrole/OH ratio of 1.9 ± 0.1 (average ± standard deviation). Because this ratio deviates from pseudo-first order conditions, as is typical for CRM, a correction needed to be applied (see Sect. 3.2.4). Sampling air was continuously drawn into the system and the instrument was switched between C3 (measured for 22-24 minutes) and C2 (measured for 6-8 min) modes. The longer C2 measurements were used when ambient humidity was unstable. C1 was determined every 5−7 days (average ± standard deviation over the whole campaign: 60.71 ± 1.18 ppb of pyrrole). Changes in pyrrole mixing ratio were monitored by a Proton Transfer Reaction-Quadrupole Mass Spectrometer (PTR−QMS, Ionicon Analytik, Innsbruck, Austria (Lindinger and Jordan, 1998) at m/z = 68 (dwell time: 5 s). The PTR−QMS was calibrated every week. It was operated at 60 °C drift temperature, 2.2 mbar drift pressure and 600 V drift voltage (E/N = 137 Td). In parallel, a PTR−Time of Flight (ToF)−MS was deployed to monitor VOCs and OVOCs (m/z up to 280), and a gas chromatograph with flame ionization detector (GC−FID) to monitor non-methane hydrocarbons (NMHCs; 20 compounds). Average detection limits for the different NMHCs ranged from 1−25 ppt. The NMHC and methane measurements are described in detail elsewhere (Bourtsoukidis et al., 2019). The PTR-ToF-MS was deployed at 60 °C drift temperature, 2.2 mbar drift pressure and 600 V drift voltage (E/N = 137 Td). 1,3,5-trichlorobenzene was fed continuously into the sample stream for mass scale calibration. The time resolution of the measurement was 1 min and background measurements were performed every 3 h for 10 min. The PTR-ToF-MS was calibrated with a multicomponent pressurized gas VOC standard (Apel-Riemer Environmental Inc., Colorado, USA). Mass resolution (full width at half maximum) at 96 amu ranged between ~3500 and ~4500. Average detection limits for the compounds measured by PTR-ToF-MS ranged from 1−107 ppt. A full list of the trace gases measured by GC-FID and PTR-ToF-MS can be found in Table S1.

Formaldehyde (HCHO) and inorganic trace gases (NO, NO_2, O_3, SO_2) were measured sampling from the same chimney (the instruments used are specified in Table S1). Based on SO_2, NO_x and ethene measurements, a filter was applied to exclude sampling periods that were influenced by the vessel's own exhaust.

3.3.4 Total OH reactivity data analysis

CRM data analysis was conducted following the general procedures described in Keßel (2016) and Pfannerstill et al. (2018).

Humidity in C2 (background) measurements can differ from that of C3 (ambient) measurements because C2 was measured only twice per hour. As the amount of OH radicals generated in the CRM reactor depends on humidity, C2 data were corrected for these C2/C3 humidity differences by applying an empirical relationship of the pyrrole signal vs. the PTR−MS water cluster signal as described in Michoud et al. (2015). The C2 correction applied to match C3 humidity decreased pyrrole levels by on average 0.05 ± 0.04 ppb, corresponding to an OH reactivity of ≈ 0.3 s^{-1}. NO, NO_2 and ozone cause interferences in CRM due to OH recycling induced by HO_2, which is formed in the reactor simultaneously with OH (Sinha et al., 2008; Michoud et al., 2015; Fuchs et al., 2017). Ozone, NO and NO_2 interferences were quantified in the laboratory (details of the experiments can be found in Sect. S1). NO_2 loss and conversion to NO in the mass flow controller during tests was monitored by an NO/NO_2 analyzer (Two-channel-chemiluminescence detector). The combined NO, NO_2 and ozone corrections amounted to a median of ~24 % of total OH reactivity or an average of 0.36 ± 0.19 ppb of pyrrole over the whole campaign, which equals ≈ 1.9 s^{-1}, with a maximum absolute correction of 1.39 ppb (7.4 s^{-1} / 27 % of total OH reactivity) under the influence of closely located ship emissions (high NO_x). A frequency distribution of the corrected fraction of total OH reactivity is displayed in Fig. S1.

The calculation of total OH reactivity with the CRM equation (see Sinha et al., 2008) assumes pseudo-1st-order conditions inside the reactor, which can, however, not be met while preserving a reasonable sensitivity (C3−C2 difference). The correction for deviation from pseudo-1st-order conditions inside the reactor was derived from empirical test gas measurements adapted from the approach in Michoud et al. (2015). The deviation from pseudo-1st-order depends on the pyrrole/OH ratio and on the reaction rate constant of the measured trace gas towards OH. Trace gases with fast reaction rates (comparable to that of pyrrole) require the largest correction because their concentration inside the reactor decreases at a similar rate as that of pyrrole, leading to an underestimation of their reactivity. Such gases, namely alkenes, were sometimes present during AQABA (e.g. a C_5H_8-alkene which was not isoprene). This is why we did not use an average correction factor for all gas mixes as in Michoud et al. (2015), but applied a correction where the composition of the air mass is taken into account. Test gases used were toluene (for aromatics correction), isoprene and propene (for alkenes correction), propane and cyclohexane (correction for other species). These test gases are representative of the relevant trace gases and ranges of reaction rate coefficients observed during AQABA. In test experiments, these trace gases were added to the CRM system in known amounts, i.e. known total OH reactivities, at pyrrole/OH ratios representative for the campaign. The correction factors resulting from comparing the observed reactivity with the expected reactivity were weighted according to the measured composition of the ambient air at the moment of observation:

$$F = a\,X_{aromatic} + b\,X_{alkenes} + c\,(1 - X_{arom} - X_{alkenes})$$ Eq. (3.1),

where F is the total correction factor and the weighted compound-class-specific correction factors are a = 1.22, b = 2.89 and c = 1.44. X is the speciated OH reactivity fraction (in s^{-1} s) of the respective class of compounds (aromatics, alkenes). This correction increased OH reactivity by a factor of 1.4 to 2.5 (average ± standard deviation: F = 1.5 ± 0.1, median = 1.5).

The dilution of ambient air with humidified nitrogen was accounted for with a dilution factor of 1.34.

The 5 min detection limit (LOD) was 5.4 s^{-1}, derived from the 2σ standard deviation of clean air measurements in the Arabian Sea. Total uncertainty (1 σ) of the measurements was ~ 50 % (median and average), with a precision of 10−76 % over 5 min depending on the quantity of reactivity.

3.3.5 Calculated OH reactivity from individually measured compounds (speciated OH reactivity)

The speciated OH reactivity is the sum of the OH reactivities attributed to individual (measured) trace gases:

$$R = \Sigma\, k_{M+OH}\,[M]$$ Eq. (3.2)

Contributions of trace gases (M, where *[M]* is their respective concentration in molecules cm^{-3}) to OH reactivity (R in s^{-1}) are calculated using the reaction rate constants (k_{M+OH} in cm^3 $molecule^{-1}$ s^{-1}) of the respective trace gases (M) with the OH radical. The difference between measured total OH reactivity and the sum of individual trace gas contributions to OH reactivity is termed "unattributed" or "missing" OH reactivity. The trace gases taken into account here for calculating speciated OH reactivity and their reaction rate constants used are listed in Table S1. Out of a total of 120 chemical species that were considered for the calculation of speciated reactivity, 42 chemical species (specified in Table S1), including many of the known important contributors to OH reactivity, were calibrated with gas standards and therefore have low uncertainties in their concentrations as well as in their reaction rate coefficients (5−15 %). A further 78 exact masses (specified in Table S1) monitored by PTR−ToF−MS were attributed to molecular formulae, and their concentrations derived using a theoretical approach (Lindinger and Jordan, 1998), which has an uncertainty of ca. 50 %. In cases where several trace gases could be responsible for the measured mass, an average of the known reaction rate coefficients with OH was used for calculating the speciated OH reactivity. In the few cases where rate coefficients were unknown in literature, the rate coefficient of a trace gas with comparable functional groups was applied (see Table S1). The uncertainty of the reaction rate coefficients k_{M+OH} is estimated to be 100 % due to the occasional large differences in rate coefficients between possible structures. The uncertainty of the resulting

speciated (i.e. calculated) OH reactivity depends on the fraction of gas-standard calibrated compounds in the ambient air at any given point of time and varies between 10 % and 92 %, with an average and median of 45 % over the whole campaign. In accordance with the time resolution of the GC-FID, which monitored compounds with a significant share of OH reactivity, speciated OH reactivity was calculated in 50 min time resolution.

3.3.6 Air mass back trajectories

To investigate the origin of air masses encountered, back trajectories were derived using the Hybrid Single-Particle Lagrangian Integrated Trajectory model (HYSPLIT, version 4, 2014). This model is a hybrid between a Lagrangian and an Eulerian model for tracing small imaginary air parcels forward or back in time (Draxler and Hess, 1998). Back trajectories were calculated based on a start height of 200 m above sea level, going 216 h back in time on an hourly grid beginning at the ship position.

3.3 Results and discussion

3.3.1 Overview of total OH reactivity around the Arabian Peninsula

The air masses encountered during the AQABA campaign were delineated according to the geographical region (Fig. 3.1a/b). A notable difference between leg 1 and leg 2 was the general wind direction over the Arabian Gulf, which changed from north-west (from Iraq/Kuwait) to northeast (from Iran). The range of observed total OH reactivities over the whole campaign was from below the detection limit over the Arabian Sea (north-west Indian Ocean) up to $303.6 \pm 83.9\ s^{-1}$ during fueling/bunkering of the ship at the port of Fujairah (United Arab Emirates), due to fresh fuel emissions. The largest fraction of attributed OH reactivity was provided by OVOCs in almost all AQABA regions (9−35 %), which is comparable to previous studies in the oil impacted region of Houston, where between 11 % and 24 % of the OH sink was due to OVOCs (Mao et al., 2010). There were notable regional differences in both the total OH reactivity and the contributing trace gases, which will be discussed hereafter. An overview is displayed in Table 3.1, which divides the reactivity into different chemical families. A list of chemical species attributed to each chemical family is available in Table S1.

The measured sulfur-containing VOCs (SVOCs) and halogenated VOCs (HalVOCs) played virtually no role for OH reactivity in any of the AQABA regions (Table 3.1). The OH reactivity of the monitored NVOCs (nitrogen-containing VOCs) was also very minor with not more than 1 % of total OH reactivity over the whole campaign.

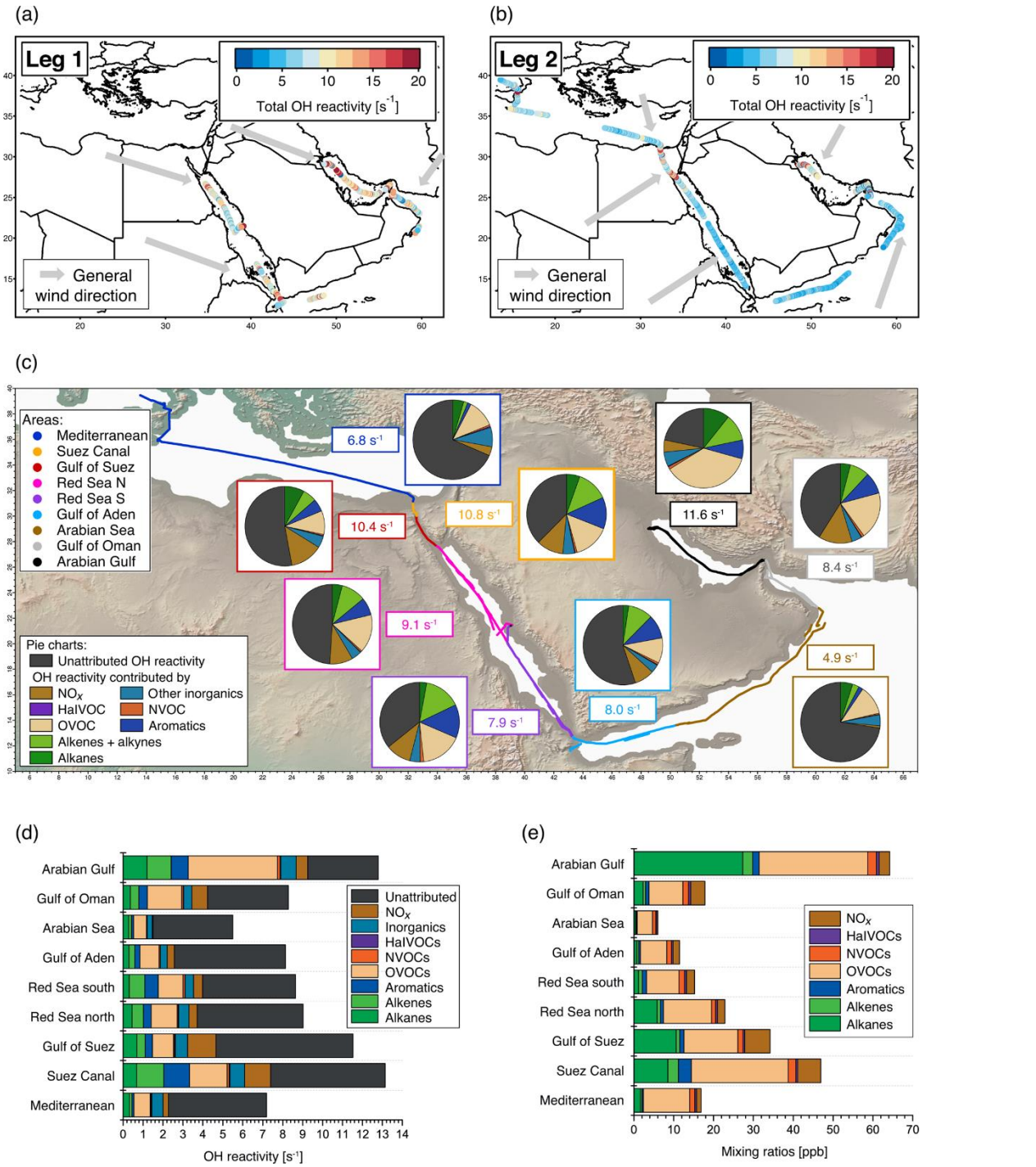

Figure 3.1: Overview of total OH reactivity around the Arabian Peninsula during the AQABA campaign. OH reactivity during (a) leg 1 (July 5−July 31, 2017) and (b) leg 2 (August 3−August 31, 2017). The maximum in the color scales is set to 20 s^{-1} for better visibility of differences, although there are a few datapoints above this value. Arrows depict general wind directions for the respective regions. (c) Total OH reactivity medians by region, and pie charts showing the contribution of compound classes for datapoints where speciated OH reactivity ≥ LOD (exception: pie charts of Mediterranean and Arabian Seas show average of all datapoints, due to low number of points above LOD). (d) Average OH reactivity and speciation by region for all datapoints, including those where speciated OH reactivity was below the LOD. Error bars show the total uncertainty of the measurement. (e) Average mixing ratio of VOCs/trace gases in ppb by compound class and region (except for the class of inorganic compounds other than NO_x). The individual compounds included in each class are listed in Table S1. Port calls and bunkering are excluded from all averages.

Table 3.1: Overview of measured and speciated OH reactivity by region. "≥ LOD" signifies the use of exclusively those datapoints where speciated OH reactivity is equal to or above the LOD. Percentages of contribution to total OH reactivity by group were calculated from all datapoints in 50 min time resolution. The chemical species attributed to each group are listed in Table S1. For an explanation of unattributed or speciated OH reactivity and "theoretical approach" species refer to Sect. 3.2.5. The 10 most important species are the species with largest average OH reactivity over the respective region. The ratios of C_3 or C_5 carbonyls vs. their precursors or toluene vs. benzene are indicators for air mass age. *Note that the detection limit was 5.4 s^{-1}. (Medit. = Mediterranean.)

	Medit. Sea	Suez Canal	Gulf of Suez	Red Sea north	Red Sea south	Gulf of Aden	Arabian Sea	Gulf of Oman	Arabian Gulf
Aromatic hydrocarbons	1 %	10 %	3 %	4 %	8 %	3 %	2 %	5 %	7 %
Alkanes	4 %	5 %	6 %	5 %	4 %	4 %	5 %	4 %	9 %
Alkenes	2 %	10 %	4 %	6 %	9 %	4 %	3 %	5 %	9 %
OVOCs	11 %	14 %	9 %	14 %	14 %	12 %	12 %	21 %	35 %
NVOCs	1 %	1 %	0 %	1 %	1 %	1 %	1 %	1 %	1 %
SVOCs	0 %	0 %	0 %	0 %	0 %	0 %	1 %	1 %	0 %
Halogenated VOCs	0 %	0 %	0 %	0 %	0 %	0 %	0 %	0 %	0 %
Inorganics	8 %	6 %	5 %	6 %	5 %	4 %	4 %	5 %	6 %
NO_x	4 %	10 %	12 %	5 %	5 %	4 %	1 %	9 %	5 %
Unattributed OH reactivity fraction (all datapoints) ± 1 σ total uncertainty	68 ± 52 %	44 ± 43 %	59 ± 44 %	59 ± 50 %	54 ± 54 %	68 ± 51 %	72 ± 57 %	49 ± 55 %	27 ± 55 %
Unattributed OH reactivity fraction ≥ LOD ± 1 σ total uncertainty	none	37 ± 35 %	53 ± 34 %	49 ± 39 %	35 ± 55 %	55 ± 38 %	none	41 ± 52 %	22 ± 56 %
Fraction of species with concentrations derived from theoretical approach	28 %	28 %	22 %	38 %	51 %	46 %	42 %	46 %	46 %
Speciated (calculated) OH reactivity [s^{-1}], averages ± standard deviation	**2.3** ± 1.2	**7.4** ± 5.8	**4.7** ± 2.2	**3.7** ± 1.7	**4.0** ± 2.1	**2.6** ± 1.1	**1.5** ± 0.2	**4.3** ± 1.2	**9.3** ± 5.6
Speciated (calculated) OH reactivity [s^{-1}], medians, 25th−75th percentile	**2.0** 1.9−2.2	**5.4** 2.7−13.4	**4.3** 3.0−5.9	**3.3** 2.5−4.5	**3.7** 2.2−5.5	**2.4** 2.0−2.9	**1.5** 1.4−1.7	**4.0** 3.2 −5.2	**7.6** 5.2 −11.9
Measured OH reactivity [s^{-1}], averages ± standard deviation	**7.2** ± 2.9	**13.2** ± 6.9	**11.6** ± 4.2	**9.1** ± 3.3	**8.7** ± 4.2	**8.2** ± 3.1	**5.6*** ± 2.0	**8.3** ± 3.6	**12.9** ± 6.2
Measured OH reactivity [s^{-1}], medians, 25th−75th percentile	**6.8** 5.8−7.8	**10.8** 7.4−18.8	**10.4** 8.2−15.0	**8.5** 7.0−10.5	**7.9** 5.7−10.9	**8.0** 5.9−10.1	**4.9*** 4.1−6.5	**8.4** 5.9−10.5	**11.2** 8.9−15.2
OH reactivity of 10 most important species [s^{-1}]	1.7	3.8	3.1	2.1	2.2	1.7	1.1	3.3	4.9
Fraction of total OH reactivity contributed by 10 most important species	24 %	29 %	27 %	23 %	25 %	21 %	20 %	39 %	38 %
C_3 carbonyls / propane [ppb ppb^{-1}], medians	8.6	3.4	2.6	1.9	9.4	6.8	none	2.4	0.9
C_5 carbonyls / pentanes [ppb ppb^{-1}], medians	3.0	1.7	1.1	1.3	1.9	2.4	3.8	1.2	2.8
Toluene / benzene[ppb ppb^{-1}], medians	0.24	0.88	0.80	0.39	0.78	0.33	0.18	0.79	0.47

3.3.1.1 Strongly polluted regions: Arabian Gulf, Gulf of Suez and Suez Canal

Compounds with short lifetimes are generally more relevant for total OH reactivity than long-lived species (see also Sect. 3.3.3). Since emissions from oil and gas production and cities contain high mixing ratios of reactive alkenes, the Arabian Gulf, the Gulf of Suez and the Suez Canal, where such sources abound, showed the highest average OH reactivities (Fig. 3.1c/d). In these regions, obvious nearby emission sources were cities, industrial complexes, and especially oil/gas production/processing (Fig. 3.2). The large alkane mixing ratios associated with oil and gas production (Fig. 1e; Bourtsoukidis et al., 2019) were not reflected in an equally large share of total OH reactivity due to the slow reaction rate coefficient of alkanes with the OH radical (Fig. 3.1d). The average total OH reactivity (± standard deviation) was 12.9 ± 6.2 s^{-1} (median: 11.2 s^{-1}) over the Arabian Gulf, 13.2 ± 6.9 s^{-1} (median: 10.8 s^{-1}) over the Suez Canal and 11.6 ± 4.2 s^{-1} (median: 10.4 s^{-1}) over the Gulf of Suez. There were short periods with higher total OH reactivities (± total uncertainties) up to 32.8 ± 9.6 s^{-1} over the Arabian Gulf and 26.6 ± 8.2 s^{-1} over the Suez Canal (see Sect. 3.3.2). These ranges are comparable to OH reactivities reported from some urban areas, e.g. Beijing, China (Williams et al., 2016), Houston, Texas (Mao et al., 2010), New York City (Ren et al., 2006), and to OH reactivities calculated from ship-based VOC observations in the fossil fuel production impacted Houston/Galveston Bay (Gilman et al., 2009). The AQABA observations are, however, more than three times as high as VOC-attributed OH reactivity calculated from observations downwind of gas and oil production in south Texas (Schade and Roest, 2016) and twice as high as at the Boulder Atmospheric Observatory when impacted by gas wells (Swarthout et al., 2013).

The largest percentage of attributed OH reactivity over the Arabian Gulf was provided by OVOCs (35 % of total, in contrast to 14 % observed over the Houston/Galveston Bay (Gilman et al., 2009). This was surprising, as the Gulf region was expected to be similarly dominated by direct hydrocarbon emissions from the fossil fuel industry as the Houston/Galveston Bay. Although the alkanes and OVOCs had broadly equivalent mixing ratios over the Arabian Gulf (Fig. 3.1e), the former have generally lower OH reactivity. Conditions in the Gulf region during summer favor rapid photooxidation of hydrocarbon emissions to OVOCs, due to high temperatures (on average 34.5 °C), high humidity (up to 92 % RH) and strong irradiation. It should also be noted that as the ship passed through the Arabian Gulf, it was only exposed to primary emissions for relatively short periods of time, when located directly downwind of the sources. The more oxidized regional background air was sampled for longer periods. Furthermore, a bias towards OVOCs in the assessment of speciated OH reactivity is also possible in this study, because they were well covered by PTR−ToF−MS measurements, while longer-chain or branched alkenes and alkanes, which are components of oil and other fuels (D'Auria et al., 2009; Gueneron et al., 2015) were in the AQABA

measurements limited to C_2-C_8 compounds. Nonetheless, considering the whole campaign, the Arabian Gulf was the region with the highest OH reactivity from alkanes (on average ~1.2 s^{-1} or ~9 % of total OH reactivity). An important influence of oil and gas production on total OH reactivity in the Arabian Gulf is therefore evident in our data.

Petroleum extraction facilities and refineries are located at both shores of the Gulf of Suez and Canal, (Fig. 3.2), and wind from both east and west lead to a relatively large contribution of alkanes (5−6 %; Fig. 3.1d/e).

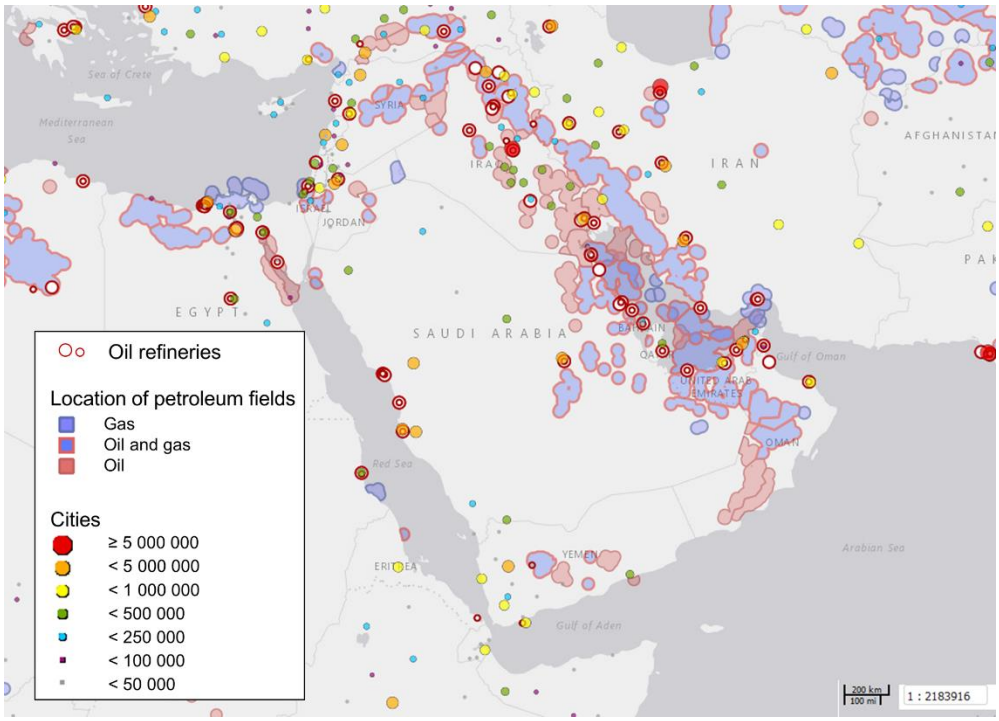

Figure 3.2: Oil refineries, petroleum fields and cities in the Arabian Basin. City markers are scaled with the number of inhabitants as denoted in the legend. Source: Harvard WorldMap Project (https://worldmap.harvard.edu/maps/6718/dJT).

By virtue of their double bond, alkenes are more reactive towards OH than alkanes. Indeed, in Saudi Arabian cities, OH reactivity of alkenes has been reported to be twice as high as the reactivity of alkanes, despite higher abundance of the latter (Barletta et al., 2017). Similarly, over the Arabian Gulf, the AQABA campaign results show an equivalent average share of OH reactivity from alkenes and alkanes (both ~1.2 s^{-1}, which equals ~9 %), despite a ~11 times larger average mixing ratio of alkanes. Certainly a fraction of highly reactive alkenes emitted on land will have already been oxidized before the emission impacted air mass reached the point of observation on the ship. Alkene-attributed OH reactivity was slightly higher in the Suez Canal (1.4 s^{-1} vs. 1.2 s^{-1}), where the distance to emission sources is generally shorter due to the narrowness of the canal. Additionally, and probably more importantly, alkenes are only minor components in fossil fuel

emissions generally. They are emitted from vehicle exhausts (a possible source near the Suez Canal) due to incomplete combustion (Koppmann, 2007). Alkanes, on the other hand, can be so abundant in emissions from oil and gas production that they dominate OH reactivity, as was observed in Colorado, where 60 % of OH reactivity calculated from VOC measurements (not total OH reactivity) was due to alkanes and only 8 % from alkenes (Gilman et al., 2013). In another study at the same site, alkanes contributed 26 %, alkenes 3 %, and aromatics 2 % of total OH reactivity (Swarthout et al., 2013). In contrast to that, alkenes (41 %) dominated over alkanes (23 %) in the OH reactivity calculated from VOC observations over the Houston/Galveston Bay (Gilman et al., 2009).

Aromatics are important components of fossil fuels besides alkanes and alkenes (Koppmann, 2007). In Egyptian cities, ambient VOC mixing ratios from traffic have been reported to be dominated by aromatics (Matysik et al., 2010), whereas in Saudi Arabian cities, alkanes were more abundant (Barletta et al., 2017). Consistent with these findings, we observed higher average speciated OH reactivity from aromatics (1.3 s^{-1}) in the Suez Canal (influenced by air from Cairo, roads next to the Canal, a refinery, and a power plant) compared to the Arabian Gulf (0.9 s^{-1}, influenced by oil/gas industry emissions and partly by urban air from Saudi Arabia, Iraq and Kuwait).

A strong influence of maritime traffic in the narrow and highly frequented Suez Canal and Gulf is evident from the large NO_x contribution to total OH reactivity (~10 and ~12 %, respectively). Here, other vessels and their exhaust plumes passed by closely during waiting periods (before entering the Suez Canal in the northern Gulf of Suez and inside the Canal).

The Arabian Gulf and Suez Canal will be discussed in more detail in case studies in Sect. 3.3.2.

3.3.1.2 Seaways influenced by maritime traffic: Red Sea, Gulf of Aden and Gulf of Oman

The Red Sea, the Gulf of Aden, and the Gulf of Oman displayed similar total OH reactivities with medians of 7.9−8.5 s^{-1} during the AQABA campaign (northern Red Sea: median 8.5 s^{-1} / mean ± standard deviation 9.1 ± 3.3 s^{-1}, southern Red Sea: 7.9 s^{-1} / 8.7 ± 4.2 s^{-1}, Gulf of Aden: 8.0 s^{-1} / 8.2 ± 3.1 s^{-1}, Gulf of Oman: 8.4 s^{-1}/ 8.4 ± 3.1 s^{-1}, also see Table 3.1 and Fig. 3.1c/d). These values are comparable to urban observations in the lower range, such as in in Helsinki, Finland (Praplan et al., 2017), or Mainz, Germany (Sinha et al., 2008).

The OH reactivity over the Red Sea, Gulf of Aden and Gulf of Oman can largely be attributed to the influence of maritime transport in these busy, relatively constricted seaways. Refineries at the eastern shore of the northern Red Sea (Fig. 3.2) are not thought to have influenced our measurements due to prevailing wind from north-west and west.

Among the three regions, the Gulf of Aden was the one with the lowest average total OH reactivity. Likely, this is due to its location in the transition zone to the open north-western Indian Ocean (see Fig. 3.1c). Here, air masses were less influenced by pollution than over the Red Sea or Gulf of Oman, as the AQABA cruise took place during northern hemisphere summer, when the ITCZ is over India and comparably clean air is drawn north over the north-western Indian Ocean (Ajith Joseph et al., 2018). In accordance with this finding, Bourtsoukidis et al. (2019) showed by lifetime-variability regression of alkanes that the Gulf of Aden was the area with the most remote character during AQABA.

In ship exhausts, the highest emission factors (apart from CO_2) have been found for NO_x (Endresen, 2003; Eyring, 2005; Huang et al., 2018). Large ship engines emit an average of 76 kg of NO_x per ton of fuel combusted (Eyring, 2005). This is reflected in the OH reactivity share of NO_x, which was in these relatively narrow seaway regions in the range of 4−9 % (Table 3.1). OVOCs accounted for 12−21 % of total OH reactivity there, alkenes 4−9 %, inorganics (dominated by SO_2 and CO) 4−6 %, aromatics 3−8 % and alkanes 4−5 %. All those classes of compounds can stem from fuel combustion in ships (Endresen, 2003; Eyring, 2005; Huang et al., 2018; Xiao et al., 2018), which emit an average of 43 kg of SO_x, 4.7 kg of CO and 7 kg of hydrocarbons per ton of fuel combusted (Eyring, 2005).

The C_3 carbonyls (C_3H_6O) vs. propane (C_3H_8), C_5 oxidation products ($C_5H_{10}O$) vs. pentanes (C_5H_{12}) and toluene vs. benzene ratios (Table 3.1) were used here as indicators of the oxidation state (and, thereby, the extent of photochemical ageing) of the air. We note that this approach is based on two assumptions: 1) that production of the carbonyls by oxidation dominates over direct emission, although some direct combustion emissions cannot be excluded, and 2) that the only carbonyl precursor is the corresponding C_3 or C_5 compound without significant fragmentation of larger VOCs. The toluene vs. benzene relationship is based on the assumption of simultaneous emission of both compounds. Notably, a distinct difference between northern (less oxidized, $[C_3H_6O]/[C_3H_8] \approx 1.9$ and $[C_5H_{10}O]/[C_5H_{12}] \approx 1.3$) and southern Red Sea (oxidized, $[C_3H_6O]/[C_3H_8] \approx 9.4$ and $[C_5H_{10}O]/[C_5H_{12}] \approx 1.9$) was observed. Although it did not result in large differences in total OH reactivity values (median of 7.9 s^{-1} in the photochemically aged air masses in the south Red Sea and 8.5 s^{-1} in the north Red Sea), it reflects the origin of air masses: urban centers in northeast Africa for the north Red Sea, and the less populated and more distant Sudan and Chad for the south Red Sea.

3.3.1.3 Cleaner regions: Mediterranean and Arabian Sea

Over the more open seas, notably the Mediterranean and Arabian Sea (north-western Indian Ocean), the air was aged, cleaner, and less reactive to OH. Here, total OH reactivities were mostly close to the detection limit of 5.4 s^{-1}. The median over the Mediterranean was 6.8 s^{-1} (average ± standard

deviation: 7.2 ± 2.9 s^{-1}), which compares to the lower limits of observations from suburban areas such as Whiteface Mountain (Ren et al., 2006), Norfolk, UK (Ingham et al., 2009), Central Pennsylvania (Ren et al., 2005) or Arenosillo at the Spanish coast (Sinha et al., 2012), and more remote locations such as the Rocky Mountains (Nakashima et al., 2014). Total OH reactivity measured over the Arabian Sea during AQABA was with a median of 4.9 s^{-1} (average ± standard deviation: 5.6 ± 2.0 s^{-1}) below the detection limit of 5.4 s^{-1}. The marine OH reactivity calculated from trace gas measurements over the central Gulf of Mexico was 1.01 s^{-1} (Gilman et al., 2009), a value which was slightly exceeded in our observations over the open Arabian Sea with a speciated OH reactivity of 1.5 ± 0.2 s^{-1}.

Larger OH reactivity occurred over the Mediterranean Sea during short episodes of polluted air from the mainland in the Strait of Messina (between Sicily and Italy), visible in Fig. 3.1b. In the Strait of Messina and surroundings, total OH reactivity amounted to between 6.7 ± 3.6 s^{-1} and 26.7 ± 8.2 s^{-1} for 5 h, whereas before and after, it was close to the detection limit. OVOCs were with ~11−12 % of total OH reactivity the largest group of identified OH sinks in both the Mediterranean and Arabian Sea. Over the Mediterranean, the influence of shipping emissions was larger than over the Arabian Sea, evident from NO_x-attributed OH reactivity, which was on average 0.26 s^{-1} or ~4 % of the total in the Mediterranean in contrast to 0.05 s^{-1} or ~1 % of the total in the Arabian Sea. Johansson et al. (2017) found that ship traffic over the Arabian Sea causes 3 % of the global NO_x emissions from maritime transport, which explains why even here the conditions were not completely pristine.

3.3.2 Case studies

3.3.2.1 Arabian Gulf

Figure 3.1 shows the average OH reactivity composition for the Arabian Gulf. However, the air measured over the Arabian Gulf originated partly from Kuwait/Iraq, partly from Iran and partly from the south. The composition of total OH reactivity between the different regions of origin displayed distinct differences, and can therefore be divided according to origin of the measured air masses, shown in Fig. 3.3.

Notably, the air from Iraq and/or Kuwait showed obvious influence from oil extraction industries with large fractions of alkanes, alkenes and aromatics (Fig. 3.3). Here, emission sources were closest to the point of observation, which was reflected in highest total OH reactivity (median: 18.8 s^{-1}, average ± standard deviation: 18.7 ± 7.9 s^{-1}) and low C_3 carbonyls/propane and high toluene/benzene ratio medians of 0.3 and 0.8, respectively. In contrast, OH reactivity in the air originating from Iran was lower (median: 9.8 s^{-1}, average ± standard deviation: 10.8 ± 3.4 s^{-1}), with a slightly higher C_3 carbonyls/propane and a lower toluene/benzene ratio (both 0.4). The OH

reactivity here was similar to that found in air from the south (Saudi Arabia) with a median of 9.8 s^{-1} and a mean of 9.7 ± 3.3 s^{-1}, however, the C_3 carbonyls/propane ratio of 2.0 points to more oxidized air masses. The high OH reactivity in air originating from Kuwait and Iraq can be attributed to emissions from petrochemical extraction and processing industries that would explain the large contribution of alkanes, alkenes and aromatics. Apart from two notable exceptions, the distribution of OH reactivity did not differ significantly between air from Iran and the south. In air from Iran, the alkene fraction was larger than in air from the south, probably due to closer and different emission sources (gas extraction at the Iranian coast), which would also explain the lower C_3 carbonyls/propane ratio. The NO_x fraction was larger in air from south, most likely for reasons of ship traffic influence.

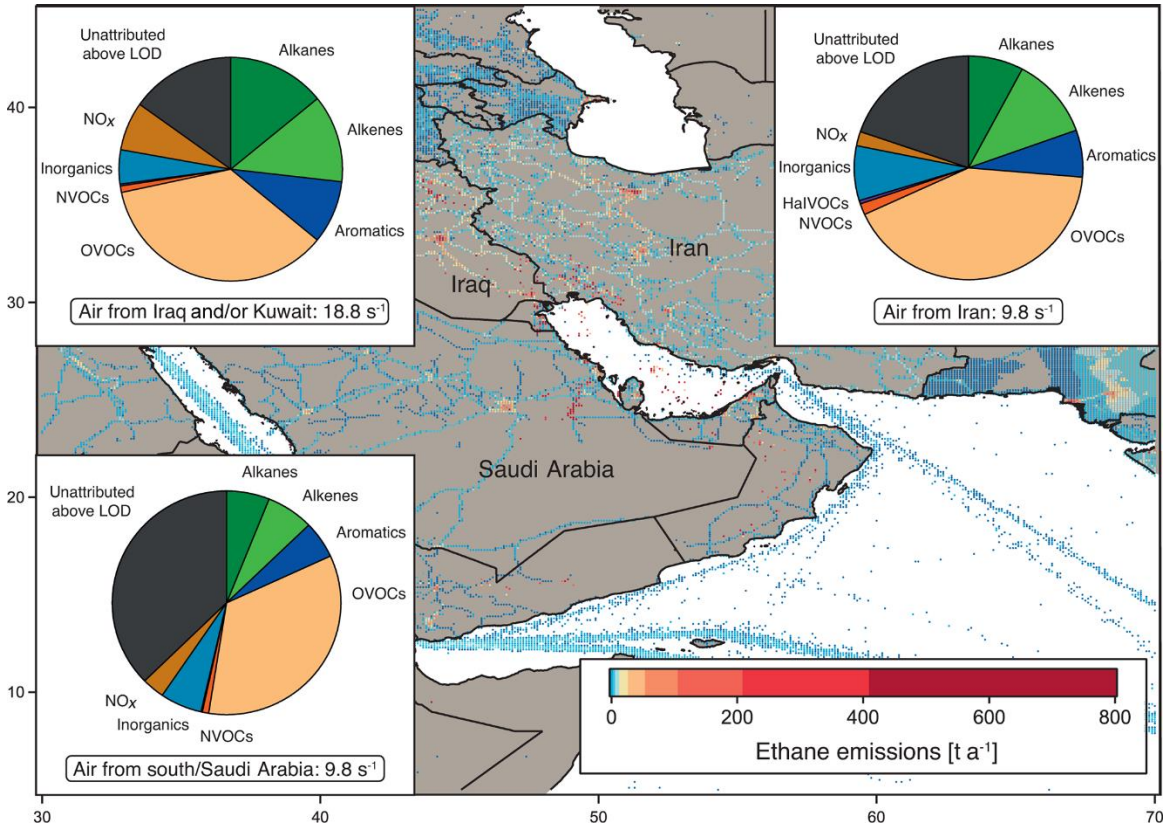

Figure 3.3: OH reactivity composition and average ± standard deviation in the Arabian Gulf, separated by origin of the measured air masses: from Iraq/Kuwait, from Iran from southern Arabian Gulf/Saudi Arabia. Background: Ethane emissions map using data from the EDGAR database (http://edgar.jrc.ec.europa.eu, for 2012) as an indicator for the distribution of petroleum extraction and other anthropogenic sources.

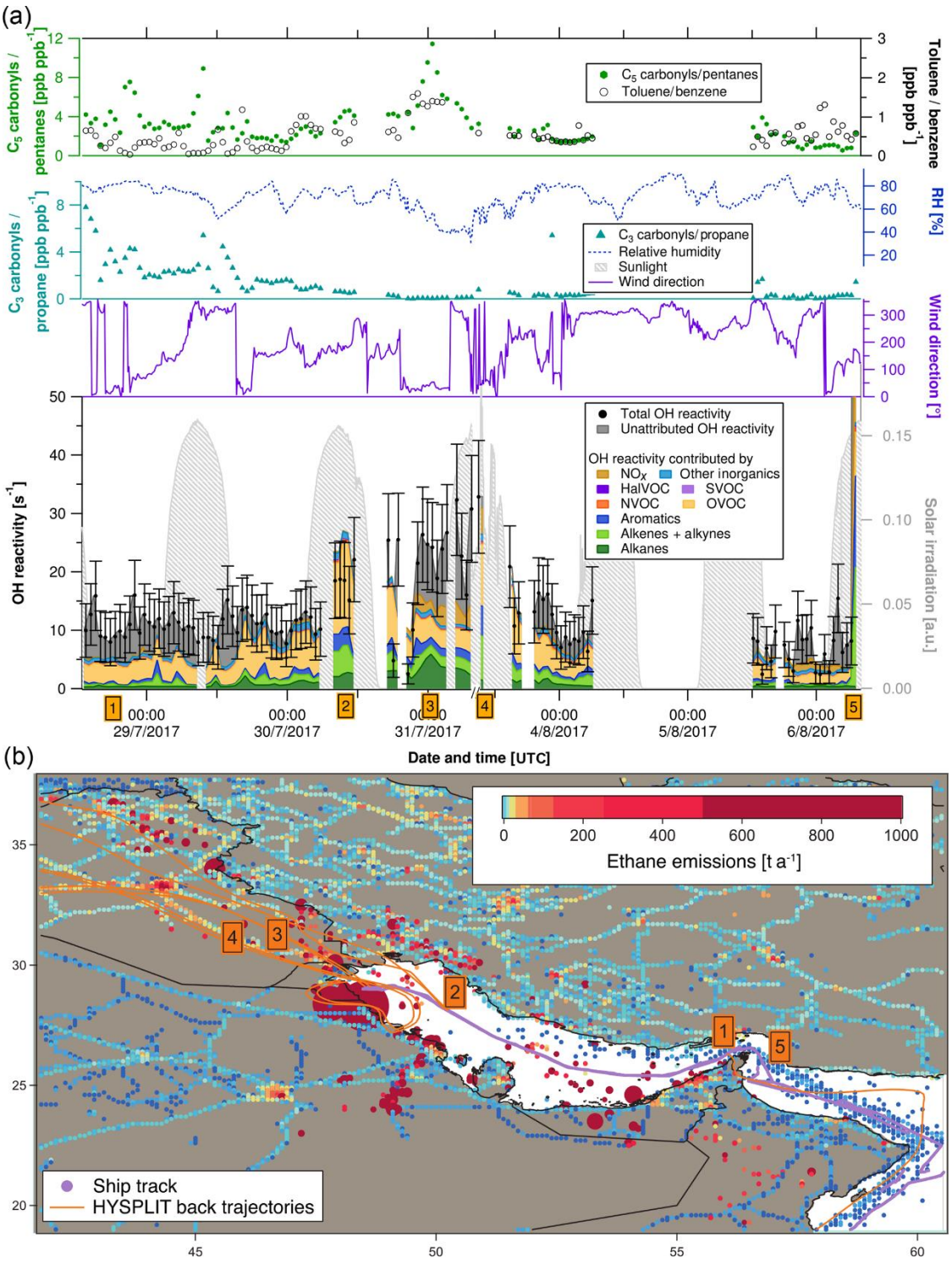

Figure3.4: (a) C_3 carbonyls/propane ratio, C_5 carbonyls/pentane ratio, toluene/benzene ratio, relative humidity, solar irradiation, wind direction, speciated and measured OH reactivity in the Arabian Gulf. Error bars of total OH reactivity display the 1 σ total uncertainty of the measurement. (b) Ship track of the campaign in the Arabian Gulf with HYSPLIT air mass back trajectories and numbered labels of case study points. Ethane emissions from the EDGAR database (http://edgar.jrc.ec.europa.eu, for 2012) as an indicator for petroleum extraction/processing and other anthropogenic sources are shown on a logarithmic colour scale. Emissions out of scale (> 1000 t a^{-1}) are shown with larger circles.

Figure 3.4 (a) depicts a time series of measurements along the ship track from entering the Arabian Gulf to Kuwait and back. The upper part of the graph shows indicators of the photochemical age of the air mass. The $[C_3H_6O]/[C_3H_8]$ ratio decreases and the toluene/benzene ratio increases when getting closer to Kuwait, meaning that the research vessel was approaching the emission sources (refineries, oil platforms). Both these indicators show opposite patterns, as expected. The $[C_5H_{10}O]/[C_5H_{12}]$ ratio follows the $[C_3H_6O]/[C_3H_8]$ ratio except for an increase towards Kuwait, which shows that the fresh emissions observed here were richer in propane than in pentanes, and indicates a mix of fresh emissions with aged air masses. This observation will be discussed in more detail in Sect. 3.3.4.2. Changes in relative humidity indicate the varying influence of dry desert air and more humid air masses.

The following five case studies (orange numbered labels in Fig. 3.4 with corresponding air mass back trajectories) will go into more detail regarding the origin of OH reactivity (reported with ± 1 σ total uncertainty) in the Arabian Gulf:

1) At the entrance to the Arabian Gulf after passing the Strait of Hormuz, total OH reactivity was comparably low (8.0 ± 4.0 s^{-1}). Sampled air had traversed the open Indian Ocean, but passed over the Musandam Peninsula, where urban areas probably contributed some OH reactivity. OVOCs dominated (36 ± 20 % of OH reactivity), with an insignificant unattributed fraction of 38 ± 76 %.

2) At this location in the northern part of the Arabian Gulf, ca. 100 km from the coast of Saudi Arabia, total OH reactivity amounted to 22.1 ± 7.2 s^{-1}, mainly due to OVOCs (57 ± 29 %), with large fractions of alkanes (10 ± 1 %), alkenes (16 ± 8 %) and aromatics (10 ± 5 %). The back trajectories originate from eastern Iraq, with the urban areas of Amara and Basra. The large fraction of OVOCs is an indicator for chemically aged air. The aromatics, alkenes and alkanes probably were emitted from offshore oil/gas extraction platforms (Fig. 3.4b) and mixed with the oxidized air contaminants coming from larger distance. Within the uncertainty of the measurement, there is no unattributed OH reactivity at this location; with values of 19.4 ± 9.9 s^{-1} for the speciated OH reactivity and 22.1 ± 7.2 s^{-1} for the measured total OH reactivitiy.

3) Approximately 30 km from the coast of Kuwait, the back trajectories indicate that the sampled air masses travelled over the Rumaila oil field in Basra (Iraq). Consequently, the total OH reactivity of 26.4 ± 8.1 s^{-1} was mainly due to alkanes from oil extraction (24 ± 2 %). In contrast to the previous case study, significant unattributed OH reactivity was observed here (40 ± 37 %), which might be due to components of oil such as higher than C_8 and/or branched hydrocarbons that were not measured on board the *Kommandor Iona*.

4) Just after departure from the port of Kuwait, the highest observed OH reactivity (32.8 ± 9.6 s^{-1}) of the campaign was measured (except for refueling). HYSPLIT back trajectories show that it likely

originated from large pollution sources at the coast: refineries (Saudi Aramco refinery and industrial area with storage tanks in Khafji, Saudi Arabia) and oil fields (Wafra oil field in Kuwait; oil platforms at the sea). Notably, alkenes (23 ± 14 %) were a much larger OH sink here than alkanes (5 ± 0.5 %), and the unattributed OH reactivity was zero within the uncertainty.

5) The largest OH reactivity measured during the whole campaign was 303.6 ± 83.9 s^{-1} during refueling of the vessel in front of the port of Fujairah (United Arab Emirates). A back trajectory would not be relevant here, as these are direct diesel fuel evaporation emissions, mainly composed of alkenes (27 ± 18 % of speciated OH reactivity) and aromatics (21 ± 10 %), mixed with NO_x (39 ± 4 %) from the bunker ship's own fuel combustion. Wu et al. (2015) measured total OH reactivity from gasoline evaporation with the CRM method. In their study, alkenes contributed 40 % of measured OH reactivity, and they found an unattributed OH reactivity fraction of 43 %. In our study, a larger percentage (75 ± 42 %) of total OH reactivity remains unexplained in the fuel evaporation measurement, which is most likely due to the fact that less of the higher and branched hydrocarbons were measured.

3.3.2.2 Suez Canal

The Suez Canal transit on August 24, 2017, was among the episodes of highest total OH reactivities during the whole campaign and will therefore be discussed in more detail here. In August 2017, 49 ships transited the Canal per day (Suez Canal Authority, 2018). It is one of the world's most heavily used shipping lanes and there are no regulations concerning the fuel used or emission limitations. The Suez Canal is 193 km long and at the water surface 313 m wide (Suez Canal Authority, 2017). Given its narrowness, other vessels and their exhausts, as well as urban areas or streets were relatively close to the *Kommandor Iona* while it was traveling along the Canal. Consequently, variations in OH reactivity can mainly be attributed to local emissions. Therefore, back trajectories are usually not helpful for explaining OH reactivity over the Suez Canal.

Four case studies (orange numbered labels in Fig. 3.5) will elucidate the origin of OH reactivity (reported with ± 1 σ total uncertainty) measured over the Suez Canal:

1) This 4 h period of higher OH reactivity (15.2 ± 5.8 s^{-1} to 19.1 ± 6.6 s^{-1}) occurred during a waiting period at the southern entrance to the Suez Canal, in the port area of Suez City. Interestingly, OH reactivity was dominated by alkanes here (~10−15 %). This can be explained by the wind coming from north where directly at the shore a petrol storage area is located (Nasr Petroleum Company, Suez, Egypt). The toluene/benzene ratio was between 1 and 3, indicating fuel combustion emissions as a source in Suez City and/or from ships, rather than biomass burning which tends to be richer in benzene.

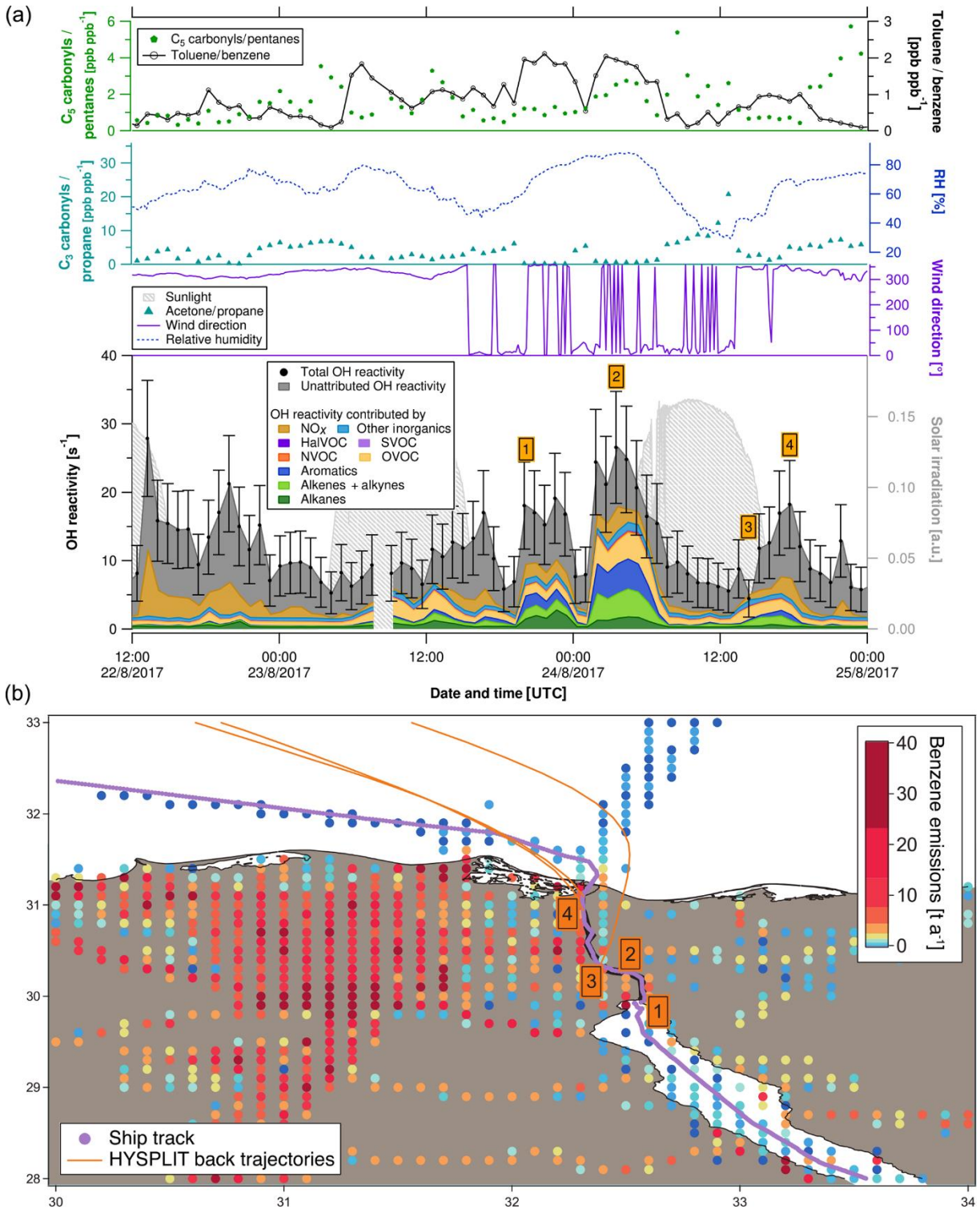

Figure 3.5: (a) C_3 carbonyls/propane ratio, C_5 carbonyls/pentane ratio, toluene/benzene ratio, relative humidity, solar irradiation, wind direction, speciated and measured OH reactivity in the Suez Canal. Error bars of total OH reactivity display the total uncertainty of the measurement. (b) Ship track of the cruise in the Suez Canal with HYSPLIT air mass back trajectories and numbered labels of case study points. Benzene emissions as an indicator for anthropogenic sources from the EDGAR database (http://edgar.jrc.ec.europa.eu, for 2012) are shown on a logarithmic colour scale.

2) The Great Bitter Lake is part of the Suez Canal and is used by ships as a "passing lane". During the 4 h waiting time in the lake, the highest OH reactivity of the transit was observed (20.6 ± 6.9 s^{-1} to 26.6 ± 8.2 s^{-1}). Alkenes, aromatics and OVOCs contributed almost equally to this value (~16 %, ~17 %, and ~17 %, respectively). Especially the large amount of aromatics is notable. With 7 ± 1 % contribution, alkanes were less relevant here than in the Suez City port (case study 1). A visible source of nearby emissions at the northern lakeshore (with northerly winds) was a power plant running on natural gas and/or heavy fuel oil (Abu Sultan Power Station, Ismailia, Egypt (Global Energy Observatory, 2015). Its emissions may have been mixed with those from the lakeshore settlements and from bypassing cargo ships, with a toluene/benzene ratio between 1 and 3, characteristic for fuel combustion emissions.

3) This point of observation was low in OH reactivity (5.5 ± 3.2 s^{-1}) as well as in relative humidity (29.2 %). Combined with the back trajectory, this indicates that the air mass sampled here had passed over the Sinai Desert. In this location, the C_3 carbonyls/propane ratio was 20.7, indicating a photochemically aged air mass. For comparison, the ratio was never above 10 anywhere else in the area, and in case studies 1 and 2 even between 0 and 1. Similarly, the C_5 carbonyls/pentanes ratio was elevated (2.6) and the toluene/benzene ratio was low (0.5).

4) The wind direction at case study point 4 was north/north-west. Total OH reactivity was in a 4 h peak of 11.8 ± 5.0 s^{-1} to 18.2 ± 6.4 s^{-1}. Ca. 15 % of it was caused by NO_x and ~ 9 % by alkenes. The toluene/benzene ratio was ~1, which indicates a fuel combustion source. There is a highway located west of this northern part of the Canal (Ismailia−Port Said Road), but given the wind direction, exhaust plumes of other vessels sailing in front of the research ship were probably relevant for the OH reactivity as well as traffic on land.

3.3.3 How many and which chemical species contribute to total OH reactivity around the Arabian Peninsula?

Many studies of ambient total OH reactivity show significant unattributed or "missing" OH reactivity (Yang et al., 2016). Care must be taken in interpreting this missing fraction as it depends on which individual compounds are taken into account, although forest studies have tended to show greater missing reactivity fractions than urban (Williams and Brune, 2015). Using a total of 120 chemical species (listed in Table S5.2), we calculated the speciated OH reactivity in 50 min time resolution for the whole AQABA campaign. For the datapoints with speciated OH reactivity above the CRM detection limit, the unattributed fraction of total OH reactivity is plotted against the number of compounds taken into account in Fig. 3.6. Only datapoints above the detection limit were chosen in order to exclude seemingly unattributed OH reactivity which is actually due to the detection limit (unattributed fractions for all datapoints are shown along with those for above the LOD in Table 3.1). The graph shows that when up to ca. 100 species are considered, the

unattributed OH reactivity fraction decreases. The remaining compounds collectively contribute only minor additional OH reactivity (less than 0.012 s^{-1}). Total OH reactivity is best explained by measured trace gases in the Arabian Gulf (22 ± 56 % unattributed), in the Suez Canal and southern Red Sea (37 ± 34 % and 35 ± 55% unattributed, respectively). The largest unattributed OH reactivity was found in the Gulf of Aden (55 ± 38 %). Other regions with significant unattributed fractions were the northern Red Sea (49 ± 39 %) and the Gulf of Suez (53 ± 35 %). The unattributed reactivity fraction does not correlate with the indicators used for estimating the air mass age.

Figure 3.7 shows the average OH reactivity of VOCs by molecular mass (NO_x and other inorganic compounds are not considered in this graph) and color-coded for groups of compounds for the Arabian Gulf and the Suez Canal. Higher-mass aromatics play a larger role in the Suez Canal while the same OVOCs are important in both regions. Generally, less VOCs in the higher mass ranges were measured, which is likely due to larger molecules being partially lost in the ca. 10 m long, 50 °C inlet line. This means that some less volatile components of total OH reactivity might have been missed in this setup. As the same inlet was used for VOC and OH reactivity measurements, however, this does not impact the unattributed reactivity fraction.

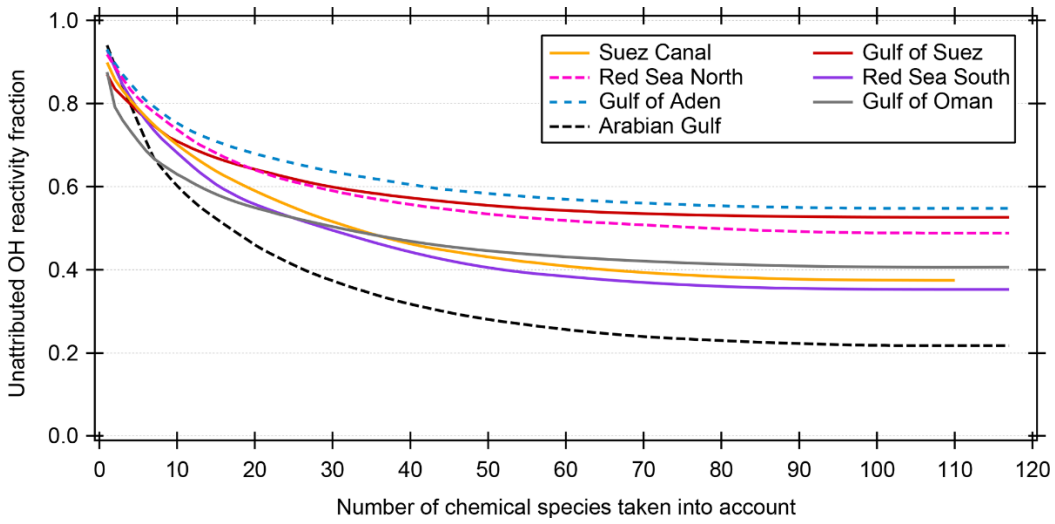

Figure 3.6: Unattributed OH reactivity fraction as a function of the number of compounds/chemical species taken into account for calculating speciated OH reactivity. The chemical species are taken into account with decreasing average OH reactivity. Only datapoints where the summed speciated OH reactivity is larger than or equal to the detection limit (LOD) of the CRM measurement are considered here. The Mediterranean and Arabian Sea are not shown because of insignificant number of datapoints above the LOD.

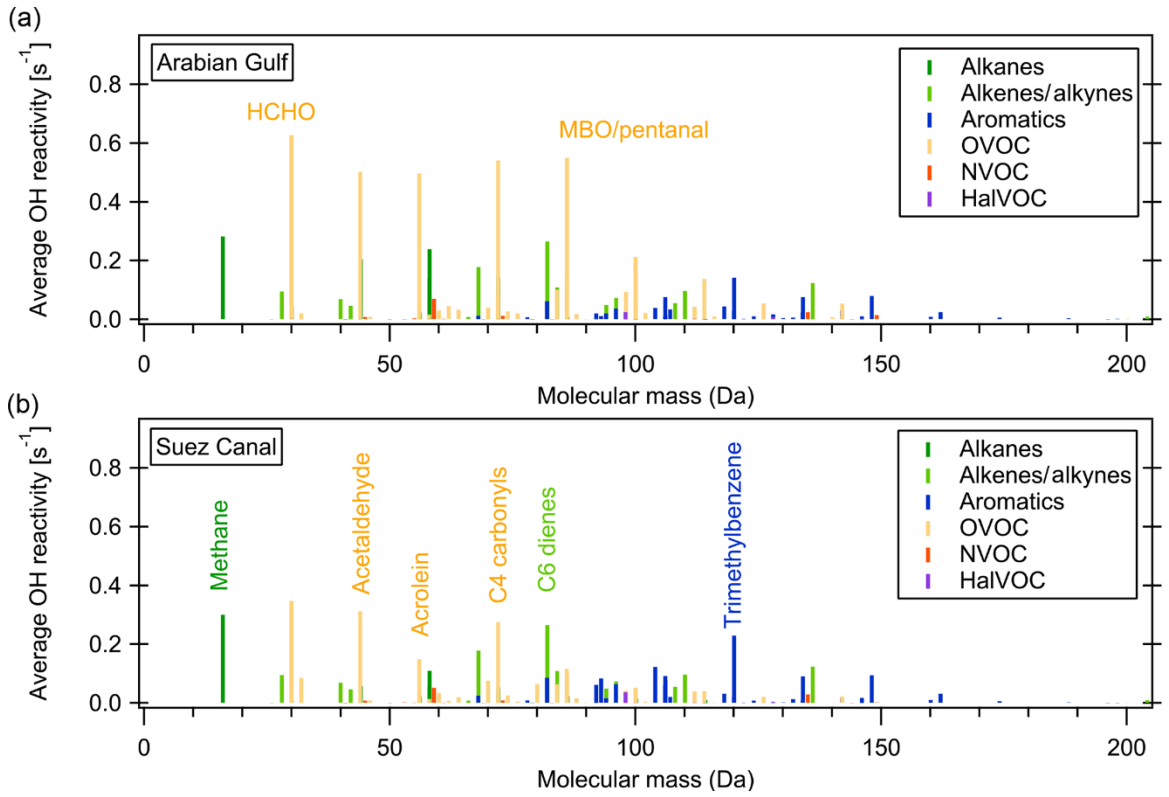

Figure 3.7: Average OH reactivity of VOCs by molecular mass in the Suez Canal and Arabian Gulf. Colors show the compound class.

The 10 chemical species which contributed most to OH reactivity in each region traversed during the AQABA campaign are displayed in Fig. 3.8. Generally, in no regional average was one single compound responsible for an OH reactivity of more than 1.4 s^{-1}. This reflects the previous discussion highlighting the necessity of considering a large number of species to get a complete picture of total OH reactivity. The concentrations of some of the compounds among the 10 most relevant ones were derived with the theoretical approach (see Sect. 3.2.5) and therefore have larger uncertainties. However, their potential importance underlines that a focus on the 14 compounds calibrated with a typical PTR−MS gas standard would not be sufficient for a comprehensive understanding of OH reactivity. Overall, the contribution of the 78 species derived by the theoretical approach amounts to between 22 % (Gulf of Suez) and 51 % (southern Red Sea) of speciated OH reactivity (see Table 3.1).

The highest percentage contribution to total OH reactivity by the 10 most important compounds was seen in the Gulf of Oman (39 ± 20 %) and the Arabian Gulf (38 ± 20 %), amongst which were the four theoretically calibrated exact masses of acrolein, MBO/pentanal, C_4 carbonyls and C_6 dienes.

The importance of the seaways around the Arabian Peninsula for maritime transport is reflected in the large contribution of NO_2 and CO (associated with fuel combustion), which are among the three highest contributors to OH reactivity in most of the regions and among the top 10 in all of them. Oxygenated species such as aldehydes and ketones were important OH sinks in all the areas, in particular formaldehyde, acetaldehyde and, to a lesser extent, the C_4 and C_5 carbonyls. Directly emitted hydrocarbons were among the 10 most important OH reactivity contributors only in areas closer to emission sources: e.g. n-butane and propane in the Gulf of Suez, or unsaturated hydrocarbons such as C_6 dienes, C_5 dienes (without isoprene) and ethene in the Suez Canal. The importance of oxygenates in the air composition during AQABA reflects the fast photooxidation of direct emissions during this summertime campaign (also see Sect. 3.3.1.1). In winter, the directly emitted hydrocarbons would have longer lifetimes and therefore gain importance in the OH reactivity budget at the expense of oxygenates.

In the Arabian Sea, which was the area with the lowest total OH reactivities (Fig. 3.1, Table 3.1), the global background OH reactivity from methane was a major OH sink. Dimethyl sulfide (DMS), a biogenic molecule emitted by algae which has been observed in this part of the ocean before (Warneke and Gouw, 2001) and will be discussed elsewhere for the AQABA campaign (Edtbauer et al., 2019, in preparation), appears among the 10 most important OH sinks here despite a reactivity of only 0.02 s^{-1}. This is evidence for relatively clean air due to the influence of open ocean air, although even here emissions from shipping are evident from the CO and NO_2 contributions. In the Mediterranean, methane was the second-most important single contributor to total OH reactivity after CO.

Generally, anthropogenic VOCs and their oxidation products dominated OH reactivity around the Arabian Peninsula. For example, acrolein was among the 10 most important contributors almost everywhere during AQABA (Fig. 3.8). Acrolein is a major product of the oxidation of 1,3-butadiene, which is among the most abundant alkenes emitted from anthropogenic sources (Grosjean et al., 1994). The C_4 carbonyls (butanal or methyl ethyl ketone (MEK), are major contributors to total OH reactivity over the Arabian Basin, and both can be directly emitted from fossil fuel combustion (Schauer et al., 2002) or be the result of ambient oxidation processes. Carbonyl photolysis has been found recently to be a possible source of ozone formation in an oil and gas production area (Edwards et al., 2014).

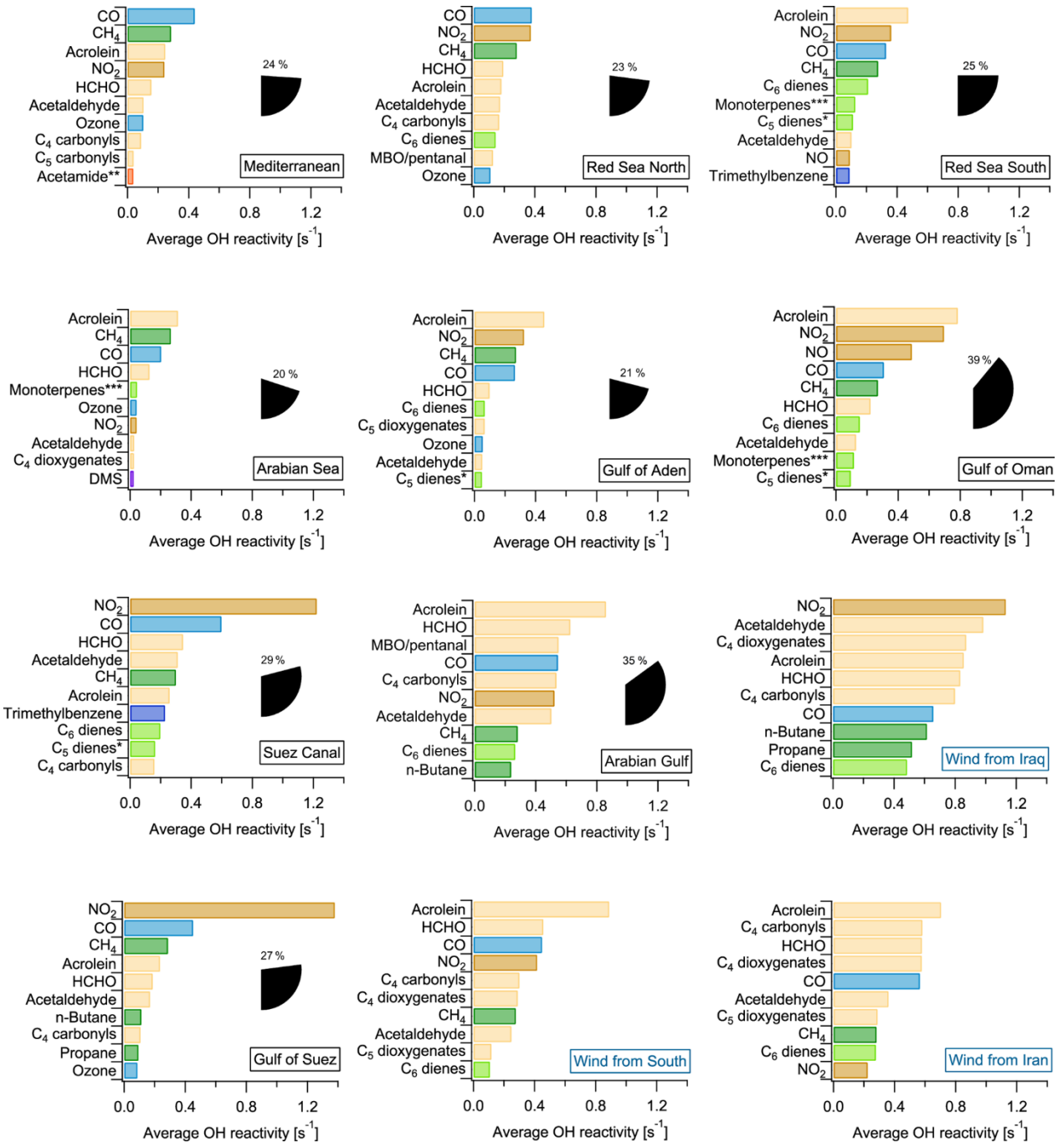

Figure 3.8: Regional average OH reactivity of each of the 10 most important contributors to OH reactivity. The percentage of total OH reactivity from these 10 compounds is shown as pie wedges. The Arabian Gulf was split by air mass origin (plots with blue labels). *C_5 dienes do not include isoprene. **Acetamide or *N*-methyl formamide. ***"Monoterpenes" may include anthropogenic C_{10} trienes. **Abbreviations: MBO: 2-Methyl-3-buten-2-ol.**

3.3.4 OH reactivity and ozone

3.3.4.1 Ozone production regimes

Ozone and OH reactivity are connected via a chemical cycle that involves NO_x and VOCs (Sillman, 1999; Ren et al., 2013): OH oxidizes VOCs to form peroxy radicals, which, in turn, oxidize NO to NO_2. NO_2 thus formed is subsequently photolyzed to result in ozone production. Ozone formation is, however, neither linearly dependent on NO_x concentration nor VOC reactivity, and a decrease in one parameter does not necessarily lead to a decrease in ozone formation (Pusede and Cohen, 2012).

Defining ozone production regimes in terms of the OH reactivities of VOCs and NO_x is a way of assessing the sensitivity of ozone production to the prevailing conditions (Kirchner et al., 2001; Sinha et al., 2012). The method and underlying chemistry has been extensively evaluated for different conditions and compared to other methods in Kirchner et al. (2001). The amount of peroxy radicals produced by VOC oxidation is linked to the OH reactivity of VOCs. The OH reactivity of VOCs was calculated here as the difference of measured total OH reactivity (in 5 min time resolution) and OH reactivity of measured NO_x. Only data at daytime (06:00–18:00 local time) was considered, because the method is inherently limited to daytime chemistry. Figure 3.9 shows ozone production regime plot examples, where "s" denotes the relative reactivity of OH towards NO_x and VOCs. Based on the analysis of Kirchner et al. (2001), which was developed for urban VOC mixtures, in between the lines labelled s = 0.2 and s = 0.01, ozone production is favored by a suitable ratio of NO_x and OH reactivity of VOCs, whereas s > 0.2 indicates VOC limitation, and s < 0.01 NO_x limitation. The Arabian Sea with its comparably clean air was a region with partially NO_x limited ozone production (Fig. 3.9a). Here, 20 % of the datapoints do not fall within the regime of ozone production, mostly due to NO_x limitation. This is reflected in relatively low ozone mixing ratios. The Gulf of Suez (Fig. 3.9b) is characterized in part by a strong VOC limitation associated with high NO_x (69 % of datapoints indicate an ozone formation regime). This NO_x can be attributed to emissions from other vessels at close proximity while waiting at the entrance of the Suez Canal. The low ozone mixing ratios associated with high NO_x in the fresh combustion emissions (Fig. 9b/c) point to ozone titration, which will be discussed in greater detail in Sect. 3.3.4.2. In the Suez Canal (Fig. 3.9c), the datapoints are also grouped more towards VOC sensitivity whereas the opposite is true for the Arabian Gulf (Fig. 3.9d). Nevertheless, in both the Suez Canal and the Arabian Gulf, almost all datapoints (97 % in the Arabian Gulf and 91 % in the Suez Canal) fall into the regime of ozone formation, meaning that a suitable ratio of VOC and NO_x molecules for ozone formation was present nearly all the time. The same is true for the other environments (not shown in graph) with favored ozone formation 97 % of the time in the Mediterranean, 93 % in the

northern Red Sea, 88 % in the southern Red Sea, 87 % in the Gulf of Aden, and 82 % in the Gulf of Oman.

The ozone production favoring conditions with both high NO_x- and VOC-attributed OH reactivities may be contributing factors to the high ozone levels observed and modeled above the Arabian Gulf (Lelieveld et al., 2009; Fountoukis et al., 2018). Ozone formation favorable conditions resulting in ozone mixing ratios up to 145 ppb have been reported from other sites influenced by oil and gas production (Edwards et al., 2014; Wei et al., 2014). Moradzadeh et al. (2019) found that a hydrocarbon processing plant at the shore of the Arabian Gulf impacted ozone levels even in 300 km distance. Generally, emissions in lower latitudes (e.g. below 30° N as in the Arabian Gulf) lead to more efficient formation of tropospheric ozone than in higher latitudes, because the meteorological conditions lead to faster reaction rates and strong convection (Zhang et al., 2016).

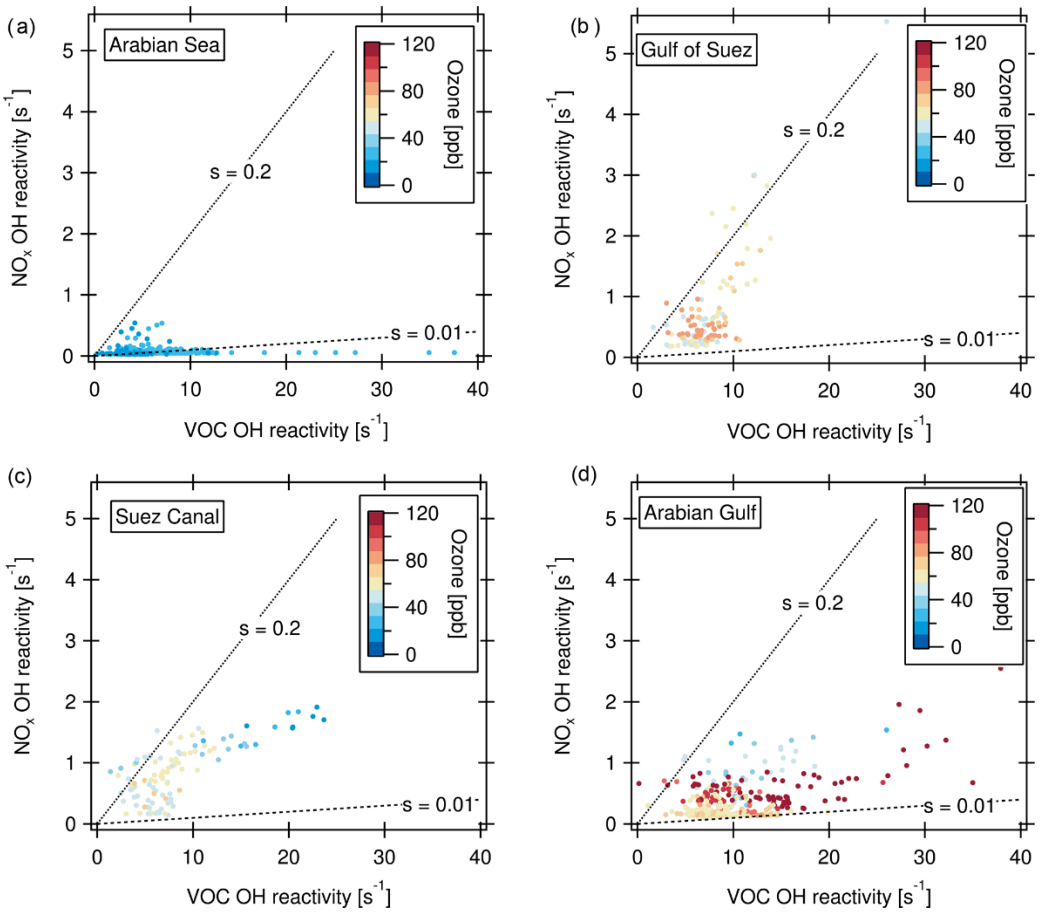

Figure 3.9: Ozone production regimes for (a) Arabian Sea, (b) Gulf of Suez (c) Suez Canal, and (d) Arabian Gulf. "s" denotes the relative reactivity of OH towards NO_x and VOCs. For s > 0.2: VOC limitation, for s < 0.01: NO_x limitation of the ozone formation.

3.3.4.2 OH reactivity/ozone correlations

The relationship between ozone and total OH reactivity during the AQABA campaign is depicted in Fig. 3.10. Data from most regions display a negative correlation between ozone mixing ratio and total OH reactivity. This is exemplified for the Mediterranean, the Suez Canal and Gulf of Suez in Fig. 3.10a (correlation for Suez Canal: slope = -0.2; $r^2 = 0.61$). Additionally, there is a large group of datapoints located at lower OH reactivity (below 10 s^{-1}) and ozone mixing ratios of 50 to 70 ppb.

The reason for the negative correlation seen in parts of the data is displayed in Fig. 3.10b. Higher OH reactivities in this part of the plot coincide with higher NO_x, stemming from the exhaust plumes of vessels passing close by. In these ship plumes, high levels of VOCs are co-emitted with NO_x. This combination leads to elevated total OH reactivity. At the same time, ozone is depleted by the NO emissions in the fresh ship plumes ($NO + O_3 \rightarrow NO_2 + O_2$, Sillman, 1999). This effect is seen when an emission source co-emitting NO_x and VOCs is very close (Akimoto, 2016), as ozone values recover rapidly downwind through NO_2 photolysis and mixing. The ozone titration effect has similarly been observed in negative ozone-CO correlations (Parrish et al., 1998).

The bulk of datapoints between 50 and 70 ppb of ozone associated with lower OH reactivity and no trend is, on the other hand, more representative of a campaign background/average, uninfluenced by immediate emission sources and with lower NO_x (Fig. 3.10b). Here, a possible longer-term effect of the co-emission of VOC and NO_x from marine transport and other anthropogenic sources can be seen. As a secondary pollutant and being suppressed by NO, ozone can often be elevated at distance to the pollution sources (Sudo and Akimoto, 2007). Large quantities of ozone can be produced during long-range transport under sunlight influence (Parrish et al., 1998; Akimoto, 2016; Moradzadeh et al., 2019). Consequently, in the seaways around the Arabian Peninsula, ozone mixing ratios were mostly between 50 and 80 ppb, which is the range of daytime values in polluted Beijing (Williams et al., 2016; Yang et al., 2017).

Over the Arabian Gulf, the same negative relationship between OH reactivity and ozone as in the Suez Canal, Gulf of Suez and Mediterranean existed in those datapoints where ozone was below 70 ppb. In contrast, at ozone mixing ratios above ca. 80 ppb, no trend or a slightly positive correlation between ozone mixing ratio and OH reactivity can be ascertained (Fig. 3.10a). Ozone mixing ratios above 70 ppb over the Arabian Gulf were associated with a high fraction of OVOCs (Fig. 3.10c), indicating more photochemically processed air. Additionally, when OH reactivity was high at the same time as ozone, alkene OH reactivity was also elevated (Fig. 3.10d). This points to a mixing in of fresh emissions (associated with short-lived alkenes) into photochemically aged, oxidized air contaminants (high OVOCs and high ozone) over the Arabian Gulf. Polluted air masses from urban or industrial areas on land were probably oxidized during their transport to the

coast/sea, where they were mixed with emissions from oil and gas extraction facilities, as has been discussed in detailed case studies of such occasions in Sect. 3.3.2.

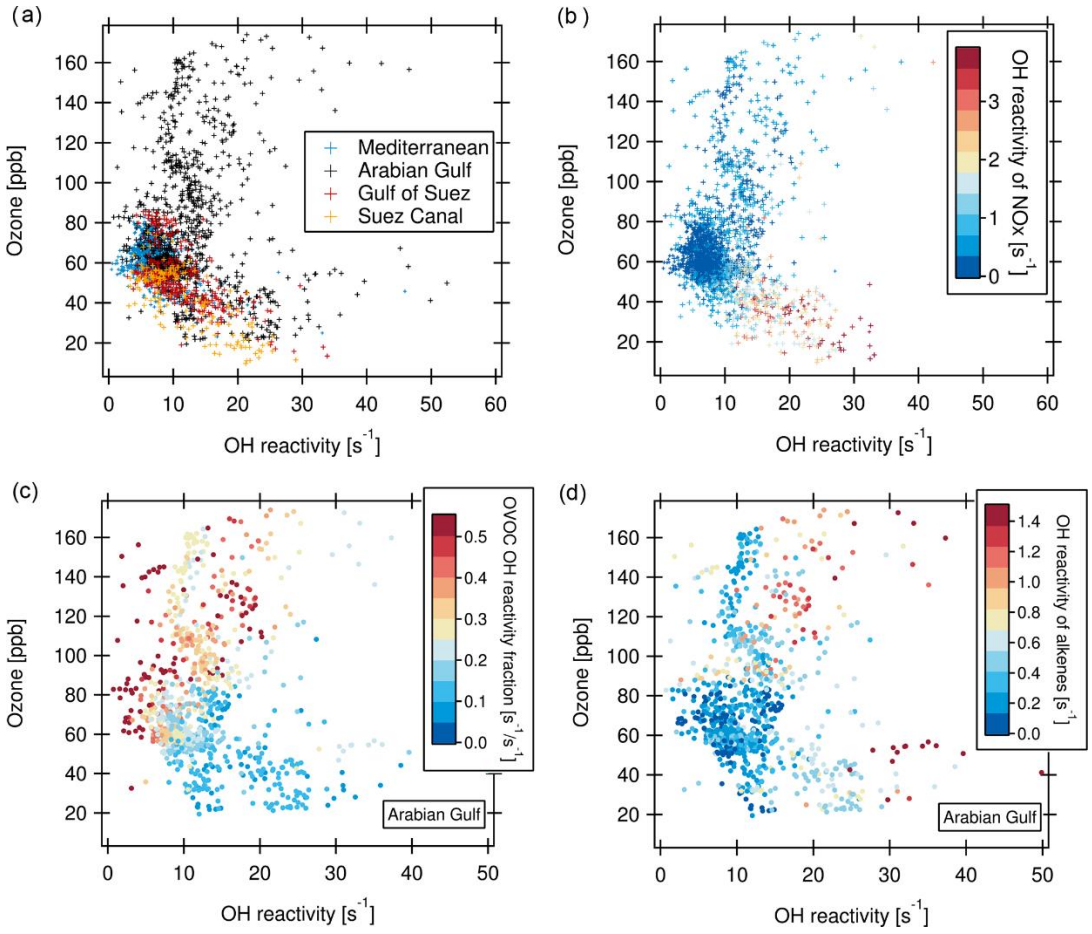

Figure 3.10: (a) Ozone vs. total OH reactivity for four regions. (b) Same as (a), but with OH reactivity of NO_x as color scale (no datapoints when NO_x values are missing). (c) Ozone vs. OH reactivity for the Arabian Gulf with the fraction of OVOC in total OH reactivity as color scale. (d) Ozone vs. OH reactivity for the Arabian Gulf with OH reactivity of alkenes as color scale.

3.4 Summary and conclusions

In July and August 2017, during the AQABA campaign, the first ship-based direct measurements of total OH reactivity were conducted using the Comparative Reactivity Method. The total OH reactivity in ambient air around the Arabian Peninsula was predominantly related to anthropogenic influence. Particularly, reactive hydrocarbons from oil and gas extraction/production and inorganic reactants such as NO_x and CO from fuel combustion by shipping were major OH sinks during the whole campaign. Total OH reactivity over the Arabian Basin varied, with periods below the detection limit over the Arabian Sea, regional medians of 7.9–8.5 s^{-1} under permanent maritime traffic influence over the seaways of the Red Sea, Gulf of Aden and Gulf of Oman, and episodes of up to 32.8 ± 9.6 s^{-1} when air masses were influenced by emissions from oil/gas extraction

facilities, urban centers and/or ships in close proximity. The largest regional median OH loss rate of 18.8s^{-1} was observed over the Arabian Gulf when air originated from Iraq/Kuwait, where large oil fields and refineries at the shore provided high emissions. Over the Suez Canal, median OH reactivities of 10.8 s^{-1} and up to 26.6 ± 8.2 s^{-1} were attributed to local emissions from a petroleum storage facility, a power plant and traffic on sea and land. The cleanest environment was the Arabian Sea, where the marine biogenic compound dimethyl sulfide was among the 10 most important known contributors to OH reactivity.

In all the regions around the Arabian Peninsula, OVOCs were the class of compounds that provided the largest identified OH sink. They were formed efficiently because photochemistry was highly active due to intense solar irradiation and high temperatures in summer. Photochemically aged air mixed with fresh nearby emissions over the Arabian Gulf, leading to extremely high ozone mixing ratios. Using ozone production regime plots, we found that the ratio of VOC- and NO_x-attributed OH reactivities was favorable for ozone formation nearly all along the ship track. In the Arabian Gulf, large OH reactivity from VOCs due to oil and gas sources together with NO_x from marine traffic lead to a regime of ozone production 97 % of the time. The only regions where ozone production was limited for a significant fraction of time were the Gulf of Suez with VOC limitation when affected by NO_x-rich plumes, and the Arabian Sea with a slight NO_x limitation due to clean air from the open Indian Ocean. Ozone versus OH reactivity correlation plots were found to be a valuable tool in identifying different chemical regimes with regards to ozone formation and loss: ozone destruction in NO_x-rich ship plumes was clearly distinguishable from a mix of fresh petroleum extraction emissions with photochemically aged air.

Studies of ambient total OH reactivity often show a significant "missing" or unattributed fraction of OH reactivity, although this tends to be smaller in anthropogenic environments (Williams and Brune, 2015). In an attempt to close the OH reactivity budget, the OH reactivity of compounds with unidentified structure from PTR−ToF−MS measurements was calculated using averages of the reaction rate constants of all possible structures attributed to each chemical formula. These species were important OH sinks, accounting for 22−51 % of the regional speciated OH reactivity. With this approach, the measured total OH reactivity can be explained within the uncertainty for the Suez Canal, the southern Red Sea, the Gulf of Oman and the Arabian Gulf. Significant unattributed fractions remain in the Gulf of Suez, the northern Red Sea and the Gulf of Aden. Overall, ~ 100 chemical species needed to be identified to explain the measured total OH reactivity within the uncertainty, while the 10 most important compounds contributed 20−39 % of the reactivity. Unattributed reactivity in plumes from hydrocarbon processing facilities may be due to branched and/or higher hydrocarbons not captured with the techniques available on board the *Kommandor Iona*. In order to get a more comprehensive picture of the chemical species relevant

for OH chemistry in the region, measurements with even greater chemical detail in the hydrocarbons would be necessary.

The range and composition of OH reactivity (and the ozone mixing ratios) around the Arabian Peninsula were, despite the marine measurement locations, broadly comparable to observations from highly populated urban areas, except for an unusually large contribution of OVOCs (Kovacs et al., 2003; Mao et al., 2010; Dolgorouky et al., 2012; Kim et al., 2016; Williams et al., 2016; Praplan et al., 2017; Yang et al., 2017). The "urban-like" OH reactivity is related to intensive international ship traffic in the seaways in the Arabian Basin and to major emissions from oil and gas industries on sea platforms and at the coasts. Oil and gas related VOCs were important sources of OH reactivity, and could be a relevant factor for the extremely high ozone concentrations and the photochemical air pollution usually seen in summer in the region (Lelieveld et al., 2009; Smoydzin et al., 2012; Farahat, 2016; Barkley et al., 2017).

Most predictions assume that oil and natural gas production will increase in the Middle East during the coming decades (Balat, 2006; Khatib, 2014; Holz et al., 2015; Overland, 2015). Similarly, ship emissions around the Arabian Peninsula have been projected to grow on the short term due to intensifying traffic (Eyring et al., 2007), although new emission regulations set by the International Maritime Organization (IMO, 2019), effective from 2020, might lead to a long-term decrease. Given that the conditions favor ozone production and will increase to do so due to rising temperatures (Wasimi, 2010; Lelieveld et al., 2012; Lelieveld et al., 2016), emission regulations in the region appear to be the only way to prevent a further increase in photochemical air pollution in the future.

Data availability. The data used in this study will be available from August 2019 to all scientists agreeing to the AQABA protocol at https://doi.org/10.5281/zenodo.3354117.

Supplement. The supplement related to this article is available on- line at: https://doi.org/10.5194/acp-19-11501-2019-supplement.

Author contributions. EP and NW were responsible for OH reactivity measurements and data. EP conducted further data analysis and wrote the first draft of the manuscript. AE, EB, LE and CS contributed VOC and NMHC measurements and data. Ozone and SO_2 data were provided by JC and PE, formaldehyde and NO_x data by DD, BH, IT and HF, methane and carbon monoxide by JP. DW calculated the back trajectories. JL designed and realized the campaign. JW supervised the study. All authors contributed to manuscript writing and revision, read and approved the submitted version.

Acknowledgements. We thankfully acknowledge the cooperation with the Cyprus Institute (CyI), the King Abdullah University of Science and Technology (KAUST) and the Kuwait Institute for Scientific Research (KISR). We thank Hays Ships Ltd, Captain Pavel Kirzner and the ship crew for their support on-board the *Kommandor Iona*. We would like to express our gratitude to the

whole AQABA team, particularly Hartwig Harder for daily management of the campaign; and Marcel Dorf, Claus Koeppel, Thomas Klüpfel and Rolf Hofmann for logistical organization and help with preparation and setup. We are grateful for Uwe Parchatka's assistance with NO_2 loss characterizations and Jan Schuladen's solar radiance data. The campaign was funded by the Max Planck Society. The position of Nijing Wang was funded by the European Union's Horizon 2020 research and innovation programme under the Marie Skłodowska-Curie grant agreement No. 674911.

Financial support. The AQABA campaign was funded by the Max Planck Society. The position of Nijing Wang was funded by the European Union's Horizon 2020 Research and Innovation program under the Marie Skłodowska-Curie grant agreement no. 674911.

The article processing charges for this open-access publication were covered by the Max Planck Society.

Review statement. This paper was edited by Frank Keutsch and re-viewed by two anonymous referees.

References

Abdelkader, M., Metzger, S., Mamouri, R. E., Astitha, M., Barrie, L., Levin, Z., and Lelieveld, J.: Dust–air pollution dynamics over the eastern Mediterranean, Atmos. Chem. Phys., 15, 9173–9189, doi:10.5194/acp-15-9173-2015, 2015.

Ajith Joseph, K., Jayaram, C., Nair, A., George, M. S., Balchand, A. N., and Pettersson, L. H.: Remote Sensing of Upwelling in the Arabian Sea and Adjacent Near-Coastal Regions, in: Remote Sensing of the Asian Seas, 1st edition 2019, Barale, V., and Gade, M. (Eds.), Springer International Publishing, Cham, 467–483, 2018.

Akimoto, H.: Tropospheric Reaction Chemistry, in: Atmospheric Reaction Chemistry, Springer Japan, Tokyo, 285–386, 2016.

Balat, M.: The Position of Oil in the Middle East: Potential Trends, Future Perspectives, Market and Trade, Energy Sources, Part A: Recovery, Utilization, and Environmental Effects, 28, 821–828, doi:10.1080/009083190951384, 2006.

Barkley, M. P., González Abad, G., Kurosu, T. P., Spurr, R., Torbatian, S., and Lerot, C.: OMI air-quality monitoring over the Middle East, Atmos. Chem. Phys., 17, 4687–4709, doi:10.5194/acp-17-4687-2017, 2017.

Barletta, B., Simpson, I. J., Blake, N. J., Meinardi, S., Emmons, L. K., Aburizaiza, O. S., Siddique, A., Zeb, J., Yu, L. E., Khwaja, H. A., Farrukh, M. A., and Blake, D. R.: Characterization of carbon monoxide, methane and nonmethane hydrocarbons in emerging cities of Saudi Arabia and Pakistan and in Singapore, J Atmos Chem, 74, 87–113, doi:10.1007/s10874-016-9343-7, 2017.

Boersma, K. F., Vinken, G. C. M., and Tournadre, J.: Ships going slow in reducing their NOx emissions: Changes in 2005–2012 ship exhaust inferred from satellite measurements over Europe, Environ. Res. Lett., 10, 74007, doi:10.1088/1748-9326/10/7/074007, 2015.

Bourtsoukidis, E., Ernle, L., Crowley, J. N., Lelieveld, J., Paris, J.-D., Pozzer, A., Walter, D., and Williams, J.: Non Methane Hydrocarbon (C2-C8) sources and sinks around the Arabian Peninsula, Atmos. Chem. Phys. Discuss., 1–45, doi:10.5194/acp-2019-92, 2019.

Buzcu, B. and Fraser, M. P.: Source identification and apportionment of volatile organic compounds in Houston, TX, ATMOSPHERIC ENVIRONMENT, 40, 2385–2400, doi:10.1016/j.atmosenv.2005.12.020, 2006.

Chenoweth, J., Hadjinicolaou, P., Bruggeman, A., Lelieveld, J., Levin, Z., Lange, M. A., Xoplaki, E., and Hadjikakou, M.: Impact of climate change on the water resources of the eastern Mediterranean and Middle East region: Modeled 21st century changes and implications, Water Resour. Res., 47, 45, doi:10.1029/2010WR010269, 2011.

Cook, B. I., Anchukaitis, K. J., Touchan, R., Meko, D. M., and Cook, E. R.: Spatiotemporal drought variability in the Mediterranean over the last 900 years, Journal of geophysical research. Atmospheres JGR, 121, 2060–2074, doi:10.1002/2015JD023929, 2016.

D'Auria, M., Emanuele, L., Racioppi, R., and Velluzzi, V.: Photochemical degradation of crude oil: Comparison between direct irradiation, photocatalysis, and photocatalysis on zeolite, Journal of hazardous materials, 164, 32–38, doi:10.1016/j.jhazmat.2008.07.111, 2009.

Dolgorouky, C., Gros, V., Sarda-Esteve, R., Sinha, V., Williams, J., Marchand, N., Sauvage, S., Poulain, L., Sciare, J., and Bonsang, B.: Total OH reactivity measurements in Paris during the 2010 MEGAPOLI winter campaign, Atmos. Chem. Phys., 12, 9593–9612, doi:10.5194/acp-12-9593-2012, 2012.

Donat, M. G., Peterson, T. C., Brunet, M., King, A. D., Almazroui, M., Kolli, R. K., Boucherf, D., Al-Mulla, A. Y., Nour, A. Y., Aly, A. A., Nada, T. A. A., Semawi, M. M., Al Dashti, H. A., Salhab, T. G., El Fadli, K. I., Muftah, M. K., Dah Eida, S., Badi, W., Driouech, F., El Rhaz, K., Abubaker, M. J. Y., Ghulam, A. S., Erayah, A. S., Mansour, M. B., Alabdouli, W. O., Al Dhanhani, J. S., and Al Shekaili, M. N.: Changes in extreme temperature and precipitation in the Arab region: long-term trends and variability related to ENSO and NAO, Int. J. Climatol., 34, 581–592, doi:10.1002/joc.3707, 2014.

Doskey, P. V., Fukui, Y., Sultan, M., Al Maghraby, A., and Taher, A.: Source Profiles for Nonmethane Organic Compounds in the Atmosphere of Cairo, Egypt, Journal of the Air & Waste Management Association (1995), 49, 814–822, doi:10.1080/10473289.1999.10463850, 1999.

Draxler, R. R. and Hess, G. D.: An Overview of the HYSPLIT_4 Modelling System for Trajectories, Dispersion, and Deposition, Australian Meteorological Magazine, 295–308, 1998.

Edwards, P. M., Brown, S. S., Roberts, J. M., Ahmadov, R., Banta, R. M., deGouw, J. A., Dubé, W. P., Field, R. A., Flynn, J. H., Gilman, J. B., Graus, M., Helmig, D., Koss, A., Langford, A. O., Lefer, B. L., Lerner, B. M., Li, R., Li, S.-M., McKeen, S. A., Murphy, S. M., Parrish, D. D., Senff, C. J., Soltis, J., Stutz, J., Sweeney, C., Thompson, C. R., Trainer, M. K., Tsai, C., Veres, P. R., Washenfelder, R. A., Warneke, C., Wild, R. J., Young, C. J., Yuan, B., and Zamora, R.: High winter ozone pollution from carbonyl photolysis in an oil and gas basin, Nature, 514, 351–354, doi:10.1038/nature13767, 2014.

Endresen, Ø.: Emission from international sea transportation and environmental impact, J. Geophys. Res., 108, 29,239, doi:10.1029/2002JD002898, 2003.

Eyring, V.: Emissions from international shipping: 1. The last 50 years, J. Geophys. Res., 110, 127, doi:10.1029/2004JD005619, 2005.

Eyring, V., Stevenson, D. S., Lauer, A., Dentener, F. J., Butler, T., Collins, W. J., Ellingsen, K., Gauss, M., Hauglustaine, D. A., Isaksen, I. S. A., Lawrence, M. G., Richter, A., Rodriguez, J. M., Sanderson, M., Strahan, S. E., Sudo, K., Szopa, S., van Noije, T. P. C., and Wild, O.: Multi-model simulations of the impact of international shipping on Atmospheric Chemistry and Climate in 2000 and 2030, Atmos. Chem. Phys., 7, 757–780, doi:10.5194/acp-7-757-2007, 2007.

Ezhova, E., Ylivinkka, I., Kuusk, J., Komsaare, K., Vana, M., Krasnova, A., Noe, S., Arshinov, M., Belan, B., Park, S.-B., Lavrič, J. V., Heimann, M., Petäjä, T., Vesala, T., Mammarella, I., Kolari, P., Bäck, J., Rannik, Ü., Kerminen, V.-M., and Kulmala, M.: Direct effect of aerosols on solar radiation and gross primary production in boreal and hemiboreal forests, Atmos. Chem. Phys., 18, 17863–17881, doi:10.5194/acp-18-17863-2018, 2018.

Farahat, A.: Air pollution in the Arabian Peninsula (Saudi Arabia, the United Arab Emirates, Kuwait, Qatar, Bahrain, and Oman): Causes, effects, and aerosol categorization, Arab J Geosci, 9, 276, doi:10.1007/s12517-015-2203-y, 2016.

Fountoukis, C., Ayoub, M. A., Ackermann, L., Perez-Astudillo, D., Bachour, D., Gladich, I., and Hoehn, R. D.: Vertical Ozone Concentration Profiles in the Arabian Gulf Region during Summer and Winter: Sensitivity of WRF-Chem to Planetary Boundary Layer Schemes, Aerosol Air Qual. Res., 18, 1183–1197, doi:10.4209/aaqr.2017.06.0194, 2018.

Fuchs, H., Novelli, A., Rolletter, M., Hofzumahaus, A., Pfannerstill, E. Y., Kessel, S., Edtbauer, A., Williams, J., Michoud, V., Dusanter, S., Locoge, N., Zannoni, N., Gros, V., Truong, F., Sarda-Esteve, R., Cryer, D. R., Brumby, C. A., Whalley, L. K., Stone, D., Seakins, P. W., Heard, D. E., Schoemaecker, C., Blocquet, M., Coudert, S., Batut, S., Fittschen, C., Thames, A. B., Brune, W. H., Ernest, C., Harder, H., Muller, J. B. A., Elste, T., Kubistin, D., Andres, S., Bohn, B., Hohaus, T., Holland, F., Li, X., Rohrer, F., Kiendler-Scharr, A., Tillmann, R., Wegener, R., Yu, Z., Zou, Q., and Wahner, A.: Comparison of OH reactivity measurements in the atmospheric simulation chamber SAPHIR, Atmos. Meas. Tech., 10, 4023–4053, doi:10.5194/amt-10-4023-2017, 2017.

Gilman, J. B., Kuster, W. C., Goldan, P. D., Herndon, S. C., Zahniser, M. S., Tucker, S. C., Brewer, W. A., Lerner, B. M., Williams, E. J., Harley, R. A., Fehsenfeld, F. C., Warneke, C., and Gouw, J. A. de: Measurements of volatile organic compounds during the 2006 TexAQS/GoMACCS campaign: Industrial influences, regional characteristics, and diurnal dependencies of the OH reactivity, J. Geophys. Res., 114, doi:10.1029/2008JD011525, 2009.

Gilman, J. B., Lerner, B. M., Kuster, W. C., and Gouw, J. A. de: Source signature of volatile organic compounds from oil and natural gas operations in northeastern Colorado, Environmental science & technology, 47, 1297–1305, doi:10.1021/es304119a, 2013.

Global Energy Observatory: Abu Sultan Thermal Power Plant Egypt: http://globalenergyobservatory.org/geoid/1977, last access: 2 January 2019.

Goldstein, A. H. and Galbally, I. E.: Known and Unexplored Organic Constituents in the Earth's Atmosphere, Environ. Sci. Technol., 41, 1514–1521, doi:10.1021/es072476p, 2007.

Grosjean, D. and Seinfeld, J. H.: Parameterization of the formation potential of secondary organic aerosols, Atmospheric Environment (1967), 23, 1733–1747, doi:10.1016/0004-6981(89)90058-9, 1989.

Grosjean, E., Williams, E. L., and Grosjean, D.: Atmospheric chemistry of acrolein, Science of The Total Environment, 153, 195–202, doi:10.1016/0048-9697(94)90198-8, 1994.

Gueneron, M., Erickson, M. H., VanderSchelden, G. S., and Jobson, B. T.: PTR-MS fragmentation patterns of gasoline hydrocarbons, International Journal of Mass Spectrometry, 379, 97–109, doi:10.1016/j.ijms.2015.01.001, 2015.

Haagen-Smit, A. J.: Chemistry and Physiology of Los Angeles Smog, Ind. Eng. Chem., 44, 1342–1346, doi:10.1021/ie50510a045, 1952.

Hansen, R. F., Blocquet, M., Schoemaecker, C., Léonardis, T., Locoge, N., Fittschen, C., Hanoune, B., Stevens, P. S., Sinha, V., and Dusanter, S.: Intercomparison of the comparative reactivity method (CRM) and pump–probe technique for measuring total OH reactivity in an urban environment, Atmos. Meas. Tech., 8, 4243–4264, doi:10.5194/amt-8-4243-2015, 2015.

Holz, F., Richter, P. M., and Egging, R.: A Global Perspective on the Future of Natural Gas: Resources, Trade, and Climate Constraints, Review of Environmental Economics and Policy, 9, 85–106, doi:10.1093/reep/reu016, 2015.

Huang, C., Hu, Q., Wang, H., Qiao, L., Jing, S.'a., Wang, H., Zhou, M., Zhu, S., Ma, Y., Lou, S., Li, L., Tao, S., Li, Y., and Lou, D.: Emission factors of particulate and gaseous compounds from a large cargo vessel operated under real-world conditions, Environmental pollution (Barking, Essex 1987), 242, 667–674, doi:10.1016/j.envpol.2018.07.036, 2018.

IMO: Prevention of Air Pollution from Ships: Revised MARPOL Annex VI: http://www.imo.org/en/OurWork/Environment/PollutionPrevention/AirPollution/Pages/Air-Pollution.aspx, last access: 1 March 2019.

Ingham, T., Goddard, A., Whalley, L. K., Furneaux, K. L., Edwards, P. M., Seal, C. P., Self, D. E., Johnson, G. P., Read, K. A., Lee, J. D., and Heard, D. E.: A flow-tube based laser-induced fluorescence instrument to measure OH reactivity in the troposphere, Atmos. Meas. Tech. Discuss., 2, 621–657, doi:10.5194/amtd-2-621-2009, 2009.

Johansson, L., Jalkanen, J.-P., and Kukkonen, J.: Global assessment of shipping emissions in 2015 on a high spatial and temporal resolution, ATMOSPHERIC ENVIRONMENT, 167, 403–415, doi:10.1016/j.atmosenv.2017.08.042, 2017.

Keßel, S. U.: Entwicklung und Charakterisierung der Comparative Reactivity Method zur Messung von Hydroxylradikal- und Chlorradikal-Reaktivitäten - Troposphärische Oxidationschemie in drei unterschiedlich stark anthropogen beeinflussten Gebieten, Dissertation, Johannes-Gutenberg-Universität, Mainz, 2016.

Khalil, M. A. K., Butenhoff, C. L., Porter, W. C., Almazroui, M., Alkhalaf, A., and Al-Sahafi, M. S.: Air quality in Yanbu, Saudi Arabia, Journal of the Air & Waste Management Association (1995), 66, 341–355, doi:10.1080/10962247.2015.1129999, 2016.

Khatib, H.: Oil and natural gas prospects: Middle East and North Africa, Energy Policy, 64, 71–77, doi:10.1016/j.enpol.2013.07.091, 2014.

Kim, S., Sanchez, D., Wang, M., Seco, R., Jeong, D., Hughes, S., Barletta, B., Blake, D. R., Jung, J., Kim, D., Lee, G., Lee, M., Ahn, J., Lee, S.-D., Cho, G., Sung, M.-Y., Lee, Y.-H., Kim, D. B., Kim, Y., Woo, J.-H., Jo, D., Park, R., Park, J.-H., Hong, Y.-D., and Hong, J.-H.: OH reactivity in urban and suburban regions in Seoul, South Korea - an East Asian megacity in a rapid transition, Faraday discussions, 189, 231–251, doi:10.1039/c5fd00230c, 2016.

Kirchner, F., Jeanneret, F., Clappier, A., Krüger, B., van den Bergh, H., and Calpini, B.: Total VOC reactivity in the planetary boundary layer: 2. A new indicator for determining the sensitivity of the ozone production to VOC and NO x, J. Geophys. Res., 106, 3095–3110, doi:10.1029/2000JD900603, 2001.

Koppmann, R.: Volatile Organic Compounds in the Atmosphere, Blackwell Publishing Ltd, Oxford, UK, 2007.

Kovacs, T. A., Brune, W. H., Harder, H., Martinez, M., Simpas, J. B., Frost, G. J., Williams, E., Jobson, T., Stroud, C., Young, V., Fried, A., and Wert, B.: Direct measurements of urban OH reactivity during Nashville SOS in summer 1999, J. Environ. Monitor., 5, 68–74, doi:10.1039/b204339d, 2003.

Kroll, J. H. and Seinfeld, J. H.: Chemistry of secondary organic aerosol: Formation and evolution of low-volatility organics in the atmosphere, ATMOSPHERIC ENVIRONMENT, 42, 3593–3624, doi:10.1016/j.atmosenv.2008.01.003, 2008.

Krotkov, N. A., McLinden, C. A., Li, C., Lamsal, L. N., Celarier, E. A., Marchenko, S. V., Swartz, W. H., Bucsela, E. J., Joiner, J., Duncan, B. N., Boersma, K. F., Veefkind, J. P., Levelt, P. F., Fioletov, V. E., Dickerson, R. R., He, H., Lu, Z., and Streets, D. G.: Aura OMI observations of regional SO_2 and NO_2 pollution changes from 2005 to 2015, Atmos. Chem. Phys., 16, 4605–4629, doi:10.5194/acp-16-4605-2016, 2016.

Lelieveld, J., Evans, J. S., Fnais, M., Giannadaki, D., and Pozzer, A.: The contribution of outdoor air pollution sources to premature mortality on a global scale, Nature, 525, 367–371, doi:10.1038/nature15371, 2015.

Lelieveld, J., Hadjinicolaou, P., Kostopoulou, E., Chenoweth, J., El Maayar, M., Giannakopoulos, C., Hannides, C., Lange, M. A., Tanarhte, M., Tyrlis, E., and Xoplaki, E.: Climate change and impacts in the Eastern Mediterranean and the Middle East, Climatic change, 114, 667–687, doi:10.1007/s10584-012-0418-4, 2012.

Lelieveld, J., Hoor, P., Jöckel, P., Pozzer, A., Hadjinicolaou, P., Cammas, J.-P., and Beirle, S.: Severe ozone air pollution in the Persian Gulf region, Atmos. Chem. Phys., 9, 1393–1406, doi:10.5194/acp-9-1393-2009, 2009.

Lelieveld, J., Proestos, Y., Hadjinicolaou, P., Tanarhte, M., Tyrlis, E., and Zittis, G.: Strongly increasing heat extremes in the Middle East and North Africa (MENA) in the 21st century, Climatic change, 137, 245–260, doi:10.1007/s10584-016-1665-6, 2016.

Lindinger, W. and Jordan, A.: Proton-transfer-reaction mass spectrometry (PTR–MS): On-line monitoring of volatile organic compounds at pptv levels, Chem. Soc. Rev., 27, 347, doi:10.1039/a827347z, 1998.

Mao, J., Ren, X., Chen, S., Brune, W. H., Chen, Z., Martinez, M., Harder, H., Lefer, B., Rappenglück, B., Flynn, J., and Leuchner, M.: Atmospheric oxidation capacity in the summer of Houston 2006: Comparison with summer measurements in other metropolitan studies, ATMOSPHERIC ENVIRONMENT, 44, 4107–4115, doi:10.1016/j.atmosenv.2009.01.013, 2010.

Matysik, S., Ramadan, A. B., and Schlink, U.: Spatial and temporal variation of outdoor and indoor exposure of volatile organic compounds in Greater Cairo, Atmospheric Pollution Research, 1, 94–101, doi:10.5094/APR.2010.012, 2010.

Mertens, M., Grewe, V., Rieger, V. S., and Jöckel, P.: Revisiting the contribution of land transport and shipping emissions to tropospheric ozone, Atmos. Chem. Phys., 18, 5567–5588, doi:10.5194/acp-18-5567-2018, 2018.

Michoud, V., Hansen, R. F., Locoge, N., Stevens, P. S., and Dusanter, S.: Detailed characterizations of the new Mines Douai comparative reactivity method instrument via laboratory experiments and modeling, Atmos. Meas. Tech., 8, 3537–3553, doi:10.5194/amt-8-3537-2015, 2015.

Milazzo, M. F., Ancione, G., and Lisi, R.: Emissions of volatile organic compounds during the ship-loading of petroleum products: Dispersion modelling and environmental concerns, Journal of environmental management, 204, 637–650, doi:10.1016/j.jenvman.2017.09.045, 2017.

Moradzadeh, M., Ashrafi, k., and Shafiepour-Motlagh, M.: The Evaluation of Tropospheric Ozone Formation in the Downwind of the South Pars Industrial Zone, Pollution, 5, 361–375, doi:10.22059/poll.2018.269218.539, 2019.

Nakashima, Y., Kato, S., Greenberg, J., Harley, P., Karl, T., Turnipseed, A., Apel, E., Guenther, A., Smith, J., and Kajii, Y.: Total OH reactivity measurements in ambient air in a southern Rocky mountain ponderosa pine forest during BEACHON-SRM08 summer campaign, ATMOSPHERIC ENVIRONMENT, 85, 1–8, doi:10.1016/j.atmosenv.2013.11.042, 2014.

Overland, I.: Future Petroleum Geopolitics: Consequences of Climate Policy and Unconventional Oil and Gas, in: Handbook of Clean Energy Systems, Yan, J. (Ed.), Wiley, Weinheim, 1–29, 2015.

Parrish, D. D., Trainer, M., Holloway, J. S., Yee, J. E., Warshawsky, M. S., Fehsenfeld, F. C., Forbes, G. L., and Moody, J. L.: Relationships between ozone and carbon monoxide at surface sites in the North Atlantic region, J. Geophys. Res., 103, 13357–13376, doi:10.1029/98JD00376, 1998.

Pfannerstill, E. Y., Nölscher, A. C., Yáñez-Serrano, A. M., Bourtsoukidis, E., Keßel, S., Janssen, R. H. H., Tsokankunku, A., Wolff, S., Sörgel, M., Sá, M. O., Araújo, A., Walter, D., Lavrič, J., Dias-Júnior, C. Q., Kesselmeier, J., and Williams, J.: Total OH Reactivity Changes Over the Amazon Rainforest During an El Niño Event, Front. For. Glob. Change, 1, 600, doi:10.3389/ffgc.2018.00012, 2018.

Praplan, A. P., Pfannerstill, E. Y., Williams, J., and Hellén, H.: OH reactivity of the urban air in Helsinki, Finland, during winter, ATMOSPHERIC ENVIRONMENT, 169, 150–161, doi:10.1016/j.atmosenv.2017.09.013, 2017.

Pusede, S. E. and Cohen, R. C.: On the observed response of ozone to NO_x and VOC reactivity reductions in San Joaquin Valley California 1995–present, Atmos. Chem. Phys., 12, 8323–8339, doi:10.5194/acp-12-8323-2012, 2012.

Pusede, S. E., Gentner, D. R., Wooldridge, P. J., Browne, E. C., Rollins, A. W., Min, K.-E., Russell, A. R., Thomas, J., Zhang, L., Brune, W. H., Henry, S. B., DiGangi, J. P., Keutsch, F. N., Harrold, S. A., Thornton, J. A., Beaver, M. R., St. Clair, J. M., Wennberg, P. O., Sanders, J., Ren, X., VandenBoer, T. C., Markovic, M. Z., Guha, A., Weber, R., Goldstein, A. H., and Cohen, R. C.: On the temperature dependence of organic

reactivity, nitrogen oxides, ozone production, and the impact of emission controls in San Joaquin Valley, California, Atmos. Chem. Phys., 14, 3373–3395, doi:10.5194/acp-14-3373-2014, 2014.

Ren, X., Brune, W. H., Cantrell, C. A., Edwards, G. D., Shirley, T., Metcalf, A. R., and Lesher, R. L.: Hydroxyl and Peroxy Radical Chemistry in a Rural Area of Central Pennsylvania: Observations and Model Comparisons, J Atmos Chem, 52, 231–257, doi:10.1007/s10874-005-3651-7, 2005.

Ren, X., Brune, W. H., Oliger, A., Metcalf, A. R., Simpas, J. B., Shirley, T., Schwab, J. J., Bai, C., Roychowdhury, U., Li, Y., Cai, C., Demerjian, K. L., He, Y., Zhou, X., Gao, H., and Hou, J.: OH, HO 2 and OH reactivity during the PMTACS-NY Whiteface Mountain 2002 campaign: Observations and model comparison, J. Geophys. Res., 111, n/a-n/a, doi:10.1029/2005JD006126, 2006.

Ren, X., van Duin, D., Cazorla, M., Chen, S., Mao, J., Zhang, L., Brune, W. H., Flynn, J. H., Grossberg, N., Lefer, B. L., Rappenglück, B., Wong, K. W., Tsai, C., Stutz, J., Dibb, J. E., Thomas Jobson, B., Luke, W. T., and Kelley, P.: Atmospheric oxidation chemistry and ozone production: Results from SHARP 2009 in Houston, Texas, J. Geophys. Res. Atmos., 118, 5770–5780, doi:10.1002/jgrd.50342, 2013.

Salameh, T., Afif, C., Sauvage, S., Borbon, A., and Locoge, N.: Speciation of non-methane hydrocarbons (NMHCs) from anthropogenic sources in Beirut, Lebanon, Environmental science and pollution research international, 21, 10867–10877, doi:10.1007/s11356-014-2978-5, 2014.

Salameh, T., Sauvage, S., Afif, C., Borbon, A., and Locoge, N.: Source apportionment vs. emission inventories of non-methane hydrocarbons (NMHC) in an urban area of the Middle East: Local and global perspectives, Atmos. Chem. Phys., 16, 3595–3607, doi:10.5194/acp-16-3595-2016, 2016.

Schade, G. W. and Roest, G.: Analysis of non-methane hydrocarbon data from a monitoring station affected by oil and gas development in the Eagle Ford shale, Texas, Elem Sci Anth, 4, 96, doi:10.12952/journal.elementa.000096, 2016.

Schauer, J. J., Kleeman, M. J., Cass, G. R., and Simoneit, B. R. T.: Measurement of Emissions from Air Pollution Sources. 5. C 1 −C 32 Organic Compounds from Gasoline-Powered Motor Vehicles, Environ. Sci. Technol., 36, 1169–1180, doi:10.1021/es0108077, 2002.

Sillman, S.: The relation between ozone, NOx and hydrocarbons in urban and polluted rural environments, ATMOSPHERIC ENVIRONMENT, 33, 1821–1845, doi:10.1016/S1352-2310(98)00345-8, 1999.

Simpson, I. J., Aburizaiza, O. S., Siddique, A., Barletta, B., Blake, N. J., Gartner, A., Khwaja, H., Meinardi, S., Zeb, J., and Blake, D. R.: Air quality in Mecca and surrounding holy places in Saudi Arabia during Hajj: Initial survey, Environmental science & technology, 48, 8529–8537, doi:10.1021/es5017476, 2014.

Sinha, V., Williams, J., Crowley, J. N., and Lelieveld, J.: The Comparative Reactivity Method – a new tool to measure total OH Reactivity in ambient air, Atmos. Chem. Phys., 8, 2213–2227, doi:10.5194/acp-8-2213-2008, 2008.

Sinha, V., Williams, J., Diesch, J. M., Drewnick, F., Martinez, M., Harder, H., Regelin, E., Kubistin, D., Bozem, H., Hosaynali-Beygi, Z., Fischer, H., Andrés-Hernández, M. D., Kartal, D., Adame, J. A., and Lelieveld, J.: Constraints on instantaneous ozone production rates and regimes during DOMINO derived using in-situ OH reactivity measurements, Atmos. Chem. Phys., 12, 7269–7283, doi:10.5194/acp-12-7269-2012, 2012.

Sinha, V., Williams, J., Lelieveld, J., Ruuskanen, T. M., Kajos, M. K., Patokoski, J., Hellen, H., Hakola, H., Mogensen, D., Boy, M., Rinne, J., and Kulmala, M.: OH reactivity measurements within a boreal forest: evidence for unknown reactive emissions, Environmental science & technology, 44, 6614–6620, doi:10.1021/es101780b, 2010.

Smoydzin, L., Fnais, M., and Lelieveld, J.: Ozone pollution over the Arabian Gulf - role of meteorological conditions, Atmos. Chem. Phys. Discuss., 12, 6331–6361, doi:10.5194/acpd-12-6331-2012, 2012.

Sudo, K. and Akimoto, H.: Global source attribution of tropospheric ozone: Long-range transport from various source regions, J. Geophys. Res., 112, 1609, doi:10.1029/2006JD007992, 2007.

Suez Canal Authority: Canal Characteristics: https://www.suezcanal.gov.eg/English/About/SuezCanal/Pages/CanalCharacteristics.aspx, last access: 1 February 2019.

Suez Canal Authority: Navigation Statistics: https://www.suezcanal.gov.eg/English/Navigation/Pages/NavigationStatistics.aspx, last access: 1 February 2019.

Swarthout, R. F., Russo, R. S., Zhou, Y., Hart, A. H., and Sive, B. C.: Volatile organic compound distributions during the NACHTT campaign at the Boulder Atmospheric Observatory: Influence of urban and natural gas sources, J. Geophys. Res. Atmos., 118, 10,614-10,637, doi:10.1002/jgrd.50722, 2013.

Tanarhte, M., Hadjinicolaou, P., and Lelieveld, J.: Intercomparison of temperature and precipitation data sets based on observations in the Mediterranean and the Middle East, J. Geophys. Res., 117, n/a-n/a, doi:10.1029/2011JD017293, 2012.

Terink, W., Immerzeel, W. W., and Droogers, P.: Climate change projections of precipitation and reference evapotranspiration for the Middle East and Northern Africa until 2050, Int. J. Climatol., 33, 3055–3072, doi:10.1002/joc.3650, 2013.

Warneke, C. and Gouw, J. A. de: Organic trace gas composition of the marine boundary layer over the northwest Indian Ocean in April 2000, ATMOSPHERIC ENVIRONMENT, 35, 5923–5933, doi:10.1016/S1352-2310(01)00384-3, 2001.

Wasimi, S. A.: Climate change in the Middle East and North Africa (MENA) region and implications for water resources project planning and management, Int J of Cl Chan Strat and Man, 2, 297–320, doi:10.1108/17568691011063060, 2010.

Wei, W., Cheng, S., Li, G., Wang, G., and Wang, H.: Characteristics of ozone and ozone precursors (VOCs and NOx) around a petroleum refinery in Beijing, China, Journal of Environmental Sciences, 26, 332–342, doi:10.1016/S1001-0742(13)60412-X, 2014.

Williams, J. and Brune, W.: A roadmap for OH reactivity research, ATMOSPHERIC ENVIRONMENT, 106, 371–372, doi:10.1016/j.atmosenv.2015.02.017, 2015.

Williams, J., Keßel, S. U., Nölscher, A. C., Yang, Y., Lee, Y., Yáñez-Serrano, A. M., Wolff, S., Kesselmeier, J., Klüpfel, T., Lelieveld, J., and Shao, M.: Opposite OH reactivity and ozone cycles in the Amazon rainforest and megacity Beijing: Subversion of biospheric oxidant control by anthropogenic emissions, ATMOSPHERIC ENVIRONMENT, 125, 112–118, doi:10.1016/j.atmosenv.2015.11.007, 2016.

Wu, Y., Yang, Y.-D., Shao, M., and Lu, S.-H.: Missing in total OH reactivity of VOCs from gasoline evaporation, Chinese Chemical Letters, 26, 1246–1248, doi:10.1016/j.cclet.2015.05.047, 2015.

Xiao, Q., Li, M., Liu, H., Fu, M., Deng, F., Lv, Z., Man, H., Jin, X., Liu, S., and He, K.: Characteristics of marine shipping emissions at berth: profiles for particulate matter and volatile organic compounds, Atmos. Chem. Phys., 18, 9527–9545, doi:10.5194/acp-18-9527-2018, 2018.

Yang, Y., Shao, M., Keßel, S., Li, Y., Lu, K., Lu, S., Williams, J., Zhang, Y., Zeng, L., Nölscher, A. C., Wu, Y., Wang, X., and Zheng, J.: How the OH reactivity affects the ozone production efficiency: case studies in Beijing and Heshan, China, Atmos. Chem. Phys., 17, 7127–7142, doi:10.5194/acp-17-7127-2017, 2017.

Yang, Y., Shao, M., Wang, X., Nölscher, A. C., Kessel, S., Guenther, A., and Williams, J.: Towards a quantitative understanding of total OH reactivity: A review, ATMOSPHERIC ENVIRONMENT, 134, 147–161, doi:10.1016/j.atmosenv.2016.03.010, 2016.

Yoshino, A., Sadanaga, Y., Watanabe, K., Kato, S., Miyakawa, Y., Matsumoto, J., and Kajii, Y.: Measurement of total OH reactivity by laser-induced pump and probe technique—comprehensive observations in the urban atmosphere of Tokyo, ATMOSPHERIC ENVIRONMENT, 40, 7869–7881, doi:10.1016/j.atmosenv.2006.07.023, 2006.

Zhang, X., Aguilar, E., Sensoy, S., Melkonyan, H., Tagiyeva, U., Ahmed, N., Kutaladze, N., Rahimzadeh, F., Taghipour, A., Hantosh, T. H., Albert, P., Semawi, M., Karam Ali, M., Said Al-Shabibi, M. H., Al-

Oulan, Z., Zatari, T., Al Dean Khelet, I., Hamoud, S., Sagir, R., Demircan, M., Eken, M., Adiguzel, M., Alexander, L., Peterson, T. C., and Wallis, T.: Trends in Middle East climate extreme indices from 1950 to 2003, J. Geophys. Res., 110, 1959, doi:10.1029/2005JD006181, 2005.

Zhang, Y., Cooper, O. R., Gaudel, A., Thompson, A. M., Nédélec, P., Ogino, S.-Y., and West, J. J.: Tropospheric ozone change from 1980 to 2010 dominated by equatorward redistribution of emissions, Nature Geosci, 9, 875–879, doi:10.1038/ngeo2827, 2016.

Zhao, Y., Saunois, M., Bousquet, P., Lin, X., Hegglin, M. I., Canadell, J. G., Jackson, R. B., Hauglustaine, D. A., Szopa, S., Stavert, A. R., Abraham, N. L., Archibald, A. T., Bekki, S., Deushi, M., Jöckel, P., Josse, B., Kinnison, D., Kirner, O., Marécal, V., O&apos, Connor, F. M., Plummer, D. A., Revell, L. E., Rozanov, E., Stenke, A., Strode, S., Tilmes, S., Dlugokencky, E. J., and Zheng, B.: Inter-model comparison of global hydroxyl radical (OH) distributions and their impact on atmospheric methane over the 2000-2016 period, Atmos. Chem. Phys. Discuss., 1–47, doi:10.5194/acp-2019-281, 2019.

Chapter 4. Emission rates of volatile organic compounds (VOCs) from humans: breath, skin and whole body characterizations

Abstract

Human occupancy is a major source of volatile organic compounds (VOCs) in the indoor environment. VOCs are emitted into the air via breath and dermal emission, which can further react with oxidants in the air to produce secondary VOCs, some of which have adverse effects on human health. In this study, we continuously measured VOCs in a well-conditioned steel walled chamber (22.5 m^3, air exchange rate at 3.2 h^{-1}) occupied by four human subjects, using a proton transfer reaction time of flight mass spectrometry. Experiments of human whole body, breath and dermal emissions were performed separately under ozone-free and ozone-present conditions. For breath emissions, the dominant VOCs were endogenous compounds namely: acetone, isoprene and methanol, accounting for 91% of the total VOCs emission rate (ER) at 1290 μg h^{-1} p^{-1}. Ozone exposure had a negligible effect on most of the VOCs but slightly increased the ER of oxygenated VOCs. For dermal emissions, acetic acid, acetone and $C_2H_2OH^+$ (fragment of acids) were the most abundant species under no ozone condition. However, with ozone present the total ER increased to 4453 μg h^{-1} p^{-1} with acetone, 6-methyl-5-hepten-2-one (6MHO),and 4-oxopentanal (4OPA) being the most dominant VOCs, accounting for 35%, which are known as first and secondary ozone oxidation products of squalene (major skin oil component). The average whole-body total ER was 2165 ± 978 μg h^{-1} p^{-1} under ozone-free condition and doubled when ozone was added in the chamber. The same dominant species were also identified for whole-body emissions with and without ozone exposure. The study indicates breath emitted VOCs dominate the indoor total VOCs emission under the ozone free condition, while skin related VOCs increase dramatically with ozone exposure. The ERs of VOCs derived from the study can help models better predict indoor air quality.

4.1 Introduction

Human beings are a potent mobile source of volatile organic compounds (VOCs) in the indoor environment. Several hundred VOCs are known to enter the air via breath and dermal emission (de Lacy Costello et al. 2014). Although building materials, decorations, furniture and consumer products were previously frequently reported as important indoor VOCs sources, (Afshari, 2003; Cheng et al., 2015; Hodgson et al., 2002; Hodgson et al., 1993; Nazaroff and Weschler, 2004; Simon et al., 2020), the role of humans beings as an important indoor VOCs source will become more and more prominent due to regulatory driven emission decreases from indoor furnishings and building materials.. With oxidants present in indoor air (e.g. ozone or OH radicals), VOCs can be produced on the surface of human beings (clothing, hair and skin) as well as in the gas phase via secondary formation (Abbatt and Wang, 2020; Weschler, 2006; Weschler, 2016). Some of these species have adverse effects on human health. For example, exposure to 4OPA, one of the major squalene ozonolysis products, can cause irritancy and allergic responses (Anderson et al., 2012). Therefore, it is important to understand the species and the abundance of VOCs released from human natural emissions and the effect of indoor oxidants.

Human VOCs emission rates (ERs) have been reported in several public indoor environments: a university classroom (Tang et al., 2016), a cinema (Stonner et al., 2017) and a gallery room in a museum (Pagonis et al., 2019). Several VOC species (e.g. methanol, ethanol, monoterpenes and siloxanes) showed large variations due to previous alcohol or food consumption and the use of personal care products. A few studies have also reported separate breath and dermal emissions of VOCs performed in a sealed chamber with single subject (Mochalski et al., 2014; Mochalski et al., 2018; Zou et al., 2020). However, a comprehensive chemical characterization of "natural" human ERs including whole-body, breath-only and skin-only ERs under controlled environments as well as the effect from ozone is lacking.

This study is a part of the Indoor Chemical Human Emissions and Reactivity (ICHEAR) project, which used online VOCs measuring techniques (mainly proton transfer reaction time of flight mass spectrometry) to monitor the variation of VOCs emitted from human beings in a climate chamber under controlled conditions. The total ERs together with their species contributions of whole body, separate breath and skin were derived under ozone-free and ozone-present conditions, respectively, and were compared to the ERs reported in the literature.

4.2 Materials/Methods

4.2.1 Chamber experiments

Experiments were performed in two identical stainless-steel chambers under controlled conditions (temperature, relative humidity (RH) and air change rate (ACR)). A detailed description of the

experimental set-up and procedures were given in (Bekö et al., 2020). In order to derive the human emission rates of whole body, breath and skin under normal conditions (temperature ~25°C, RH ~30%) as well as under the ozone-present condition, seven experiments listed in Table 4.1 were selected for this study, involving three groups of young adults in the age of 19 to 30. In each experiment, four volunteers wearing identical new laundered long clothing (pants + long sleeve shirts) except for Exp.12 and 13 in which volunteers wore short clothing (shorts + T-shirts) entered the chamber in the morning and sat inside the chamber for about 3 hours followed by a short lunch break outside the chamber. Afterwards volunteers re-entered the chamber for 10 minutes, and ozone (~ 100 ppb) was added into the supply air to achieve the ozone-present condition in the chamber. Volunteers stayed for around 2 - 2.5 hours for the afternoon ozone-present condition. Breath and dermal emission separation was achieved by the use of facial masks connected by tubing to the other identical chamber.

Table 4.1 Experimental information (numbers in parentheses refer to replicate measurements)

Experiment No*. (replicate)	Experiment type	Temperature (°C) (replicate)	Relative humidity (%) (replicate)
1	Whole-body: group A1	26.2 - 30.3	31 - 35
6 (21)	Whole-body: group A2	23.7 - 27.5 (23.3 - 27.7)	16 – 23 (17 - 25)
10	Whole-body: group A3	25.3 - 28.8	28 - 31
12	Breath: group A3	32.2 - 32.6	56 - 62
13	Skin: group A3	26.3 - 29.9	24 - 28

* Experiment numbers are identical to those in Bekö et al.[37].

4.2.2 VOCs measurements

A proton transfer reaction time of flight mass spectrometer (PTR-ToF-MS, 8000, Ionicon Analytik) was used to continuously measure VOCs in the chamber's exhaust air. The PTR-ToF-MS sampled the sub-flow of ~ 100mL min^{-1} via the FEP (fluorinated ethylene propylene) tubing (i.d. = 3.18 mm) from the main chamber exhaust line (flow rate 7 L min^{-1}, length 5 m, i.d. = 12.7 mm). With protonated water (H_3O^+) as the primary ions, VOCs having proton affinity higher than water (697 kJ/mol) undergo proton-transfer reactions and are detected on the its protonated mass to charge ratio (*m/z*) without significant fragments (Lindinger et al., 1998). The mass resolution was around 4000 at mass 96 amu. The measurement time resolution was 20 s and mass range was up to 500 amu. Measured ions were attributed to chemical formulas based on the exact *m/z*, followed by the assignment of specific chemical species. As the mass becomes larger, the chances of existence of isomeric compounds also increase. Therefore, chemical formulas having multiple isomeric compounds were only further attributed to specific compounds that has been previously reported as being related to human body emissions as well as human-involved ozone initiated chemistry in

the literature. A full calibration including the humidity dependence was performed throughout the campaign by using a standard gas mixture containing methanol, acetonitrile acetaldehyde, acetone, dimethyl sulfide (DMS), isoprene, methyl vinyl ketone (MVK), methacrolein, methyl ethyl ketone (MEK), benzene, toluene, xylene, 1,3,5-Trimethylbenzene and α-pinene (Apel-Riemer Environmental Inc.). The limit of detection of calibrated species ranged from 8 ppt for 1,3,5-trimethylbenzene to 171 ppt for methanol with the uncertainty ≤ 11% (Table 4.2). For VOC species without gas standard calibrations, the mixing ratios were calculated based on a theoretical method by using a constant proton transfer reaction rate coefficient at 2×10^{-9} cm^3 $molecule^{-1}$ s^{-1} with the uncertainty of ~ 50% (Sekimoto et al., 2017; Zhao and Zhang, 2004).

To compensate for the inability of PTR-ToF-MS to quantify isoprene and propanal in this study (due to interferences at the corresponding masses), the mixing ratios of those two species were taken from a custom-made fast gas chromatograph-mass spectrometer (fast-GC) with LOD < 25 ppt and total uncertainty < 10%, which sampled the sub-stream from the same main inlet as PTR-ToF-MS. The time resolution of the fast-GC was 3 minutes running under the selected ion monitoring mode. Details of the instrument operation were mentioned elsewhere (Bourtsoukidis et al., 2017). It is mainly because $C_5H_8H^+$ (*m/z* 69.070) could also be affected by contributions from fragments of long chain aldehydes (Ruzsanyi et al., 2013) and propanal can not be separated from acetone by PTR-MS with H_3O^+ as the primary ions.

Table 4.2 Limits of detection and total uncertainty of calibrated species for PTR-ToF-MS

Mass (H+)	Compounds	LOD (3std) ppt	Total uncertainty %
m33.034	Methanol	171	11
m42.033	Acetonitrile	26	7
m45.033	Acetaldehyde	130	6
m59.048	Acetone	84	6
m63.026	Dimethyl Sulfide (DMS)	14	6
m71.048	Methyl vinyl ketone/Methacrolein	35	5
m73.064	Methyl ethyl ketone	30	6
m79.053	Benzene	11	6
m93.070	Toluene	11	6
m107.086	Xylene	10	6
m121.101	1,3,5-Trimethylbenzene	8	7
m137.132	Monoterpenes	11	6

4.2.3 Other trace gas measurements

CO_2 was continuously monitored by a cavity ring-down spectrometer (Picarro G2401; Picarro Inc.) sampling the sub-flow from the same main inlet as PTR-ToF-MS and fast-GC. Ozone added into the supply air was generated via a Jelight 600UV ozone generator (Jelight Company Inc.). The

ozone level inside the chamber or supply air was monitored by an ozone monitor (Model 205, 2B Technologies). Detailed information of those instruments can be found in (Bekö et al., 2020).

4.2.4 Emission rates calculation

The emission rate (μg h^{-1} p^{-1}) of a VOC species *i* was calculated according to Eq. 4.1 by using the concentrations measured during the steady-state period (15 minutes before volunteers exiting the chamber) in which occupants are the only source constantly emitting VOCs that is in equilibrium with the loss of VOCs through air exchange.

$$ER = V_{chamber} \times ACR \times (C_{i(steady-state)} - C_{i\ (background)})/4 \quad \text{Eq. 4.1}$$

$V_{chamber}$ is the chamber volume (22.5 m^3). *ACR* is the air change rate (3.2 h^{-1}), which was determined from CO_2 and Freon®134a tracer gas decay as described in (Bekö et al., 2020). $C_{i(steady\text{-}state)}$ represents the mean concentration of species *i* (μg m^{-3}) over the steady-state period. $C_{i(background)}$ is the mean background concentration of species *i* in the empty chamber before volunteer entered the chamber for each experiment. 4 is the number of volunteers in the chamber. In total, 185 species and ions were identified related to human occupants with the criteria that $C_{i(steady\text{-}state)}$ - $C_{i(background)}$ is larger than the standard deviation of concentrations measured over the steady-state period.

4.3 Results and discussion

4.3.1 Time series of major human related VOCs

Figure 4.1 shows the time series of several important marker compounds from breath and skin lipids ozonolysis for a complete experiment of whole-body emissions (Exp. 10). Human endogenous breath compounds including acetone, isoprene and methanol (Fenske and Paulson, 1999) immediately increased along with CO_2 when volunteers entered the chamber in the morning. This phenomenon also appeared when the volunteers re-entered the chamber in the early afternoon before ozone addition. After ozone (~ 100 ppb) was introduced into the chamber, squalene ozonolysis products 6-methyl-5-hepten-2-one (6MHO), acetone and 4-oxopentanal (4OPA) (Petrick and Dubowski, 2009; Wisthaler and Weschler, 2010) had significant elevations. The increase of acetone was even comparable to the increase due to exhaled acetone without ozone present. 6MHO and 4OPA were slightly elevated after subjects entered the chamber in the morning when there was no ozone, which was probably due to prior exposure to outside ozone before the experiment. However, this tiny increase is insignificant compared to the later increase. The steady-state ozone level was around 37 ppb in the afternoon, indicating a huge ozone loss (~ 63 ppb) due to human occupants. Isoprene showed slightly lower mixing ratios in the afternoon compared to those of the morning, which is likely caused by ozone oxidation while methanol had comparable levels. After the subjects left the chamber, all major trace gases except for 4OPA plummeted. 4OPA

had a tiny decrease when the chamber door opened (subjects exited the chamber) and slightly elevated when the chamber door closed, which is consistent with 4OPA being a secondary formed compound produced through squalene ozonolysis. In Figure 4.1, the simultaneous increase of CO_2 as well as most of the species in the middle of each half-day experiment was due to preplanned movements by the volunteers (standing up and some stretching movements), which changed the air mixing state inside the chamber.

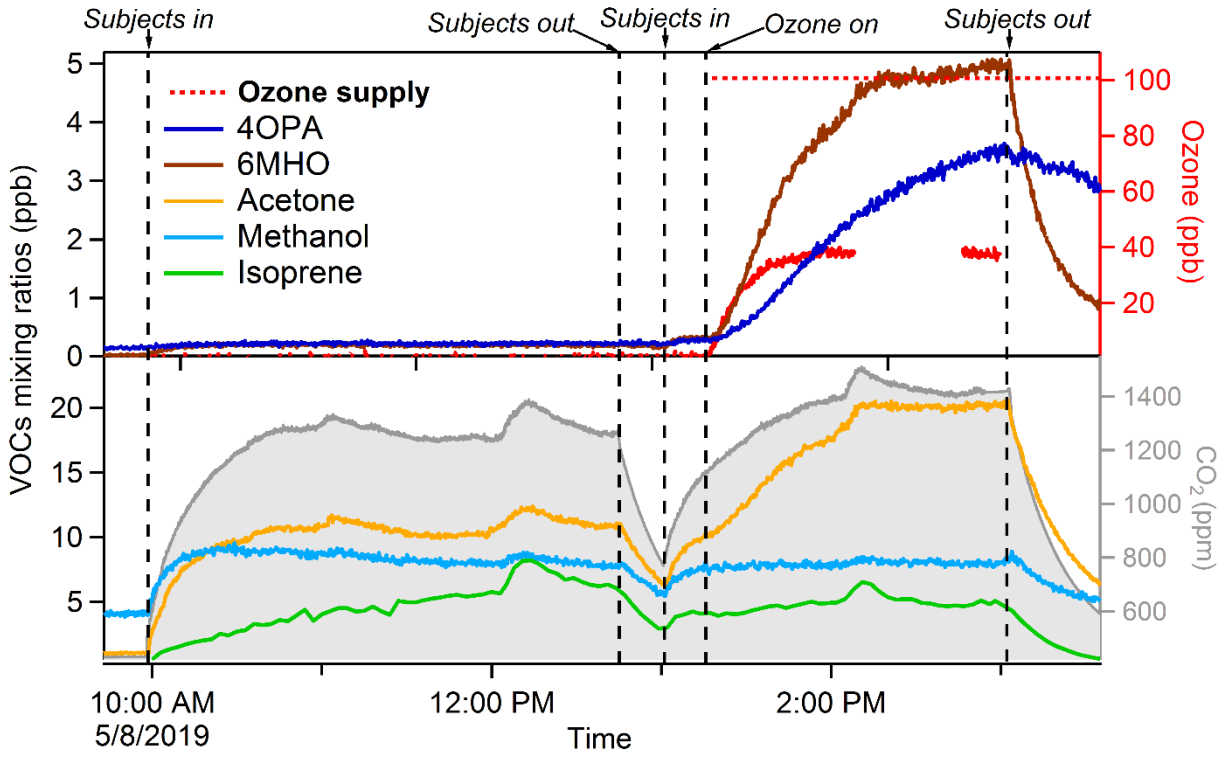

Figure 4.1 Time series of major VOCs related to human emissions (data from Exp. 10 was used).

4.3.2 Emission rates (ERs) under ozone-free condition

Benchmark experiments (Exp. 1, 6, 10 and 21) among three groups of volunteers were included to derive the whole-body VOCs emission rates as the variance of steady-state mixing ratios among groups were small for most of species. The total whole-body ER under the condition without ozone was 2165 ± 978 μg h^{-1} p^{-1}. The standard deviation was mainly driven by the top three contributors that accounted for 67% of the total whole-body ER: acetone (max: 1824 μg h^{-1} p^{-1} for Exp. 6; min: 424 μg h^{-1} p^{-1} for Exp. 10), isoprene (max: 324 μg h^{-1} p^{-1} for Exp. 10; min: 204 μg h^{-1} p^{-1} for Exp. 21) and methanol (max: 181 μg h^{-1} p^{-1} for Exp. 6; min: 89 μg h^{-1} p^{-1} for Exp. 10). Acetone, isoprene and methanol are major breath borne endogenous compounds that can vary from person to person and even with time for the same person due to the human metabolism (de Lacy Costello et al., 2014; Schubert et al., 2012; Turner et al., 2006b). As the experiments were performed among different

volunteer groups on different days, it is therefore not surprising to see some variations. Those three compounds were also ranked as the top three species (by mixing ratio) contributing to the total ER of breath (Figure 4.2 b), accounting for 91% of the total (1290 μg h^{-1} p^{-1}). Only acetone was also ranked within three most contributing species to the total skin ER with much lower ER at 182 μg h^{-1} p^{-1}. This indicates that more than 60% of the total whole-body ER were contributed by exhaled breath when the indoor ozone was not present. Besides those three compounds, the other species ranking within the top ten contributing species for whole-body emissions were mostly identified as the top ten species for skin (dermal) emissions (see Figure 4.2) as well, indicating those species were more likely related to skin emissions. $C_6H_{10}H^+$ (general fragment of large aldehydes) (Ruzsanyi et al., 2013) and 6MHO were not present in the top ten contributing species for the total skin ER, they were actually ranked as 12th and 14th place. Three top ten species tolualdehyde, $C_4H_8O_2H^+$ and phenol (Figure 4.2 c) might be only specific to that group of volunteers (A3) as the ERs of those three species were found much higher for whole-body Exp. 10 (A3) than the ERs for other two groups (Exp. 1, 6 and 21). Besides top ten contributing species, the rest of the measured species were categorized to C_xH_y (hydrocarbons), $C_xH_yO_{1-3}$ (species containing one, two or three oxygen atoms), species containing nitrogen, species containing sulfur and others (rest of species). It can be inferred from Figure 4.2 that the whole-body ER of the sum of those rest categories (474 ± 122 μg h^{-1} p^{-1}, 22% of the total ER) should be mostly contributed by dermal emissions as the contribution from breath emissions was insignificant. Top ten species explained 97%, 63% and 78% of the total breath ER, skin ER and whole-body ER, respectively. Thus, our findings further prove that the chemical profile for dermal emissions is much more diverse and complicated than the breath emissions (de Lacy Costello et al., 2014).

It is known that breath and skin can also act as sinks of VOCs through inhalation and dermal uptake (He et al., 2019; Weschler and Nazaroff, 2014). The sum of total breath ER and the total skin ER was ~ 300 μg h^{-1} p^{-1} higher than mean whole-body total ER but within its standard deviation. As experiments of separate breath and skin emissions were only performed for one group of volunteers (A3), it is more reasonable to compare the sum of separate breath and skin ERs to the whole-body ER of Exp. 10 with the same group of volunteers. The total whole-body ER of group A3 is 1593 μg h^{-1} p^{-1}, about 900 μg h^{-1} p^{-1} lower than the summed ER of separate breath and skin emissions, which might be partially explained by breath and dermal uptake. However, the dermal emissions in the skin-separate experiment (Exp. 13) was probably higher than the dermal emissions contributed to the whole-body emissions for Exp. 10 due to more bare skin being exposed to the air ("short" clothing for volunteers in Exp. 13). Therefore, the uptake via breath and skin may exist but it is difficult to quantify the amount based on current results.

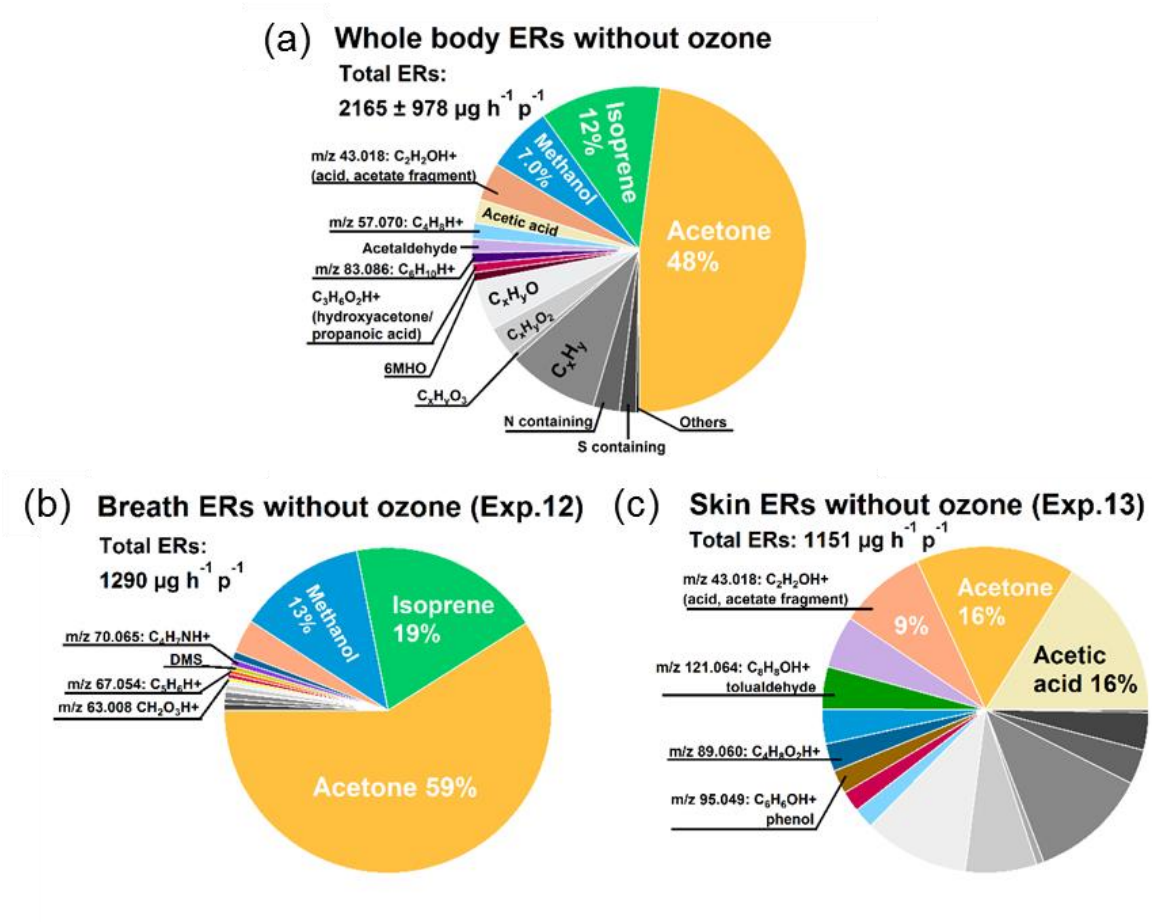

Figure 4.2 Total emission rates (ERs) fractional contributions from top ten species and other species for (a) whole-body emissions (mean values of Exp. 1, 6, 10 and 21); (b) breath emissions (Exp. 12) and (c) skin emissions (Exp. 13) under ozone-free condition. Top three contributing species were always labelled with the percentage. Species not presented in (a) were listed additionally in (b) and (c).

4.3.3 Emission rates (ERs) under ozone-present condition

As mentioned in section 4.3.1, when ozone was added into the chamber, products of squalene ozonlysis (e.g. 6MHO and 4OPA) had a substantial increase, indicating the significance of ozone oxidation of skin lipids, which was reflected by the total skin-only ER (4453 μg h^{-1} p^{-1}), three times as the skin-only ER when there was no ozone present. As shown in Figure 4.3 c, the three highest contributors to the total skin ER altered with acids being replaced by 6MHO and 4OPA. Other species $C_6H_{10}H^+$ (general fragment of long-chain aldehydes), decanal, hydroxyacetone/propanoic acid and 1,4-butanedial were ranked within the top ten species, which are all reported as products of skin lipids ozonolysis (Wisthaler and Weschler, 2010). For breath ERs, the effect from ozone was much less significant. Although endogenous breath compounds acetone, isoprene and methanol had slightly less ERs compared to the ERs under ozone-free condition, the ranking

remained the same (see Figure 4.3 b). The decreased ER of isoprene is likely due to reaction with ozone. Different metabolic states in the afternoon may also be a reason for those endogenous compound changes as steady-state CO_2 was always relatively higher in the afternoon session after a lunch break (Bekö et al., 2020). The breath-only ER increased about 280 μg h^{-1} p^{-1}, which was mainly contributed by oxygenated compounds. The increase may be related to the changed metabolic state after a light lunch. However, as the ozone was introduced into the chamber that only contained exhaled breath, those oxygenated compounds were more likely to be products of ozone reacting with the surface of the chamber and facilities inside the chamber (chairs and tables) which contained small amount of human skin lipids left from previous experiments. Therefore, only terminal compounds produced from squalene ozonolysis like 4OPA and 1,4-butanedial were ranked within the top ten contributing species (Figure 4.3 b) as they cannot undergo further ozonolysis.

The mean total ER of the whole-body under the ozone-present condition (4607 ± 1064 μg h^{-1} p^{-1}) doubled compared to the total ER under ozone-free condition. The whole-body total ER was ~ 1400 μg h^{-1} p^{-1} smaller than the sum of breath-only ER and skin-only ER, much more significant than the difference under ozone-free condition. Although breath and dermal uptake may explain part of the "loss" ER, more skin area exposed to ozone due to less clothing for Exp. 13 was more likely the reason for the large ER derived from the skin-only experiment. The top three contributing species to the total whole-body ER were acetone (31%, 1443 ± 620 μg h^{-1} p^{-1}), 6MHO (9%, 429 ± 50 μg h^{-1} p^{-1}) and 4OPA (6%, 292 ± 36 μg h^{-1} p^{-1}). Endogenous breath compounds isoprene and methanol ranked as the 4^{th} and 9^{th} positions. Other top ten species contributing to the whole-body ER were slightly different from the top ten species contributing to the skin ER (see Figure 4.3). As with decanal, nonanal was an ozone degradation product of unsaturated fatty acids (on of skin lipid components) (Wisthaler and Weschler, 2010). The difference may be caused by the only variable – clothing.

To better understand the species contribution to the huge increase induced by ozone, for each benchmark experiment, the delta ER of each species was calculated ($ER_{ozone\text{-}present} - ER_{ozone\text{-}free}$). If the absolute delta ER for one species is less than the standard deviations of the steady-state ERs for both under ozone-free and ozone-present conditions, the change of that species due to ozone is considered to be insignificant (i.e. delta ER is 0). Figure 4.4 shows the mean delta ERs of all species derived from benchmark experiments. More than 100 species and ions had a significant increase while limited species had decreases (mainly methanol and isoprene) under the ozone-present condition. Species with an increase of ER above 10 μg h^{-1} p^{-1} were mainly oxygenated VOCs containing one or two oxygen and hydrocarbon fragments. Among the top ten species which had the most significant elevation, 9 species were also ranked within the top ten species contributing to

the total whole-body ER and skin-only ER, and 8 species (including aldehyde fragment $C_6H_{10}H^+$) belong to carbonyl compounds that are reported as products of skin lipids ozonolysis. Therefore, indoor ozone not only enhances the total ER but also changes the chemical composition of human emissions. Meanwhile, the standard deviations (variability among each group) of the delta ERs of top ten elevated species were small (ranging from 4% to 15%), indicating skin-involved ozone chemistry has good consistency among different people.

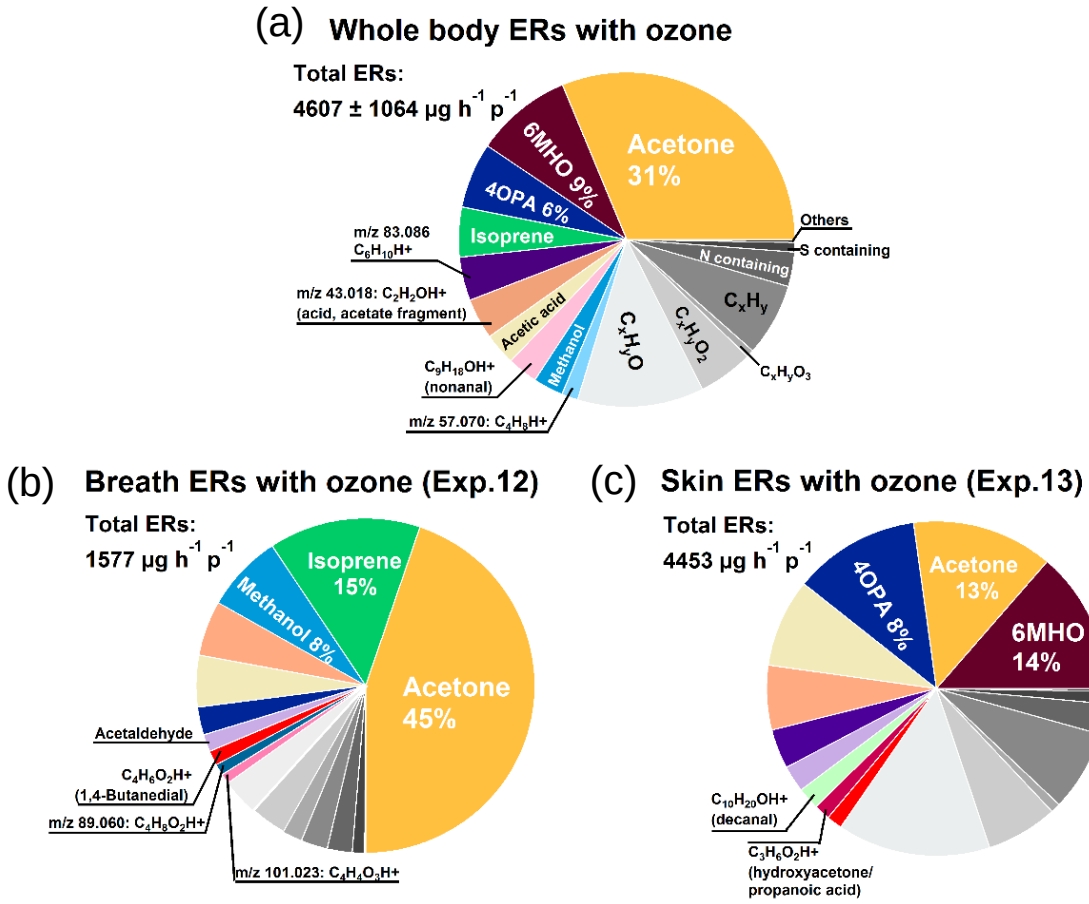

Figure 4.3 Total emission rates (ERs) fractional contributions from top ten species and other species for (a) whole-body emissions (mean values of Exp. 1, 6, 10 and 21); (b) breath emissions (Exp. 12) and (c) skin emissions (Exp. 13) under ozone-present condition. Top three contributing species were always labelled with the percentage. Species not presented in (a) were listed additionally in (b) and (c).

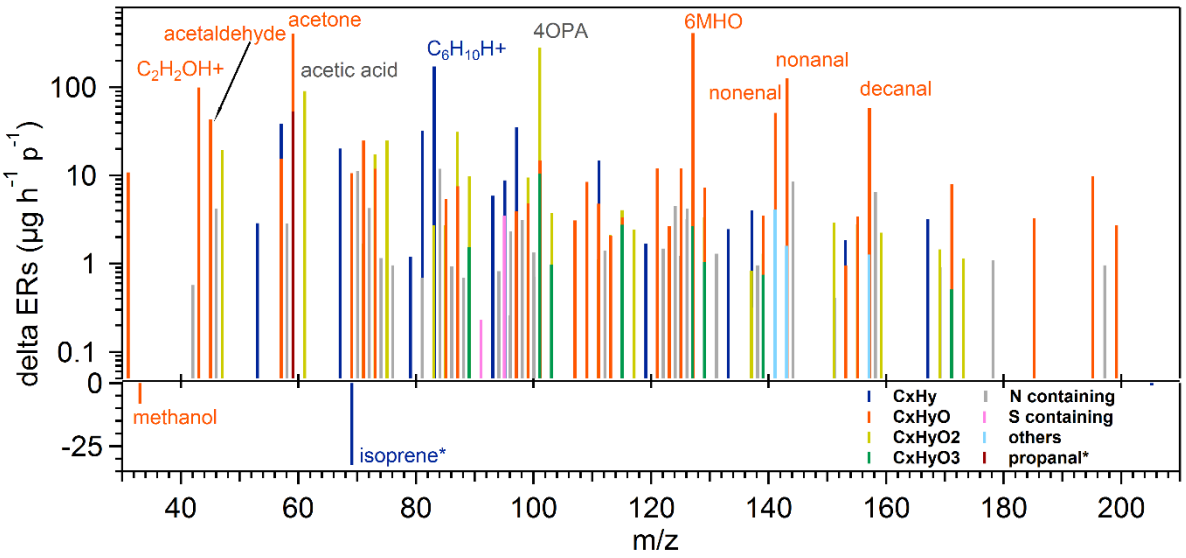

Figure 4.4 Mean emission rate changes (delta ERs) of all measured species due to ozone effect (averaged from Exp. 1, 6, 10 and 21). Ten species having most significant increase and two species having most significant decrease were labeled.

4.3.4 Human emission rates (ERs) reported in literatures

For this study (ICHEAR chamber study), the effects which may be caused by individual volunteer were kept as low as possible (using specific personal care products, monitored diet with certain restrictions, wearing prepared clothing, excluding smokers etc.) Therefore, the total whole-body ER obtained under ozone-free conditions should be close to the lower limit of natural human VOCs ER. Tang et al. (2016) reported the total occupant ER of VOCs measured by PTR-MS in a classroom to be 6250 μg h^{-1} p^{-1} with the top contribution from cyclic volatile methylsiloxanes (cVMS) (45%) that are commonly present in personal care products. The ER of cVMS (mainly decamethylcyclopentasiloxane (D5) and dodecamethylcyclohexasiloxane (D6)) for the ICHEAR chamber was much lower (below 5 μg h^{-1} p^{-1}) as the volunteers were not allowed to use other personal care products besides the specific soap, shampoo and toothpaste offered by the experiment organizers. By subtracting the ER of cVMS, the total ER in the classroom would be 3450 μg h^{-1} p^{-1}, which is higher than the whole-body ER under ozone-free condition (2165 ± 978 μg h^{-1} p^{-1}). Although the exact ozone level was not reported in Tang et al. (2016), ozone loss along with the mixing ratio increase of squalene ozonolysis products (6MHO and 4OPA) were observed when the classroom was occupied. Thus, the higher ER obtained in the classroom was probably caused by enhanced ERs of those products produced from skin lipids ozonolysis as well as other VOCs emitted from personal care products.

Several studies done in various human occupied indoor environments using PTR-MS have reported the emission rates of different VOCs (Pagonis et al., 2019; Stonner et al., 2017; Tang et al., 2016).

Species that were commonly measured were selected to compare with the ERs as shown in Figure 4.5. For 6MHO and 4OPA, as the ozone initially exposed to subjects in the chamber (~ 100 ppb) was at the upper limit of normal indoor ozone level, the ERs for those compounds derived under ozone-present condition should also be close to the upper limit. Therefore, the ERs of 6MHO and 4OPA in the classroom and the gallery room (ozone below 5 ppb) were in the range of the ERs from the ICHEAR ozone-free condition and ozone-present condition. While for the cinema audience, the ER of 6MHO was even lower than that in the chamber without ozone and 4OPA was not detected. Limited indoor ozone due to low outside ozone may be the reason, as was suggested in their study. However it can not explain the lower ERs compared to ICHEAR no-ozone condition. Previous skin exposure to the outside ozone might explain the difference as the cinema study was performed in winter (Germany) when people tend to have less skin exposed to outside air while the ICHEAR study was done in April to May (Denmark). For endogenous breath compounds acetone, isoprene and methanol where large variability can be expected due to different populations, the ERs under ozone-free conditions were in the same order of magnitude (around or within factor of 2) as those reported in other studies. One exception is for the much higher ER of methanol in the cinema where the methanol was considered more likely to be exogenous compound due to fruit or fruit juice intake. Although acetone can also be generated via squalene ozonolysis, as the ozone level in other studies were much lower compared to the ozone level in the ICHEAR chamber, the dominant source of acetone in other studies should be human breath. The ERs of ethanol were comparable before and after ozone addition in the chamber and were much lower than the ER reported in other studies. Ethanol is both an endogenous and exogenous compound emitted from human breath due to body metabolism and food/drink intake, respectively (Turner et al., 2006a). Volunteers participating in the ICHEAR chamber study were requested not to consume any alcohol over the experimental period. Studies done in the cinema and gallery room demonstrated that alcohol consumption before the movie and the opening event might be the reason for the high ethanol ER. This may also explain the higher ERs of acetaldehyde and acetic acid reported in other studies as they were produced in the process of body ethanol metabolism and detected in human breath (Smith et al., 2010). Due to restrictions in using personal care products for volunteers in the chamber study, the ER of monoterpenes was much lower than the ERs reported in the cinema and the classroom but comparable to the ER in a gallery room. Little use of personal care products or decay over the day (the event in the gallery room was held in late afternoon) might be the reason as suggested by the author.

Several studies have characterized the ERs of breath-borne and skin-born VOCs emissions in a sealed chamber occupied by one subject (Mochalski et al., 2014; Sun et al., 2017; Zou et al., 2020). VOCs measured in common with ICHEAR chamber study were compared as shown in Table 4.3 and Table 4.4. As the ozone level was kept as low as possible in other studies, we only include the

ERs obtained under ozone-free condition of our chamber study for comparison. The breath ER of isoprene is higher than the mean values reported by Sun et al. (2017) and the ER of monoterpenes is lower. But they are in the range of their measurements obtained from 117 volunteers. The ER of acetone reported by Sun et al. (2017) showed little variation among individuals and is much lower compared to the ER of acetone from the ICHEAR chamber study. The author claimed that semi-quantification of acetone might be a reason as the calibration linear fit was not good enough. Other VOCs were not detected in our study, which may be due to lack of repetitive experiments among different volunteers. For dermal emissions (see Table 4.4), our results generally agree better with the results from Mochalski et al. (2014) except for 6MHO. Exposure to the outside ozone before the experiments might be the reason for the much higher 6MHO ER even under ozone-free condition. The generally lower ERs of VOCs reported by Zou et al. (2020) was probably due to showering directly before the experiment. The ERs of chain aldehydes were found in general to be lower than the values reported in two other studies. Bias from the quantification using constant k rate instead of gas standards may be one of the reasons.

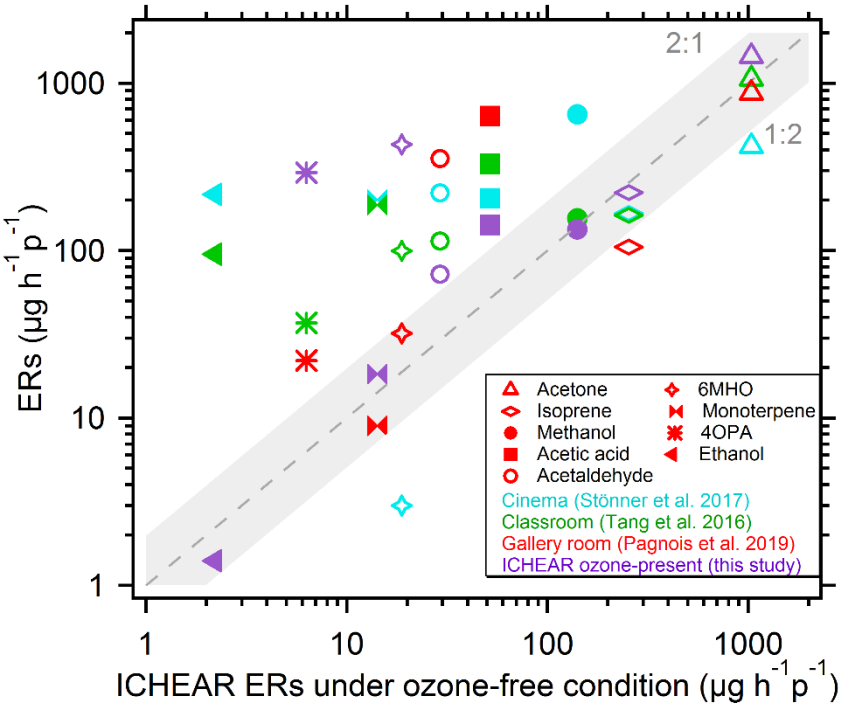

Figure 4.5 Comparison of selected VOC human emission rates between ICHEAR chamber study and other studies. (The emission rate of ethanol for gallery room was not included as it was over 12000 μg h^{-1} p^{-1}; The emission rate of methanol was not reported in the study of gallery room; 4OPA was not measured in the cinema).

Table 4.3 Human breath emission rates (μg h^{-1} p^{-1}) of selected species in the literature

Species	Sun et al. (2017) Mean (range)	ICHEAR Exp. 12* Mean over steady state
Acetone	24.84 (24.08 - 37.27)	761
Isoprene	36.71 (0.98 - 288.25)	246
Acetic acid	2.29 (0.16 – 11.8)	Not detected
Monoterpenes	6.51 (0.25 – 514.23)	2.4
Methyl ethyl ketone	0.44 (0.13 – 2.06)	Not detected
Phenol	4.8 (0.49 – 193.79)	Not detected
Ethanol	1.31 (0.03- 5.52)	Not detected

*Under ozone-free condition

Table 4.4 Human skin emission rates (μg h^{-1} p^{-1}) selected species in the literature

Species	Zou et al. (2020) Mean of replicates for one subject	Mochalski et al. (2014) Mean of 10 subjects	ICHEAR Exp. 13* Mean over steady state
Monoterpenes	2.6	6.2	7.3
Acetic acid	19.1	Not reported	185
$C_4H_8O_2$ (ester)	19.8	Not reported	31.9
Acetaldehyde	6.5	Not reported	60.1
Acetone	39.7	156	182
Methyl ethyl ketone	Not reported	17	7.9
Methyl vinyl ketone	Not reported	24.2	14.9
6MHO	4	5	181.7
Geranyl acetone	8.8	Not reported	5.4
Decanal	39	Not reported	8.2
Nonanal	32.6	13	6.19
Octanal	5.4	7.6	0.89
Hexanal	6.5	11.9	1.19

*Under ozone-free condition

4.4 Limitations and implications

Uncertainty up to 50% is expected for the ER of species that were not calibrated using gas standards. Therefore, the total uncertainty of whole-body ER under ozone-free condition was up to 36%, lower than that under ozone-present condition (up to 45%) since the fractional contribution of standard-calibrated species was higher under ozone-free condition compared to the ozone-present

condition. Better quantification of the major contributing species would help to lower the uncertainty of the ERs. Meanwhile, those carbonyl compounds (e.g. 6MHO, 4OPA and aldehydes) generated when ozone was present may not be entirely from the skin/clothing surface as they can be secondarily generated in the gas phase which probably can not be strictly called direct human emissions. Salvador et al. (2019) studied the ozone effect on soiled shirts using the same climate chamber as this study and found that 30% of 6MHO and 40% of 4OPA were actually produced in the gas phase when ozone was present in the chamber without subjects present.

Geranyl acetone, one of the major squalene ozonolysis products was measured at very low mixing ratios in the study, around 40 times lower than the mixing ratio of 6MHO. Salvador et al. (2019) reported that the steady-state mixing ratio of geranyl acetone was comparable or even higher than 6MHO when ozone was added into the chamber where four worn T-shirts were placed under similar conditions. As Salvador et al. (2019) calibrated those two compounds with prepared standards, bias from using constant k rate to calculate the mixing ratios of geranyl acetone and 6MHO in our study may partly explain the large variation. However, as mentioned before, with the uncertainty up to 50%, the mixing ratio of geranyl acetone would still be one order of magnitude lower than the mixing ratio of 6MHO if we consider the extreme scenario that the mixing ratios of geranyl acetone and 6MHO were underestimated and overestimated by 50%, respectively. This indicates the existence of other factors causing the bias. Absorption of geranyl acetone to the inlet surface may be one of the reason as the vapor pressure of geranyl acetone (3.35 Pa at 298K) is much lower than 6MHO (235 Pa at 298K) (Table 1.4 in Chapter 1). The inlet used in the study was longer than the inlet used in Salvador et al. (2019). Under ozone-present conditions, geranyl acetone on the inlet surface can be converted to 6MHO by ozone itself, causing less geranyl acetone and more 6MHO to be measured by the PTR-MS.

The skin-only experiment was achieved by introducing only the exhaled air into the other chamber via masks and tubing. Therefore, human flatus which is also a source emitting various VOCs (de Lacy Costello et al., 2014) may also contribute to the dermal emissions characterized in our study.

With the specially designed chamber experiments and real-time VOCs measurements, this study was able to characterize human bioeffluents and the effect of ozone on human emissions. The study indicates that breath emitted VOCs dominate the indoor total VOCs emissions under ozone-free conditions, while skin emitted VOCs and their reaction products increased substantially with the presence of ozone. The obtained ERs of VOCs can help to improve existing indoor air quality models. In particular, through comparison of ERs with other studies, the ERs derived under ozone-free condition can serve as the bottom limit of natural human emissions.

References

Abbatt, J. P. D. and Wang, C.: The atmospheric chemistry of indoor environments, Environ Sci Process Impacts, 22, 25-48, 2020.

Afshari, A., Lundgren, B. and Ekberg, L.E.: Comparison of three small chamber test methods for the measurement of VOC emission rates from paint, Indoor Air, 13, 156-165, 2003.

Anderson, S. E., Franko, J., Jackson, L. G., Wells, J. R., Ham, J. E., and Meade, B. J.: Irritancy and allergic responses induced by exposure to the indoor air chemical 4-oxopentanal, Toxicol Sci, 127, 371-381, 2012.

Bekö, G., Wargocki, P., Wang, N., Li, M., Weschler, C. J., Morrison, G., Langer, S., Ernle, L., Licina, D., Yang, S., Zannoni, N., and Williams, J.: The Indoor Chemical Human Emissions and Reactivity project (ICHEAR): Overview of experimental methodology and preliminary results, Indoor Air, 00, 1-16, 2020.

Bourtsoukidis, E., Helleis, F., Tomsche, L., Fischer, H., Hofmann, R., Lelieveld, J., and Williams, J.: An aircraft gas chromatograph–mass spectrometer System for Organic Fast Identification Analysis (SOFIA): design, performance and a case study of Asian monsoon pollution outflow, Atmos. Meas. Tech., 10, 5089-5105, 2017.

Cheng, Y.-H., Lin, C.-C., and Hsu, S.-C.: Comparison of conventional and green building materials in respect of VOC emissions and ozone impact on secondary carbonyl emissions, Building and Environment, 87, 274-282, 2015.

de Lacy Costello, B., Amann, A., Al-Kateb, H., Flynn, C., Filipiak, W., Khalid, T., Osborne, D., and Ratcliffe, N. M.: A review of the volatiles from the healthy human body, J Breath Res, 8, 014001, 2014.

Fenske, J. D. and Paulson, S. E.: Human breath emissions of VOCs, J Air Waste Manag Assoc, 49, 594-598, 1999.

He, J., Sun, X., and Yang, X.: Human respiratory system as sink for volatile organic compounds: Evidence from field measurements, Indoor Air, 29, 968-978, 2019.

Hodgson, A. T., Beal, D., and McIlvaine, J. E. R.: Sources of formaldehyde, other aldehydes and terpenes in a new manufactured house, Indoor Air, 12, 235-242, 2002.

Hodgson, A. T., Wooley, J. D., and Daisey, J. M.: Emissions of volatile organic compounds from new carpets measured in a large-scale environmental chamber, Air & Waste, 43, 316-324, 1993.

Lindinger, W., Hansel, A., and Jordan, A.: On-line monitoring of volatile organic compounds at pptv levels by means of proton-transfer-reaction mass spectrometry (PTR-MS) medical applications, food control and environmental research, International Journal of Mass Spectrometry and Ion Processes, 173, 191-241, 1998.

Mochalski, P., Unterkofler, K., Hinterhuber, H., and Amann, A.: Monitoring of selected skin-borne volatile markers of entrapped humans by selective reagent ionization time of flight mass spectrometry in NO+ mode, Anal Chem, 86, 3915-3923, 2014.

Mochalski, P., Wiesenhofer, H., Allers, M., Zimmermann, S., Guntner, A. T., Pineau, N. J., Lederer, W., Agapiou, A., Mayhew, C. A., and Ruzsanyi, V.: Monitoring of selected skin- and breath-borne volatile organic compounds emitted from the human body using gas chromatography ion mobility spectrometry (GC-IMS), J Chromatogr B Analyt Technol Biomed Life Sci, 1076, 29-34, 2018.

Nazaroff, W. W. and Weschler, C. J.: Cleaning products and air fresheners: exposure to primary and secondary air pollutants, Atmospheric Environment, 38, 2841-2865, 2004.

Pagonis, D., Price, D. J., Algrim, L. B., Day, D. A., Handschy, A. V., Stark, H., Miller, S. L., de Gouw, J., Jimenez, J. L., and Ziemann, P. J.: Time-Resolved Measurements of Indoor Chemical Emissions, Deposition, and Reactions in a University Art Museum, Environ Sci Technol, 53, 4794-4802, 2019.

Petrick, L. and Dubowski, Y.: Heterogeneous oxidation of squalene film by ozone under various indoor conditions, Indoor Air, 19, 381-391, 2009.

Ruzsanyi, V., Fischer, L., Herbig, J., Ager, C., and Amann, A.: Multi-capillary-column proton-transfer-reaction time-of-flight mass spectrometry, J Chromatogr A, 1316, 112-118, 2013.

Salvador, C. M., Beko, G., Weschler, C. J., Morrison, G., Le Breton, M., Hallquist, M., Ekberg, L., and Langer, S.: Indoor ozone/human chemistry and ventilation strategies, Indoor Air, 29, 913-925, 2019.

Schubert, R., Schwoebel, H., Mau-Moeller, A., Behrens, M., Fuchs, P., Sklorz, M., Schubert, J. K., Bruhn, S., and Miekisch, W.: Metabolic monitoring and assessment of anaerobic threshold by means of breath biomarkers, Metabolomics, 8, 1069-1080, 2012.

Sekimoto, K., Li, S.-M., Yuan, B., Koss, A., Coggon, M., Warneke, C., and de Gouw, J.: Calculation of the sensitivity of proton-transfer-reaction mass spectrometry (PTR-MS) for organic trace gases using molecular properties, International Journal of Mass Spectrometry, 421, 71-94, 2017.

Simon, V., Uitterhaegen, E., Robillard, A., Ballas, S., Veronese, T., Vilarem, G., Merah, O., Talou, T., and Evon, P.: VOC and carbonyl compound emissions of a fiberboard resulting from a coriander biorefinery: comparison with two commercial wood-based building materials, Environ Sci Pollut Res Int, 27, 16121-16133, 2020.

Smith, D., Pysanenko, A., and Spanel, P.: Kinetics of ethanol decay in mouth- and nose-exhaled breath measured on-line by selected ion flow tube mass spectrometry following varying doses of alcohol, Rapid Commun Mass Spectrom, 24, 1066-1074, 2010.

Stonner, C., Edtbauer, A., and Williams, J.: Real-world volatile organic compound emission rates from seated adults and children for use in indoor air studies, Indoor Air, 28, 164-172, 2017.

Sun, X., He, J., and Yang, X.: Human breath as a source of VOCs in the built environment, Part II: Concentration levels, emission rates and factor analysis, Building and Environment, 123, 437-445, 2017.

Tang, X., Misztal, P. K., Nazaroff, W. W., and Goldstein, A. H.: Volatile Organic Compound Emissions from Humans Indoors, Environ Sci Technol, 50, 12686-12694, 2016.

Turner, C., Spanel, P., and Smith, D.: A longitudinal study of ethanol and acetaldehyde in the exhaled breath of healthy volunteers using selected-ion flow-tube mass spectrometry, Rapid Commun Mass Spectrom, 20, 61-68, 2006a.

Turner, C., Spanel, P., and Smith, D.: A longitudinal study of methanol in the exhaled breath of 30 healthy volunteers using selected ion flow tube mass spectrometry, SIFT-MS, Physiol Meas, 27, 637-648, 2006b.

Weschler, C. J.: Ozone's Impact on Public Health: Contributions from Indoor Exposures to Ozone and Products of Ozone-Initiated Chemistry, Environmental Health Perspectives, 114, 1489-1496, 2006.

Weschler, C. J.: Roles of the human occupant in indoor chemistry, Indoor Air, 26, 6-24, 2016.

Weschler, C. J. and Nazaroff, W. W.: Dermal Uptake of Organic Vapors Commonly Found in Indoor Air, Environmental Science & Technology, 48, 1230-1237, 2014.

Wisthaler, A. and Weschler, C. J.: Reactions of ozone with human skin lipids: sources of carbonyls, dicarbonyls, and hydroxycarbonyls in indoor air, Proceedings of the National Academy of Sciences, 107, 6568-6575, 2010.

Zhao, J. and Zhang, R.: Proton transfer reaction rate constants between hydronium ion (H3O+) and volatile organic compounds, Atmospheric Environment, 38, 2177-2185, 2004.

Zou, Z., He, J., and Yang, X.: An experimental method for measuring VOC emissions from individual human whole-body skin under controlled conditions, Building and Environment, 181, 107137, 2020.

Chapter 5. Total OH reactivity of emissions from humans: in-situ measurement and budget analysis

This entire chapter is reproduced with permission from:

Nijing Wang, Nora Zannoni, Lisa Ernle, Gabriel Bekö, Pawel Wargocki, Mengze Li, Charles J. Weschler, and Jonathan Williams *Environmental Science & Technology* **2021** 55 (1), 149-159 DOI: 10.1021/acs.est.0c04206 https://doi.org/10.1021/acs.est.0c04206 **Only the numbering of sections, figures, tables and equations have been adapted to match the thesis structure.**

Contribution to this publication by Nijing Wang: participated the experimental design; conducted VOCs measurement and raw data processing; contributed to OH reactivity measurements and raw data processing; performed further data analysis of VOCs and OH reactivity including; drafted the entire article and is the corresponding author of the article.

Abstract

Humans are a potent mobile source of various volatile organic compounds (VOCs) in indoor environments. Such direct anthropogenic emissions are gaining importance as those from furnishings and building materials become better regulated and energy efficient homes may reduce ventilation. While previous studies have characterized human emissions in indoor environments, the question remains whether VOCs remain unidentified by current measuring techniques. In this study conducted in a climate chamber occupied by four people, the total OH reactivity of air was quantified, together with multiple VOCs measured by PTR-ToF-MS and fast-GC-MS. Whole-body, breath and dermal emissions were assessed. Comparison of directly measured OH reactivity and that of the summed reactivity of individually measured species revealed no significant shortfall. Ozone exposure (37 ppb) was found to have little influence on breath OH reactivity but enhanced dermal OH reactivity significantly. Without ozone, the whole-body OH reactivity was dominated by breath emissions, mostly isoprene (76%). With ozone present, OH reactivity nearly doubled, the increase being mainly caused by dermal emissions of mostly carbonyl compounds (57%). No significant difference in total OH reactivity was observed for different age groups (teenagers/young-adults/seniors) without ozone. With ozone present, total OH reactivity decreased slightly with increasing age.

5.1 Introduction

People spend on average 80% ~ 90% of their time indoors, and more than 60% in their home residence.[1-5] Therefore, indoor air quality plays an important role in human health as people are exposed to numerous chemical compounds for long periods within their indoor home environment.[6, 7] The degree of exposure is even higher while movement restrictions are in force e.g. associated with pandemic outbreaks.

For the last 20-30 years, the main focus of the indoor research has been on building-related emissions such as building materials, furnishings, and paints; numerous volatile organic compounds (VOCs) have been measured from such sources.[8-13] However, with improved manufacturing techniques, these emissions gradually decreased, increasing the relative importance of emissions from occupants themselves.

Humans are a potent, mobile source of chemicals in indoor environments. Several hundred bioeffluent VOCs are known to be emitted via breath and skin.[14] In the presence of oxidants such as ozone or the hydroxyl radical (OH), oxidation products can be formed.[15-19] Besides, indoor OH concentrations have been measured and modelled in several studies which indicate the common occurrence of levels on the order of 10^5 molecules cm^{-3}.[20-24] Despite the application of advanced measurement technology in recent studies, the question remains: are we measuring all of the OH reactive species related to indoor human emissions? The question can be addressed by measurements of total OH reactivity, which provides a direct measurement of the total loss rate of OH radicals in the air. When this value is compared to the sum of the OH reactivity contributed by the individually measured species, any difference will indicate that the characterization of species has been insufficient. Studies made outdoors have revealed significant differences between measured and calculated reactivity.[25-28] The missing fraction in comparison to known species gives important insights into possible unknown primary emission sources and secondary products.

The OH reactivity in this study is determined using the comparative reactivity method (CRM)[29] which has been applied in various outdoor locations worldwide from megacities to rainforests.[25, 26, 30-32] A recent inter-comparison of OH reactivity methods has shown that the CRM method accurately measures OH reactivity[33], especially under high OH reactivity conditions. Therefore, indoor environments, where high OH reactivity can be expected, present a good application for this method.

Several studies have characterized VOCs from people in various real world indoor environments including aircraft cabins, offices, classrooms, movie theaters and museums.[34-39] These results inevitably represent emissions from people combined with inputs from clothing, detergents, fragrances, furnishings and furniture. While limited indoor studies have considered the OH

reactivity contributions of measured indoor VOCs,[40] to our knowledge, none to date has compiled a budget based on a direct total OH reactivity measurement. Therefore, measuring the total OH reactivity and VOCs exclusively from human emissions is needed to answer whether current indoor air trace gas measurements provide a complete chemical characterization of human emissions from different sources (breath and skin), including their variations under different well controlled conditions. Of special interest is total OH reactivity of human emissions in the presence of ozone, one of the most important indoor oxidants.[41]

This study is a part of the Indoor Chemical Human Emissions and Reactivity (ICHEAR) project, which aims to comprehensively characterize the human contribution to indoor air chemistry. The goals of this work are: (1) define the OH reactivity of indoor air resulting from whole-body human emissions, as well as isolated breath and dermal emissions; (2) identify if any missing reactivity exists and the fractional composition of the OH reactivity; (3) examine the effect of ozone; (4) examine the effect of human age.

5.2 Methods

5.2.1 Chamber Experiment Set-Up

Two 22.5 m^3 stainless-steel climate chambers at the Technical University of Denmark were used for all experiments. The stainless steel chamber minimizes the influence of surface effects and emissions from furnishings and decorative materials. Detailed information about the experimental design and the instrumental set-up are given by Bekö, et al.[42] In brief, pre-cleaned chambers were ventilated with filtered outdoor air at an air change rate (ACR) of 3.2 ± 0.11 h^{-1} (mean value calculated from measurement of CO_2 decay as well as Freon®134a tracer gas, details in Bekö, et al.[42]). The temperature and the relative humidity of the chambers were controlled and monitored. For the duration of an experiment, four volunteers were asked to stay inside the chamber wearing standardized long-sleeve shirts, pants and calf socks ("long" clothing) or t-shirts, shorts and ankle socks ("short" clothing), which were prewashed with fragrance-free detergent and tumble-dried after purchase. In the subset of experiments designed to characterize the impact of ozone, ozone was generated using a Jelight 600 UV ozone generator and introduced into the chamber supply air to achieve the targeted mixing ratio of ~ 100 ppb in an unoccupied chamber. With four people present, the steady-state ozone level fell to 37 ppb. The ozone loss due to the chamber surface without people present was relatively small (~5%).[42] The experiments were performed with three groups of young adults, a teenage group and a senior group.

In this study (Table 1), the identical experiments with the five groups (benchmark experiments, Experiment 1, 6, 10, 16, 18) and their replicates (Experiment 21, 25 and 26) were selected to determine the total OH reactivity of human whole-body emissions under ozone-free and ozone-

present conditions, as well as the potential variation of total OH reactivity with age. For each benchmark experiment, volunteers wearing "long" clothing stayed in the chamber for ~ 3 hours in the morning. Then, after a short lunch break (10 - 15 minutes), volunteers re-entered the chamber for the afternoon period (~ 2.5 hours). Ozone was introduced approximately 10 minutes after they re-entered the chamber. In addition to the benchmark conditions, additional experiments were performed in order to examine breath and skin emissions separately. This was achieved by using two identical chambers and asking the volunteers to breathe through a mask (Sperian ValuAir Plus 6100V series RP155). They inhaled air from the chamber in which they sat, and exhaled air into the second chamber. As the main inlet for all measurement instruments was fixed in the primary chamber, where the whole-body experiments were performed, the skin-only Experiment 13 was performed by asking the volunteers to sit in the primary chamber, while the breath-only Experiment 12 was achieved by having the volunteers sit in the second chamber. Ozone was always introduced into the primary chamber.

Table 5.1. Experimental conditions and information.

Experiment No*. (replicate)	Experiment type	Temperature (°C) (replicate)	Relative humidity (%) (replicate)	Age
1	Whole-body: young adult (group A1)	26.2 - 30.3	31 - 35	
6 (21)	Whole-body: young adult (group A2)	23.7 - 27.5 (23.3 - 27.7)	16 - 23 (17 - 25)	mean: 25 (19 - 30)
10	Whole-body: young adult (group A3)	25.3 - 28.8	28 - 31	
18 (26)	Whole-body: teenager (group T4)	24.6 - 28.4 (25.8 - 30.0)	29 - 37 (30 - 36)	mean: 13.8 (13 - 15)
16 (25)	Whole-body: senior (group S5)	25.3 - 29.7 (25.4 - 29.0)	24 - 30 (24 - 28)	mean: 70.5 (68 - 72)
12	Breath: young adult (group A3)	32.2 – 32.6	56 - 62	
13	Skin: young adult (group A3)	26.3 - 29.9	24 - 28	

* Experiment numbers are identical to those in Bekö et al.[42]. Numbers in parentheses refer to replicate measurements.

5.2.2 Total OH Reactivity Measurement and Data Analysis

A common inlet for all instruments (i.d. = 12.7 mm, length 5m, fluorinated ethylene propylene tubing) was attached inside the chamber air outlet, to draw air exiting the chamber to instruments at 7 L min^{-1}. The inlet was manually controlled via a 3-way valve (Galtek® Solenoid Valves, Entegris, Inc.) to allow switching between the chamber's supply air and exhaust airstreams. A subflow (i.d. = 6.35 mm) of ~ 300 mL min^{-1} from the main inlet was taken by the CRM system

which mainly consists of a glass reactor and a detector (a proton transfer quadrupole mass spectrometer, PTR-QMS produced by Ionicon Analytik).

The principle of the CRM is to monitor the concentration variations of a reference molecule with a known OH rate constant (pyrrole in this study, Westfalen AG), when it reacts with OH radicals alone, or when mixed with ambient air in a glass reactor[29]. The OH radicals were generated by flushing humidified nitrogen (6.0 grade, Westfalen AG) through a Hg-Ar UV lamp (LOT Quantum Design). The pyrrole variations were detected by the PTR-QMS at *m/z* 68 operated under drift pressure at 2.2 mbar, temperature at 60 °C and voltage at 600 V (E/N =137 Td)[29]. The detailed CRM operating procedures can be found in the Supporting Information (SI). Due to a failure of the drift tube temperature control in PTR-QMS during the experiments with the senior group (Experiment 16 and 25), the measured total OH reactivity data for those particular experiments are not available.

The measured OH reactivity was corrected for possible interferences (humidity and non-pseudo-first-order condition) according to previous studies.[29, 33, 43] Interference from NOx (NO and NO_2) was deemed negligible due to their low mixing ratios (mostly of time near and below the limits of detection, 1 ppb). The interferences were described in greater details in the SI. The limit of detection (LOD, 3σ) during the campaign was 5 s^{-1}. The total uncertainty of the OH reactivity data was ~ 50% (median and mean), with the precision error ranging from 12% - 54% for the experiments included in this study. The detailed calculations of total uncertainty and precision can be found in the SI.

5.2.3 VOCs and Other Trace Gas Measurements

A proton transfer time of flight mass spectrometer (PTR-ToF-MS 8000, Ionicon Analytik) was used to measure VOCs in the chamber. The instrument sampled the same main inlet air as the CRM instrument by taking another sub-stream of ~ 100 mL min^{-1} (i.d. = 3.18mm). The PTR-ToF-MS was operated under standard conditions (same as PTR-QMS used in CRM) using protonated water (H_3O^+) as the primary ions. Compounds with proton affinity higher than water are detected at their protonated mass (MH^+).[44] 4-point calibrations were performed throughout the campaign using a standard gas mixture containing the 14 compounds listed in Table S5.2 (Apel-Riemer Environmental Inc.). The time resolution of the measurement was 20 s with mass resolution of 4000 at mass 96 amu. The LOD (3σ) for the VOCs measured by PTR-ToF-MS ranged from 7 ppt to 171 ppt for compounds calibrated with the gas standard. For other detected masses, empirical formulas were assigned and the mixing ratios of those masses were calculated using the theoretical calculation method assuming a constant proton transfer rate coefficient, with an associated uncertainty of ~ 50%.[45] Here, an exception was made for 6-methyl-5-hepten-2-one (6MHO), which

is a main product of squalene ozonolysis. [37] The mixing ratio was corrected to the reported proton transfer rate coefficient[46]. Due to high abundance of 6MHO (above 4 ppb when ozone was present reported in Bekö, et al.[42]) and its measured fast reaction rate with OH radicals (1.57×10^{-10} cm^3 $molecules^{-1}$ s^{-1}, see Table S5.2), the uncertainty of calculated reactivity (see section 2.4) for 6MHO as well as the total reactivity would be overestimated if no correction was applied.

The mixing ratios of isoprene and propanal (i.e., propionaldehyde) were taken from a custom-made fast gas chromatograph-mass spectrometer (fast-GC) deployed for the campaign with LOD < 25 ppt and total uncertainty < 10%. This is because the PTR-Tof-MS was found to have interferences for isoprene since $C_5H_8H^+$ (m/z 69.070) could also result from fragmentation of aldehydes with carbon number larger than four[47], and the instrument could not distinguish propanal and acetone. The fast-GC was operated in selected ion monitoring (SIM) mode to measure certain VOCs at a time resolution of 3 minutes. Details of the operation method were described in Bourtsoukidis et al.[48].

Ammonia (NH_3) was measured by a manufacturer-calibrated cavity ring-down spectrometer (Picarro G2103). A detailed description of the NH_3 measurement was reported by Li, et al. [49] Ozone was measured by an ozone monitor (Model 205, 2B Technologies). NO and NO_2 were continuously monitored by a chemiluminescence NO/NOx analyzer (ECO PHYSICS, model CLD 700 AL).

5.2.4 Calculated OH Reactivity

In order to compare the directly measured total OH reactivity with the OH reactivity from all measured species, the total "calculated OH reactivity" was obtained based on measured trace gas concentrations using the following equation:

$$R = \sum k_{X_i+OH}[X_i] \qquad \text{Eq. (5.1)}$$

where $[X_i]$ is the concentration of trace gas species i and the k_{X_i+OH} refers to the rate constant (cm^3 $molecule^{-1}$ s^{-1}) of species i reacting with the OH radical. In total, 78 species with assigned empirical formulas and chemical structures were considered in the calculation; these compounds were detected above the LODs most of the time, and are related to human emissions (higher mixing ratios detected with volunteers inside the chamber in comparison with the empty chamber). These species were grouped into hydrocarbons (HC), oxygenated volatile organic compounds (OVOCs), nitrogen containing compounds and sulfur containing compounds. OVOCs were further divided into five subgroups: alcohols, acids, oxygenated aromatics, carbonyls and others. The list of species with corresponding k_{X_i+OH} taken from published literature is shown in Table S5.2. As some measured PTR-ToF-MS masses can be isomeric compounds, an averaged k_{X_i+OH} was derived for isomeric compounds with known rate constants (Table S5.2). However, for some isomeric

carbonyls, specific compounds were assigned to the formula according to Wisthaler and Weschler [37] who reported carbonyl products from human skin lipid reaction with ozone. For some compounds whose rate constants with the OH radical are unknown, rate constants for compounds with similar chemical structure were used. The uncertainty of the k_{X_i+OH} for standard-calibrated compounds and specifically assigned compounds was estimated to be ~ 10%. While for the averaged k_{X_i+OH} derived from isomeric compounds, large uncertainty (100%) was estimated.[30] The uncertainty of calculated reactivity for each species is a propagation of uncertainties from the mixing ratio and the k_{X_i+OH}. Therefore, the total uncertainty of the total calculated OH reactivity is highly dependent on the reactivity fraction of the species having less uncertainty (i.e. standard calibrated compounds), with mean and median uncertainty of 29% for the experiments in this study.

Data from each experiment during the steady state condition before volunteers exit the chamber were selected and averaged for both measured and calculated OH reactivity. Steady state was assumed when the relative change of the calculated reactivity was small at the end of each experiment (see details in the SI.), meaning the total production rate of reactive species due to human occupants was equivalent to their total loss rate, which included air exchange and deposition to chamber surfaces. The data during the steady state period reported in this study were background corrected by subtracting the measured mean value in the empty chamber before volunteers entered.

5.3 Results and discussion

5.3.1 Total OH Reactivity of Whole-Body Emissions

Four benchmark experiments (1, 6, 21 and 10) involving three different groups of young adult volunteers were selected to represent the whole-body emission from adults, with the mean levels of measured and calculated OH reactivity shown in Figure 5.1. In general, the OH reactivity due to occupancy by four adults was 14 ± 3 s^{-1} under ozone-free condition and increased to 33 ± 6 s^{-1} with ozone present. There was good agreement with the calculated OH reactivity of 16 ± 2 s^{-1} and 33 ± 1 s^{-1} under ozone-free and ozone-present conditions, respectively. In other words, the calculated OH reactivity matched well with the measurements, considering the associated uncertainty (Figure S5.1). The OH reactivities of whole-body emissions from four people in the ventilated chamber (16 s^{-1} under ozone-free condition and 33 s^{-1} under ozone-present condition) were comparable to reactivities measured in mega cities[50].

As shown in Figure 5.1, under ozone-free condition hydrocarbons contributed the largest fraction (81%) to the total OH reactivity (dominated by isoprene, 76%, 12 s^{-1}), followed by carbonyls (14%). Although more than 70 species were considered in the calculation, the top ten species accounted for 90% of the total OH reactivity (Table 5.2). Besides isoprene, the reactivity of the other nine

species individually was less than 1 s^{-1}. In contrast, after ozone was introduced into the chamber, the total OH reactivity doubled compared to the ozone-free condition. Carbonyl compounds constituted the largest fraction (57%, 19 s^{-1}). The OH reactivity of hydrocarbons showed a small decrease when ozone was present, while the OH reactivity of OVOCs (except for alcohols) increased. In particular, the reactivity attributed to carbonyl compounds increased by almost an order of magnitude from 2 s^{-1} without ozone to 19 s^{-1} with ozone present. 6MHO alone accounted for 28% of the total reactivity under the ozone-present condition, which is comparable with the fractional contribution by isoprene (33%). This occurred because of their abundance and fast reaction rate constants with OH radicals (1.0×10^{-10} cm^3 $molecules^{-1}$ s^{-1} for isoprene and 1.57×10^{-10} cm^3 $molecules^{-1}$ s^{-1} for 6MHO).[51,52] Isoprene is one of the most abundant VOCs observed in human breath[53]. 6MHO is a major product of the reaction of ozone with squalene, one of the main components of skin lipids[15]. It should be noted that acetone was found to be much more abundant than isoprene, with and without ozone. It is not only a major breath compound[53] but also a squalene-ozone reaction product[15]. However, due to its much smaller rate constant with the OH radical at 1.8×10^{-13} cm^3 $molecules^{-1}$ s^{-1},[54] its contribution to the total OH reactivity is relatively small (< 0.15 s^{-1}).

The reported OH reactivity of 16 s^{-1} under ozone-free and 33 s^{-1} under ozone-present conditions with four seated people inside the chamber (temperature range: 23 - 30 °C), gave a reactivity of 4.0 and 8.3 s^{-1} per person, respectively. No other direct indoor OH reactivity measurement results are available for comparison. However, as no significant missing reactivity was observed, we can compare our results to previous studies that reported calculated OH reactivity. For studies that reported concentrations of gas-phase species, the OH reactivity can be estimated using Eq. (5.1). At identical occupancy, the mixing ratios of indoor gas-phase species are impacted by the room volume, the ACR and the surface removal rate. Bigger room volume and larger ACR lead to more dilution, which results in lower mixing ratios. In order to compare our results with other studies, we adjusted the estimated per-person OH reactivity in other studies for the differences in room volume and ACR between those studies and our data. The surface removal of a compound can be ignored if it reaches steady state. Since the major compounds (isoprene and 6MHO) contributing to the OH reactivity could quickly reach steady-state, the surface removal was not considered. Details of the adjustment method are given in SI.

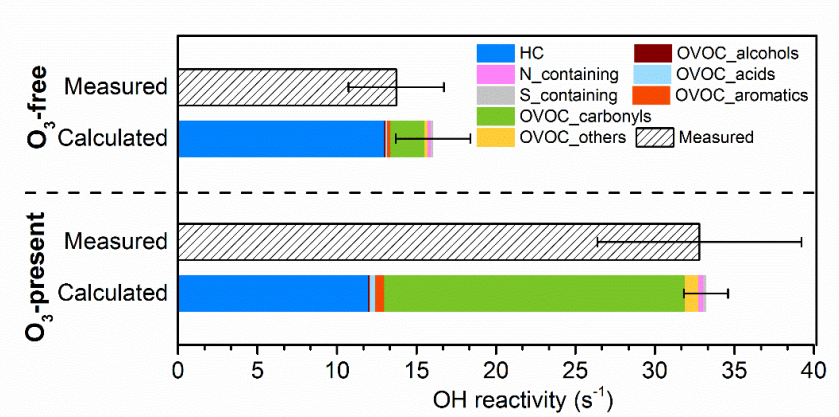

Figure 5.1. Calculated and measured OH reactivity of adult whole-body emissions under ozone-free and ozone-present conditions. Error bars represent the standard deviation derived from the data of four benchmark experiments (Experiment 1, 6, 10, 21).

Table 5.2. Top ten species contributing to the calculated OH reactivity of adult whole-body emissions (average levels and standard deviations of Experiment 1, 6, 10 and 21) under ozone-free and ozone-present conditions.

	Mass (H^+)	Compounds	OH Reactivity ± SD (s^{-1})	Fraction ± SD %
Ozone-free	*	isoprene	12 ± 2.4	76 ± 3.8
	137.132	limonene	0.6 ± 0.1	3.6 ± 1.0
	127.112	6MHO	0.4 ± 0.1	2.6 ± 1.3
	45.034	acetaldehyde	0.3 ± 0.2	2.0 ± 0.9
	#	ammonia	0.2 ± 0.1	1.2 ± 0.5
	195.186	geranyl acetone	0.2 ± 0.1	1.1 ± 0.6
	87.044	1,4-butanedial	0.1 ± 0.0	0.9 ± 0.1
	33.034	methanol	0.1 ± 0.0	0.8 ± 0.3
	91.057	C4H10S	0.1 ± 0.1	0.7 ± 0.5
	71.049	C4H6O	0.1 ± 0.0	0.7 ± 0.2
	Sum of top 10 species		**14 ± 2.4**	**90 ± 1.6**
	Sum of all species		**16 ± 2.3**	
Ozone-present	*	isoprene	11.0 ± 1.2	33 ± 3.8
	127.112	6MHO	9.3 ± 1.1	28 ± 1.2
	101.096	4OPA	1.9 ± 0.2	5.8 ± 0.1
	143.143	nonanal	1.2 ± 0.1	3.5 ± 0.1
	87.044	1,4-butanedial	0.8 ± 0.1	2.5 ± 0.1
	45.034	acetaldehyde	0.8 ± 0.2	2.5 ± 0.8
	137.132	limonene	0.7 ± 0.1	2.2 ± 1.0
	141.127	nonenal	0.7 ± 0.1	2.0 ± 0.1
	*	propanal	0.6 ± 0.1	1.8 ± 0.0
	195.186	geranyl acetone	0.4 ± 0.1	1.3 ± 0.5
	Sum of top 10 species		**27 ± 1.4**	**82 ± 0.8**
	Sum of all species		**33 ± 1.4**	

*isoprene and propanal data were obtained from fast-GC.

#ammonia data was obtained from a cavity ring-down spectrometer (Picarro G2103).

Table 5.3 compares the OH reactivity per person ($s^{-1}p^{-1}$) of this study with those estimated for other human occupied indoor environments. The adjusted values for OH reactivity per person obtained in various occupied environments are comparable, and within the range of our chamber results without and with ozone. In the museum gallery study, the total OH reactivity with high occupant density was roughly 73% higher than the total OH reactivity with low occupant density. This comparison underlines the significant effect of occupancy on total OH reactivity in real-world indoor environments. The major species contributing to the OH reactivity in a classroom[36] and a museum gallery[40] were isoprene, monoterpenes and 6MHO. In a cinema,[35] besides isoprene and monoterpenes, acetaldehyde, a common human bioeffluent compound,[14] was the third compound contributing the most to the reactivity. Less OH reactivity contribution from 6MHO was probably caused by the lower level of ozone in winter leading to less skin-initiated oxidation products.[35] The major species contributing to OH reactivity in our study (Table 5.2) agree well with those in other studies. However, when ozone was present in our chamber, carbonyls (not including 6MHO) contributed to the reactivity more than monoterpenes (Table 5.2). This likely reflects the fact that the volunteers in our study did not use fragranced personal care products, which often contain monoterpenes (e.g. limonene).[55] Overall, the comparable per-person OH reactivity and the similar major OH reactivity contributing species observed in various studies indicates the relative consistency of the OH reactivity budget of human emissions. The present study reveals the extent to which ozone in an occupied environment can amplify the total OH reactivity of human emissions.

Table 5.3. Per-person OH reactivity from human emissions in various studies

Indoor Environments	OH reactivity per person before adjustment ($s^{-1}p^{-1}$)	Indoor volume (m^3)	Outdoor ACR (h^{-1})	Indoor ozone level (ppb)	OH reactivity per person after adjustment ($s^{-1}p^{-1}$)
Present study					
Chamber (ozone-free)	4.0	22.5	3.2	< 1	4.0
Chamber (ozone-present)	8.3	22.5	3.2	37	8.3
Other studies					
Classroom (Tang et al.[36])	0.12[a]	670	5	Not reported	5.4
Cinema (Stönner et al.[35])	0.055[a]	1300	5	Low	5.0
Gallery room (high occupancy event) (Price et al.[40])	0.080[b]	6000	0.8	5	5.3

[a] OH reactivity per person before adjustment was estimated using reported VOCs emission rates, details shown in the *Supporting Information*.

[b] OH reactivity per person before adjustment was estimated based on reported OH reactivity and occupancy number, details shown in the *Supporting Information*.

5.3.2 Total OH Reactivity of Breath and Dermal Emissions

To better understand the relative contributions of breath and dermal emissions to the total whole-body OH reactivity, results from Experiment 10 (whole-body, adult group A3) are shown in Figure 5.2, alongside the results from the separate breath and dermal emission experiments performed with the same group of volunteers. In general, the measured OH reactivity and the calculated OH reactivity were comparable. For breath-only emissions, the total OH reactivity without ozone (13 s^{-1}) was similar to the total OH reactivity with ozone present (14 s^{-1}). Hydrocarbon reactivity dominated the total reactivity under both ozone-free and ozone-present conditions. Although ozone had a negligible effect on the reactivity of breath-only emissions, the contribution of carbonyls showed an obvious increase under the ozone-present condition (Figure 5.2), accounting for 13% (2 s^{-1}) of the total calculated OH reactivity. It is likely due to ozone reacting with species in the air (e.g. isoprene and monoterpenes) as well as with a small amount of less volatile organic species (squalene, unsaturated fatty acids etc.) remaining on the chamber surfaces. As for dermal emissions, the calculated reactivity was 5 s^{-1} under ozone-free condition, which was close to the LOD (5 s^{-1}) of the measured reactivity. With ozone present, the OH reactivity increased significantly to 31 s^{-1}, with carbonyl reactivity contributing the most (84%, 26 s^{-1}). 6MHO alone accounted for 42% of the total (13 s^{-1}). The sum of OH reactivity for breath and dermal emissions exceeded the whole-body OH reactivity, especially when ozone was present. The dermal-only experiment was performed with "short" clothing, while the other experiments were performed with "long" clothing. More skin area was exposed to ozone in the dermal-only experiment, leading to greater release of reactive species. In addition, the breath-only experiment was performed under higher temperature and relative humidity, which made the comparison imperfect.

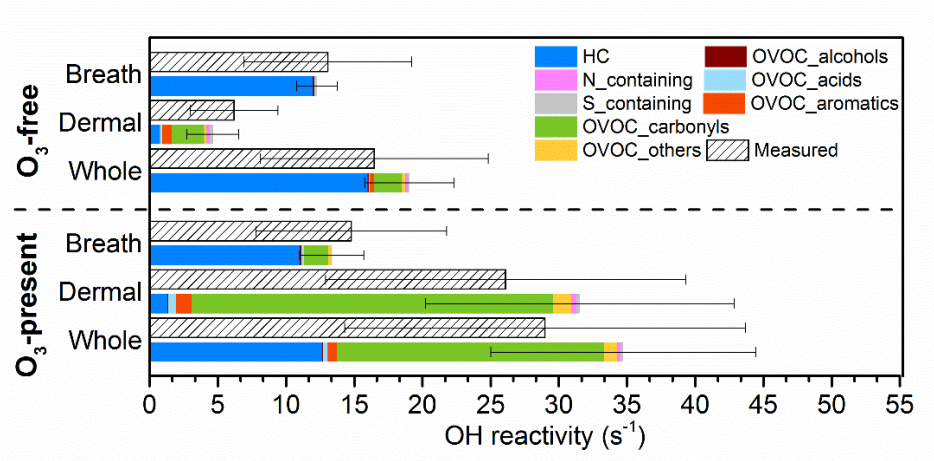

Figure 5.2. Measured and calculated OH reactivity of breath (Experiment 12), dermal (Experiment 13) and corresponding whole-body emissions (Experiment 10) under ozone-free and ozone-present conditions. Error bars represent the total uncertainty of the measured and calculated OH reactivity.

The top ten OH reactivity contributing species accounted for nearly all of the calculated total OH reactivity of breath emissions (99% at ozone-free, 94% at ozone-present conditions, Table S5.3). In contrast, the top ten OH reactivity contributing species accounted for 63% (3 s^{-1}) of the calculated total OH reactivity of dermal emissions under ozone free and for 75% (24 s^{-1}) under ozone-present condition (Table S5.4). The OH reactivity stemming from dermal emissions is more chemically diverse, especially under elevated ozone conditions. Similarly, for the whole-body emissions, the fraction that could not be explained by the top ten contributing species increased from 10% (2 s^{-1}) without ozone to 18 % (6 s^{-1}) with ozone (Table 5.2), indicating that a diverse array of reactive species were released into the gas-phase due to ozone-initiated oxidation. The top ten species contributing to the whole-body OH reactivity (Table 5.2) could also be found in either the top ten species of breath or dermal emissions (Tables S5.2 and S5.3). Taken together, the above results indicate that the reactivity of the whole-body emissions under ozone-free condition was mostly determined by the reactivity of the breath emissions. A small additional carbonyl reactivity of whole-body emissions was presumably attributable to reactivity of dermal emissions which was possibly induced by direct dermal emissions or exposure to ambient ozone prior to the experiments. The large increase in OH reactivity for whole-body emissions in the presence of ozone was attributable to the dramatic increase in products of reactions between ozone and dermal emissions (mainly carbonyls).

With ozone present, the OH reactivity budget was more broadly shared by a mix of carbonyls, especially aldehydes, due to dermal emissions (Figure 5.2 and Table 5.2). Mochalski, et al. [56] measured dermally emitted VOCs using GC-MS from 31 healthy volunteers and detected more aldehyde species compared with ketone species. Aldehydes and ketones with the same empirical formula are difficult to distinguish when using PTR-MS with H_3O^+ as the primary reagent ion. According to Mochalski et al.[56], carbonyls measured by PTR-MS in our study, especially mono carbonyls with larger molecular weight (carbon number > 4), are more likely to be aldehydes than ketones. Exceptions are certain ketones known as major skin lipid ozonolysis products (i.e. 6MHO and geranyl acetone). Aldehydes including 4-oxopantanal, nonanal, 1,4-butanedial and nonenal ranked within the top ten species contributing to the total reactivity under ozone-present condition and have all been reported as ozone oxidation products from skin lipids.[37, 38, 57, 58]

5.3.3 Total OH Reactivity for Volunteers of Different Ages

Similar to the results obtained with young adults (YA), the total OH reactivity for teenagers (T) and seniors (S) increased by a factor of ~ 2 when ozone was present in the chamber (Figure 5.3), compared to when it was absent. Consistently, the increase was mainly caused by increased carbonyls > OVOC others > aromatic OVOCs > nitrogen containing species. The contribution from alcohol, acids and sulfur containing species were not shown in the plot, since they contributed

negligible fractions to the total reactivity (below 0.2 s^{-1} and 0.5 s^{-1} under ozone-free and ozone-present condition, respectively). The measured OH reactivity was generally in good agreement with calculated reactivity for teenagers when ozone was absent. However, higher OH reactivity was measured (42 ± 3 s^{-1}) compared to the calculated OH reactivity (34 ± 2 s^{-1}) for teenagers when ozone was present. Since this difference (missing reactivity of 8 s^{-1}, 19%) was within the uncertainty of the measured reactivity (49%), we can't confidently interpret whether or not it was indicative of unmeasured species in this case.

Skin lipid emission rates tend to decrease with age,[59] which may lead to less ozone-initiated chemistry on the skin, and lower OH reacivity from dermal emissions in the presence of ozone among older individual. Figure 5.3 shows that young adults and teenagers had similar calculated total OH reactivity when ozone was present (33 ± 1 s^{-1} for YA, 34 ± 2 s^{-1} for T), while the senior group showed slightly lower reactivity (29 ± 4 s^{-1}). A similar pattern was observed for the OH reactivity contribution from carbonyls (Figure 5.3). This trend of decreasing OH reactivity from carbonyls in the presence of ozone with increasing age appears to support the view that less skin lipids are generated with increasing age. Another major contributor to the total reactivity is isoprene from exhaled breath, as discussed previously. The OH reactivity from isoprene was comparable under ozone-free and ozone-present conditions for all groups. As shown in Figure 5.3, seniors had slightly lower reactivity attributable to isoprene compared to young adults and teenagers. This is in agreement with Kushch, et al. [60], who found isoprene levels in breath to decrease with age for men above 20 years. In contrary, other studies have found that younger children (aged 7-13) and young people in general (age below 30) emit less isoprene than elderly people.[61, 62] Besides age and sex, isoprene in breath was found to be related to physiological parameters like respiratory rate or cardiac output.[63, 64] The large error bars for isoprene reactivity indicate large variations even for the same group of people (Figure 5.3). The level of isoprene was likely influenced by multiple factors. In summary, due to the mixed gender character of the groups and the limited number of volunteers in the teenager and senior groups, it is not possible to discern a potential dependency of OH reactivity on age under ozone-free conditions.

In the absence of ozone, the top ten species were similar among the age groups, together accounting for roughly 90% of the total OH reactivity (Figure S5.2a). Interestingly, nonenal was ranked within the top ten species only for seniors; 2-nonenal is found to be involved in aging-related body odor change. [65] The sum of the top ten species for each age group accounted for a smaller fraction of the total OH reactivity when ozone was present (79% for teenagers, 83% young adults and 79% for seniors, Figure S5.2b) than when ozone was absent. Many of the top species under ozone-free conditions were also among the top ten consumers of OH in the presence of ozone. However, 6MHO rose to the 2nd spot in the top-ten list. Two chemicals that were not in the top ten when

ozone was absent (4OPA and nonanal), were the 3rd and 4th ranked sinks for OH in the presence of ozone in each age group. Although the amount of skin lipids per unit area decreases with age, the proportion of different skin lipid constituents remains similar regardless of age.[59] Consistent with this, in the top ten lists, the carbonyl species derived from ozone oxidation of skin lipids were similar across the three age groups (Figure S5.2).

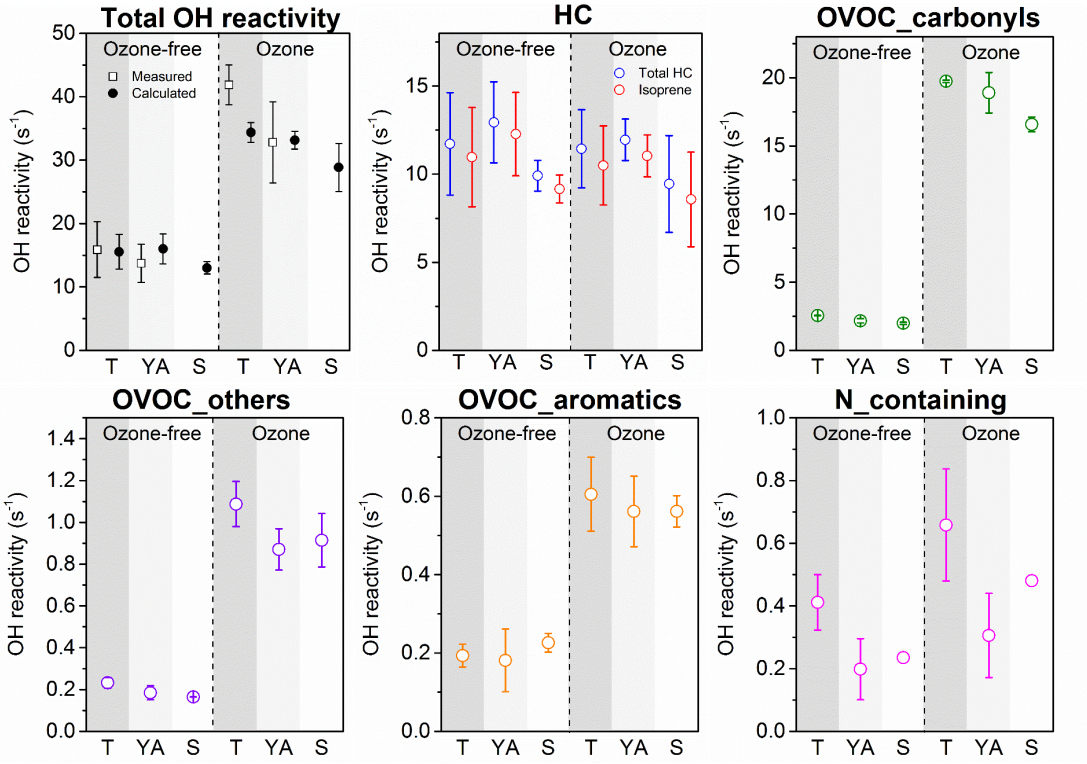

Figure 5.3. The total calculated and measured OH reactivity and the calculated OH reactivity for five chemical subgroups (those making the greatest contributions) for whole-body emissions from teenagers (T, n=2), young adults (YA, n=4) and seniors (S, n=2). Error bars refer to the standard deviations obtained from benchmark experiments in each age group. Since nitrogen containing species were dominated by ammonia (due to its high mixing ratios[52]) and the data were only available for one benchmark experiment, the variation (error bars) for the senior group (Experiment 25) could not be derived.

5.4 Limitations and Implications of the Study

When ozone reacts with squalene, 6MHO and geranyl acetone are generated as primary products in roughly equal amounts (see Fig. 1 in Wisthaler and Weschler[35]). These compounds are also generated by secondary reactions between ozone and other primary products of ozone/squalene chemistry. [37] In the present study, the measured mixing ratios of geranyl acetone were much smaller,

relative to the concentration of 6MHO, than that measured in a simulated office[37] or that measured in the present chamber[66] under similar conditions. Geranyl acetone has a lower vapor pressure and larger octanol/air partition coefficient (K_{oa}) than 6MHO, and hence it has a greater tendency to sorb to surfaces, including those that constitute the sampling train. The sampling train for this study consisted of the main inlet tubing, a three-way valve, and subflows to the instruments, which is longer and more complex than those used in the earlier studies. Furthermore, the FEP tubing used in this study has been reported to have a greater tendency to sorb gas-phase organics than the PFA tubing [67, 68] used by Salvador et al.[64] We speculate that in our study a significant fraction of geranyl acetone sorbed to the sampling train, and that some of the sorbed geranyl acetone subsequently reacted with ozone passing through the sampling lines, generating 6MHO. The length of the sampling tubing for the instrument that measured total OH reactivity and the instruments that measured speciated gas-phase organics was similar. Hence, measured total OH reactivity and calculated total OH reactivity would have been comparably impacted by such an artifact – the air that reached the instruments would have had lower geranyl acetone and higher 6MHO concentrations than the chamber air. To some extent, the loss of geranyl acetone during sampling would be partially compensated by the production of 6MHO that resulted from ozone reacting with sorbed geranyl acetone. Hence, the measured total OH reactivity is more reliable than the individual measured concentrations of 6-MHO and geranyl acetone. However, this compensation is not expected to be perfect, as the OH rate constant for geranyl acetone (two double bonds) is expected to be higher than that for 6MHO (one double bond). The net result is that the total OH reactivity and the fractional contribution of geranyl acetone may be higher, while the fractional contribution of 6MHO may be lower, than what we have reported in this study under the ozone-present condition. This sampling artifact should not have a large impact on the comparisons shown in Table 3, since the results from other studies have been obtained under conditions with much lower indoor ozone concentrations. We expect the per-person OH reactivity in the other studies to be closer to those measured for the ozone-free condition in the current study, as indeed they are. Meanwhile, the artifacts from hydroperoxide decomposition catalyzed by any metal surface were considered negligible in this study (see details in the SI).

It is worth noting that the agreement between measured and calculated reactivity is a sensitive test of budget completeness for those organic compounds that have higher OH reactivity. This method is however insensitive to the presence of unreactive species and blind to chemically inert species.

Ozone was the variable we deliberately changed during each experiment. However, the light lunch may be an unintended variable; subsequent changes in metabolism may slightly alter human breath and skin emissions as suggested by Li et al.[49] in the case of NH_3. The reactivity with ozone present is highly driven by isoprene and 6MHO. Isoprene, as an endogenous breath compound, would be

more impacted by metabolism. However, exhaled isoprene levels can be affected by a number of variables as mentioned in section 3.3. Further experiments are needed to better define the influence of food intake on isoprene levels. Another limitation is the small number of subjects constituting the teenager and senior groups; this limited the power of statistical comparisons among the age groups.

Measuring the total OH reactivity is a novel method that supplements specific analytical methods used to measure individual species. This study demonstrates the application and feasibility of the OH reactivity measurement in indoor environments. Although no significant unattributed reactivity was observed with and without ozone, differences were observed in the contributions of various chemical species. This study focused on human emissions in the absence of personal care products; further studies are needed to quantify the effect of such products (e.g., fragrances or deodorants) on OH reactivity. Meanwhile, during periods of lower traffic intensity (e.g., weekends or holiday periods, or lockdowns), lower NOx emissions from vehicles may result in elevated ozone concentrations, especially in cities[69,70]. This can lead to higher indoor reactivity and potentially to increased exposure to reaction products derived from occupant generated compounds.

AUTHOR INFORMATION

Corresponding Author: Nijing Wang (nijing.wang@mpic.de) - Air chemistry department, Max Planck Institute for Chemistry, Hahn-Meitner-Weg 1, 55128, Mainz, Germany

Notes

The authors declare no competing financial interest.

ACKNOWLEDGMENTS

This study was funded by the Alfred P. Sloan Foundation (Grant Number G-2018-11233). We thank Dr. Sarka Langer for the support of NO/NO_x analyzer. We appreciate the participation of all volunteers.

References

1. Brasche, S.; Bischof, W., Daily time spent indoors in German homes – Baseline data for the assessment of indoor exposure of German occupants. *International Journal of Hygiene and Environmental Health* **2005,** *208*, (4), 247-253.

2. Leech, J. A.; Nelson, W. C.; Burnett, R. T.; Aaron, S.; Raizenne, M. E., It's about time: A comparison of Canadian and American time–activity patterns. *Journal of Exposure Science & Environmental Epidemiology* **2002,** *12*, (6), 427-432.

3. Moya, J.; Phillips, L.; Schuda, L.; Wood, P.; Diaz, A.; Lee, R.; Clickner, R.; Birch, R.; Adjei, N.; Blood, P., Exposure factors handbook: 2011 edition. *US Environmental Protection Agency* **2011**.

4. Duan, X., *Highlights of the Chinese exposure factors handbook*. Academic Press: **2015**.

5. Klepeis, N. E.; Nelson, W. C.; Ott, W. R.; Robinson, J. P.; Tsang, A. M.; Switzer, P.; Behar, J. V.; Hern, S. C.; Engelmann, W. H., The National Human Activity Pattern Survey (NHAPS): a resource for assessing exposure to environmental pollutants. *Journal of Exposure Science & Environmental Epidemiology* **2001,** *11*, (3), 231-252.

6. Salthammer, T.; Zhang, Y.; Mo, J.; Koch, H. M.; Weschler, C. J., Assessing Human Exposure to Organic Pollutants in the Indoor Environment. *Angew Chem Int Ed Engl* **2018,** *57*, (38), 12228-12263.

7. Bernstein, J. A.; Alexis, N.; Bacchus, H.; Bernstein, I. L.; Fritz, P.; Horner, E.; Li, N.; Mason, S.; Nel, A.; Oullette, J., The health effects of nonindustrial indoor air pollution. *Journal of Allergy and Clinical Immunology* **2008,** *121*, (3), 585-591.

8. Levin, H., Building materials and indoor air quality. *Occupational Medicine (Philadelphia, Pa.)* **1989,** *4*, (4), 667-693.

9. Hodgson, A. T.; Beal, D.; McIlvaine, J. E. R., Sources of formaldehyde, other aldehydes and terpenes in a new manufactured house. *Indoor Air* **2002,** *12*, (4), 235-242.

10. Weschler, C. J., Changes in indoor pollutants since the 1950s. *Atmospheric Environment* **2009,** *43*, (1), 153-169.

11. Nazaroff, W. W.; Weschler, C. J., Cleaning products and air fresheners: exposure to primary and secondary air pollutants. *Atmospheric Environment* **2004,** *38*, (18), 2841-2865.

12. Rudel, R. A.; Camann, D. E.; Spengler, J. D.; Korn, L. R.; Brody, J. G., Phthalates, Alkylphenols, Pesticides, Polybrominated Diphenyl Ethers, and Other Endocrine-Disrupting Compounds in Indoor Air and Dust. *Environmental Science & Technology* **2003,** *37*, (20), 4543-4553.

13. Hodgson, A. T.; Wooley, J. D.; Daisey, J. M., Emissions of volatile organic compounds from new carpets measured in a large-scale environmental chamber. *Air & Waste* **1993,** *43*, (3), 316-324.

14. de Lacy Costello, B.; Amann, A.; Al-Kateb, H.; Flynn, C.; Filipiak, W.; Khalid, T.; Osborne, D.; Ratcliffe, N. M., A review of the volatiles from the healthy human body. *J Breath Res* **2014,** *8*, (1), 014001.

15. Petrick, L.; Dubowski, Y., Heterogeneous oxidation of squalene film by ozone under various indoor conditions. *Indoor Air* **2009,** *19*, (5), 381-91.

16. Young, C. J.; Zhou, S.; Siegel, J. A.; Kahan, T. F., Illuminating the dark side of indoor oxidants. *Environ Sci Process Impacts* **2019,** *21*, (8), 1229-1239.

17. Weschler, C. J., Ozone in indoor environments: concentration and chemistry. *Indoor air* **2000,** *10*, (4), 269-288.

18. Abbatt, J. P. D.; Wang, C., The atmospheric chemistry of indoor environments. *Environ Sci Process Impacts* **2020,** *22*, (1), 25-48.

19. Weschler, C. J.; Carslaw, N., Indoor Chemistry. *Environ Sci Technol* **2018,** *52*, (5), 2419-2428.

20. Weschler, C. J.; Shields, H. C., Production of the hydroxyl radical in indoor air. *Environmental Science & Technology* **1996**, 30, (11), 3250-3258.21.

21. Weschler, C. J.; Shields, H. C., Measurements of the hydroxyl radical in a manipulated but realistic indoor environment. *Environmental Science & Technology* **1997**, 31, (12), 3719-3722.

22. White, I. R.; Martin, D.; Muñoz, M. P.; Petersson, F. K.; Henshaw, S. J.; Nickless, G.; Lloyd-Jones, G. C.; Clemitshaw, K. C.; Shallcross, D. E., Use of Reactive Tracers To Determine Ambient OH Radical Concentrations: Application within the Indoor Environment. *Environmental Science & Technology* **2010**, 44, (16), 6269-6274.

23. Gómez Alvarez, E.; Amedro, D.; Afif, C.; Gligorovski, S.; Schoemaecker, C.; Fittschen, C.; Doussin, J.-F.; Wortham, H., Unexpectedly high indoor hydroxyl radical concentrations associated with nitrous acid. *Proceedings of the National Academy of Sciences* **2013,** *110*, (33), 13294.

24. Carslaw, N.; Fletcher, L.; Heard, D.; Ingham, T.; Walker, H., Significant OH production under surface cleaning and air cleaning conditions: Impact on indoor air quality. *Indoor Air* **2017**, 27, (6), 1091-1100.

25. Yang, Y.; Shao, M.; Keßel, S.; Li, Y.; Lu, K.; Lu, S.; Williams, J.; Zhang, Y.; Zeng, L.; Nölscher, A. C.; Wu, Y.; Wang, X.; Zheng, J., How the OH reactivity affects the ozone production efficiency: case studies in Beijing and Heshan, China. *Atmos. Chem. Phys.* **2017,** *17*, (11), 7127-7142.

26. Nölscher, A. C.; Yanez-Serrano, A. M.; Wolff, S.; de Araujo, A. C.; Lavric, J. V.; Kesselmeier, J.; Williams, J., Unexpected seasonality in quantity and composition of Amazon rainforest air reactivity. *Nat Commun* **2016,** *7*, 10383.

27. Di Carlo, P.; Brune, W. H.; Martinez, M.; Harder, H.; Lesher, R.; Ren, X.; Thornberry, T.; Carroll, M. A.; Young, V.; Shepson, P. B.; Riemer, D.; Apel, E.; Campbell, C., Missing OH Reactivity in a Forest: Evidence for Unknown Reactive Biogenic VOCs. *Science* **2004,** *304*, (5671), 722.

28. Zannoni, N.; Gros, V.; Sarda Esteve, R.; Kalogridis, C.; Michoud, V.; Dusanter, S.; Sauvage, S.; Locoge, N.; Colomb, A.; Bonsang, B., Summertime OH reactivity from a receptor coastal site in the Mediterranean Basin. *Atmos. Chem. Phys.* **2017,** *17*, (20), 12645-12658.

29. Sinha, V.; Williams, J.; Crowley, J.; Lelieveld, J., The Comparative Reactivity Method–a new tool to measure total OH Reactivity in ambient air. *Atmospheric Chemistry and Physics* **2008,** *8*, (8), 2213-2227.

30. Pfannerstill, E. Y.; Wang, N.; Edtbauer, A.; Bourtsoukidis, E.; Crowley, J. N.; Dienhart, D.; Eger, P. G.; Ernle, L.; Fischer, H.; Hottmann, B.; Paris, J.-D.; Stönner, C.; Tadic, I.; Walter, D.; Lelieveld, J.; Williams, J., Shipborne measurements of total OH reactivity around the Arabian Peninsula and its role in ozone chemistry. *Atmospheric Chemistry and Physics* **2019,** *19*, (17), 11501-11523.

31. Zannoni, N.; Gros, V.; Lanza, M.; Sarda, R.; Bonsang, B.; Kalogridis, C.; Preunkert, S.; Legrand, M.; Jambert, C.; Boissard, C.; Lathiere, J., OH reactivity and concentrations of biogenic volatile organic compounds in a Mediterranean forest of downy oak trees. *Atmospheric Chemistry and Physics* **2016,** *16*, (3), 1619-1636.

32. Williams, J.; Keßel, S. U.; Nölscher, A. C.; Yang, Y.; Lee, Y.; Yáñez-Serrano, A. M.; Wolff, S.; Kesselmeier, J.; Klüpfel, T.; Lelieveld, J.; Shao, M., Opposite OH reactivity and ozone cycles in the Amazon rainforest and megacity Beijing: Subversion of biospheric oxidant control by anthropogenic emissions. *Atmospheric Environment* **2016,** *125*, 112-118.

33. Fuchs, H.; Novelli, A.; Rolletter, M.; Hofzumahaus, A.; Pfannerstill, E. Y.; Kessel, S.; Edtbauer, A.; Williams, J.; Michoud, V.; Dusanter, S.; Locoge, N.; Zannoni, N.; Gros, V.; Truong, F.; Sarda-Esteve, R.; Cryer, D. R.; Brumby, C. A.; Whalley, L. K.; Stone, D.; Seakins, P. W.; Heard, D. E.; Schoemaecker, C.; Blocquet, M.; Coudert, S.; Batut, S.; Fittschen, C.; Thames, A. B.; Brune, W. H.; Ernest, C.; Harder, H.; Muller, J. B. A.; Elste, T.; Kubistin, D.; Andres, S.; Bohn, B.; Hohaus, T.; Holland, F.; Li, X.; Rohrer, F.; Kiendler-Scharr, A.; Tillmann, R.; Wegener, R.; Yu, Z.; Zou, Q.; Wahner, A., Comparison of OH reactivity measurements in the atmospheric simulation chamber SAPHIR. *Atmospheric Measurement Techniques* **2017,** *10*, (10), 4023-4053.

34. Pagonis, D.; Price, D. J.; Algrim, L. B.; Day, D. A.; Handschy, A. V.; Stark, H.; Miller, S. L.; de Gouw, J.; Jimenez, J. L.; Ziemann, P. J., Time-Resolved Measurements of Indoor Chemical Emissions, Deposition, and Reactions in a University Art Museum. *Environ Sci Technol* **2019,** *53*, (9), 4794-4802.

35. Stonner, C.; Edtbauer, A.; Williams, J., Real-world volatile organic compound emission rates from seated adults and children for use in indoor air studies. *Indoor Air* **2017,** *28*, (1), 164-172.

36. Tang, X.; Misztal, P. K.; Nazaroff, W. W.; Goldstein, A. H., Volatile Organic Compound Emissions from Humans Indoors. *Environ Sci Technol* **2016,** *50*, (23), 12686-12694.

37. Wisthaler, A.; Weschler, C. J., Reactions of ozone with human skin lipids: sources of carbonyls, dicarbonyls, and hydroxycarbonyls in indoor air. *Proceedings of the National Academy of Sciences* **2010,** *107*, (15), 6568-6575.

38. Weschler, C. J.; Wisthaler, A.; Cowlin, S.; Tamás, G.; Strøm-Tejsen, P.; Hodgson, A. T.; Destaillats, H.; Herrington, J.; Zhang, J.; Nazaroff, W. W., Ozone-initiated chemistry in an occupied simulated aircraft cabin. *Environmental Science & Technology* **2007,** *41*, (17), 6177-6184.

39. Liu, S.; Li, R.; Wild, R. J.; Warneke, C.; de Gouw, J. A.; Brown, S. S.; Miller, S. L.; Luongo, J. C.; Jimenez, J. L.; Ziemann, P. J., Contribution of human-related sources to indoor volatile organic compounds in a university classroom. *Indoor Air* **2016,** *26*, (6), 925-938.

40. Price, D. J.; Day, D. A.; Pagonis, D.; Stark, H.; Algrim, L. B.; Handschy, A. V.; Liu, S.; Krechmer, J. E.; Miller, S. L.; Hunter, J. F.; de Gouw, J. A.; Ziemann, P. J.; Jimenez, J. L., Budgets of Organic Carbon Composition and Oxidation in Indoor Air. *Environ Sci Technol* **2019,** *53*, (22), 13053-13063.

41. Weschler, C. J., Ozone's Impact on Public Health: Contributions from Indoor Exposures to Ozone and Products of Ozone-Initiated Chemistry. *Environmental Health Perspectives* **2006,** *114*, (10), 1489-1496.

42. Bekö, G.; Wargocki, P.; Wang, N.; Li, M.; Weschler, C. J.; Morrison, G.; Langer, S.; Ernle, L.; Licina, D.; Yang, S.; Zannoni, N.; Williams, J., The Indoor Chemical Human Emissions and Reactivity project (ICHEAR): Overview of experimental methodology and preliminary results. *Indoor Air* **2020,** *00*, 1-16.

43. Michoud, V.; Hansen, R. F.; Locoge, N.; Stevens, P. S.; Dusanter, S., Detailed characterizations of the new Mines Douai comparative reactivity method instrument via laboratory experiments and modeling. *Atmospheric Measurement Techniques* **2015,** *8*, (8), 3537-3553.

44. Lindinger, W.; Hansel, A.; Jordan, A., On-line monitoring of volatile organic compounds at pptv levels by means of proton-transfer-reaction mass spectrometry (PTR-MS) medical applications, food control and environmental research. *International Journal of Mass Spectrometry and Ion Processes* **1998,** *173*, (3), 191-241.

45. Zhao, J.; Zhang, R., Proton transfer reaction rate constants between hydronium ion (H3O+) and volatile organic compounds. *Atmospheric Environment* **2004,** *38*, (14), 2177-2185.

46. Amelynck, C.; Schoon, N.; Kuppens, T.; Bultinck, P.; Arijs, E., A selected ion flow tube study of the reactions of H3O+, NO+ and O2+ with some oxygenated biogenic volatile organic compounds. *International Journal of Mass Spectrometry* **2005,** *247*, (1-3), 1-9.

47. Ruzsanyi, V.; Fischer, L.; Herbig, J.; Ager, C.; Amann, A., Multi-capillary-column proton-transfer-reaction time-of-flight mass spectrometry. *J Chromatogr A* **2013**, 1316, 112-8.

48. Bourtsoukidis, E.; Helleis, F.; Tomsche, L.; Fischer, H.; Hofmann, R.; Lelieveld, J.; Williams, J., An aircraft gas chromatograph–mass spectrometer System for Organic Fast Identification Analysis (SOFIA): design, performance and a case study of Asian monsoon pollution outflow. *Atmos. Meas. Tech.* **2017,** *10*, (12), 5089-5105.

49. Li, M.; Weschler, C. J.; Beko, G.; Wargocki, P.; Lucic, G.; Williams, J., Human ammonia emission rates under various indoor environmental conditions. *Environmental Science & Technology* **2020**, 54, (9), 5419-5428.

50. Yang, Y.; Shao, M.; Wang, X.; Nölscher, A. C.; Kessel, S.; Guenther, A.; Williams, J., Towards a quantitative understanding of total OH reactivity: A review. *Atmospheric Environment* **2016**, 134, 147-161.

51. Smith, A. M.; Rigler, E.; Kwok, E. S. C.; Atkinson, R., Kinetics and Products of the Gas-Phase Reactions of 6-Methyl-5-hepten-2-one and trans-Cinnamaldehyde with OH and NO3 Radicals and O3 at 296 ± 2 K. *Environmental Science & Technology* **1996,** *30*, (5), 1781-1785.

52. Atkinson, R.; Arey, J., Atmospheric Degradation of Volatile Organic Compounds. *Chemical Reviews* **2003,** *103*, (12), 4605-4638.

53. Fenske, J. D.; Paulson, S. E., Human breath emissions of VOCs. *J Air Waste Manag Assoc* **1999,** *49*, (5), 594-8.

54. Atkinson, R.; Baulch, D.; Cox, R.; Crowley, J.; Hampson, R.; Hynes, R.; Jenkin, M.; Rossi, M.; Troe, J., Evaluated kinetic and photochemical data for atmospheric chemistry: Volume I-gas phase reactions of Ox, HOx, NOx and SOx species. *Atmospheric chemistry and physics* **2004,** *4*, (6), 1461-1738.

55. Steinemann, A. C.; MacGregor, I. C.; Gordon, S. M.; Gallagher, L. G.; Davis, A. L.; Ribeiro, D. S.; Wallace, L. A., Fragranced consumer products: Chemicals emitted, ingredients unlisted. *Environmental Impact Assessment Review* **2011,** *31*, (3), 328-333.

56. Mochalski, P.; King, J.; Unterkofler, K.; Hinterhuber, H.; Amann, A., Emission rates of selected volatile organic compounds from skin of healthy volunteers. *J Chromatogr B Analyt Technol Biomed Life Sci* **2014,** *959*, 62-70.

57. Weschler, C. J., Roles of the human occupant in indoor chemistry. *Indoor Air* **2016,** *26*, (1), 6-24.

58. Wisthaler, A.; Tamás, G.; Wyon, D. P.; Strøm-Tejsen, P.; Space, D.; Beauchamp, J.; Hansel, A.; Märk, T. D.; Weschler, C. J., Products of ozone-initiated chemistry in a simulated aircraft environment. *Environmental Science & Technology* **2005,** *39*, (13), 4823-4832.

59. Waller, J. M.; Maibach, H. I., Age and skin structure and function, a quantitative approach (II): protein, glycosaminoglycan, water, and lipid content and structure. *Skin Research and Technology* **2006,** *12*, (3), 145-154.

60. Kushch, I.; Arendacka, B.; Stolc, S.; Mochalski, P.; Filipiak, W.; Schwarz, K.; Schwentner, L.; Schmid, A.; Dzien, A.; Lechleitner, M.; Witkovsky, V.; Miekisch, W.; Schubert, J.; Unterkofler, K.; Amann, A., Breath isoprene--aspects of normal physiology related to age, gender and cholesterol profile as determined in a proton transfer reaction mass spectrometry study. *Clin Chem Lab Med* **2008,** *46*, (7), 1011-8.

61. Lechner, M.; Moser, B.; Niederseer, D.; Karlseder, A.; Holzknecht, B.; Fuchs, M.; Colvin, S.; Tilg, H.; Rieder, J., Gender and age specific differences in exhaled isoprene levels. *Respir Physiol Neurobiol* **2006,** *154*, (3), 478-83.

62. Smith, D.; Španěl, P.; Enderby, B.; Lenney, W.; Turner, C.; Davies, S. J., Isoprene levels in the exhaled breath of 200 healthy pupils within the age range 7–18 years studied using SIFT-MS. *Journal of Breath Research* **2009,** *4*, (1), 017101.

63. Sukul, P.; Schubert, J. K.; Oertel, P.; Kamysek, S.; Taunk, K.; Trefz, P.; Miekisch, W., FEV manoeuvre induced changes in breath VOC compositions: an unconventional view on lung function tests. *Sci Rep* **2016,** *6*, 28029.

64. Schubert, R.; Schwoebel, H.; Mau-Moeller, A.; Behrens, M.; Fuchs, P.; Sklorz, M.; Schubert, J. K.; Bruhn, S.; Miekisch, W., Metabolic monitoring and assessment of anaerobic threshold by means of breath biomarkers. *Metabolomics* **2012,** *8*, (6), 1069-1080.

65. Haze, S.; Gozu, Y.; Nakamura, S.; Kohno, Y.; Sawano, K.; Ohta, H.; Yamazaki, K., 2-Nonenal newly found in human body odor tends to increase with aging. *J Invest Dermatol* **2001,** *116*, (4), 520-4.

66. Salvador, C. M.; Beko, G.; Weschler, C. J.; Morrison, G.; Le Breton, M.; Hallquist, M.; Ekberg, L.; Langer, S., Indoor ozone/human chemistry and ventilation strategies. *Indoor Air* **2019,** *29*, (6), 913-925.

67. Liu, X.; Deming, B.; Pagonis, D.; Day, D. A.; Palm, B. B.; Talukdar, R.; Roberts, J. M.; Veres, P. R.; Krechmer, J. E.; Thornton, J. A.; de Gouw, J. A.; Ziemann, P. J.; Jimenez, J. L., Effects of gas–wall interactions on measurements of semivolatile compounds and small polar molecules. *Atmospheric Measurement Techniques* **2019,** *12*, (6), 3137-3149.

68. Deming, B. L.; Pagonis, D.; Liu, X.; Day, D. A.; Talukdar, R.; Krechmer, J. E.; de Gouw, J. A.; Jimenez, J. L.; Ziemann, P. J., Measurements of delays of gas-phase compounds in a wide variety of tubing materials due to gas–wall interactions. *Atmospheric Measurement Techniques* **2019,** *12*, (6), 3453-3461.

69. Wang, L.; Li, M.; Yu, S.; Chen, X.; Li, Z.; Zhang, Y.; Jiang, L.; Xia, Y.; Li, J.; Liu, W.; Li, P.; Lichtfouse, E.; Rosenfeld, D.; Seinfeld, J. H., Unexpected rise of ozone in urban and rural areas, and sulfur dioxide in rural areas during the coronavirus city lockdown in Hangzhou, China: implications for air quality. Environmental Chemistry Letters 2020.

70. Sicard, P.; De Marco, A.; Agathokleous, E.; Feng, Z.; Xu, X.; Paoletti, E.; Rodriguez, J. J. D.; Calatayud, V., Amplified ozone pollution in cities during the COVID-19 lockdown. Sci Total Environ 2020, 735, 139542.

Supporting Information

Comparative reactivity method (CRM) operating procedures

The reference molecule used in CRM is pyrrole (C_4H_5N)[1], which reacts with OH radicals at comparable rates with reactive species and is not commonly presented in the measured air. Pyrrole can be sensitively detected by PTR-MS due to its higher proton affinity than water. For CRM, three measurement modes were implemented to quantify the total OH reactivity: (1) pyrrole together with an OH radical scavenger[2] was introduced to define the initial pyrrole level (C1 mode); (2) the OH radical scavenger was stopped and the level of pyrrole after reaction with OH radicals was recorded (C2 mode); (3) finally sample air from the chamber was introduced into the reactor with the pyrrole, the resulting competition for the available OH leading to a third pyrrole level (C3 mode). Based on these three modes, the total reactivity (R, s^{-1}) was calculated using the following equation:

$$R = \frac{(C3-C2)}{(C1-C3)} \cdot C1 \cdot k_{Pyrrol+OH}$$

where *C1*, *C2* and *C3* refer to previously mentioned pyrrole concentrations (molecules cm^{-3}) in the corresponding mode and $k_{Pyrrol+OH}$ refers to the rate constant of pyrrole reacting with OH radicals[3]. During an experiment, the OH reactivity measurement was switched between C2 mode and C3 mode every 5 minutes, and the C1 mode was usually measured at the end of the day. The pyrrole level measured by PTR-QMS was calibrated frequently using a gas standard (Westfalen AG, Germany).

Interference and corrections of OH reactivity data analysis

- **Pyrrole photolysis**

The pen ray mercury lamp used for water photolysis would also lead to pyrrole photolysis, which would complicate the system[1]. Therefore, the initial pyrrole level (C1) was determined when the lamp was on, which already considered the loss of pyrrole due to photolysis.

- **Humidity correction**

As the OH radical concentration is dependent on the water vapor inside the reactor, any difference in humidity between the C2 and C3 modes must also be taken into account. The humidity correction was done by humidifying the air flow of CRM at different degrees under C2 mode[1]. The humidity was monitored by the ratio of *m/z* 37 (water cluster) and *m/z*19 (primary ions). Then a correction factor can be derived from the slope of humidity vs. C2 pyrrole level, with an error of 29%. The correction factor was then applied to the C2 level during measurements to correct the humidity

difference between C2 mode and C3 mode. The correction of the C2 level was on average 0.06 ± 0.04 ppb, leading to a reactivity of 0.4 ± 0.2 s^{-1}.

- **Correction factor for not being at pseudo-first-order conditions**

Equation (1), used to derive the OH reactivity, is based on the assumption of pseudo-first-order conditions. These conditions cannot be entirely fulfilled under normal operating conditions when maintaining a reasonable sensitivity. Therefore, a correction factor was applied as a function of the pyrrole/OH ratios. The method used to derive the correction factor is based on Michoud, et al. [4]. The correction factor was obtained from injecting known amount of a standard gas under different pyrrole/OH ratios conditions. A factor can be obtained from measured reactivity vs. calculated reactivity for that gas. Total of five standard gases with different rate constants reacting with the OH radical including propane, propene, isoprene, α-pinene and acetaldehyde were tested within the pyrrole/OH range observed during the entire campaign. A linear fit was applied among all the factors derived from the tests, resulting in a linear relationship between the correction factor and pyrrole/OH ratio (f = a[pyrrole/OH]+b), with an error of 31%. Throughout the campaign, the pyrrole/OH ratio ranged from 2.0 - 3.0, which increased the OH reactivity by a factor of 1.3 to 2.7.

- **NO_x interference**

Previous studies have also shown that NO_x can potentially cause an interference to CRM measurements by producing OH radicals via reactions with HO_2 radicals. Relevant corrections should be applied if the measured conditions have abundant NO_x (NO > 10ppb[1]) and it should be noted that NO has a more significant interference compared to NO_2 at the same level[4-6]. NO and NO_2 were continuously monitored by a chemiluminescence NO/NO_x analyzer (ECO PHYSICS, model CLD 700 AL). The mixing ratios of NO and NO_2 in the occupied chamber were near or below the detection limit (1 ppb) for most of the time during the entire experimental period. By taking into account the dilution factor of the CRM (1.37), NO and NO_2 levels in the glass reactor would be lower than the detection limit most of the time. Therefore, NO_x interference to the CRM could be neglected and no correction was applied. NO and NO_2 have OH rate constants comparable to some VOCs shown in Table S1 (9.70×10^{-12} cm^3 $molecules^{-1}$ s^{-1} and 9.80×10^{-12} cm^3 $molecules^{-1}$ s^{-1} for NO and NO_2, respectively[7]). The upper limit of the NO_x contribution to the total reactivity (assuming 2 ppb of NO or NO_2) would be 0.5 s^{-1} (3.0% of the total reactivity under ozone-free condition and 1.5% under ozone-present condition). This is comparable to some top ten OH reactivity contributing species (Table 2). The NOx data were mostly at or below the detection limit and no clear trend can be observed due to human occupancy; the 2 ppb of NOx assumption represents an upper limit estimate rather than a measurement. Therefore, NOx was not included in the calculation of OH reactivity in the study.

- **Ozone interference**

High level of ozone was also found to cause interference depending on the CRM system[5]. For ozone interference test, different levels of ozone (0 -110 ppb) was introduced to the empty chamber. The measured OH reactivity interference due to ozone was less than 3 s^{-1} at the highest ozone level, which is lower than the limit of detection for CRM during this campaign (5 s^{-1}). The ozone level in the chamber during the afternoon steady state when occupied was around 37 ppb, resulting in 1 s^{-1} difference in the measured reactivity which was much smaller than the total uncertainty of the measured reactivity (16 – 22 s^{-1}). As the ozone interference is negligible and extra uncertainty would be introduced from the correction factor, no correction was applied.

Calculations of precision and total uncertainty of CRM

When a test gas is injected into the CRM at several known concentrations, the corresponding mean reactivity at each concentration can be obtained together with the standard deviation. By plotting the relative reactivity (standard deviation/mean reactivity, $R_{relative}$) against the mean reactivity ($R_{measured}$), an exponential curve is obtained that can be fit with the equation:

$$R_{relative} = a + b * \exp(c * R_{measured})$$

where parameters a, b and c are derived from curve fitting and the relative reactivity defines the precision. For this study, results from test gases mentioned in "Correction factor for not being at pseudo-first-order conditions" were included to derive the fitting results. Based on the measured reactivity of real measurements, the precision can be calculated by applying this equation to each data point.

The accuracy of the CRM is the propagation of uncertainties from the pyrrole standard gas concentration, the dilution factors derived from flow measurements, the OH rate constant of pyrrole, the humidity correction, and the non-pseudo-first-order correction. Detailed numbers can be found in Table S5.1.

Table S5.1 Uncertainties in the CRM

Uncertainties from	**Uncertainties (%)**
Pyrrole standard gas	10
Dilution factors	0.16
OH rate constant of pyrrole	14
Humidity correction	29
Non-pseudo-first-order correction	31
Propagated accuracy	46
Total uncertainty (mean and median)	50

Empty-chamber background

The background obtained from the empty chamber before volunteers entered was in general very stable for calculated reactivity (3 s^{-1} on average with a variability of 10%). For measured total reactivity, the background was typically around or under the detection limit (5 s^{-1}).

Definition of steady-state condition

As the calculated reactivity has less uncertainty than measured reactivity, the steady-state condition was verified by the relative change of calculated reactivity during the 15 minutes before volunteers exited the chamber. This is to avoid any effect left due to requested movements by the volunteers (standing up and stretching) every hour during each experimental period. For all the experiments, the relative changes ((max-min)/mean) were below 5% (0.8-5.0%, mean 2.1%), which is much less than the uncertainty of the calculated OH reactivity (21% - 45%, median and mean 29%). Therefore, the time period of 15 minutes is suitable to be considered as steady-state condition.

Adjustment method applied for OH reactivity per person comparison

To be able to compare the OH reactivity per person ($s^{-1}p^{-1}$) in the ICHEAR chamber experiments with other studies, the OH reactivity per person obtained from other studies were adjusted for the room volume and the air change rate (ACR) applied in the ICHEAR chamber experiments using the following equations:

$$RP_a = \frac{Room\ volume\ (other\ studies)}{22.5\ m^3} \times \frac{ACR\ (other\ studies)}{3.2\ h^{-1}} \times RP_b$$

where RP_a refers to the OH reactivity per person after the adjustment and RP_b refers to the OH reactivity per person before the adjustment, which is obtained from the total OH reactivity divided by the number of occupants in that environment. 22.5 m^3 is the ICHEAR chamber volume and 3.2 h^{-1} is the ACR for the chamber. The per-person OH reactivity before the adjustment (RP_b) for the other studies mentioned in Table 3 were estimated using reported values. For the museum gallery room study[70], RP_b is derived from the incremental total OH reactivity (14 s^{-1}) during the high occupancy event (compared to the low occupancy condition) divided by the number of occupants (176 on average). For the classroom study[71] and cinema study[72], the RP_b was calculated based on the VOC emission rates (μg $h^{-1}p^{-1}$) reported in each work. As both studies used PTR-ToF-MS, some masses could only be assigned to chemical formulas instead of specific compounds. Therefore, we only included masses with specific compound assignments reported in those two studies to calculate the total OH reactivity per person. Those included VOCs were mostly measured during the present experiments as well. The emission rates were first converted to mixing ratios per person (ppb p^{-1}) based on the indoor space volume and the ACR reported in each study. Then

the total OH reactivity per person was calculated using Eq.5.1 in the main text. The estimated RP_b of those two studies may slightly underestimate the actual values as those masses without a specific compound assignment (accounting for < 20% of the total VOC emission rates) were not included in the calculation.

Potential artifacts from decomposition of hydroperoxides

It has been reported that metal surface can act as a catalyst for the decomposition of organic hydroperoxides, and that this is temperature dependent.[73] It has been further reported that with stainless tubing, the conversion rates for ISOPOOH to formaldehyde at room temperature were not significant (below 10%) but increased to 50% at 160 °C[73]. As the temperature in the ICHEAR chamber study was always less than ~ 31°C, this artifact on the stainless-steel chamber walls is not anticipated to be important. However, for the PTR-ToF-MS instrument, this interference may still exist as the drift tube was heated to 60 °C, converting a small amount of ISOPOOH to other products. Another important factor to consider is that in the ICHEAR chamber study, the main oxidant was ozone instead of OH radicals (which are the major oxidant outdoors). MVK and MACR, rather than ISOPOOH, are the major products of isoprene ozonolysis[74]. Furthermore, the reaction between ozone and isoprene is relatively slow (1.1×10^{-3} ppb/h at 298 K)[7]; at the average ozone concentration (37 ppb) used in ICHEAR, the O_3/isoprene reaction occurs at a rate ($0.04\ h^{-1}$) substantially slower than the air change rate ($3.2\ h^{-1}$). Hence, production of ISOPOOH via ozone reaction was quite small in ICHEAR. The formation of ISOPOOH, to the extent that it occurred in ICHEAR, was probably from isoprene/OH oxidation as OH radicals can be generated during the ozonolysis of unsaturated compounds. Assuming the extreme scenario that measured MVK/MACR were half decomposed from ISOPOOH, it would increase the calculated reactivity during ozone-present condition by $0.6\ s^{-1}$ as ISOPOOH has a faster reaction rate constant compared to MVK/MACR ($9.65 \times 10^{-11}\ cm^3\ molecules^{-1}\ s^{-1}$, averaged of (1,2)-ISOPOOH and (4,3)-ISOPOOH)[75]. The calculated increase of $0.6\ s^{-1}$ is within the standard deviation of the total calculated reactivity ($1.4\ s^{-1}$). Therefore, we judge that the interference should be small. In terms of reactivity measurement, as the PTR-QMS measured the air coming out of the glass reactor and temperature inside the reactor was around 35-40 °C, there should be no interference.

Table S5.2. List of compounds used in calculating the estimated OH reactivity.

Compound group	Protonated *m/z* from PTR-MS	Formula assignment	Possible compound assignment	k_{Xi+OH} (cm^3 $molecules^{-1}$ s^{-1}) at 298K*	Remarks**	Reference
Hydrocarbons (HC)		C5H8	isoprene	1.00×10^{-10}	Data from fast-GC	7 (IUPAC)
	79.053	C6H6	benzene	1.20×10^{-12}	PTR calibrated	7 (IUPAC)
	93.070	C7H8	toluene	5.60×10^{-12}	PTR calibrated	7 (IUPAC)
	105.070	C8H8	styrene	5.80×10^{-11}		8
	107.086	C8H10	xylene	1.70×10^{-11} (1.36 -2.31) $\times 10^{-11}$	PTR calibrated; k rate averaged from listed isomeric compounds	8
	119.086	C9H10	2-phenylpropene	5.30×10^{-11}		9
	121.101	C9H12	trimethylbenzene	4.06×10^{-11} (3.25 -5.67) $\times 10^{-11}$	PTR calibrated; k rate averaged from listed isomeric compounds	8
	133.101	C10H12	benzene,(2-methyl-1-propenyl)-	3.30×10^{-11}		9
	137.132	C10H16	monoterpenes	1.64×10^{-10}	PTR calibrated using α-pinene; k rate of limonene was taken	7 (IUPAC)
OVOC Alcohols	33.034	CH4O	methanol	9.00×10^{-13}	PTR calibrated	7 (IUPAC)
	47.049	C2H6O	ethanol	3.20×10^{-12}		7 (IUPAC)
OVOC Acids	43.018 61.029	C2H4O2	acetic acid	8.00×10^{-13}		10
	73.029	C3H4O2	acrylic acid	1.75×10^{-11}		11
	89.023	C3H4O3	pyruvic acid	1.24×10^{-13}		12
OVOC Aromatics	95.049	C6H6O	phenol	3.27×10^{-11}		13
	107.049	C7H6O	benzaldehyde	1.20×10^{-11}		7 (IUPAC)
	109.029	C6H4O2	1,4-benzoquinone	4.60×10^{-12}		14
	109.065	C7H8O	methylphenol/methoxybenzene/toluene-1,2-oxide 3/2-methyloxepin	7.74×10^{-11} (2.54 -21.0) $\times 10^{-11}$	k rate averaged from listed isomeric compounds	15-17

OVOC Aromatics	121.065	C8H8O	tolualdehyde	1.60×10^{-11}		8
	123.044	C7H6O2	p-benzoquinone, 2-methyl-	2.35×10^{-11}		14
	123.081	C8H10O	dimethylphenol	8.48×10^{-11}		16
	125.060	C7H8O2	4-methoxyphenol /3-methoxyphenol/2-methoxyphenol	8.94×10^{-11} ($7.44\text{-}9.80) \times 10^{-11}$	k rate averaged from listed isomeric compounds	16
	135.081	C9H10O	dimethylbenzaldehyde	2.74×10^{-11} ($2.46\text{-}3.70) \times 10^{-11}$	k rate averaged from listed isomeric compounds	18
	137.060	C8H8O2	1,4-benzodioxane	2.52×10^{-11}		19
	149.096	C10H12O	2,4,5-trimethylbenzaldehyde	4.27×10^{-11}		20
OVOC Carbonyls	31.018	CH2O	formaldehyde	9.37×10^{-12}		8
	45.033	C2H4O	acetaldehyde	1.50×10^{-11}	PTR calibrated	7 (IUPAC)
	57.034	C3H4O	acrolein	2.00×10^{-11}		21
	59.048	C3H6O	acetone	1.80×10^{-13}	PTR calibrated	7 (IUPAC)
	71.048	C4H6O	methyl vinyl ketone (MVK)/methacrolein (MACR)/isoprene hydroxy hydroperoxide (ISOPOOH)	2.45×10^{-11} ($2.0\text{ -}2.9) \times 10^{-11}$	PTR calibrated; k rate averaged from MVK and MACR	7 (IUPAC)
	73.064	C4H8O	methyl ethyl ketone	1.10×10^{-12}	PTR calibrated	7 (IUPAC)
	75.044	C3H6O2	hydroxyacetone	3.00×10^{-12}		22
	83.049	C5H6O	4-oxopentanal fragment; methylfuran	2.00×10^{-11}	k rate of 4OPA was taken	23
	85.028	C4H4O2	butenedial	5.21×10^{-11}		24
	85.065	C5H8O	2-pentenal	4.37×10^{-11}		25
	87.044	C4H6O2	1,4-butanedial	5.70×10^{-11}	k rate of 4-hydroxy-2-butenal was taken	26
	87.081	C5H10O	pentanal	2.80×10^{-11}		8
	97.020	C5H4O2	2 or 3-furancarboxaldehyde	4.18×10^{-11} ($3.50\text{-}4.85) \times 10^{-11}$	k rate averaged from listed isomeric compounds	27
	97.065	C6H8O	2,4-hexadienal	5.90×10^{-11}		28
	99.045	C5H6O2	4-oxo-2-pentenal	5.58×10^{-11}		24

OVOC Carbonyls	99.081	C6H10O	cis-3-hexenal; (2e)-2-hexenal; 2-pentenal, 2-methyl-	4.64×10^{-11} $(3.93 - 6.60) \times 10^{-11}$	k rate averaged from listed isomeric compounds	29-31
	101.060	C5H8O2	4-oxopentanal (4-OPA)	2.00×10^{-11}		23
	101.096	C6H12O	hexanal	3.00×10^{-11}		8
	103.075	C5H10O2	1-hydroxy-2-methyl-3-butanone	1.62×10^{-11}		32
	109.101 127.112	C8H14O	6-methyl-5-hepten-2-one (6-MHO)	1.57×10^{-10}		33
	111.081	C7H10O	4-methylenehex-5-enal/(3z)-4-methylhexa-3,5-dienal/(3e)-4-methylhexa-3,5-dienal/4-methylcyclohex-3-en-1-one	1.69×10^{-10} $(1.10 - 3.10) \times 10^{-10}$	k rate averaged from listed isomeric compounds	34
	113.096	C7H12O	(e)-2-hepten-1-al	4.39×10^{-11}		25
	115.112	C7H14O	2, 3-dimethylpentanal; heptanal	3.20×10^{-11} $(2.96 - 4.20) \times 10^{-11}$	k rate averaged from listed isomeric compounds	35, 36
	127.076	C7H10O2	3-methyl-3-hexene-2,5-dione	9.40×10^{-11}		20
	129.127	C8H16O	octanal	3.00×10^{-11}	k rate estimated, same as hexanal	
	139.112	C9H14O	bicyclo[2.2.1]heptan-2-one,3,3-dimethyl-/sabinaketone/ bicyclo[3.1.1]heptan-2-one, 6,6-dimethyl-	8.85×10^{-12} $(5.15 - 14.3) \times 10^{-12}$	k rate averaged from listed isomeric compounds	37, 38
	123.117 141.127	C9H16O	trans-2-nonenal	4.35×10^{-11}		30
	125.132 143.143	C9H18O	nonanal	3.60×10^{-11}		39
	153.127	C10H16O	camphor	3.80×10^{-12}		40
	155.154	C10H18O	geraniol; citronellal	1.90×10^{-10} $(1.50 - 2.31) \times 10^{-10}$	k rate averaged from listed isomeric compounds	41, 42

OVOC Carbonyls	137.097 155.107	C9H14O2	4-methyl-4-octene-1,8-dial (4-MOD)	1.57×10^{-10}	k rate estimated, same as 6-MHO	
	139.148 157.159	C10H20O	C10 aliphatic carbonyls (decanal)	3.60×10^{-11}	k rate estimated, same as nonanal	
	151.112 169.123	C10H16O2	4-methyl-8-oxo-noennal (4-MON)	1.57×10^{-10}	k rate estimated, same as 6-MHO	
	171.175	C11H22O	C11 aliphatic carbonyls (undecanal)	3.60×10^{-11}	k rate estimated, same as nonanal	
	177.164 195.175	C13H22O	geranyl acetone	1.57×10^{-10}	k rate estimated, same as 6-MHO	
		C3H6O	propanal	2.00×10^{-11}	Data from fast-GC	7 (IUPAC)
OVOC others	69.034	C4H4O	furan	4.04×10^{-11}		43
	89.060	C4H8O2	acetic acid, ethyl ester; formic acid, 1-methylethyl ester	2.04×10^{-12} $(1.69 - 2.4) \times 10^{-12}$	k rate averaged from listed isomeric compounds	44, 45
	111.044	C6H6O2	aromatic phenol/e,z- and e,e-2,4-hexadienedial/2-furancarbocaldehyde, 5-methyl-/1,2-dihydroxybenzene/1,4-benzenediol/1,3-benzenediol	5.19×10^{-11} $(0.44 - 10.3) \times 10^{-11}$	k rate averaged from listed isomeric compounds	14, 46, 47
	113.060	C5H10O2	formic acid, tert-butyl ester/butanoic acid, methyl ester/formic acid, butyl ester/propanoic acid, 2-methyl-, methyl ester/	2.63×10^{-12} $(0.68 - 3.82) \times 10^{-12}$	k rate averaged from listed isomeric compounds	48-52
	115.075	C6H10O2	ethyl crotonate/3-methyl-2,4-pentanedione/2,5-hexanedione/methacrylic acid ethyl ester	3.25×10^{-11} $(0.67 - 4.96) \times 10^{-11}$	k rate averaged from listed isomeric compounds	53-56

OVOC others	117.091	C6H12O2	butanoic acid, 2-methyl-, methyl ester/methyl valerate/acetic acid, butyl ester/isobutyl acetate/propanoic acid, propyl ester/butanoic acid, ethyl ester	4.17×10^{-12} $(0.56\text{ -}6.33) \times 10^{-12}$	k rate averaged from listed isomeric compounds	48, 49, 52, 57-59
	129.091	C7H12O2	n-butyl acrylate/4-pentenyl acetate	3.28×10^{-11} $(2.28\text{ -}4.33) \times 10^{-11}$	k rate averaged from listed isomeric compounds	60, 61
	143.107	C8H14O2	1-hydroxy-6-methyl-5-hepten-2-one (OH-6MHO)	6.60×10^{-11}	k rate of butyl methacrylate was taken	60
Nitrogen containing	42.033	C2H3N	acetonitrile	2.20×10^{-14}	PTR calibrated	7 (IUPAC)
		NH3	ammonia	1.57×10^{-13}	Data from Picarro	7 (IUPAC)
	46.029	CH3NO	formamide/formaldoxime	2.97×10^{-12} $(1.50\text{ -}4.44) \times 10^{-12}$	k rate averaged from listed isomeric compounds	62, 63
	70.065	C4H7N	butyronitrile	2.56×10^{-13}		64
	74.024	C2H3NO2	nitroethene	1.20×10^{-12}		65
Sulfur containing	49.011	CH4S	methanethiol	3.30×10^{-11}		7 (IUPAC)
	63.026	C2H6S	dimethyl sulfide	4.80×10^{-12}	PTR calibrated	7 (IUPAC)
	91.057	C4H10S	tert-butylthiol; 2-butanethiol; 1-propanethiol, 2-methyl-; 1-butanethiol;	4.22×10^{-11} $(2.91\text{ -}5.60) \times 10^{-11}$	k rate averaged from listed isomeric compounds	66
	95.016	C2H6O2S	dimethyl sulfone	3.00×10^{-13}		67

IUPAC: preferred values recommend by IUPAC were taken.

* rate constant ranges listed in parentheses refer to the range of rate constants of listed isomeric compounds.

**Compounds without mentioning as “PTR calibrated”, “fast-GC” nor “Piccaro” refer to the mixing ratios of species measured by PTR-ToF-MS were calculated based on theoretic method using a constant rate coefficient (2.0E-9 cm^3s^{-1}) for the reactions with H_3O^+ [68], except for 6-MHO where a known rate coefficient (3.8E-9 cm^3s^{-1}) was used [69].

Table S5.3. Top ten species contributing to the calculated OH reactivity of breath emissions (Experiment 12, adult group A3) under ozone-free and ozone-present conditions.

	Mass (H^+)	Compounds	OH Reactivity (s^{-1})	Fraction
Ozone-free	*	isoprene	11.9	95.3%
	33.034	methanol	0.15	1.2%
	137.132	limonene	0.09	0.7%
	59.048	acetone	0.08	0.6%
	69.034	furan	0.04	0.3%
	61.029	acetic acid	0.04	0.3%
	87.044	1,4-butanedial	0.03	0.2%
	127.112	6MHO	0.02	0.2%
	91.057	C4H10S	0.02	0.2%
	63.026	DMS	0.01	0.1%
		Sum of top 10 species	**12.3**	**99.1%**
		Sum of all species	**12.5**	
Ozone-present	*	isoprene	11.2	82.5%
	87.044	1,4-butanedial	0.5	3.4%
	101.096	4OPA	0.3	2.0%
	45.034	acetaldehyde	0.2	1.5%
	127.112	6MHO	0.1	0.9%
	*	propanal	0.1	0.9%
	71.049	C4H6O	0.1	0.8%
	33.034	methanol	0.1	0.8%
	69.034	furan	0.1	0.7%
	61.029	acetic acid	0.1	0.7%
		Sum of top 10 species	**12.8**	**94.3%**
		Sum of all species	**13.5**	

*isoprene and propanal data were obtained from fast-GC

Table S5.4. Top ten species contributing to the calculated OH reactivity of dermal emissions (Experiment 13, adult group A3) under ozone-free and ozone-present conditions.

	Mass (H^+)	Compounds	OH Reactivity (s^{-1})	Fraction
Ozone-free	45.034	acetaldehyde	0.7	15.1%
	69.070	isoprene	0.3	7.2%
	127.112	6MHO	0.3	7.0%
	95.049	phenol	0.3	6.6%
	137.133	limonene	0.3	6.3%
	#	ammonia	0.2	4.6%
	121.065	tolualdehyde	0.2	4.5%
	91.057	C4H10S	0.2	4.3%
	87.044	1,4-butanedial	0.2	4.1%
	71.049	C4H6O	0.2	3.8%
		Sum of top 10 species	**2.9**	**63.4%**
		Sum of all species	**4.6**	
Ozone-present	127.112	6MHO	13.2	41.8%
	101.096	4OPA	3.6	11.3%
	87.044	1,4-butanedial	1.5	4.6%
	45.034	acetaldehyde	1.3	4.1%
	157.159	decanal	0.7	2.3%
	143.143	nonanal	0.7	2.3%
	141.127	nonenal	0.7	2.2%
	143.107	OH-6MHO	0.7	2.2%
	137.133	limonene	0.6	2.0%
	195.186	geranal acetone	0.5	1.7%
		Sum of top 10 species	**23.5**	**74.5%**
		Sum of all species	**31.5**	

#ammonia data was from Picarro.

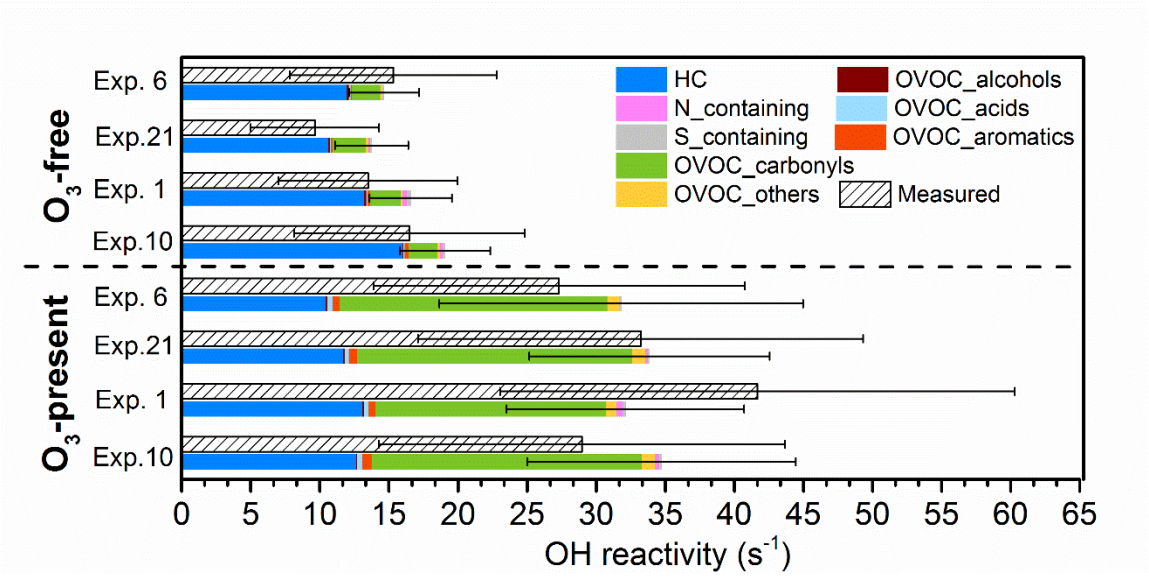

Figure S5.1. Calculated and measured OH reactivity during ozone-free and ozone-present steady-state conditions of the benchmark experiments with young adults. Error bars represent the total uncertainty of measured OH reactivity and calculated OH reactivity. Experiment 21 is a replicate of Experiment 6.

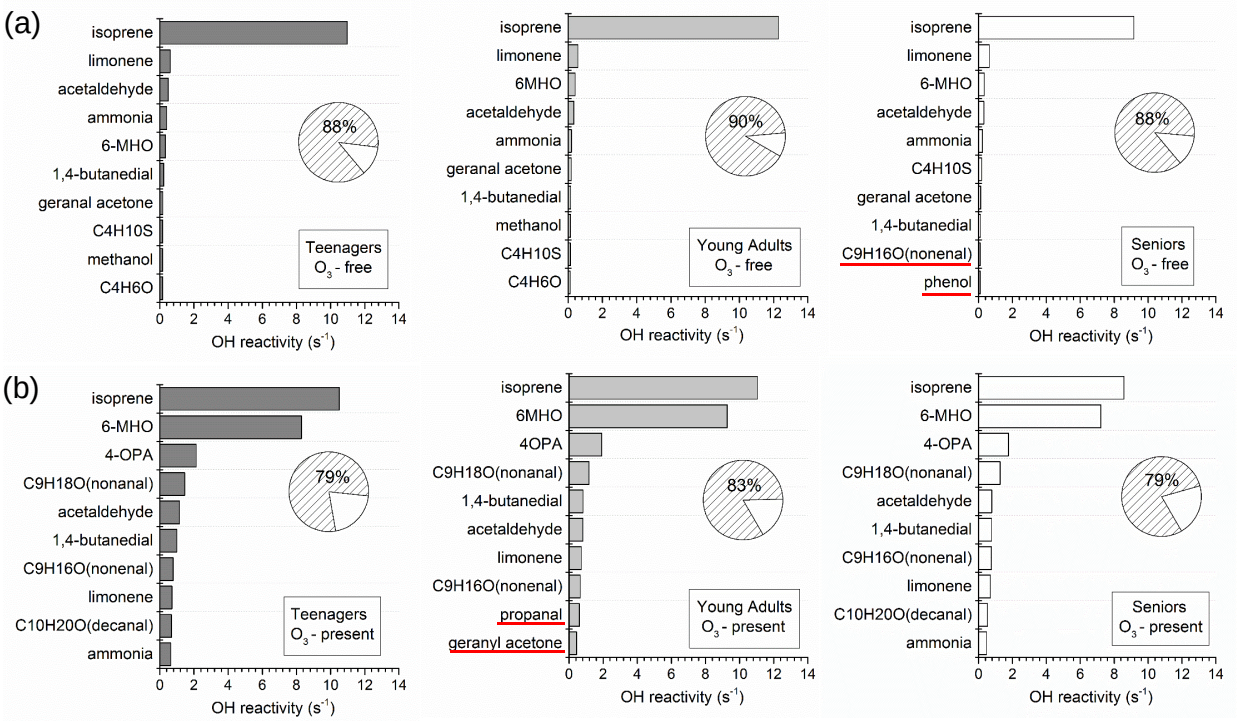

Figure S5.2. Top ten species contributing to the total OH reactivity for teenagers, young adults and seniors under (a) ozone-free condition and (b) ozone-present condition. The species marked with red underline represent unique species that do not appear among the top ten species of the other two groups. The pie chart in each plot represents the fractions of the total reactivity attributable to the top ten species (hatched) and remaining species (blank).

References

1. Sinha, V.; Williams, J.; Crowley, J.; Lelieveld, J., The Comparative Reactivity Method–a new tool to measure total OH Reactivity in ambient air. *Atmospheric Chemistry and Physics* **2008,** *8*, (8), 2213-2227.

2. Zannoni, N.; Dusanter, S.; Gros, V.; Sarda Esteve, R.; Michoud, V.; Sinha, V.; Locoge, N.; Bonsang, B., Intercomparison of two comparative reactivity method instruments inf the Mediterranean basin during summer 2013. *Atmospheric Measurement Techniques* **2015,** *8*, (9), 3851-3865.

3. Dillon, T. J.; Tucceri, M. E.; Dulitz, K.; Horowitz, A.; Vereecken, L.; Crowley, J. N., Reaction of Hydroxyl Radicals with C4H5N (Pyrrole): Temperature and Pressure Dependent Rate Coefficients. *The Journal of Physical Chemistry A* **2012,** *116*, (24), 6051-6058.

4. Michoud, V.; Hansen, R. F.; Locoge, N.; Stevens, P. S.; Dusanter, S., Detailed characterizations of the new Mines Douai comparative reactivity method instrument via laboratory experiments and modeling. *Atmospheric Measurement Techniques* **2015,** *8*, (8), 3537-3553.

5. Fuchs, H.; Novelli, A.; Rolletter, M.; Hofzumahaus, A.; Pfannerstill, E. Y.; Kessel, S.; Edtbauer, A.; Williams, J.; Michoud, V.; Dusanter, S.; Locoge, N.; Zannoni, N.; Gros, V.; Truong, F.; Sarda-Esteve, R.; Cryer, D. R.; Brumby, C. A.; Whalley, L. K.; Stone, D.; Seakins, P. W.; Heard, D. E.; Schoemaecker, C.; Blocquet, M.; Coudert, S.; Batut, S.; Fittschen, C.; Thames, A. B.; Brune, W. H.; Ernest, C.; Harder, H.; Muller, J. B. A.; Elste, T.; Kubistin, D.; Andres, S.; Bohn, B.; Hohaus, T.; Holland, F.; Li, X.; Rohrer, F.; Kiendler-Scharr, A.; Tillmann, R.; Wegener, R.; Yu, Z.; Zou, Q.; Wahner, A., Comparison of OH reactivity measurements in the atmospheric simulation chamber SAPHIR. *Atmospheric Measurement Techniques* **2017,** *10*, (10), 4023-4053.

6. Pfannerstill, E. Y.; Wang, N.; Edtbauer, A.; Bourtsoukidis, E.; Crowley, J. N.; Dienhart, D.; Eger, P. G.; Ernle, L.; Fischer, H.; Hottmann, B.; Paris, J.-D.; Stönner, C.; Tadic, I.; Walter, D.; Lelieveld, J.; Williams, J., Shipborne measurements of total OH reactivity around the Arabian Peninsula and its role in ozone chemistry. *Atmospheric Chemistry and Physics* **2019,** *19*, (17), 11501-11523.

7. IUPAC Task Group on Atmospheric Chemical Kinetic Data Evaluation: Datasheets - gas phase: http://iupac.pole-ether.fr/

8. Atkinson, R.; Arey, J., Atmospheric Degradation of Volatile Organic Compounds. *Chemical Reviews* **2003,** *103*, (12), 4605-4638.

9. Chiorboli, C.; Maldotti, A.; Bignozzian, C.; Carassitik, V. Atmospheric photochemistry: kinetics and mechanism of reactions between aromatic olefins and hydroxyl radical, *Proceedings of the Second European Symposium on Physico-Chemical Behaviour of Atmospheric Pollutants (conference)*, ***1981***, pp 228-233.

10. Atkinson, R.; Baulch, D.; Cox, R.; Crowley, J.; Hampson Jr, R.; Kerr, J.; Rossi, M.; Troe, J., Summary of evaluated kinetic and photochemical data for atmospheric chemistry. *IUPAC Subcommittee on gas kinetic data evaluation for atmospheric chemistry* **2001,** *20*.

11. Teruel, M. A.; Blanco, M. B.; Luque, G. R., Atmospheric fate of acrylic acid and acrylonitrile: rate constants with Cl atoms and OH radicals in the gas phase. *Atmospheric Environment* **2007,** *41*, (27), 5769-5777.

12. Mellouki, A.; Mu, Y., On the atmospheric degradation of pyruvic acid in the gas phase. *Journal of Photochemistry and Photobiology A: Chemistry* **2003,** *157*, (2-3), 295-300.

13. Sørensen, M.; Hurley, M.; Wallington, T.; Dibble, T.; Nielsen, O., Do aerosols act as catalysts in the OH radical initiated atmospheric oxidation of volatile organic compounds? *Atmospheric Environment* **2002,** *36*, (39-40), 5947-5952.

14. Olariu, R. I.; Barnes, I.; Becker, K. H.; Klotz, B., Rate coefficients for the gas-phase reaction of OH radicals with selected dihydroxybenzenes and benzoquinones. *International Journal of Chemical Kinetics* **2000,** *32*, (11), 696-702.

15. Coeur-Tourneur, C.; Henry, F.; Janquin, M.-A.; Brutier, L., Gas-phase reaction of hydroxyl radicals with m-, o- and p-cresol. *International Journal of Chemical Kinetics* **2006,** *38*, (9), 553-562.

16. Coeur-Tourneur, C.; Cassez, A.; Wenger, J. C., Rate Coefficients for the Gas-Phase Reaction of Hydroxyl Radicals with 2-Methoxyphenol (Guaiacol) and Related Compounds. *The Journal of Physical Chemistry A* **2010,** *114*, (43), 11645-11650.

17. Klotz, B.; Barnes, I.; Golding, B. T.; Becker, K.-H., Atmospheric chemistry of toluene-1,2-oxide/2-methyloxepin. *Physical Chemistry Chemical Physics* **2000,** *2*, (2), 227-235.

18. Clifford, G. M.; Wenger, J. C., Rate coefficients for the gas-phase reaction of hydroxyl radicals with the dimethylbenzaldehydes. *International journal of chemical kinetics* **2006,** *38*, (9), 563-569.

19. Atkinson, R.; Arey, J.; Tuazon, E. C.; Aschmann, S. M., Gas-phase reactions of 1, 4-benzodioxan, 2, 3-dihydrobenzofuran, and 2, 3-benzofuran with OH radicals and O3. *International journal of chemical kinetics* **1992,** *24*, (4), 345-358.

20. Aschmann, S. M.; Arey, J.; Atkinson, R., Rate Constants for the Reactions of OH Radicals with 1,2,4,5-Tetramethylbenzene, Pentamethylbenzene, 2,4,5-Trimethylbenzaldehyde, 2,4,5-Trimethylphenol, and 3-Methyl-3-hexene-2,5-dione and Products of OH + 1,2,4,5-Tetramethylbenzene. *The Journal of Physical Chemistry A* **2013,** *117*, (12), 2556-2568.

21. Magneron, I.; Thevenet, R.; Mellouki, A.; Le Bras, G.; Moortgat, G.; Wirtz, K., A study of the photolysis and OH-initiated oxidation of acrolein and trans-crotonaldehyde. *The Journal of Physical Chemistry A* **2002,** *106*, (11), 2526-2537.

22. Mason, S. A.; Arey, J.; Atkinson, R., Kinetics and Products of the OH Radical-Initiated Reaction of 1,4-Butanediol and Rate Constants for the Reactions of OH Radicals with 4-Hydroxybutanal and 3-Hydroxypropanal. *Environmental Science & Technology* **2010,** *44*, (2), 707-713.

23. Fruekilde, P.; Hjorth, J.; Jensen, N. R.; Kotzias, D.; Larsen, B., Ozonolysis at vegetation surfaces: a source of acetone, 4-oxopentanal, 6-methyl-5-hepten-2-one, and geranyl acetone in the troposphere. *Atmospheric Environment* **1998,** *32*, (11), 1893-1902.

24. Bierbach, A.; Barnes, I.; Becker, K. H.; Wiesen, E., Atmospheric chemistry of unsaturated carbonyls: Butenedial, 4-oxo-2-pentenal, 3-hexene-2, 5-dione, maleic anhydride, 3H-furan-2-one, and 5-methyl-3H-furan-2-one. *Environmental science & technology* **1994,** *28*, (4), 715-729.

25. Davis, M.; Gilles, M.; Ravishankara, A.; Burkholder, J. B., Rate coefficients for the reaction of OH with (E)-2-pentenal,(E)-2-hexenal, and (E)-2-heptenal. *Physical Chemistry Chemical Physics* **2007,** *9*, (18), 2240-2248.

26. Baker, J.; Arey, J.; Atkinson, R., Formation and reaction of hydroxycarbonyls from the reaction of OH radicals with 1, 3-butadiene and isoprene. *Environmental science & technology* **2005,** *39*, (11), 4091-4099.

27. Bierbach, A.; Barnes, I.; Becker, K., Product and kinetic study of the OH-initiated gas-phase oxidation of furan, 2-methylfuran and furanaldehydes at≈ 300 K. *Atmospheric Environment* **1995,** *29*, (19), 2651-2660.

28. Renbaum-Wolff, L.; Smith, G. D., "Virtual Injector" Flow Tube Method for Measuring Relative Rates Kinetics of Gas-Phase and Aerosol Species. *The Journal of Physical Chemistry A* **2012,** *116*, (25), 6664-6674.

29. Grosjean, D.; Williams II, E. L., Environmental persistence of organic compounds estimated from structure-reactivity and linear free-energy relationships. Unsaturated aliphatics. *Atmospheric Environment. Part A. General Topics* **1992,** *26*, (8), 1395-1405.

30. Gao, T.; Andino, J. M.; Rivera, C. C.; Márquez, M. F., Rate constants of the gas-phase reactions of OH radicals with trans-2-hexenal, trans-2-octenal, and trans-2-nonenal. *International Journal of Chemical Kinetics* **2009,** *41*, (7), 483-489.

31. Xing, J.-H.; Ono, M.; Kuroda, A.; Obi, K.; Sato, K.; Imamura, T., Kinetic study of the daytime atmospheric fate of (Z)-3-hexenal. *The Journal of Physical Chemistry A* **2012,** *116*, (33), 8523-8529.

32. Aschmann, S. M.; Arey, J.; Atkinson, R., Atmospheric chemistry of selected hydroxycarbonyls. *The Journal of Physical Chemistry A* **2000,** *104*, (17), 3998-4003.

33. Smith, A. M.; Rigler, E.; Kwok, E. S. C.; Atkinson, R., Kinetics and Products of the Gas-Phase Reactions of 6-Methyl-5-hepten-2-one and trans-Cinnamaldehyde with OH and NO3 Radicals and O3 at 296 ± 2 K. *Environmental Science & Technology* **1996,** *30*, (5), 1781-1785.

34. Baker, J.; Arey, J.; Atkinson, R., Kinetics of the Gas-Phase Reactions of OH Radicals, NO3 Radicals and O3 with Three C7-Carbonyls Formed From The Atmospheric Reactions of Myrcene, Ocimene and Terpinolene. *Journal of Atmospheric Chemistry* **2004,** *48*, (3), 241-260.

35. Albaladejo, J.; Ballesteros, B.; Jiménez, E.; Martín, P.; Martínez, E., A PLP–LIF kinetic study of the atmospheric reactivity of a series of C4–C7 saturated and unsaturated aliphatic aldehydes with OH. *Atmospheric environment* **2002,** *36*, (20), 3231-3239.

36. Tuazon, E. C.; Aschmann, S. M.; Nguyen, M. V.; Atkinson, R., H-atom abstraction from selected C · H bonds in 2, 3-dimethylpentanal, 1, 4-cyclohexadiene, and 1, 3, 5-cycloheptatriene. *International Journal of Chemical Kinetics* **2003,** *35*, (9), 415-426.

37. Atkinson, R.; Aschmann, S. M., Atmospheric chemistry of the monoterpene reaction products nopinone, camphenilone, and 4-acetyl-1-methylcyclohexene. *Journal of atmospheric chemistry* **1993,** *16*, (4), 337-348.

38. Carrasco, N.; Picquet-Varrault, B.; Doussin, J.-F., Kinetic and product study of the gas-phase reaction of sabinaketone with OH radical. *International Journal of Chemical Kinetics* **2007,** *39*, (7), 415-421.

39. Bowman, J. H.; Barket, D. J.; Shepson, P. B., Atmospheric chemistry of nonanal. *Environmental science & technology* **2003,** *37*, (10), 2218-2225.

40. Ceacero-Vega, A. A.; Ballesteros, B.; Bejan, I.; Barnes, I.; Jiménez, E.; Albaladejo, J., Kinetics and mechanisms of the tropospheric reactions of menthol, borneol, fenchol, camphor, and fenchone with hydroxyl radicals (OH) and chlorine atoms (Cl). *The Journal of Physical Chemistry A* **2012,** *116*, (16), 4097-4107.

41. Forester, C. D.; Ham, J. E.; Wells, J., Geraniol (2, 6-dimethyl-2, 6-octadien-8-ol) reactions with ozone and OH radical: Rate constants and gas-phase products. *Atmospheric Environment* **2007,** *41*, (6), 1188-1199.

42. Harrison, J.; Ham, J.; Wells, J., Citronellal reactions with ozone and OH radical: Rate constants and gas-phase products detected using PFBHA derivatization. *Atmospheric Environment* **2007,** *41*, (21), 4482-4491.

43. Atkinson, R., Kinetics and mechanisms of the gas-phase reactions of the hydroxyl radical with organic compounds under atmospheric conditions. *Chemical Reviews* **1986,** *86*, (1), 69-201.

44. Picquet, B.; Heroux, S.; Chebbi, A.; Doussin, J. F.; Durand-Jolibois, R.; Monod, A.; Loirat, H.; Carlier, P., Kinetics of the reactions of OH radicals with some oxygenated volatile organic compounds under simulated atmospheric conditions. *International journal of chemical kinetics* **1998,** *30*, (11), 839-847.

45. Pimentel, A. S.; Tyndall, G. S.; Orlando, J. J.; Hurley, M. D.; Wallington, T. J.; Sulbaek Andersen, M. P.; Marshall, P.; Dibble, T. S., Atmospheric chemistry of isopropyl formate and tert-butyl formate. *International Journal of Chemical Kinetics* **2010,** *42*, (8), 479-498.

46. Bierbach, A.; Barnes, I.; Becker, K., Rate coefficients for the gas-phase reactions of hydroxyl radicals with furan, 2-methylfuran, 2-ethylfuran and 2, 5-dimethylfuran at 300±2 K. *Atmospheric Environment. Part A. General Topics* **1992,** *26*, (5), 813-817.

47. Klotz, B.; Barnes, I.; Becker, K.-H., Kinetic study of the gas-phase photolysis and OH radical reaction of E,Z- and E,E-2,4-Hexadienedial. *International Journal of Chemical Kinetics* **1999,** *31*, (10), 689-697.

48. Ferrari, C.; Roche, A.; Jacob, V.; Foster, P.; Baussand, P., Kinetics of the reaction of OH radicals with a series of esters under simulated conditions at 295 K. *International Journal of Chemical Kinetics* **1996,** *28*, (8), 609-614.

49. Cometto, P. M.; Daële, V.; Idir, M.; Lane, S. I.; Mellouki, A., Reaction Rate Coefficients of OH Radicals and Cl Atoms with Ethyl Propanoate, n-Propyl Propanoate, Methyl 2-Methylpropanoate, and Ethyl n-Butanoate. *The Journal of Physical Chemistry A* **2009,** *113*, (40), 10745-10752.

50. Le Calve, S.; Le Bras, G.; Mellouki, A., Temperature dependence for the rate coefficients of the reactions of the OH radical with a series of formates. *The Journal of Physical Chemistry A* **1997,** *101*, (30), 5489-5493.

51. Szilágyi, I.; Dóbé, S.; Bérces, T.; Márta, F.; Viskolcz, B., Direct kinetic study of reactions of hydroxyl radicals with alkyl formates. *Zeitschrift für Physikalische Chemie* **2004,** *218*, (4), 479-492.

52. Schütze, N.; Zhong, X.; Kirschbaum, S.; Bejan, I.; Barnes, I.; Benter, T., Relative kinetic measurements of rate coefficients for the gas-phase reactions of Cl atoms and OH radicals with a series of methyl alkyl esters. *Atmospheric Environment* **2010,** *44*, (40), 5407-5414.

53. Blanco, M. B.; Taccone, R. A.; Lane, S. I.; Teruel, M. A., On the OH-initiated degradation of methacrylates in the troposphere: Gas-phase kinetics and formation of pyruvates. *Chemical physics letters* **2006,** *429*, (4-6), 389-394.

54. Dagaut, P.; Wallington, T. J.; Liu, R.; Kurylo, M. J., A kinetic investigation of the gas-phase reactions of hydroxyl radicals with cyclic ketones and diones: mechanistic insights. *The Journal of Physical Chemistry* **1988,** *92*, (15), 4375-4377.

55. Holloway, A.-L.; Treacy, J.; Sidebottom, H.; Mellouki, A.; Daële, V.; Le Bras, G.; Barnes, I., Rate coefficients for the reactions of OH radicals with the keto/enol tautomers of 2, 4-pentanedione and 3-methyl-2, 4-pentanedione, allyl alcohol and methyl vinyl ketone using the enols and methyl nitrite as photolytic sources of OH. *Journal of Photochemistry and Photobiology A: Chemistry* **2005,** *176*, (1-3), 183-190.

56. Teruel, M. A.; Benitez-Villalba, J.; Caballero, N.; Blanco, M. B., Gas-Phase oxidation of methyl crotonate and ethyl crotonate. kinetic study of their reactions toward OH radicals and Cl atoms. *The Journal of Physical Chemistry A* **2012,** *116*, (24), 6127-6133.

57. Le Calvé, S.; Le Bras, G.; Mellouki, A., Kinetic studies of OH reactions with Iso-propyl, Iso-butyl, Sec-butyl, and Tert-butyl acetate. *International journal of chemical kinetics* **1997,** *29*, (9), 683-688.

58. Veillerot, M.; Foster, P.; Guillermo, R.; Galloo, J. C., Gas-phase reaction of n-butyl acetate with the hydroxyl radical under simulated tropospheric conditions: Relative rate constant and product study. *International Journal of Chemical Kinetics* **1996,** *28*, (4), 235-243.

59. Stemmler, K.; Mengon, W.; Alistair Kerr, J., Hydroxyl-radical-initiated oxidation of isobutyl isopropyl ether under laboratory conditions related to the troposphere Product studies and proposed mechanism. *Journal of the Chemical Society, Faraday Transactions* **1997,** *93*, (16), 2865-2875.

60. Blanco, M. B.; Bejan, I.; Barnes, I.; Wiesen, P.; Teruel, M. A., OH-Initiated Degradation of Unsaturated Esters in the Atmosphere: Kinetics in the Temperature Range of 287−313 K. *The Journal of Physical Chemistry A* **2009,** *113*, (20), 5958-5965.

61. Williams, D. C.; O'Rji, L. N.; Stone, D. A., Kinetics of the reactions of OH radicals with selected acetates and other esters under simulated atmospheric conditions. *International Journal of Chemical Kinetics* **1993,** *25*, (7), 539-548.

62. Nizamov, B.; Dagdigian, P. J., Spectroscopic and kinetic investigation of methylene amidogen by cavity ring-down spectroscopy. *The Journal of Physical Chemistry A* **2003,** *107*, (13), 2256-2263.

63. Borduas, N.; da Silva, G.; Murphy, J. G.; Abbatt, J. P. D., Experimental and Theoretical Understanding of the Gas Phase Oxidation of Atmospheric Amides with OH Radicals: Kinetics, Products, and Mechanisms. *The Journal of Physical Chemistry A* **2015,** *119*, (19), 4298-4308.

64. Sun, J.; Tang, Y.; Sun, H.; Pan, Y.; Jia, X.; Pan, X.; Wang, R., Mechanistic and kinetic study of the OH+ C2H5CN reaction. *Chemical Physics Letters* **2008,** *463*, (4-6), 315-321.

65. Nielsen, O. J.; Jørgensen, O.; Donlon, M.; Sidebottom, H. W.; O'Farrell, D. J.; Treacy, J., Rate constants for the gas-phase reactions of OH radicals with nitroethene, 3-nitropropene and 1-nitrocyclohexene at 298 K and 1 atm. *Chemical physics letters* **1990,** *168*, (3-4), 319-323.

66. Barnes, I.; Bastian, V.; Becker, K.; Fink, E.; Nelsen, W., Oxidation of sulphur compounds in the atmosphere: I. Rate constants of OH radical reactions with sulphur dioxide, hydrogen sulphide, aliphatic thiols and thiophenol. *Journal of atmospheric chemistry* **1986,** *4*, (4), 445-466.

67. Falbe-Hansen, H.; Sørensen, S.; Jensen, N.; Pedersen, T.; Hjorth, J., Atmospheric gas-phase reactions of dimethylsulphoxide and dimethylsulphone with OH and NO3 radicals, Cl atoms and ozone. *Atmospheric Environment* **2000,** *34*, (10), 1543-1551.

68. Lindinger, W.; Hansel, A.; Jordan, A., On-line monitoring of volatile organic compounds at pptv levels by means of proton-transfer-reaction mass spectrometry (PTR-MS) medical applications, food control and environmental research. *International Journal of Mass Spectrometry and Ion Processes* **1998,** *173*, (3), 191-241.

69. Amelynck, C.; Schoon, N.; Kuppens, T.; Bultinck, P.; Arijs, E., A selected ion flow tube study of the reactions of H3O+, NO+ and O2+ with some oxygenated biogenic volatile organic compounds. *International Journal of Mass Spectrometry* **2005,** *247*, (1-3), 1-9.

70. Price, D. J.; Day, D. A.; Pagonis, D.; Stark, H.; Algrim, L. B.; Handschy, A. V.; Liu, S.; Krechmer, J. E.; Miller, S. L.; Hunter, J. F.; de Gouw, J. A.; Ziemann, P. J.; Jimenez, J. L., Budgets of Organic Carbon Composition and Oxidation in Indoor Air. Environ Sci Technol 2019, 53, (22), 13053-13063.

71. Tang, X.; Misztal, P. K.; Nazaroff, W. W.; Goldstein, A. H., Volatile Organic Compound Emissions from Humans Indoors. Environ Sci Technol 2016, 50, (23), 12686-12694.

72. Stonner, C.; Edtbauer, A.; Williams, J., Real-world volatile organic compound emission rates from seated adults and children for use in indoor air studies. Indoor Air 2017, 28, (1), 164-172.

73. St Clair, J. M.; Rivera-Rios, J. C.; Crounse, J. D.; Praske, E.; Kim, M. J.; Wolfe, G. M.; Keutsch, F. N.; Wennberg, P. O.; Hanisco, T. F., Investigation of a potential HCHO measurement artifact from ISOPOOH. *Atmos Meas Tech* **2016,** *9*, (9), 4561-4568.

74. Wennberg, P. O.; Bates, K. H.; Crounse, J. D.; Dodson, L. G.; McVay, R. C.; Mertens, L. A.; Nguyen, T. B.; Praske, E.; Schwantes, R. H.; Smarte, M. D.; St Clair, J. M.; Teng, A. P.; Zhang, X.; Seinfeld, J. H., Gas-Phase Reactions of Isoprene and Its Major Oxidation Products. *Chem Rev* **2018,** *118*, (7), 3337-3390.

75. St. Clair, J. M.; Rivera-Rios, J. C.; Crounse, J. D.; Knap, H. C.; Bates, K. H.; Teng, A. P.; Jørgensen, S.; Kjaergaard, H. G.; Keutsch, F. N.; Wennberg, P. O., Kinetics and Products of the Reaction of the First-Generation Isoprene Hydroxy Hydroperoxide (ISOPOOH) with OH. *The Journal of Physical Chemistry A* **2016,** *120*, (9), 1441-1451.

Chapter 6. Conclusions and future perspectives

This doctoral work mainly focuses on the characterization of carbonyl compounds and their contribution to the total OH reactivity in both outside atmosphere and indoor human occupied environments. The PTR-MS is the major measurement technique applied to monitor carbonyls and the total OH reactivity. It was shown throughout this work that similar volatile carbonyl compounds can be present both outdoors and indoors, albeit at different levels caused by various emission sources and formation mechanism, influencing the air chemistry. In both situations, comparing the measured total OH reactivity and the estimated OH reactivity helped to identify the completeness of reactive species characterization and to understand to what extent carbonyls contribute to the total loss frequency of OH radicals.

For the outdoor environment, the carbonyls and the total OH reactivity were measured around the Arabian Peninsula from on-board a ship. Aliphatic carbonyls were generally more abundant than unsaturated and aromatic carbonyls over the different regions. Acetone had the highest mixing ratios ranging from several hundred ppt over the Arabian Sea to several ppb over the Arabian Gulf, followed by formaldehyde and acetaldehyde, which showed a similar regional distribution. Case studies demonstrated that photochemical oxidation of precursors and biomass burning were important sources for carbonyls over the Arabian Gulf and Suez region, respectively. Meanwhile, direct emissions from anthropogenic sources (ship emissions and oil & gas industry) could also contribute to the high mixing ratios of carbonyls. By further comparing the measured mixing ratios of major carbonyls (acetaldehyde, acetone and methyl ethyl ketone) with a comprehensive global atmospheric chemistry model (EMAC), acetaldehyde was found to have the largest bias over most of the regions, which was largely underestimated by the model simulation, up to a factor of 10. By implementing an oceanic source of acetaldehyde from photodegradation of colored dissolved organic matter reported in previous literature, the model estimation had a significant improvement especially over the northern part of the Red Sea. This finding observed in the marine atmosphere over the Arabian Peninsula supports recent studies claiming ocean may serve as an important source for atmospheric acetaldehyde (Millet et al., 2010; Read et al., 2012; Wang et al., 2019). However, measurement results of acetaldehyde concentration in the seawater are still lacking globally, leading to uncertainty in the ocean acting as a net source of acetaldehyde. Meanwhile, the contribution from other sources (e.g. from organic aerosols) via different formation pathways are still under discussion (Wang et al., 2019). Inlet sampling artifacts due to degradation of inlet surface absorbed materials can introduce bias to the measured values especially under pristine regions

(Apel et al., 2008; Northway et al., 2004). Therefore, careful instrumental characterizations and more ambient measurement comparison with model simulations are needed to better understand the budget of acetaldehyde, one of the simplest carbonyl compounds in the atmosphere.

A similar regional distribution to the carbonyls was found for the measured total OH reactivity with the highest value observed being comparable to the values obtained in polluted urban areas. By including more species measured by PTR-ToF-MS and other trace gas instruments (over 100 species), the unattributed reactivity reduced compared to only including major species. The reactivity budget can be closed within the uncertainty over half of the regions including the most polluted areas (Arabian Gulf and Suez Canal). Oxygenated VOCs were found to provide the largest OH reactivity over the Arabian Gulf with five carbonyl species ranked as the top ten most important contributors to the total OH reactivity, indicating strong photochemical reactions leading to high ozone over this region. In addition, OH reactivity versus ozone correlations plots helped to characterize the ozone formation and loss involving different chemical process. The good data coverage of the OH reactivity measurement throughout the ship campaign showed the robustness of the CRM method on a moving platform.

For the indoor environment, the carbonyls and the total OH reactivity were measured in a climate chamber occupied by human subjects under controlled conditions so that the "natural" human emissions can be ascertained. Over 150 species and ions were found related to human occupants. For the total breath emission rate, the most important contributors were acetone, isoprene and methanol (91% of the total). While for the total dermal emission rate, it was acetic acid, acetone and $C_2H_2OH^+$ (fragment of acids) contributing the most. When ozone was added in the chamber, the total emission rate of breath as well as the top contributing species showed no significant change. However, the total emission rate of skin increased dramatically with the most important contributors changed to acetone, 6MHO and 4OPA, which are major skin lipids (mainly squalene) ozonolysis products. For the whole-body emission rate, it doubled when ozone was present. The increase was driven by the dermal emissions mainly carbonyl compounds. For whole-body emissions, the same dominant species were identified without and with ozone present. The emission rates obtained from the chamber study can be used in indoor air models to better simulate the indoor environments occupied by humans. This is key information as human beings are the single common element of all living spaces. Based on measured VOCs, the estimated OH reactivity can be calculated. By comparing the calculated and the measured OH reactivity, no missing

reactivity (unattributed fraction) was observed within the uncertainty, indicating major reactive species related to human emissions under both ozone-free and ozone-present conditions have been captured by the applied trace gas measurement technique. Similar to the ozone effect observed for the emission rates, ozone had negligible effect on breath OH reactivity (dominated by isoprene) but elevated the dermal OH reactivity dramatically dominated by carbonyl compounds. The OH reactivity of whole-body emissions from four people in the ventilated chamber (16 s^{-1} under ozone-free and 33 s^{-1} under ozone-present) was comparable to the reactivity measured in big cities. The study was extended to identify the age effect. Only under ozone-present conditions, was it found that the total OH reactivity had a slight age dependence with the OH reactivity: the reactivity contributed by carbonyl compounds decreased with increasing age. It was for the first time that the CRM system was applied in indoor air measurement, showing good performance and feasibility.

Ozone formation and loss were mentioned throughout this thesis work linking

to carbonyl formation and loss for both outdoor and indoor air chemistry. We can conclude from the work that ozone plays a more significant role as an oxidant in indoor air chemistry than its role as a direct oxidant in daytime outdoor air chemistry. Although the hydroxyl radical (OH) is the main oxidant in outside air, coming from ozone photochemistry as described in section 1.1.1, indoor OH level is suppressed to a large extent. For outdoor air, secondary formation of ozone is an issue of a great concern not only due to its exposure risk but also because of production of carbonyl compounds during its formation process. The typical indoor to outdoor ozone ratio (I/O) is in the range of 0.2 to 0.7 (Weschler, 2000). More importantly, the outdoor accumulated ozone can impact the indoor ozone concentrations, indirectly affecting the indoor air quality through ozone-initiated chemistry. In contrast, ozone formation via photochemistry rarely occurs in indoor air due to lack of solar radiation but can be additionally released from devices such as printers and air purifiers. Outdoor direct VOCs emission sources have been intensively studied, which provides valuable information to better understand the source profiles of atmospheric carbonyls. However, due to much stronger solar radiation compared to indoor air, photolysis and photochemical reactions occur rapidly. Together with meteorological conditions, the formation and loss of carbonyl compounds become complicated, which can lead to missing reactivity and unbalanced source and sink budgets (as for acetaldehyde). For indoor air, ozone is the mostly studied oxidant. The formation of other oxidants (e.g. OH and NO_3) in indoor environments are known to be related to human activities but are so far much less studied. The study presented in this doctoral project

done in the climate chamber already showed abundant and diverse VOCs can be released just from human body and how ozone can alter the abundance and the chemical profile when people remain seated. Although, no missing reactivity was observed in the chamber study, some unattributed reactivity may exist under other conditions. Therefore, more studies are needed to characterize the VOCs released from different human activities and how they can interact with indoor oxidants. It was recently identified that ozone-initiated carbonyl production can be more efficiently reduced via ozone filtration compared to increasing the air exchange rate (Salvador et al., 2019). More practical studies of this type should be conducted, as they provide valuable information that can help to improve the air quality of human occupied indoor environments more efficiently.

Last but not least, although PTR-MS and the CRM method have been widely used to characterize the VOCs and OH reactivity, limitations of quantification still remain, which can cause uncertainty to measurements. PTR-MS using protonated water as the primary ions is not able to measure compounds with lower proton affinity than water and it has low efficiency to measure compounds with slightly higher proton affinity than water (e.g. formaldehyde). In addition, it is also not able to distinguish isomeric compounds. In recent years, more studies have been done by using multiple reagent ions (e.g. NO^+, O_2^+ and NH_4^+) to improve the qualification of PTR-MS (Yuan et al., 2017). Other techniques like gas chromatography (GC) was also deployed in parallel to PTR-MS to achieve wider chemical characterization (Materic et al., 2015; Romano et al., 2014). However, for measurements with fast temporal changes and large variations, switching between different ions or running modes could lead to data loss (worsen the time resolution of the data set). For the CRM system, the relative large uncertainty is caused by multiple interference corrections that remain the main issue limiting the precision of measured reactivity using this method. Instrumental improvements are needed to reduce the interferences.

References

Apel, E. C., Brauers, T., Koppmann, R., Bandowe, B., Boßmeyer, J., Holzke, C., Tillmann, R., Wahner, A., Wegener, R., Brunner, A., Jocher, M., Ruuskanen, T., Spirig, C., Steigner, D., Steinbrecher, R., Gomez Alvarez, E., Müller, K., Burrows, J. P., Schade, G., Solomon, S. J., Ladstätter-Weißenmayer, A., Simmonds, P., Young, D., Hopkins, J. R., Lewis, A. C., Legreid, G., Reimann, S., Hansel, A., Wisthaler, A., Blake, R. S., Ellis, A. M., Monks, P. S., and Wyche, K. P.: Intercomparison of oxygenated volatile organic compound measurements at the SAPHIR atmosphere simulation chamber, Journal of Geophysical Research, 113, 2008.

Materic, D., Lanza, M., Sulzer, P., Herbig, J., Bruhn, D., Turner, C., Mason, N., and Gauci, V.: Monoterpene separation by coupling proton transfer reaction time-of-flight mass spectrometry with fastGC, Anal Bioanal Chem, 407, 7757-7763, 2015.

Millet, D. B., Guenther, A., Siegel, D. A., Nelson, N. B., Singh, H. B., de Gouw, J. A., Warneke, C., Williams, J., Eerdekens, G., and Sinha, V.: Global atmospheric budget of acetaldehyde: 3-D model analysis and constraints from in-situ and satellite observations, Atmospheric Chemistry and Physics, 10, 3405-3425, 2010.

Northway, M. J., de Gouw, J. A., Fahey, D. W., Gao, R. S., Warneke, C., Roberts, J. M., and Flocke, F.: Evaluation of the role of heterogeneous oxidation of alkenes in the detection of atmospheric acetaldehyde, Atmospheric Environment, 38, 6017-6028, 2004.

Read, K. A., Carpenter, L. J., Arnold, S. R., Beale, R., Nightingale, P. D., Hopkins, J. R., Lewis, A. C., Lee, J. D., Mendes, L., and Pickering, S. J.: Multiannual observations of acetone, methanol, and acetaldehyde in remote tropical atlantic air: implications for atmospheric OVOC budgets and oxidative capacity, Environ Sci Technol, 46, 11028-11039, 2012.

Romano, A., Fischer, L., Herbig, J., Campbell-Sills, H., Coulon, J., Lucas, P., Cappellin, L., and Biasioli, F.: Wine analysis by FastGC proton-transfer reaction-time-of-flight-mass spectrometry, International Journal of Mass Spectrometry, 369, 81-86, 2014.

Salvador, C. M., Beko, G., Weschler, C. J., Morrison, G., Le Breton, M., Hallquist, M., Ekberg, L., and Langer, S.: Indoor ozone/human chemistry and ventilation strategies, Indoor Air, 29, 913-925, 2019.

Wang, S., Hornbrook, R. S., Hills, A., Emmons, L. K., Tilmes, S., Lamarque, J. F., Jimenez, J. L., Campuzano‐Jost, P., Nault, B. A., Crounse, J. D., Wennberg, P. O., Kim, M., Allen, H., Ryerson, T. B., Thompson, C. R., Peischl, J., Moore, F., Nance, D., Hall, B., Elkins, J., Tanner, D., Huey, L. G., Hall, S. R., Ullmann, K., Orlando, J. J., Tyndall, G. S., Flocke, F. M., Ray, E., Hanisco, T. F., Wolfe, G. M., St. Clair, J., Commane, R., Daube, B., Barletta, B., Blake, D. R., Weinzierl, B., Dollner, M., Conley, A., Vitt, F., Wofsy, S. C., Riemer, D. D., and Apel, E. C.: Atmospheric Acetaldehyde: Importance of Air‐Sea Exchange and a Missing Source in the Remote Troposphere, Geophysical Research Letters, doi: 10.1029/2019gl082034, 2019. 2019.

Weschler, C. J.: Ozone in indoor environments: concentration and chemistry, Indoor air, 10, 269-288, 2000.

Yuan, B., Koss, A. R., Warneke, C., Coggon, M., Sekimoto, K., and de Gouw, J. A.: Proton-Transfer-Reaction Mass Spectrometry: Applications in Atmospheric Sciences, Chem Rev, 117, 13187-13229, 2017.